



Contribution to the Triazole-Based Fe(II) Spin-Crossover (SCO) materials: some achievements and new questions

Narsimhulu Pittala

► To cite this version:

Narsimhulu Pittala. Contribution to the Triazole-Based Fe(II) Spin-Crossover (SCO) materials: some achievements and new questions. Other. Université de Bretagne occidentale - Brest, 2016. English. NNT: 2016BRES0084 . tel-01591497

HAL Id: tel-01591497

<https://theses.hal.science/tel-01591497>

Submitted on 21 Sep 2017

HAL is a multi-disciplinary open access archive for the deposit and dissemination of scientific research documents, whether they are published or not. The documents may come from teaching and research institutions in France or abroad, or from public or private research centers.

L'archive ouverte pluridisciplinaire **HAL**, est destinée au dépôt et à la diffusion de documents scientifiques de niveau recherche, publiés ou non, émanant des établissements d'enseignement et de recherche français ou étrangers, des laboratoires publics ou privés.



université de bretagne
occidentale

UNIVERSITE
BRETAGNE
LOIRE

THÈSE / UNIVERSITÉ DE BRETAGNE OCCIDENTALE

sous le sceau de l'Université Bretagne Loire

pour obtenir le titre de

DOCTEUR DE L'UNIVERSITÉ DE BRETAGNE OCCIDENTALE

Mention : Chimie Moléculaire

École Doctorale SICMA

présentée par

Narsimhulu Pittala

Préparée à l'UFR Sciences et Techniques

Contribution to the Triazole-Based Fe(II) Spin-Crossover (SCO) Materials: Some Achievements and New Questions

Thèse soutenue le 24 Novembre 2016

devant le jury composé de :

Yann Garcia

Professeur, Université catholique de Louvain, Belgique / Rapporteur

Abdelkrim El-Ghayoury

Maître de Conférences (HDR), Université d'Angers/ Rapporteur

Enrique Colacio

Professeur, Université de Grenade, Espagne/ Examineur

Kamel Boukheddaden

Professeur, Université de Paris-Saclay, Versailles / Examineur

Frédéric Gloaguen

Directeur de Recherche (CNRS), Université de Brest / Examineur

Franck Thétiot

Maître de Conférences, Université de Brest / Encadrant

Smail Triki

Professeur, Université de Brest / Directeur de thèse



La bourse de thèse associée au présent travail a été financée par la “*Région Bretagne*”
(Bourse ARED)

Acknowledgements

When referring to the people who have helped me in completing my Ph.D., I would like first of all to particularly thank my supervisors Prof. Smail Triki and Dr. Franck Thetiot for their unstinting efforts and contributions, and more generally all the members of the team “Matériaux Moléculaires et Systèmes Organisés Électroactifs (MAMSOE)” (UMR CNRS6521 - UBO).



I want also to thank Stéphane Cérantola (“Ingénieur de Recherche”), Nelly Kervarec (“Ingénieur d’études”), and Gaëlle Simon (“Assistant ingénieur”) for their momentous help in NMR data analysis, and Francois Michaud for his significant assistance in X-ray diffraction data collection.



Additionally and taking into account the wide panel of characterization techniques required for the present work, I am very thankful to our collaborators *i.e.* Dr. Guillaume Chastanet and Dr. Mathieu Marchivie (ICMCB, Bordeaux, France) for magnetic measurements and XRD analyses, respectively, and Prof. Kamel Boukheddaden (Université Paris-Saclay) for the photo-physical studies.



Finally, I would like to thank my family and my friends who have supported me over the past years in different ways to make my life happier, and to achieve this work.

Summary

General Introduction	5
Chapter I: Molecular Switches and Spin-Crossover (SCO) Phenomenon	
1. Spin-Crossover (SCO) Phenomenon: Principle and Origin	12
2. Thermal Spin-Crossover (SCO): Cooperativity and Bistability	15
2.1. Characteristics	15
2.2. Cooperativity and Types of Spin-Transitions	18
3. Light-Induced Excited Spin-State Trapping (LIESST) Effects: LIESST and Reverse LIESST	21
4. Rational Tailoring of the SCO Behavior: Combinational Influences of Chemical and Structural Factors	26
4.1. Chemical Factors: Composition of the SCO Material	27
4.2. Structural Factors: Consequences and Implications of the Chemical Factors	38
5. Aims and Strategy of the Present Work	42
5.1. Selection of the Ligand: 4-R-1,2,4-Triazole Ligands (Rtrz)	42
5.2. Selection of the Anion: Organic and Inorganic Polycyano Anions	46
5.3. Aims and Strategy	49
6. Experimental Approach of Spin-Crossover Materials	52
6.1. Crystallogenes of SCO Derivatives: The “Royal” Synthetic Pathway	52
6.2. Detection and Characterization Techniques of the SCO Behaviour: A Multi-tool Approach	55
Bibliography	63

Chapter II: New Synthetic Strategy for the Design of New One-Dimensional Fe(II) *SCO* Coordination Polymers based on Functionalized Triazole Ligands: Reliable Structural Investigations including the First Structural Studies of the High and Low Spin States

Introduction	82
Results and Discussion	85
1. Syntheses and Infrared Spectroscopy of [Fe(bntrz) ₃][Pt(CN) ₄].H ₂ O (1)	85
2. Magnetic Properties	87
3. Differential Scanning Calorimetry	88
4. Structural Investigations in both High Spin (<i>HS</i>) and Low Spin (<i>LS</i>) States	90
Conclusion	99
Experimental Section	101
Bibliography	107

Chapter III: Trinuclear Fe(II) Complexes Based on Functionalised Triazole and Cyanocarbanion Ligands with Unique Complete *SCO* Behaviour

Introduction	112
Results and Discussion	116
1. Syntheses and Spectroscopic Characterizations of [Fe ₃ (bntrz) ₆ (tcnset) ₆] (2)	116
2. Magnetic Properties	119

3. Calorimetric Studies	120
4. Crystal Structure Analyses	121
Conclusion	127
Experimental Section	128
Bibliography	136

Appendix I: Effect of the Functional Group of the Cyanocarbanion on Magneto-Structural Properties in Triazole based Fe(II) Systems: Preliminary Results.

1. Syntheses and Characterizations of Functionalized Cyanocarbanions Ligand (tcnsR ⁻)	140
2. Synthesis, Structure and Magnetic Properties of Complex [Fe ₃ (bntrz) ₆ (tcnspr) ₆] (3): Preliminary Results	151
2.1. Synthesis and Characterizations	151
2.2. Structural Studies	153
2.3. Magnetic Properties	156
2.4. Differential Scanning Calorimetry	157
3. Synthesis, Structure and Magnetic Properties of the Complex [Fe ₃ (bntz) ₈ (tcnsme) ₂][tcnsme] ₂ .4H ₂ O (4): Preliminary Results	159
3.1. Synthesis	159
3.2. Preliminary Structural Characterizations and Magnetic Properties	159
Conclusion	163

Chapter IV: Spin-Crossover (SCO) Behaviours of Three Dimensional Materials Based on Functionalized Triazole Ligand

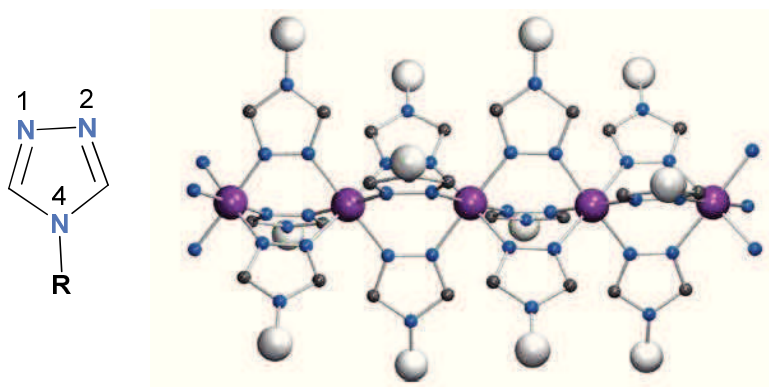
Introduction	166
Results and Discussion	169
1. Syntheses and Characterizations of $\{\text{Fe}_3(\mu_2\text{-phtptrz})_6[\mu_2\text{-Pt(CN)}_4]_3\} \cdot \text{C}_2\text{H}_5\text{OH} \cdot 5.5\text{H}_2\text{O}$ (5) and $\{\text{Fe(phtptrz)}[\text{Pt(CN)}_4] \cdot \text{H}_2\text{O}\}$ (6)	169
2. Structural Characterizations	172
3. Magnetic Properties	186
Conclusion and Perspectives	189
Experimental Section	191
Bibliography	200
 General Conclusion	 207
 Annex I: Accepted and Submitted Publications	 215

General Introduction

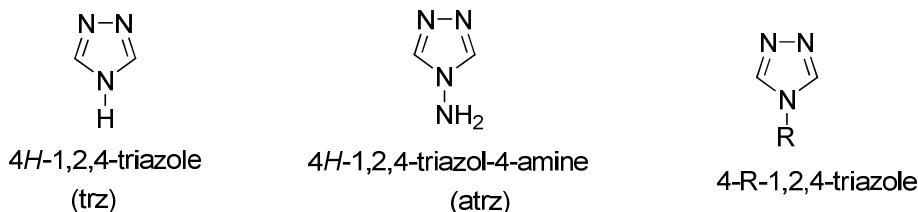
In recent years, molecular electronics and especially spin-crossover (*SCO*) materials have attracted much interest because of their many potential applications such as information storage and displays, or contrast agents for Magnetic Resonance Imaging.¹ The *SCO* phenomenon occurs mainly in some first row transition metal complexes of d^4 - d^7 electronic configurations. Depending notably on the ligand field strength, these complexes typically exhibit a reversible transition “High Spin (*HS*) \leftrightarrow Low Spin (*LS*)” under the influence of an external disturbance (e.g. temperature, radiation, magnetic field, and/or pressure).¹⁻² Among the *SCO* materials, the most studied examples to date are the Fe(II) (d^6 configuration) complexes with an all-nitrogen donor pseudo-octahedral environment ($[\text{FeN}_6]$ type), mainly constituted by nitrogen rich heterocyclic rings; the latter classically display a transition from the paramagnetic high spin (*HS*) state ($S = 2$, $^5T_{2g}$) to the diamagnetic low spin (*LS*) state ($S = 0$, $^1A_{1g}$), when the ligand field strength is close to the electron pairing energy (denoted P). The specifics of a *SCO* behavior will be mainly defined by the conditions required to trigger the spin transition (e.g. transition temperature T_{SCO}) and by the degree of cooperativity, i.e. the degree of ‘communication’ between the spin carriers in the material. In the eventuality of a high cooperativity, a hysteretic behavior may arise and provide bistability (at both the *HS* and *LS* states) with the genesis of a memory effect, where bistability is the capacity of a system to exist in the *HS* or *LS* state within a certain range of an external perturbation (e.g. T). Due to this magnetic bistability and memory effect that depend on the history of the system, the materials that show *SCO* behaviour have been identified as a viable class of applied materials, in particular for incorporation into displays and memory device units, or sensing devices.^{1,3}

In this context, the one dimensional triazole-based Fe^{II} *SCO* materials of general formulae $[\text{Fe}(\text{Htrz})_2(\text{trz})](\text{A})_x$ and $[\text{Fe}(\text{Htrz})_{3-3x}(\text{atrz})_{3x}](\text{A})_x \cdot \text{H}_2\text{O}$ (where Htrz = 4H-1,2,4-triazole, trz = 1,2,4-triazolato ligand, atrz = 4H-1,2,4-triazol-4-amine, and A is mono ($x = 1$) or di ($x=2$) anion) - with several derivatives displaying fairly abrupt spin transitions, and a tendency of wide hysteresis around or above room temperature (See Scheme 1-2 and Figure 1) - have been widely

acknowledged as the most promising systems, and so extensively investigated for the last four decades in the field of *SCO* research.¹ However, the influence of the various substituents at the 4th position of the 1,2,4-triazole ring to fine-tune the *SCO* properties have remained surprisingly unaddressed in a systematic/comparative way; the same observation can be referred to the impact of atypical or more sophisticated anionic ligands on the switching characteristics, with monoanions usually the standard sought-after candidates in most studies. Moreover, the lack of highly refined crystallographic data for those systems (intrinsically due to the high reactivity of the triazole ligands with Fe^{II} salts which tend to favor the formation of amorphous powders) remains a vital and long-lasting challenge in order to evaluate accurately and fine tune all the structural factors utterly correlated to their outstanding *SCO* behaviours.



Scheme 1. Schematic representations of a N4-substituted triazole molecule (left) and of the model/reference 1D coordination chains formed through propagation of triple N1,N2-triazole bridges connecting Fe^{II} centers (right). The R substituent is depicted as large light grey spheres. Colour code: Fe, purple; N, blue; C, dark grey.^{1e}



Scheme 2. Molecular structures of trz, atrz, and 4-R-1,2,4-triazole (where R = functional group).

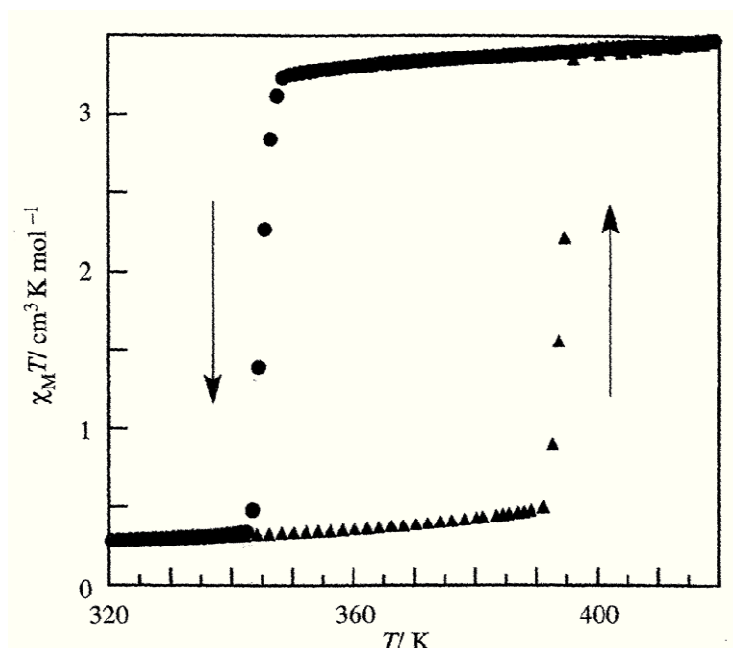
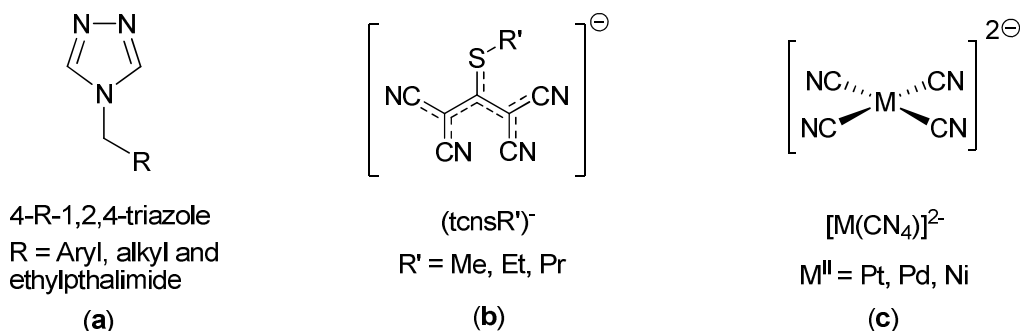


Figure 1. Magnetic thermal hysteresis of triazole-based system $\text{Fe}(\text{Htrz})_2(\text{trz})](\text{BF}_4)$ (where χ_M = magnetic susceptibility and T = temperature).^{1d}

In this regard, the present work has focused primarily on the design and the magneto-structural investigations of novel Fe^{II} SCO systems based on 4-R-1,2,4-triazole ligands including an alkyl spacer, with either (i) inorganic tetracyanometallates ($[\text{M}(\text{CN})_4]^{2-}$) or (ii) specific flexible organic cyanocarbanions ($(\text{tcnsR}')^-$) ($(\text{tcnsR}')^-$ = 1,1,3,3-tetracyano-2-thioalkylpropenide) ligands (Scheme 3). Secondly, an extensive effort has been specifically dedicated to tackle the structural knowledge gap related to triazole-based Fe^{II} SCO materials by systematically seeking access to single crystals through deep crystallogeneses investigations. Ultimately, this work aimed at methodically evaluating the impact of the functionalization of precursors 4-R-1,2,4-triazole and atypical anions such as cyanocarbanion ligands and tetracyanometallates with the establishment of magneto-structural correlations which are essential to understand the physicochemical origin of the strong cooperativity in such striking materials, but also to rationalize the tuning of the SCO properties.



Scheme 3 : Examples of (a) 4-R-1,2,4-triazole derivatives, (b) Cyanocarbanions $(tcnsR')^-$, and (c) Tetracyanometallate(II) anions $[M(CN)_4]^{2-}$.

The structure of the manuscript has been defined as followed. The content of Chapter I has been delineated to provide an overall background into the research field of *SCO* materials, in adequation with the present work. This includes the definition, the description and the characteristics of the the *SCO* phenomenon (with historical context and a focus on Fe^{II} *SCO* systems), the subjective distinction of the factors controlling the nature of the spin transition, the aims and strategy of the present work, and finally a brief overview of the experimental techniques used for the characterizations of *SCO* materials. Then, the Chapter II is devoted to the design and characterizations of a 1D Fe^{II} *SCO* polymer based on functionalized triazole ligand 4-(benzyl)-4H-1,2,4-triazole (bntrz) and tetracyanoplatinate $[Pt(CN)_4]^{2-}$ anionic moiety (including complete single crystal X-ray studies of both LS and HS states). The Chapter III deals with the substitution of the $[Pt(CN)_4]^{2-}$ anionic moiety by functionalized cyanocarbanion $(tcnsR')^-$ ($(tcnsR')^-$ = 1,1,3,3-tetracyano-2-thioalkylpropenide anion) ligands combined with the same bntrz triazole ligand that lead to atypical trinuclear and 1D systems. Finally, the Chapter IV is related to the impact of different substituents at the 4th position onto 1,2,4-triazole ligand, with two three dimensional (3D) polymers based on functionalized triazole ligand 2-(3-(4H-1,2,4-triazol-4-yl)propyl)isoindoline-1,3-dione (phtptrz) and $[Pt(CN)_4]^{2-}$ anionic moiety.

Bibliography

1. (a) O. Kahn, C. Kröber, C. Jay, *Adv. Mater.*, **1992**, *4*, 718-728; (b) O. Kahn, C. J. Martinez, *Science*, **1998**, *279*, 44-48; (c) P. J. Van Koningsbruggen, Y. Garcia, E. Codjovi, R. Lapouyade, O. Kahn, L. Fournès, L. Rabardel, *J. Mater. Chem.*, **1997**, *7*, 2069-2075; (d) J. Kröber, J. P. Audière, R. Claude, E. Codjovi, O. Kahn, J. G. Haasnoot, F. Grolire, C. Jay, A. Bousseksou, J. Linarès, F. Varret, A. Gonthier-Vassal, *Chem. Mater.*, **1994**, *6*, 1404-1412 (e). O. Roubeau, *Chem. Eur. J.*, **2012**, *18*, 15230-5244 and references therein; (f) R. N. Muller, L. V. Elst, and S. Laurent, *J. Am. Chem. Soc.*, **2003**, *125*, 8405-8407; (g) E. Coronado, J. R. Galán-Mascarós, M. Monrabal-Capilla, J. García-Martínez, and P. Pardo-Ibáñez, *Adv. Mater.*, **2007**, *19*, 1359-1361.
2. (d) P. Gülich, H. A. Goodwin, in *Spin Crossover in Transition Metal Compounds*, Springer-Verlag, Berlin/Heidelberg, **2004**, 233, 234, 235; *Topics in Current Chemistry*, Springer: Berlin, 2004; Vols. 1-3; (e) M. A. Halcrow, Spin-crossover materials: properties and applications, Wiley-VCH: Weinheim, John Wiley & Sons, Ltd., U.K., **2013**, Chapter 1, pp 1- 54. (f) P. Gülich, Y. Garcia, H. A. Goodwin, *Chem. Soc. Rev.*, **2000**, *29*, 419-427; (g) A. Bousseksou, G. molnar, L. Salmon, W. Nicolazzi, *Chem. Soc. Rev.*, **2011**, *40*, 3313-3335; (h) M. C. Muñoz, J. A. Real, *Coord. Chem. Rev.*, **2011**, *255*, 2068-2093; (i) G. Aromí, L. A. Barrios, O. Roubeau, P. Gamez, *Coord. Chem. Rev.*, **2011**, *255*, 485-546; (j) M. A. Halcrow, *Chem. Soc. Rev.*, **2011**, *40*, 4119-4142; (k) P. Gülich, A. B. Gaspar and Y. Garcia, *Beilstein J. Org. Chem.*, **2013**, *9*, 342-391.
3. (a) T. Matsumoto, G. N. Newton, T. Shiga, S. Hayami, Y. Matsui, H. Okamoto, R. Kumai, Y. Murakami, H. Oshio, *Nat. Commun.*, **2014**, *5*, 3865; (b) D. Aravena, E. Ruiz, *J. Am. Chem. Soc.*, **2012**, *134*, 777-779; (c) G. A. Craig, O. Roubeau, G. Aromí, *Coord. Chem. Rev.*, **2014**, *269*, 13-31; (d) B. Warner, J. C. Oberg, T. G. Gill, F. El Hallak, C. F. Hirjibehedin, M. Serri, S. Heutz, M. A. Arrio, P. Saintavrit, M. Mannini, G. Poneti, R. Sessoli, P. J. Rosa, *J. Phys. Chem. Lett.*, **2013**, *4*, 1546-1552; (e) J. Larionova, L. Salmon,

Y. Guari, A. Tokarev, K. Molvinger, G. Molnár, A. Bousseksou, *Angew. Chem., Int. Ed.*, **2008**, *7*, 8236-8240; (f) C. F. Wang, R. F. Li, X. Y. Chen, R. J. Wei, L. S. Zheng, J. Tao, *Angew. Chem., Int. Ed.*, **2015**, *54*, 1574-1577; (g) Y.-S. Koo, J. R. Galan-Mascaros, *Adv. Mater.*, **2014**, *26*, 6785-6789; (h) M. B. Duriska, S. M. Neville, B. Moubaraki, J. A. Cashion, G. J. Halder, K. W. Chapman, C. Balde, J. F. Létard, K. S. Murray, C. J. Kepert, S. R. Batten, *Angew. Chem., Int. Ed.*, **2009**, *48*, 2549-2552; (i) E. M. Hernandez, C. M. Quintero, O. Kraieva, C. Thibault, C. Bergaud, L. Salmon, G. Molnár, A. Bousseksou, *Adv. Mater.*, **2014**, *26*, 2889-2893; (j) H. Phan, S. M. Benjamin, E. Steven, J. S. Brooks, M. Shatruk, *Angew. Chem., Int. Ed.*, **2015**, *54*, 823-827; (k) E. Ludwig, H. Naggert, M. Kalläne, S. Rohlf, E. Kröger, A. Bannwarth, A. Quer, K. Rossnagel, L. Kipp, F. Tuczek, *Angew. Chem., Int. Ed.*, **2014**, *53*, 3019-3023; (l) V. A. Money, C. Carbonera, J. Elhaïk, M. A. Halcrow, J. A. K. Howard, J. F. Letard, *Chem. Eur. J.*, **2007**, *13*, 5503-5514; (m) E. Coronado, G. Minguez Espallargas, *Chem. Soc. Rev.*, **2013**, *42*, 1525-1539; (n) T. Liu, H. Zheng, S. Kang, Y. Shiota, S. Hayami, M. Mito, O. Sato, K. Yoshizawa, S. Kanegawa, C. Duan, *Nat. Commun.*, **2013**, *4*, 2826.

Chapter I

Molecular Switches and Spin-Crossover (*SCO*) Phenomenon

1. Spin-Crossover (<i>SCO</i>) Phenomenon: Principle and Origin	12
2. Thermal Spin-Crossover (<i>SCO</i>): Cooperativity and Bistability	15
2.1. Characteristics	15
2.2. Cooperativity and Types of Spin-Transitions	18
3. Light-Induced Excited Spin-State Trapping (LIESST) Effects: LIESST and Reverse LIESST	21
4. Rational Tailoring of the <i>SCO</i> Behavior: Combinational Influences of Chemical and Structural Factors	26
4.1. Chemical Factors: Composition of the <i>SCO</i> Material	27
4.2. Structural Factors: Consequences and Implications of the Chemical Factors	38
5. Aims and Strategy of the Present Work	42
5.1. Selection of the Ligand: 4-R-1,2,4-Triazole Ligands (Rtrz)	42
5.2. Selection of the Anion: Organic and Inorganic Polynitrile Anions	46
5.3. Aims and Strategy	49
6. Experimental Approach of Spin-Crossover Materials	52
6.1. Crystallogenes of <i>SCO</i> Derivatives: The “Royal” Synthetic Pathway	52
6.2. Detection and Characterization Techniques of the <i>SCO</i> Behaviour: A Multi-tool Approach	55
Bibliography	63

Molecular Switches and Spin-Crossover (SCO) Phenomenon

1. Spin-Crossover (SCO) Phenomenon: Principle and Origin

In the current state of molecular switch research, spin-crossover (SCO) is a unique phenomenon that represents the paradigm of molecular bistability. The change of spin state from high-spin (*HS*) to low-spin (*LS*) and *vice versa*, which occurs noticeably for some first row transition metal complexes of d^4 - d^7 electronic configurations under the application of an external perturbation, can be referred to by a number of terms *i.e.* spin crossover, spin transition or spin equilibrium. These $LS \leftrightarrow HS$ spin transitions can be triggered through a variety of external stimuli such as a change in temperature (T), application of pressure (p), irradiation with light ($h\nu$), or in a magnetic field (B). The occurrence of SCO is associated with the change of electronic structure of the central ion and also the coordination sphere volume of the compound, with drastic changes of the physical and chemical properties of the materials. The most spectacular effects are the switching of the magnetic behavior (e.g. diamagnetic \leftrightarrow paramagnetic transition) and profound modifications of the optical properties (e.g. thermo- or piezo-chromism), which have made such SCO compounds very attractive because of their applied potential as switching devices and sensors, and data storage or magneto-optical displays.^{1,2} While the deep understanding of the interaction mechanisms that lead to the cooperative nature of the transition in crystalline solids remains under intense discussion, the starting point of all the considerations at the heart of the spin transition phenomenon is mainly attributed to the “elastic interaction” between the spin-changing ions as a result of the deformation of the crystal (volume change of the lattice between the low- and high-temperature phases), and elastic frustration accompanying the transition of the ions from the *LS* to the *HS* state.³ This volume change also leads to a change of the phonon frequencies of the lattice. Thus, the larger volume of *HS* molecules induces elastic stresses in the crystalline network, hence changing the probability of other molecules to switch to the *HS* state by increasing the temperature. This elastic interaction between the molecules is commonly described as the blend of two components: a short-range interaction, statistically distributed, and a long-range interaction proportional to the average number of *HS* molecules per unit volume. While the short-range interactions depend on shape and distance between neighbor molecules

and can be correlated to the existence of covalent bonds, the long-range interactions are purely of elastic nature and are mediated by the lattice.^{3a,3b}

Regarding the historical context of *SCO* materials, the *SCO* phenomenon was discovered by Cambi *et al.* in 1931 through the observation of anomalous magnetic behavior on a series of dithiocarbamates Fe^{III} complexes.⁴ The first Co^{II} compound that showed *SCO* behaviour, namely $[\text{Co}(\text{L})_2]\text{I}_2$ ($\text{L} = \text{bis-(2,6-pyridindialdihydrazone ligand)}$), was presented by Stouffer *et al.*⁵ in 1961, followed by the discovery of the first Fe^{II} *SCO* compound $[\text{Fe}(\text{phen})_2(\text{NCS})_2]$ by Madeja and König;⁶ these first examples of Fe^{II} and Co^{II} exhibiting drastic changes of their magnetic moments as a function of temperature have been investigated extensively since the mid-1970s.⁷⁻⁸ Only during the 1980s, however, was it realized that *SCO* compounds could be used as active elements in memory devices.^{2,9} Indeed, in 1984, Decurtins *et al.* discovered that for the compound $[\text{Fe}(\text{ptz})_6](\text{BF}_4)_2$ ($\text{ptz} = 1\text{-propyltetrazole}$), a green light ($\lambda = 514 \text{ nm}$) switches the *LS* state to the *HS* and that a red light ($\lambda = 820 \text{ nm}$) switches the system back from the *HS* state to the *LS* state.¹⁰⁻¹³ The discovery of this LIESST (light-induced excited spin-state trapping) and reverse-LIESST effects suggested that the *SCO* compounds could be used as optical switches.¹ Although known for more than eight decades, the *SCO* materials have become most attractive in recent years as they have allowed the design and synthetic versatility of early optical device prototypes, the elaboration of *SCO* nanoparticles, supramolecular gels, thin films, dendrimers, contrast agents for Magnetic Resonance Imaging and liquid crystals, as well as the electrical addressing of *SCO* or the use of plasmons to detect *SCO*.¹⁴

In general, the spin transition occurs for some first row transition metal complexes of d^4 - d^7 electronic configurations (Cr^{II} , Mn^{II} , Mn^{III} , Fe^{III} , Fe^{II} , Co^{III} , Co^{II}). These derivatives in an octahedral symmetry can adopt two different electronic ground states according to the occupation of the d orbitals split into the e_g^* and t_{2g} subsets (Figure 1). When the energy difference/gap between these orbitals Δ_o is greater than pairing energy P ($\Delta_o > P$), the electrons tend to follow the Pauli Exclusion principle and to occupy the orbitals of lower energy t_{2g} in an anti-parallel fashion, and the configuration of the central metal ion is low spin (*LS*). In contrast, when the ligand field splitting energy is less than the pairing energy of the electrons ($\Delta_o < P$), this means that it becomes energetically more favourable for the paired electrons in the t_{2g} to overcome the energy barrier (Δ_o) and occupy the e_g^* level; as a result, electrons are distributed

following Hund's rule, and the metal complex adopts the high-spin state (*HS*). In-between these limits of *HS* and *LS*, a situation where the crystal field energy and pairing energy have similar values can occur; therefore, it can be seen there is a direct correlation between the two parameters of *P* and Δ_o , where for *SCO* to occur, the two must be of a similar magnitude (Figure 2).^{1f,15} In the case of Fe^{II} in a strong ligand field ($P < \Delta_o$), Fe^{II} is in its *LS* state (t_{2g}^6 , $S = 0$) while in a weak ligand field ($P > \Delta_o$), an Fe^{II} ion will reside in the *HS* state ($t_{2g}^4 e_g^{*2}$, $S = 2$, Figure 2).

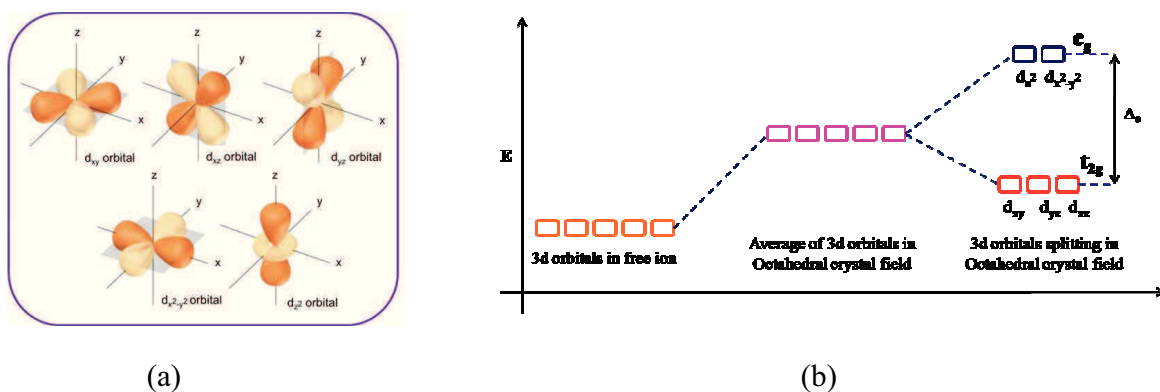


Figure 1. a) d-orbitals and their position in relations to bonding planes. b) Crystal field splitting representation of the degenerate d-orbitals of a free ion and in an octahedral field.

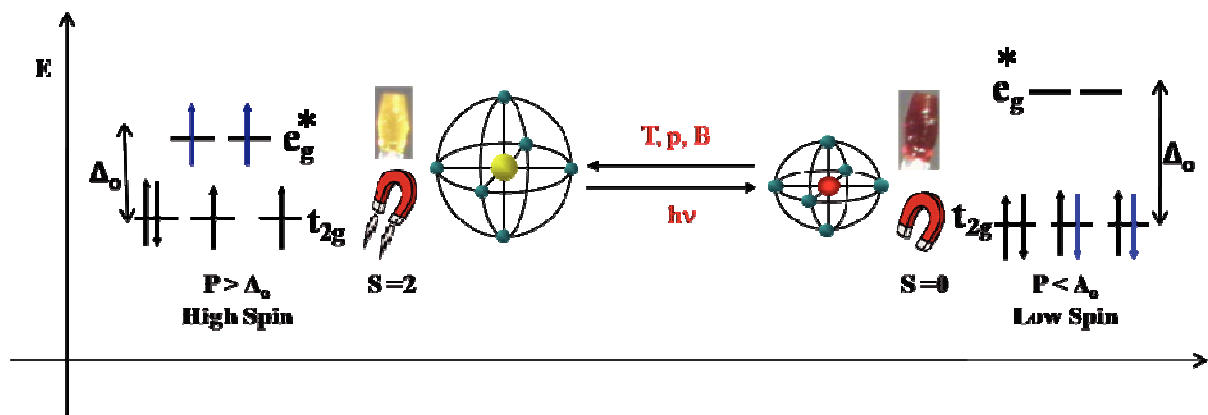


Figure 2. Schematic representation of the *SCO* phenomenon: splitting of the d-electrons in the e_g^* and t_{2g} levels in a strong ligand field and weak ligand field corresponding to the relative *P* and Δ_o parameters in a Fe^{II} d^6 .

Thus, spin transition occurs nearly exclusively with coordination complexes of 3d metal ions. Indeed, this is not expected for 4d and 5d transition element compounds on the basis of ligand field theory, because the strength of the ligand field increases notably (by ca. 50% from 3d to 4d and ca. 25% from 4d to 5d) relative to analogous 3d compounds, and is generally much greater than the spin pairing energy; hence, virtually all 4d and 5d transition metal complexes show *LS* behavior.¹⁶

2. Thermal Spin-Crossover (*SCO*): Cooperativity and Bistability

2.1. Characteristics

Despite *SCO* compounds of Fe^{II} centres not being discovered until around 1966, the most studied examples so far are those based on $\text{Fe}(\text{II})$ (d^6 configuration), for which a paramagnetic \leftrightarrow diamagnetic transition from the high spin (*HS*) state ($S = 2$, ${}^5T_{2g}$) to the low spin (*LS*) state ($S = 0$, ${}^1A_{1g}$) is observed with mainly temperature as external trigger, and so referred as a thermal spin crossover.¹⁷ More precisely, the most common spin crossover compounds are octahedral Fe^{II} complexes with an all-nitrogen donor environment (FeN_6 type), mainly constituted by nitrogen rich heterocyclic rings. Among the various ligand systems, the salicylaldimines have been attractive and popular ligands for the synthesis of transition metal complexes since they are easy to prepare and synthetically versatile.¹⁸ More recently, N_5O , N_4O_2 and P_4Cl_2 , P_4S_2 , and N_4S_2 coordinated systems have been also investigated, extending new classes of *SCO* derivatives.¹⁹ In order for thermally induced spin transitions to occur, the difference in the Gibbs free energies for the two spin states involved must be in the order of thermal energy, $k_B T$.¹ An increase in temperature favors the *HS* state, while the low temperature favors the *LS* state.

Besides the switching of the magnetic behaviour implicitly defined by the change of spin state, the *SCO* phenomenon is also strictly correlated to strong modifications in the structural and optical properties of the corresponding materials:^{17,20}

♦ Modifications of the structural properties related to *SCO*: Fe-L bond lengths and cell parameters

The mechanism for *SCO* can also be described from a thermodynamic perspective since there is a Fe-N bond length contraction accompanying *SCO* from *HS* to *LS*, with corresponding values of approximately 2.1 and 1.9 Å for Fe^{II} systems, respectively. The ligand field strength of a complex is correlated to the metal-ligand bond length and this is true for both the *HS* and *LS* state of the same complex; consequently, it is possible to define the mean difference in metal-ligand bond lengths between the *HS* and the *LS* state Δr_{HL} ($\Delta r_{HL} = r_{HS} - r_{LS}$, with r_{HS} and r_{LS} the metal-ligand bond length for the *HS* and the *LS* states, respectively, Figure 3). This means that in a configurational coordinate diagram (Figure 3), the minima of the *HS* and *LS* potential energy wells will be displaced (horizontally and vertically). So, it can be seen that for a *SCO* to occur, the zero point energy difference between the *HS* and *LS* states (given by $\Delta E^o_{HL} = E^o_{HS} - E^o_{LS}$) has to be within a thermally accessible range (Figure 3). When this situation is satisfied, all complexes will occupy the *LS* state at very low temperatures, while the entropy driven population of the *HS* state occurs at higher temperatures (the higher entropy associated with the *HS* state is derived from electronic contributions from spin degeneracy and a vibrational component). As such, the *LS* state is the quantum mechanical ground state, but at higher temperatures, the *HS* state becomes the thermodynamically stable state.¹⁵

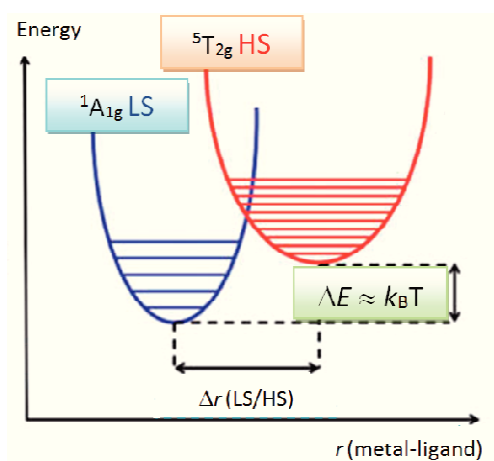


Figure 3. Potentials for the high-spin and the low-spin states along the most important reaction coordinate for spin crossover, namely the totally symmetric metal-ligand bond length denoted $r(\text{Fe-L})$.

In addition to the modifications of the Fe-L distances, the structural evolution resulting from the *SCO* can be also estimated *via* the determination of the distortion parameters Σ and Θ ; Σ is the sum of the deviation from 90° of the 12 cis-angles of the FeN_6 octahedron, while Θ is the sum of the deviation from 60° of the 24 trigonal angles of the projection of the FeN_6 octahedron onto its trigonal faces.²¹ Furthermore, the Fe-N bond length contraction and distortion parameters accompanying the *SCO* from *HS* to *LS* are also correlated to a significant variation of the cell parameters and the volume of the cell, while macroscopic repercussions on the mechanical properties of the crystal are ultimately observed. In addition, these structural modifications induce modifications of the vibrational properties of the metal complex eventually impacting the optical properties of the material upon the transition.

♦ Modifications of the optical properties related to *SCO*: Thermochromism

Thermally induced *SCO* is accompanied by a change in the magnetic moment and color (not always, but in many cases, with a distinction between liquid and solid state).²² This eventual change of color of *SCO* derivatives upon temperature is referred as thermochromism and is generally attributed to d-d electronic transitions and/or charge transfer transitions (Metal to ligand or ligand to metal charge transfer (MLCT/LMCT) depending on the configuration and nature of the coordination complexes). As examples, some 1,2,4-triazole based coordination complexes (e.g. $[\text{Fe}(\text{NH}_2\text{trz})_3]\text{Br}_2 \cdot \text{H}_2\text{O}$ (NH_2trz : 4-amino-1,2,4-triazole), solid state) exhibit a spectacular reversible purple-white thermochromic transition upon heating-cooling with a large hysteresis centered at room temperature. The thermochromic transition is related to the spin crossover (*SCO*) from the low-spin state (*LS*, purple, $S = 0$, diamagnetic) to the high-spin state (*HS*, white, $S = 2$, paramagnetic, Figure 4). Depending on the nature of the *SCO* derivatives, other colors can be involved such as red (*LS*) to yellow (*HS*) or yellow (*LS*) to green (*HS*) thermochromic transitions. As a result, this thermochromism defines a convenient preliminary characterization method to eventually detect a spin transition. It should be added that thermochromism accompanying *SCO* is of independent significance for practical applications (Figure 4). The synthesis and investigation of thermochromic compounds is an important area in materials chemistry²³ as these compounds could be used as thermochromic indicators and labels in engineering processes and in the security industry among others. The *SCO* in complexes is

also observed with changes in pressure, which allows their use as thermochromic pressure sensors.²⁴ In addition, *SCO* complexes demonstrate unusual photorefractive properties.^{24,25} Changes in spin state are also accompanied by changes in the dielectric constant^{25, 26} and electrical resistance.²⁷

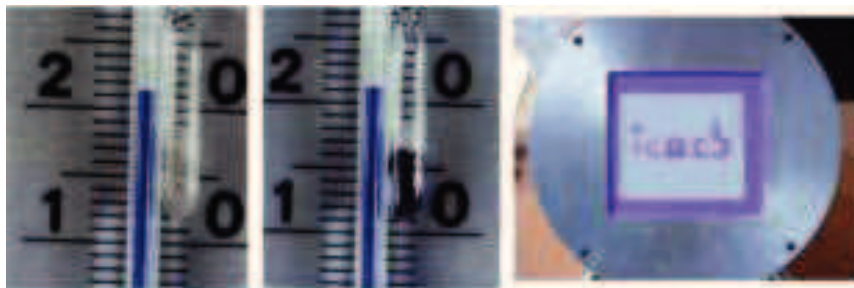


Figure 4. Left/middle: the thermochromic bistability of bulk $[\text{Fe}(\text{Htrz})_2(\text{trz})][\text{BF}_4]$ (Htrz: 1,2,4-triazole; trz: 1,2,4-triazolate anion). Right: one of the prototype displays based on $[\text{Fe}(\text{Htrz})_{3-3x}(\text{atrz})_{3x}][\text{ClO}_4]_2$ (atrz: 4-aminotriazole) pseudo-alloys developed at ICMCB, CNRS (France).¹⁴

2.2. Cooperativity and Types of Spin-Transitions

A typical spin-transition curve is generally represented as a plot of the *HS* fraction (χ_{HS}) vs. temperature (T) (Figure 5). While there are a number of *SCO* shapes/profiles that can be observed, the most important are those which display a degree of cooperativity associated with the spin-transition, where cooperativity defines the degree to which the effects of a spin-transition are conveyed throughout a crystal lattice. Thus, according to the strength of the elastic frustration correlated to the cooperativity, the system may undergo first-order transition with hysteresis, gradual, hysteretic two-step or multistep transitions, or incomplete transitions (Figure 5).^{3a,3b}

The most often encountered examples of transition curves are those which manifest in gradual transitions from *HS* to *LS* (Figure 5 (a)). The gradual transitions are indicative of a low degree of cooperativity between metal centres, while abrupt transitions (Figure 5 (b)) represent a strong cooperativity; that is a high degree of ‘communication’ of the spin-transition through the

crystal lattice, either *via* covalent linkers between metal centres or *via* intermolecular interactions (e.g. Hydrogen bonds).

Interestingly, when cooperativity is especially high, hysteresis may result. The result of hysteretic behaviour, associated with a spin-transition, and sometimes complemented by a crystallographic phase change, has come to be identified as the most important aspect of the *SCO* phenomenon. This is because hysteresis provides bistability (at both the *HS* and *LS* states) and thus a memory effect is realised, where bistability is the capacity of a system to exist in the *HS* or *LS* state between a certain ranges of an external perturbation. Using the example of temperature induced *SCO*, this means hysteresis occurs between the range of $T_{1/2}(\text{min})$ and $T_{1/2}(\text{max})$, where $T_{1/2}$ is the midpoint temperature defined as the point in which the fraction of *HS* centres exist in a 1:1 ratio with those of *LS* orientation. The $T_{1/2}(\text{max})$ is usually somewhat higher than $T_{1/2}$, and so whether the system is *HS* or *LS* between these two points indicates its history and as a result, a memory effect is observed (Figure 5 (c)). The hysteresis' mechanism can be explained by the quantum physics of phonons, which is beyond the scope of the present work; when focusing only on the chemical and physical attributes of *SCO* complexes which display hysteresis, two main origins can be proposed for the hysteresis: the first one implies a structural phase change in the lattice, caused by a *SCO* occurrence, which results in a hysteresis as each 'phase' then follows its own unique *SCO* path, and $T_{1/2}$ values for both phases are not the same; alternatively, the intramolecular structural changes that accompany the transition may be imparted to adjoining molecules by means of highly effective cooperative interactions between *SCO* centres, and then resulting in a hysteresis.

Another type of transition frequently encountered is the multi-step transition (e.g. two-step transition, Figure 5 (d)) where, as the sample is cooled, a reduction in the *HS*-fraction is interrupted by a plateau. With further cooling, the crossover proceeds again and the corresponding reduction in the *HS*-fraction is continued. This type of crossover has commonly been observed for systems involving two distinct metallic centers, where the mechanism for crossover bypasses an intermediate plateau (IP) that is usually associated with the *HS-LS* state.²⁸ Examples of two-step *SCO* will be described for 4-R-1,2,4-triazole based derivatives in chapter III and IV.

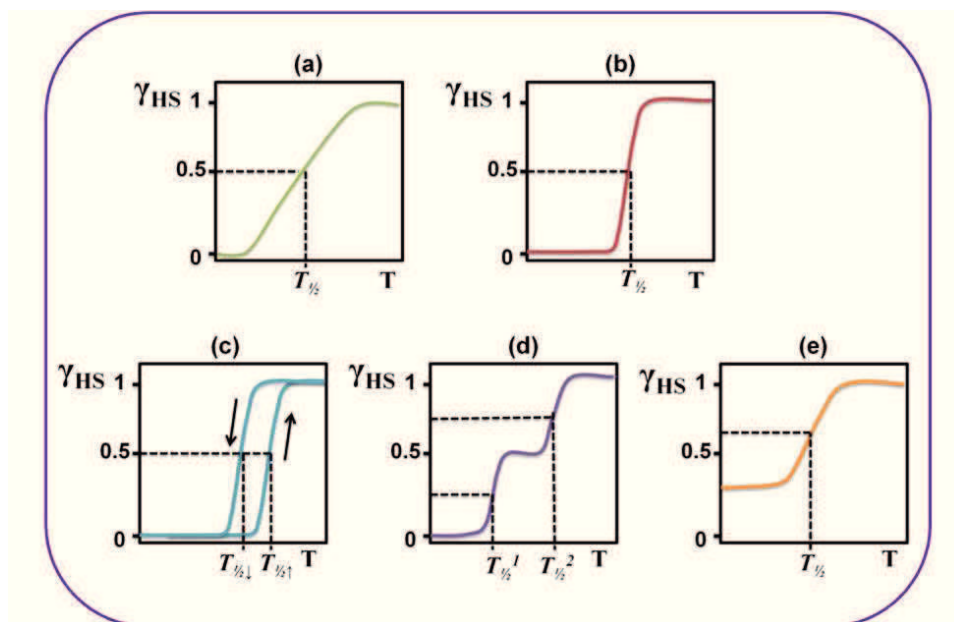


Figure 5. Main types of spin-transition curves: (a) gradual transition, (b) abrupt transition, (c) hysteresis, (d) two-step transition, (e) incomplete transition.

Finally, a spin-transition in which the entire crystal lattice fails to crossover is called an incomplete crossover (Figure 5 (e)). An incomplete crossover may occur as a result of a kinetic effect, where conversion from the *HS* to the *LS* state upon cooling happens at a very slow rate. As a consequence, a small portion of *HS* centres will contribute to the elevated susceptibility value at cryogenic temperatures. A further explanation for incomplete crossover can be a result of more than one unique Fe^{II} site existing within a given complex. Sometimes, as for example in the dinuclear complex $[\text{Fe}_2(\text{pmat})_2](\text{BF}_4)_4 \cdot \text{DMF}$ (pmat = 4-amino-3,5-bis{[(2-pyridylmethyl) amino]methyl}-4*H*-1,2,4-triazole), the *HS*-*HS* to *HS*-*LS* occurs at a $T_{1/2}$ of 224 K, but the system remains trapped in the *HS*-*LS* state, and further cooling fails to induce the transition to the *LS*-*LS* state.²⁹ As previously explained, the *SCO* property can manifest in a number of forms depending on the degree of cooperativity within the system. The parameters influencing the degree of cooperativity will be later introduced.

3. Light-Induced Excited Spin-State Trapping (LIESST) Effects: LIESST and Reverse LIESST

Besides the thermally induced spin-transition, the development of photomagnetic studies has provided deeper insight and further means into the exploration of the mechanism of *SCO*, with the possibility to control the *HS* and *LS* populations by irradiating with light of the appropriate wavelength. This photophysical phenomenon has been termed “*Light-Induced Excited Spin State Trapping*” (LIESST) effect and is associated to the irradiation into d-d or metal-ligand charge transfer (MLCT) bands of the *LS* species in the UV-VIS range below the thermal transition temperature that results in a quantitative population of the *HS* state with high quantum efficiency, generating by the same a photomagnetic bistability. The subsequent relaxation back to the *LS* ground state can then be followed by spectroscopic methods as a function of temperature up to the thermal transition temperature. This LIESST effect was first discovered in 1982 by McGarvey and Lawthers who reported that the equilibrium between the spin states of Fe^{II} spin-crossover complexes in solution at around room temperature can be photophysically perturbed *via* irradiation into the intense spin and parity allowed metal-ligand charge transfer (MLCT) absorption bands of the *LS* species.¹¹ This work was followed by the discovery of the LIESST effect in solid state by Decurtins *et al.*¹⁰ in 1984 on [Fe(ptz)₆](BF₄)₂ (ptz = 1-propyltetrazole) coordination compound which presents a phase change occurring at a spin transition temperature $T_{1/2}$ of ca. 135 K with hysteresis’ width of ca. 7 K.¹¹⁻¹² In a temperature-dependent study of the optical spectra of this compound, it was observed for the first time that a *LS* to *HS* conversion in a solid state *SCO* compound could be quantitatively ‘trapped’ in the so-called “metastable-*HS* state” following irradiation of the material - as a single-crystal, polycrystalline, or embedded in a polymer foil - with a green light ($\lambda = 514$ nm). Soon after this discovery (1986), Hauser reported the reverse process, using a near-infrared ($\lambda \sim 820$ nm) irradiation to convert the same [Fe(ptz)₆](BF₄)₂ compound from its metastable photo-induced *HS* state to the *LS* state.¹³ This so-called “reverse-LIESST” is another concept of photomagnetic behaviour and involves the conversion of the metastable-*HS* back to the *LS* state following irradiation of the *SCO* complex with a red laser. The findings of the LIESST and reverse LIESST effects have opened the possibility of using spin-crossover materials as optical data storage or processing devices, and also contributed to the growth of research in photomagnetism with early

pioneering work from Gülich,³⁰ and more recent work notably by Létard and co-workers.³¹ With the aim to generate a light-induced metastable state stable around room temperature, Bousseksou *et al.* have reported in 2005 a light-induced reversible spin transition in the *SCO* complex $[\text{Fe}(\text{C}_4\text{H}_4\text{N}_2)\{\text{Pt}(\text{CN})_4\}]$ at room temperature, using a nanosecond pulse laser.³²

The LIESST phenomenon can also be defined on the basis of the ligand field theory. The photophysical processes involved in the LIESST effect are depicted in the Jablonski diagram that illustrates the electronic states of a molecule and the transitions between them (Figure 6). Thus, the two potential wells for the *LS* and *HS* ground states are displaced due to the fact that the [metal ion - donor atom] distance in the *HS* state is longer compared to the shorter bond distance in the *LS* state (Figure 6). The green light (514 nm from an Argon ion laser) excites the *LS* state ($^1\text{A}_1$) by the spin-allowed but parity-forbidden transition to the $^1\text{T}_1$ and $^1\text{T}_2$ ligand field states ($^1\text{A}_1 \rightarrow ^1\text{T}_{1,2}$ absorption band), followed by two consecutive intersystem crossing processes (ISC) to the triplet spin states $^3\text{T}_{1,2}$, and finally to populate the *HS* state $^5\text{T}_2$ ($^1\text{T}_{1,2} \rightarrow ^3\text{T}_{1,2} \rightarrow ^5\text{T}_2$). Two factors are favorable for the occurrence of a LIESST: (i) The spin triplet states $^3\text{T}_{1,2}$ are placed energetically lower than the $^1\text{T}_1$ and $^1\text{T}_2$ ligand field states; (ii) The double ISC decay path is favored by spin-orbit coupling and therefore faster than the direct decay path back to $^1\text{A}_1$. The decay of the $^5\text{T}_2$ state to the $^1\text{A}_1$ state is highly spin and parity-forbidden, and due to the considerably larger M-L bond distance in the *HS* state as compared to the *LS* state, which builds up an energy barrier between the potential wells of the two states, the lifetime of the metastable LIESST state can be very long (e.g. on the order of days/weeks at temperatures below ca. 20 K in the case of $[\text{Fe}(\text{ptz})_6](\text{BF}_4)_2$)¹⁰; the long-lived metastable *HS* state is trapped until radiationless thermal relaxation (heat is transferred to lattice vibrations) sets in by non-adiabatic multiphonon processes.^{1c,33} Because an energy barrier exists between *HS* and *LS* states (due to metal-ligand bond lengths Δr_{HL} and zero point energy difference ΔE_{HL}) following irradiation, at low enough temperatures there is not enough energy to overcome this barrier and the sample stays trapped in the *HS* state. However, relaxation from the metastable-*HS* state to the *LS* state increases in rate as the temperature increases.

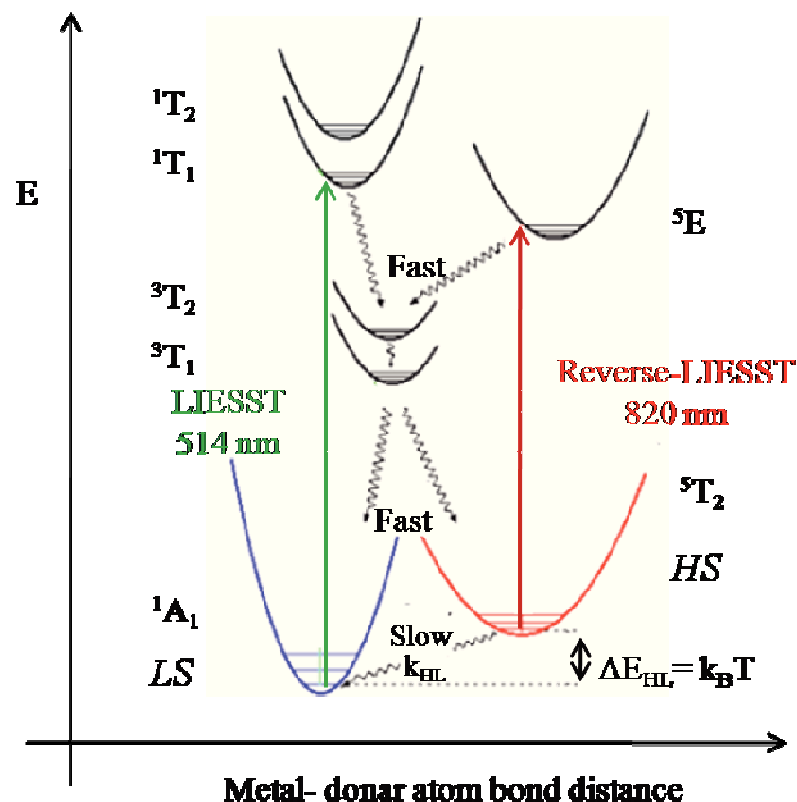


Figure 6. A Jablonski diagram for a Fe^{II} compound showing the photophysical processes of the LIESST and reverse-LIESST effects, after irradiations (laser excitations at specific wavelengths). The states are arranged vertically by energy and grouped horizontally by spin multiplicity. Non radiative (relaxation) transitions are indicated by squiggly arrows, and radiative transitions by straight arrows. The vibrational ground states of each electronic state are indicated with thick lines, and the higher vibrational states with thinner lines.

At elevated temperatures, the $HS \rightarrow LS$ relaxation is thermally activated as expected for the large horizontal and the small vertical relative displacements of the potential wells of the two states and the ensuing energy barrier between them (Figure 6). However, at low temperatures, deviations from the classical behavior towards a temperature independent rate constant indicate quantum mechanical tunneling in the shape of a non-adiabatic multi-phonon process. Moreover, it has also been shown that the reverse-LIESST phenomenon can also be performed by optical excitation into spin allowed d-d band with a relatively low quantum efficiency which eventually allows to probe the $LS \rightarrow HS$ relaxation dynamics as a function of different external perturbations

such as temperature, pressure or modulation of laser field probe. Referring to the reverse, the tunneling mechanism for this transition from the $^5T_{2g}$ to the 1A_1 state is also shown in Figure 6.

In attempts to better understand the mechanism of LIESST, and in doing so potentially decrease the rate (or increase the temperature) of relaxation from metastable *HS* to *LS*, Lènard *et al.*³⁴ have created a database of LIESST information on a large number of *SCO* Fe^{II} compounds in order to identify trends within series of complexes. As such, the parameter $T(\text{LIESST})$, which consists of systematically measuring the limit temperature above which a photomagnetic effect in a material is erased by warming the material from 10 K at a rate of 0.3 K min^{-1} , has been created as a method of drawing comparisons between the LIESST behaviour of compounds (see also paragraph 6.2.3 for experimental details). The $T(\text{LIESST})$ provides the temperature at which the metastable-*HS* state overcomes the energetic barrier between *LS* and *HS* and then begins to relax to the thermodynamically more stable *LS* state (Figure 7).

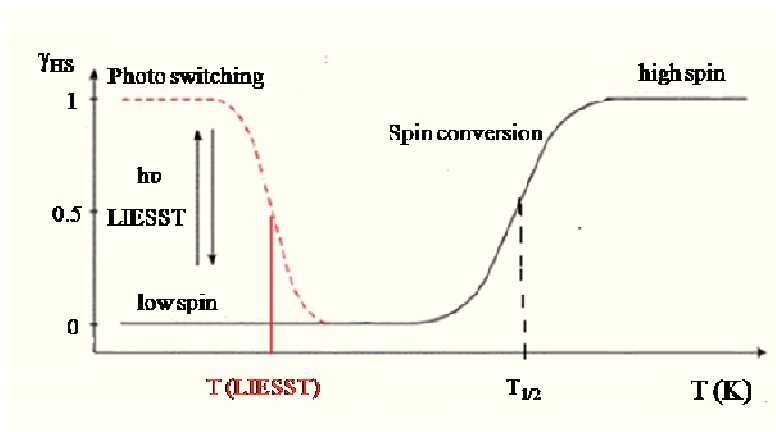


Figure 7. Schematic representation of the $T(\text{LIESST})$ effect.

The value of the $T(\text{LIESST})$ can be defined as the minimum point of the $\delta\chi_M T / \delta T$ vs. T curve. The equation for determining $T(\text{LIESST})$ is given below:

$$T(\text{LIESST}) = T_0 - 0.3 T_{1/2} \quad (1)$$

Linear correlations between $T(\text{LIESST})$ and $T_{1/2}$ have been found with different T_0 values attributed to differently coordinated Fe^{II} geometries, more specifically involving ligands with

different denticity (e.g. monodentate ($T_0 = 100$ K), bidentate ($T_0 = 120$ K) or tetra-dentate ($T_0 = 180$ K) macrocyclic ligands). As a result, for a defined T_0 line, the $T(\text{LIESST})$ decreases when $T_{1/2}$ increases, and reciprocally. Moreover, the increase of $T(\text{LIESST})$ is correlated to the stability of the light-induced state, and also to the photo-induced bistability in time. The figure 8 shows the highest $T(\text{LIESST})$ values for compounds displaying different coordination environments from the library of known LIESST active samples located along a particular T_0 line. While this approach has been established for many *SCO* derivatives, interestingly there have been also reported examples which do not follow the trend of $T(\text{LIESST})$ in relation to their denticity; a previous justification for this inconsistency has indicated that a given compound's $T(\text{LIESST})$ value may be affected by the flexibility of the ligands, in addition to the coordination environment.

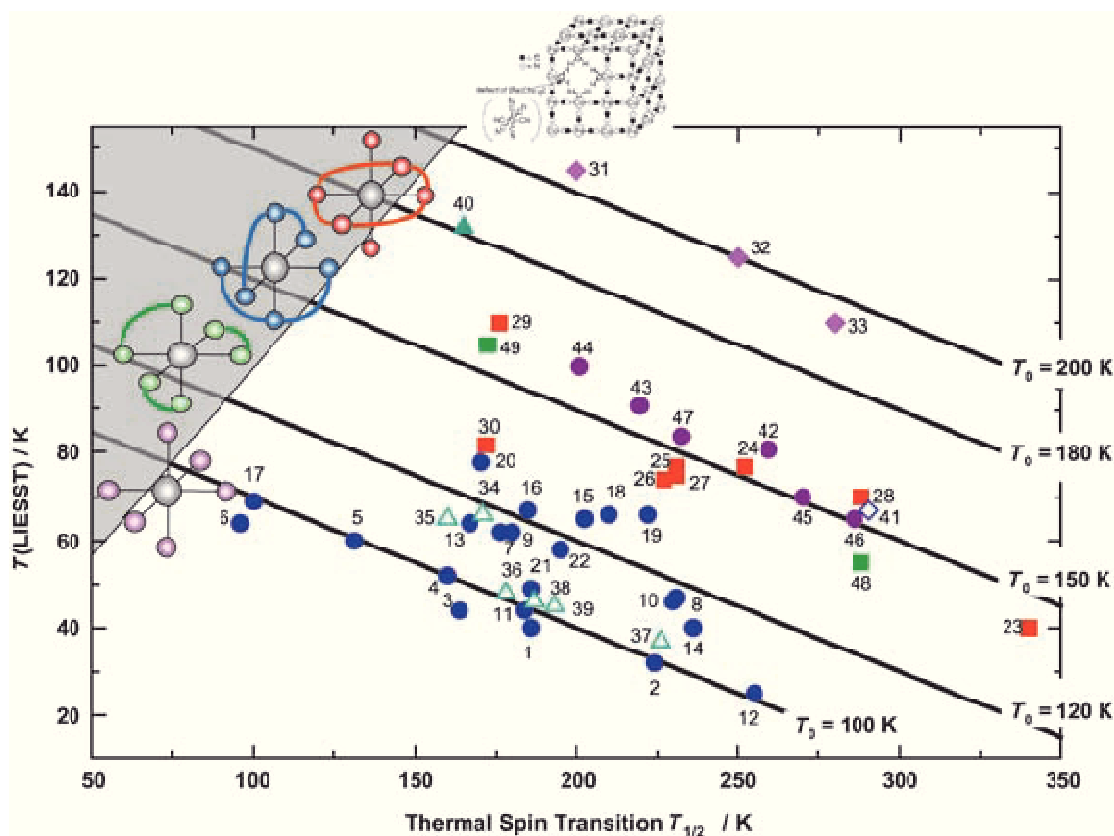


Figure 8. Plot of $T(\text{LIESST})$ vs. $T_{1/2}$ for a large number of LIESST-active *SCO* compounds, showing T_0 lines and the denticity of the ligands comprising the first coordination sphere of the LIESST-active *SCO* compounds associated with a particular T_0 line. The grey area is meaningless as $T(\text{LIESST})$ must be less than or equal to $T_{1/2}$.³⁴

4. Rational Tailoring of the *SCO* Behavior: Combinational Influences of Chemical and Structural Factors

As mentioned earlier, there are a number of factors/parameters with significant influences within the solid state of the lattice of a compound that govern a compound's ability to show *SCO*, and the ensuing properties. Although thoroughly interrelated, those factors can be subjectively distinguished in two categories:

(i) The “*chemical factors*” which relate to the nature and the intrinsic characteristics and properties of the building blocks constituting a *SCO* material, i.e. the metal ion (and eventual metal dilution), ligand(s) and co-ligand(s), anion(s) as ligands or counter-ion, and solvent(s). Another key parameter that can be defined as a “*chemical factor*” is the crystal engineering, more precisely the chemical conditions (stoichiometry, concentration, nature/mixture of the solvents, and crystallization techniques). The latter is of paramount importance in the rationalization of the tuning of *SCO* materials, as it will pave the way for possible refined structure/properties studies hardly conceivable without the access of single crystals suitable for X-ray diffraction. All these “*chemicals factors*” will implicitly condition the “*structural factors*”.

(ii) The “*structural factors*” recount the characteristics of the lattice arrangements of a *SCO* material, and can be defined as consequences and implications of the “*chemical factors*”. The latter include notably the dimensionality of the material, the specifics of the intra- and inter-molecular interactions, and also the impact of polymorphism and lattice defects. The “*structural factors*” will be the foundation to streamline a *SCO* behavior.

In fine, the rational tailoring of a *SCO* behavior implies the common approach that consists in varying only one chemical factor within a compound (e.g. ligand modification or anion substitution, or change of the crystallization conditions), and then comparing the overall impact on the structural factors and the *SCO* properties.³⁵⁻³⁷ This systematic evaluation of the combinational influences of the chemical and structural factors in *SCO* materials can be undergone with the purpose to investigate and better understand *SCO* systems, but also to optimize the properties accordingly to targeted applications; the latter comprises to either maximise the cooperativity with hysteretic behavior and $T_{1/2}$ close to room temperature, or to

enhance the factors favoring the LIESST (and reverse-LIESST) effect(s) such as the flexibility and the denticity of the ligand.

Similar to the challenge for Prussian Blue derivatives, the change of the chemical factors can also be investigated to way in single-crystallinity hardly accessible in some *SCO* systems; as an example, the 1D 1,2,4-triazole based derivatives have been studied for more than three decades because of their highly applied potential with room temperature properties display, but access to fully refined structure remains challenging task to date,³⁸ making rather difficult to undoubtedly establish rational understanding of the properties. As will be detailed in the upcoming chapters, the present work is positioned to start filling the knowledge gap in that matter.

4.1. Chemical factors: Composition of the *SCO* material

4.1.1. Nature of the ligand: Ligand substitution and/or functionalization

Beside the nature of the first row transition metal ions of d^4 - d^7 electronic configurations (Cr^{II} , Mn^{II} , Mn^{III} , Fe^{II} , Fe^{III} , Co^{II} , Co^{III}), with Fe^{II} the most prominent aspirant because of its “flexibility” related to the *SCO* requisites (e.g. coordination geometries), the nature of the ligand(s) involved in the coordination sphere will mainly dictate the eventuality of a *SCO* behavior, and so will be a key factor - although not the only one - in defining the *SCO* characteristics (e.g. $T_{1/2}$, cooperativity, thermal and light-induced specifics), and implicitly the structural ones (see paragraph 4.2), of the resulting material. More specifically, the sub-criteria to be considered about the ligand are multiple:

- The nature and number of the coordinating/donor atoms of the ligand, with a major impact on the ligand field strength of the complex.
- The constraints and distortions factors - imposed by the geometry and/or the bulkiness of the ligand in the coordination sphere - that will eventually favor the *SCO* phenomenon.
- The integration of selected free functional group(s), and/or the integration of π -electronic structure to the ligand, with a direct influence on the cooperativity through the eventuality

of intermolecular interactions involving weak bondings (e.g. H-bondings, π - π interactions, see paragraph 4.2).

- The denticity and the flexibility of the ligand, that could have notable effects on the $T(\text{LIESST})$.

It is noteworthy to specify that the aforementioned sub-criteria defining the ligand should mainly be considered jointly. Indeed, they are all interconnected and can hardly be assessed independently in a systematic way. Nevertheless, the influence of the ligand can be evaluated in some systems through either (i) ligand substitution or (ii) ligand functionalization, with the purpose to define some trends in the optimization of the *SCO* properties:

(i) *Ligand Substitution*: the judicious substitution of one ligand by another distinct analogue can generate, or alter the spin-crossover characteristics, and help to define the impact of subtle changes in the structure of the ligand on the *SCO* behavior. Empirically, for mixed complexes $[\text{FeL}_n\text{L}^1_{6-n}]$ (including two different ligands L and L^1), the rule of “averaged environment”, which states that $10Dq$ values of the complexes can be found approximately through linear interpolation between $10Dq$ values for $[\text{FeL}_6]$ and $[\text{FeL}^1_6]$, holds:³⁹

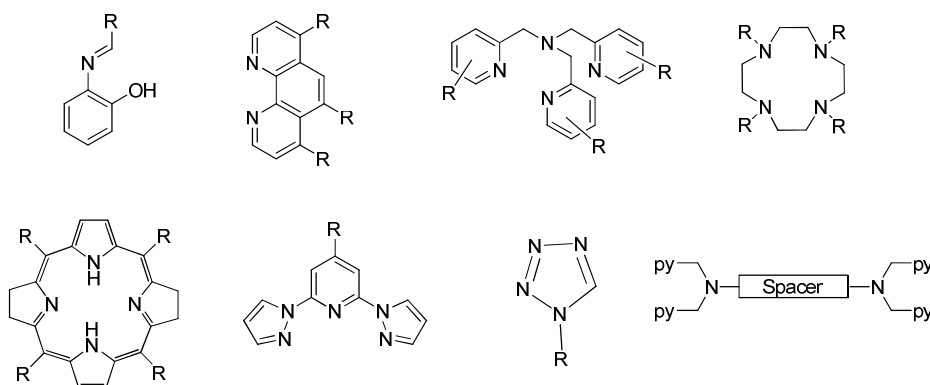
$$10Dq([\text{FeL}_n\text{L}^1_{6-n}]) \approx n/6 \, 10Dq([\text{FeL}_6]) + (6-n)/6 \, 10Dq([\text{FeL}^1_6]) \quad (2)$$

For instance, the system $[\text{Fe}(\text{py})_4(\text{NCS})_2]$ is high-spin at room temperature and does not undergo a thermal spin-transition. The substitution of two of the pyridine (py) molecules by a strong field 1,10-phenanthroline (phen) molecule gives $[\text{Fe}(\text{phen})(\text{py})_2(\text{NCS})_2]$ which does undergo a thermal transition,⁴⁰ as does the species in which the remaining two pyridines are substituted $[\text{Fe}(\text{phen})_2(\text{NCS})_2]$.⁴¹ As would be expected, $T_{1/2}$ for the former complex (106 K) is lower than that for the latter (176 K). The replacement of the two thiocyanato groups by a phenanthroline produces the totally low-spin complex cation $[\text{Fe}(\text{phen})_3]^{2+}$; their replacement by the strong field cyanide ion or the weak field chloride ion (acting as covalent ligands) produces purely low-spin $[\text{Fe}(\text{phen})_2(\text{CN})_2]$ or purely high-spin $[\text{Fe}(\text{phen})_2\text{Cl}_2]$ derivatives, respectively.^{41b}

(ii) *Functionalization of the ligand*: a similar and even more refined approach consists in finely modifying the ligand entity (and potentially affecting the ligand field strength) with various functionalizations of the ligand. This concept has been notably illustrated in 1974 by

Gütlich *et al.* with the series of $[\text{Fe}(\text{Y-phen})_3]\text{X}_2$ complexes.⁴² The exchange of -H by -CH₃ substituent, in either the 2nd or 9th position of the three phen ligands, weakens the ligand field strength due to steric hindrance (whereby the metal-donor atom distance is elongated) and the *LS* behavior of $[\text{Fe}(\text{phen})_3]\text{X}_2$ turns to a *SCO* behavior for the tris(2-CH₃-phen) analogue complex. If both the 2nd or 9th positions of the three phen ligands are substituted by -CH₃, the steric hindrance becomes even stronger and weakens the ligand field strength further, resulting in the *HS* behavior of the tris[2,9-(CH₃)₂] analogue complex down to very low temperatures. For the corresponding systems, it was found that a combination of steric hindrance (due to bulkiness), and an electronic influence of the substituent on the basicity of the coordinating N-atom, are responsible for the influence on the *SCO* behavior. The paramagnetic property of the complex series (given by the molar fraction of *HS* molecules, γ_{HS} , at a given temperature) increases in the following order $\text{Y} = \text{H} < \text{CH}_3\text{O} < \text{CH}_3 < \text{Cl}$. Moreover, the work revealed that a change of the substituents at positions not adjacent to the coordinating N-atom in the phen ligand does not influence the spin state in comparison to the unsubstituted $[\text{Fe}(\text{phen})_3]\text{X}_2$ complex.

Thus, for the last eight decades, a wide variety of ligands - with different coordination modes or denticity (mono-, bi-, tri- and tetradentate modes) - have been incorporated into *SCO* materials. Depending on the nature of the metal ion, a number of donor atoms have also been found to provide an appropriate ligand field for *SCO* to occur and these include S-donors (for Fe^{III}), O-donors (for Fe^{III}, Co^{II}, and Fe^{II}), and the more common N-donors (for Fe^{III}, Fe^{II}, and Co^{II}).⁴³ But, in the case of Fe^{II}, the N-donors are commonly from pyridyl, azole (triazole) and related groups as shown in scheme 1, often in combination with NCX (X= S, Se) unidentate ligands.



Scheme 1. Examples of ligands reported for *SCO* complexes.

4.1.2. Nature of the anions

In many *SCO* systems, the nature of the anion can drastically affect the *SCO* characteristics, noticeably with significant shifts of $T_{1/2}$ or even the disappearance of the *SCO* phenomenon. The main sub-criteria that have to be taken into account when assessing the influence of the anion(s) are:

- The geometry of the anion, which includes the symmetry, but also the bulkiness (size, volume).
- The charge of the anion, with the monoanions usually the standard sought-after candidates in most studies, but also the possibility to incorporate more complex dianions or polyanionic entities.
- The involvement of the anion in the lattice, i.e. the ability of the anion to form covalent linkage or ionic bondings to the neighboring units (e.g. metal complex) in the structural arrangement of a *SCO* material.

In the case of a *SCO* compound where the anion is directly coordinated to the metal center, the modification of the structure of the anion (e.g. functionalization with different substituents) can imply the variation of the ligand field strength and the *SCO* characteristics. This has been illustrated by Triki *et al.* in 2008 with the series of $[\text{Fe}(\text{abpt})_2(\text{A})_2]$ (abpt = 4-amino-3,5-bis(pyridin-2-yl)-1,2,4-triazole, A = terminal monoanion N ligand with A = $\text{tcm}^- = [\text{C}(\text{CN})_3]^-$ = tricyanomethanide anion; $\text{tcnome}^- = [(\text{NC})_2\text{CC}(\text{OCH}_3)\text{C}(\text{CN})_2]^-$ = 1,1,3,3-tetracyano-2-methoxypropenide anion; $\text{tcnoet}^- = [(\text{NC})_2\text{CC}(\text{OC}_2\text{H}_5)\text{C}(\text{CN})_2]^-$ = 1,1,3,3-tetracyano-2-ethoxypropenide anion) complexes involving atypical polynitrile anions (Figure 9).^{21a} Thus, the substitution of tcnome^- by tcnoet^- anion in the complex series, i.e. the replacement of $-\text{CH}_3$ by $-\text{CH}_2\text{CH}_3$ functional group, is resulting in the appearance of a *SCO* behavior for the tcnoet derivative, while the tcnome analogue remains in the *HS* state in the whole temperature range (Figure 9).

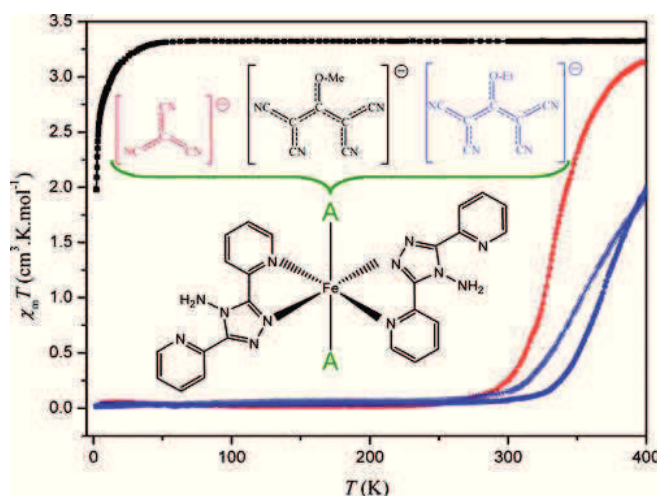


Figure 9. Illustration of the influence of the covalent anion in neutral $[\text{Fe}(\text{abpt})_2\text{A}_2]$ complexes (A = Terminal Monoanion N Ligand) on the *SCO* properties.^{21a}

In ionic lattices (with cationic *SCO* complex units and non-coordinated anions), the anion can nevertheless exercise a strong influence on the *SCO* behavior through cooperative interactions. As examples can be cited the series $[\text{Fe}(\text{2-pic})_3]\text{A}_2 \cdot \text{Solv.}$ (2-pic = 2-(aminomethyl)pyridine; A = Cl^- , Br^- , I^- , or organosulfonate anions; Solv.: EtOH or MeOH), for which the *SCO* characteristics depend strongly on the nature of the anion (Figure 10).⁴⁴

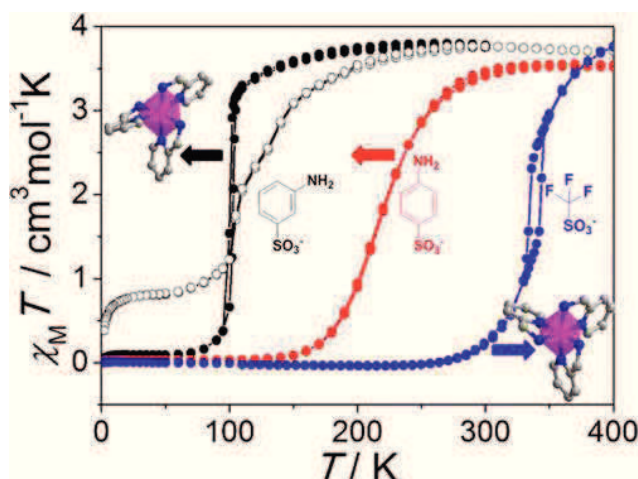
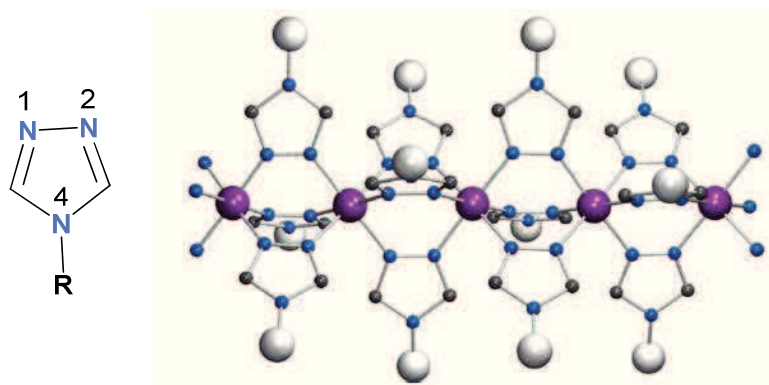


Figure 10. Illustration of the influence of the anion on the *SCO* behavior in the series $[\text{Fe}(\text{2-pic})_3]\text{A}_2 \cdot \text{MeOH}$ (2-pic = 2-(aminomethyl)pyridine; A = various organosulfonate anions).⁴⁴

The last two illustrations, associated to the strong sway induced by polynitrile and organosulfate anions on SCO properties, draw awareness to the rather unexplored aftermath in the use of uncommon anions, in comparison with the usual and more popular monoanions such as halides, BF_4^- or ClO_4^- . This facet has been decidedly addressed in the present work with the use of atypical anions.

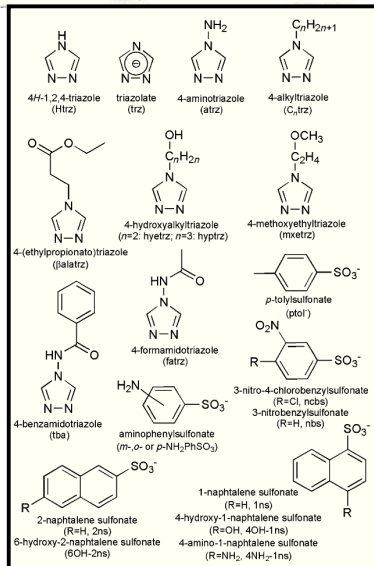
For some systems, it can be rather difficult or biased to isolate and discuss independently the influence of the ligand and the one of the anion, as both parameters can display strong influence. Thus, tables summarizing both influences can be more apt to comprehend specific systems, such as the $[\text{Fe}(4\text{-R-1,2,4-trz})_3][\text{A}]_x$ series of compounds based on the 1,2,4-triazole ligand that will define the core of the present work, and will be further discussed (Scheme 2, Table 1).^{14,22a} Indeed, the “magnetism” (so to say) of the $[\text{Fe}(4\text{-R-1,2,4-trz})_3][\text{A}]_x$ derivatives resides in the access to many synthetic variations, while maintaining a very similar chemical environment for the Fe^{II} as well as the interactions within the coordination chains. Because of the high sensitivity of the T_{SCO} to small variations in the ligand-field strength around the Fe^{II} ion, slight modifications of the R substituent or the anion is then sufficient to tune the T_{SCO} , while possibly affecting the characteristics of the transitions (e.g. abruptness). Whilst maintaining the same R substituent, the T_{SCO} is usually found to increase with the bulkiness of the anion. This is particularly well established with spherical anions, for which a near-linear relationship of T_{SCO} with the anion volume was found for both the atrz and hyetrz triazole ligands (Figure 11, Table 1). Fairly grippingly, it is possible to form $[\text{Fe}(4\text{-R-1,2,4-trz})_3][\text{A}]_x$ compounds with assortments of R or A. The mixed compounds then have intermediate T_{SCO} , allowing a fine-tuning. This was demonstrated with the $[\text{Fe}(\text{Htrz})_{3-3x}(\text{atrz})_{3x}][\text{ClO}_4]_2 \cdot \text{H}_2\text{O}$ series. The R substituent also results in variations in T_{SCO} , although in a less predictable manner (Table 1).



Scheme 2. Schematic representations of a 4-substituted triazole (left) and of the model/reference 1D coordination chains formed through propagation of triple N1,N2-triazole bridges connecting Fe^{II} centers (right). The substituent is depicted as large light grey spheres. Colour code: Fe, purple; N, blue; C, dark grey.¹⁴

Table 1. Summary tables of (a) $[\text{Fe}(\text{4-R-1,2,4-trz})_3][\text{A}]_x$ systems reported in the literature, with the influences of the nature of the R substituent and the counter-anion on the T_{SCO} ,¹⁴ and (b) trends in $T_c \uparrow$ ($T_c = T_{\text{SCO}}$) for complexes of FeL_3A_n ($L = n = 1, 2$) and $[\text{Fe}_3\text{L}_6(\text{H}_2\text{O})_6]\text{A}_6$ with different anions (ns: naphthalene sulphonate anion, tos: tosylate anion).^{22a}

(a)			(b)		
Triazole ^[a]	Anion ^[b]	T_{SCO} ^[b]	Triazole ^[a]	Anion ^[b]	T_{SCO} ^[b]
(Htrz) ₃ trz A	BF_4^-	345/385	C _n trz	ClO_4^-	165–240
(Htrz) ₂ trz B	BF_4^-	323/343		BF_4^-	180–255
Htrz	BF_4^-	323/345		Cl^-	290–361
	ClO_4^-	341/358		NO_3^- ($n = 18$)	270
	PF_6^-	269/279		CF_3SO_3^-	195–240
atrz	$\text{B}_{10}\text{H}_{10}^-$	233/246	β -alatr	ptol^-	285–335
	ClO_4^-	247/249		CF_3SO_3^-	228/232
	BF_4^-	250/260		ClO_4^-	245/255
	PF_6^-	180		BF_4^-	215/225
	$\text{Cl}^-/\text{Br}^-/\text{I}^-$	270–316		PF_6^-	195/205
	NO_3^-	310/347		$\text{Cl}^-/\text{Br}^-/\text{I}^-$	285–314
	ptol^-	279/296	hyetrz	NO_3^-	298/315
	CH_3SO_3^-	273/288		nbs	100/110
	$\text{NH}_2\text{PhSO}_3^-$ (<i>o</i> -, <i>m</i> -, <i>p</i> -)	250–320		nbs	120/168
	1ns	229/235		BF_4^-	240/244
	2ns	283/297		ClO_4^-	247/251
	4OH-1ns	230/240		NO_3^-	276/284
	4NH ₂ -1s	225/235	mxetrz	CF_3SO_3^-	224/230
	6OH-2ns	265/270		ptol^-	270/282
	Spyropan	260–340		BF_4^-	283
	ReO_4^-	225		CF_3SO_3^-	274/276
	$\text{B}_{10}\text{H}_{10}^-$	N/A		NO_3^-	297/307
	SiF_6^{2-}	241/255	fatrz	ptol^-	263/268
	MF_6^{2-} (Ti, Zr, Sn, Ge)	179–230		BF_4^-	250/258
	TaF_7^{2-}	217		CF_3SO_3^-	284/309
			tba	ptol^-	226/238
			Ligand	R	Abbreviation
			1,2,4-Triazole	H–	Htrz
			1,2,4-Triazolate ion	–	trz
			4-Amino-1,2,4-triazole	NH_2 –	NH_2trz
			4-Formylamino-1,2,4-triazole	OHCNH –	fatrz
			4-Methyl-1,2,4-triazole	CH_3 –	mtrz
			4-Ethyl-1,2,4-triazole	C_2H_5 –	etrz
			4-(2'-Hydroxyethyl)-1,2,4-triazole	$\text{HO}(\text{CH}_2)_2$ –	hettrz
			4-Propyl-1,2,4-triazole	$\text{CH}_3(\text{CH}_2)_2$ –	ptrz
			4-(3'-Hydroxypropyl)-1,2,4-triazole	$\text{HO}(\text{CH}_2)_3$ –	hptrz
			4-Isopropyl-1,2,4-triazole	$(\text{CH}_3)_2\text{CH}$ –	iptrz
			4-Butyl-1,2,4-triazole	$\text{CH}_3(\text{CH}_2)_3$ –	butrz
			4-Amyl-1,2,4-triazole	$\text{CH}_3(\text{CH}_2)_4$ –	amtrz
			4-Hexyl-1,2,4-triazole	$\text{CH}_3(\text{CH}_2)_5$ –	hektz
			4-Heptyl-1,2,4-triazole	$\text{CH}_3(\text{CH}_2)_6$ –	heptrz
			4-Octyl-1,2,4-triazole	$\text{CH}_3(\text{CH}_2)_7$ –	otrz
			4-Octadecyl-1,2,4-triazole	$\text{CH}_3(\text{CH}_2)_{17}$ –	odtrz
			4-(<i>m</i> -Methylphenyl)-1,2,4-triazole	$3\text{-CH}_3(\text{C}_6\text{H}_4)$ –	mmphtrz
			4-(<i>p</i> -Methylphenyl)-1,2,4-triazole	$4\text{-CH}_3(\text{C}_6\text{H}_4)$ –	pmphtrz
			4-(<i>m</i> -Methoxyphenyl)-1,2,4-triazole	$3\text{-CH}_3\text{O}(\text{C}_6\text{H}_4)$ –	mophtrz
			4-(2-Pyridyl)-1,2,4-triazole	$2\text{-C}_5\text{H}_4\text{N}$ –	pytrz
			4-(4'-Nitrophenyl)-1,2,4-triazole	$4\text{-NO}_2(\text{C}_6\text{H}_4)$ –	nphtrz
			$T_c \uparrow$ [K] for different anions		
			$[\text{Fe}(\text{Htrz})_3]\text{A}_n$		
			$\text{B}_{10}\text{H}_{10}^{2-}$ (246) < $\text{B}_{12}\text{H}_{12}^{2-}$ (263) < ClO_4^- (266) < Cl^- (337) < ReO_4^- (342) < NO_3^- (355) < SiF_6^{2-} (=380 with decomposition) < BF_4^- (397)		
			$[\text{Fe}(\text{NH}_2\text{trz})_3]\text{A}_n$		
			NCS^- (190) < ClO_4^- (210) < ZrF_6^{2-} (216) < ReO_4^- (228) < 1-ns (235) = 4-amino-1-ns (235) < 4-hydroxy-1-ns (240) < SiF_6^{2-} (254) < 6-hydroxy-2-ns (270) < I^- (280) < Tos (296) < 2-ns (297) < CH_3SO_3^- (299) < Br^- (312) < BF_4^- (335) < NO_3^- (342) < Cl^- (355) = SO_4^{2-} (355)		
			$[\text{Fe}(\text{etrz})_3]\text{A}_2$		
			ClO_4^- (155) < NO_3^- (232) < Br^- (275)		
			$[\text{Fe}(\text{ptrz})_3]\text{A}_2$		
			CF_3SO_3^- (140) < ClO_4^- (149) < ReO_4^- (250) < Br^- (290)		
			$[\text{Fe}(\text{hetrz})_3]\text{A}_2$		
			3-Nitrophenylsulfonate (115) < PF_6^- (205) < BF_4^- (225) < ClO_4^- (255) < I^- (297) < Br^- (312) < Cl^- (314) < NO_3^- (315)		
			$[\text{Fe}(\text{heptrz})_3]\text{A}_2$		
			ClO_4^- (180) < CF_3SO_3^- (208) < BF_4^- (221) < Tos (337)		
			$[\text{Fe}(\text{odtrz})_3]\text{A}_2$		
			ClO_4^- (210) < CF_3SO_3^- (250) < SiF_6^{2-} (310) < Tos (318)		
			$[\text{Fe}_3(\text{iptrtz})_6(\text{H}_2\text{O})_6]\text{A}_6$		
			ClO_4^- (164) < CF_3SO_3^- (187) < BF_4^- (194) < I^- (195) < Tos (242) < Br^- (355)		



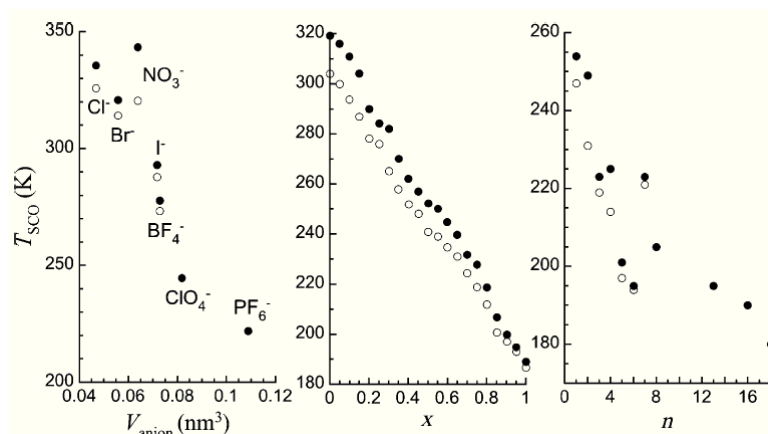


Figure 11. Left: Close to linear variation of T_{SCO} for the series $[\text{Fe}(\text{atzr})_3][\text{A}]_2$ as a function of the volume of spherical anions A. The case of $\text{A}=\text{NO}_3^-$ is included to show its peculiarity. Middle: Variation of T_{SCO} for the pseudo-alloys $[\text{Fe}(\text{Htrz})_{3-3x}(\text{atzr})_{3x}][\text{ClO}_4]_2$ as a function of the pseudo-alloy composition x . Right: Variation of T_{SCO} for the series $[\text{Fe}(\text{C}_n\text{trz})_3][\text{BF}_4]_2$ as function of the alkyl length n . Empty/full symbols represent the T_{SCO} upon cooling/warming.^{22a}

4.1.3. Nature of solvent molecules

In addition to the ligand and the anion, the variation in nature and/or numbers of the solvate molecules of the materials, as well as the total absence of solvent molecules (e.g. dehydration process), can dramatically influence the *SCO* properties. When evaluating the affect of the solvent, its implication in the lattice has also to be ascertained with distinction between coordinated and uncoordinated solvent molecules. As an illustration, the $[\text{Fe}(\text{2-pic})_3]\text{Cl}_2 \cdot \text{Solv.}$ with $\text{Solv.} = \text{EtOH}, \text{MeOH}, n\text{H}_2\text{O}$ ($n = 1$ or 2) were studied by Gütlich *et al.* with Mössbauer spectroscopy to explore the influence of the non-coordinated solvent molecules on the *SCO* behavior.⁴⁵ The ethanol shows a rather steep transition near 115 K; the methanol shows a more gradual spin-transition near 150 K; the monohydrate exhibits a very broad hysteresis loop with transition temperatures $T_{1/2\downarrow} \simeq 200$ K and $T_{1/2\uparrow} \simeq 290$ K; and the dehydrated sample exhibits no *SCO* at all, but remains in the *LS* state. Likewise, in the 1,2,4-triazole derivatives, the *SCO* characteristics of $[\text{Fe}(\text{ettrz})_3](\text{NO}_3)_2 \cdot \text{H}_2\text{O}$ and $[\text{Fe}(\text{ettrz})_3](\text{Br})_2 \cdot 2\text{H}_2\text{O}$ (ettrz = 4-ethyl-1,2,4-triazole) change upon dehydration, with a slight change in the first case in both the character of

the transition and the transition temperature (with a 2 K increase in $T_{1/2}\uparrow$), while the transition turns gradual with a decrease in $T_c\uparrow$ of 52 K for the bromide complex (Figure 12).⁴⁶ Moreover, for the $[\text{Fe}(\text{NH}_2\text{trz})_3]\text{Br}_2 \cdot n\text{H}_2\text{O}$ ($n = 0, 1.5, 3, 10$) complexes, the *SCO* temperature decreases with decreasing n (dehydration), and the transition becomes more gradual and incomplete.⁴⁷

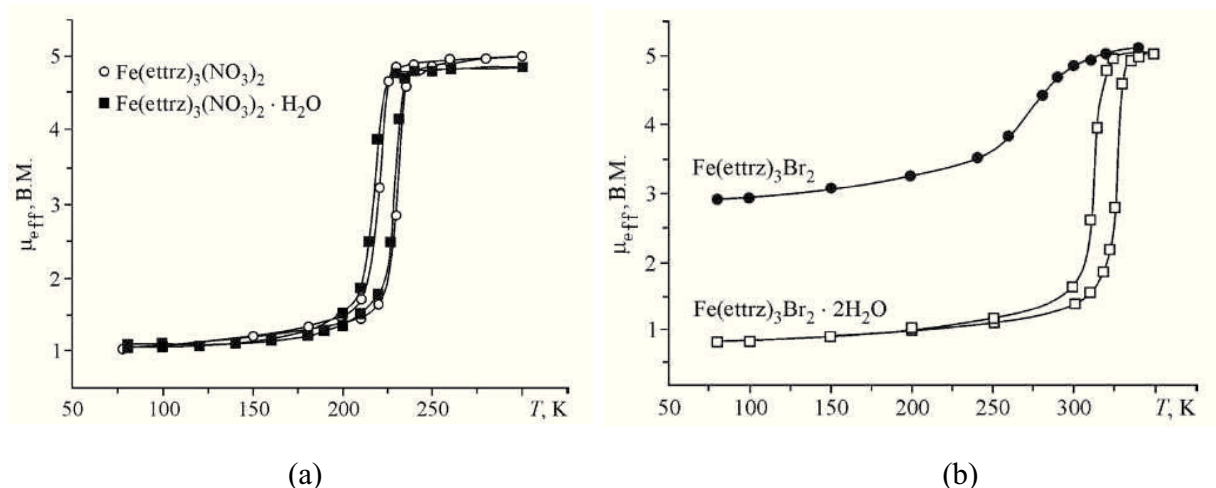


Figure 12. (a) μ_{eff} vs. T curves for $[\text{Fe}(\text{ettzr})_3](\text{NO}_3)_2 \cdot \text{H}_2\text{O}$ and $[\text{Fe}(\text{ettzr})_3](\text{NO}_3)_2$; (b) μ_{eff} vs. T curves for $[\text{Fe}(\text{ettzr})_3]\text{Br}_2 \cdot 2\text{H}_2\text{O}$ and $[\text{Fe}(\text{ettzr})_3](\text{Br})_2$.⁴⁶

The loss/alteration of *SCO* behavior upon dehydration/desolvation is commonly linked to the existence of hydrogen bonding as the communication pathways for the cooperative interactions propagating through the lattice as observed recently from our group in a series of macrocycle based Fe, but the effect of solvent is not always consistent from one system to another and is not readily predictable.⁴⁷⁻⁴⁸ Indeed, contrary to many examples in which the loss of solvent molecules is accompanied with a decline of the *SCO* behavior, Garcia *et al.* and Real *et al.* have reported two distinct examples, in 1997 and 2012 respectively, for which the appearance of the *SCO* properties are observed only in the dehydrated derivatives.⁴⁹

4.1.4. Metal dilution effect

The effect of metal dilution, into the lattice of *SCO* complexes presenting isostructural species of Fe^{II} , Zn^{II} , Cu^{II} or Co^{II} and others, has proved to be very significant in influencing the nature of spin-crossover in solids.⁴⁸ For instance, the elaborated investigations of the *SCO* behavior in the mixed-crystal series $\{[\text{Zn}_{1-x}\text{Fe}_x(\text{bbtr})_3](\text{ClO}_4)_2\}_\infty$ using SQUID measurements displayed that the *SCO* behaviour was strongly influenced by substitution of Fe^{II} by Zn^{II} (Figure 13).⁵⁰ Thus, if the transition curve is abrupt for the original Fe^{II} compound, the spin transition tend to become more gradual with decreasing Fe^{II} concentration (i.e. increasing dilution), and is shifted to lower temperatures; at high dilutions, the spin transition curve can resemble the thermal spin transition occurring in liquid solution.^{1c,50-51} The origin of such influence lies in the increase of the distances between spin-crossover centers with the decrease of their interactions.

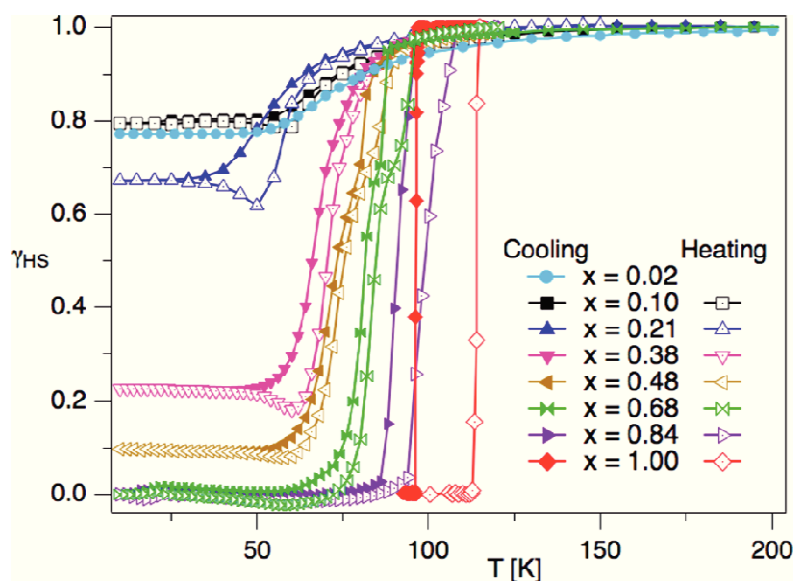


Figure 13. Thermal spin transition curves for the mixed crystal series $\{[\text{Zn}_{1-x}\text{Fe}_x(\text{bbtr})_3](\text{ClO}_4)_2\}_\infty$ ($x = 0.02, 0.10, 0.21, 0.38, 0.48, 0.68, 0.84$, and 1) obtained from optical absorption spectroscopy in cooling and heating mode (temperature sweep rate: 0.1 K/min).⁵⁰

Ultimately, all those ‘*chemicals factors*’ are also decisive in the obtention of single-crystals suitable for X-ray diffraction, which is the keystone for structure/properties correlations. In that regard, the crystal engineering conditions (stoichiometry, concentration, nature/mixture of the solvents, and crystallization technique) can be also considered as a *chemical factor*; indeed, they can have a dramatic input in some *SCO* systems, with singular crystal phases that can be obtained from the exact same starting precursors, but using different crystallization conditions.^{21a} Besides, in the 1D 1,2,4-triazole based series, the seek for single-crystals remains conspicuously a challenge that the present work has started to tackle in Chapter II.

4.2. Structural factors: Consequences and implications of the chemical factors

As previously emphasized, the strict influence of the *chemical factors* onto the *SCO* characteristics are intricate to clearly evaluate because a change in the composition of a system usually implies modifications in the structural arrangement while both factor in any resulting *SCO* behavior. In other words, the clear-cut impact of any chemical factor could be only strictly evaluated for derivatives that display the same structural arrangements/packings (e.g. isostructural derivatives), with a minority of examples to date. Among the main ‘*structural factors*’, we can define the following ones:

4.2.1. Intra- and Inter-molecular interactions

The intra- and inter-molecular interactions between *SCO* centers are directly related to the nature of metal centers, the ligand(s), anion(s), and also crystal solvent(s). For instance, the well known 1-D $[\text{Fe}(\text{4-R-1,2,4-trz})_3][\text{A}]_x$ derivatives display high degrees of cooperativity allegedly mainly arising from covalent linkers (N1-N2) between Fe^{II} *SCO* centres, but inter chain interactions will also play a part.^{14,52} Indeed, each metal center in the 1-D chain is believed to perceive its adjacent neighbours *via* changes in the metal-donor bond length and lattice volume. However, in the case of mononuclear complexes, this mode of transmission is not possible, meaning there must be further interactions, operating between complexes, and responsible for cooperative crossover. These intermolecular modes of transmission of cooperativity have been found to include hydrogen bonding and π - π stacking effects.^{21a,53-54} Thus, in the crystal lattice of

mononuclear systems, hydrogen bonds or π - π interactions between defining units are believed to play a decisive role in defining the character of the spin-transition. The importance of hydrogen bonding for the spin-crossover behavior of the $[\text{Fe}(\text{pic})_3]\text{Cl}_2$ system was investigated through the effect of isotopic exchange (H/D and $^{14}\text{N}/^{15}\text{N}$) in various positions of the ligand and the solvent molecules.⁵⁵ In a variety of polymeric triazole systems, the crystal water was found to influence substantially the abruptness of the spin-transition, whereas the loss of it resulted into gradual transition.⁵⁶ Among the most illustrative examples of the impact of π - π interactions can be cited the series of compounds $[\text{Fe}(\text{L})_2(\text{NCS})_2]$ (L =1,10-phenanthroline (phen), and dipyrrodo[3,2- α :2'3'- c]phenazine (dppz)), and $[\text{Fe}(\text{abpt})_2(\text{A})_2]$ (abpt = 4-amino-3,5-bis(pyridin-2-yl)-1,2,4-triazole, A = terminal monoanion N ligand).^{21a,57} In the first series, the crystal packing analysis shows an important number of C \cdots C contacts, with an emphasis in the dppz derivative leading to an abrupt transition with large hysteresis (~ 40 K); in the abpt series, Triki *et al.* have established a correlation between the configuration of the π - π interactions (frontal or sideways) and the corresponding magnetic properties of the *SCO* derivatives, with the sideways interactions seemingly unfavorable to *SCO*.^{21a} These observations evidenced that the *SCO* properties of materials are highly correlated with the nature and the extent of their intra- and inter-molecular interactions.

4.2.2. Dimensionality

The *SCO* phenomenon in monomeric complexes associated with the cooperativity and its rationalization in terms of effective intermolecular interactions, has led to the conclusion that enhancement of abruptness could be achieved by the use of bridging ligands capable of linking covalently the *SCO* centers. Consequently, it has been assumed some trends between the hysteresis effect (T_{SCO} , width and abruptness) in the spin-crossover derivatives and the dimensionality of the materials.⁵⁸⁻⁵⁹ For instance, it has been reported that the increase of the dimensionality from trinuclear to polymeric structures for some 1,2,4-triazole based materials shifts the transition to higher temperature, and increases the abruptness of the transition with the appearance of large hysteresis (up to *ca.* 60 K).^{56a,60-62} Other examples include the series $[\{\text{Fe}_2(\text{NCS})_2(\mu\text{-bpypz})_2\}\text{X}_n]$ (X = monodentate pyridine molecules ($n=2$),⁶³ bridging 4,4'-

bipyridine ($n=1$),⁶⁴ μ -bpypz = 3,5-bis(pyridin-2-yl)pyrazolato)) for which the increase of the dimensionality, respectively from dinuclear complexes to 1D system, leads to the appearance of a magnetic hysteresis loop in the latter compound at higher temperature. Meanwhile, the first reported two-dimensional spin-crossover coordination polymer $[\text{Fe}(\text{btr})_2(\text{NCS})_2] \cdot \text{H}_2\text{O}$ displays a strong cooperative spin-transition centered at around 134 K, with a broad hysteresis loop of *ca.* 21K width. Finally, the reported spin-crossover compound $[\text{Fe}(\text{btr})_3](\text{ClO}_4)_2$, with a three-dimensional network of covalent bonds between spin-crossover centers, shows a two-step transition with a hysteresis loop of 3 K.⁶⁵

Although relevant to discuss the dimensionality factor within specific series of *SCO* derivatives, it remains rather hazardous and fortuitous to undoubtedly extrapolate general trends between dimensionality and *SCO* behavior, with many counter-examples already reported. As an illustration, Galan-Macaros *et al.* have reported in 2015 an anionic trinuclear complex with the formula $(\text{Me}_2\text{NH}_2)_6[\text{Fe}_3(\mu\text{-L})_6(\text{H}_2\text{O})_6]$ ($\text{L} = 4\text{-(1,2,4-triazol-4-yl)ethanedisulfonate}$ which exhibits spin transition with memory effect that matches the remarkable features of triazole based coordination polymers.⁶⁶ Ultimately, the dimensionality can be a tricky structural factor to estimate, while the nature of the intra- and intermolecular interactions is positioned as a more reliable structural factor when assessing *SCO* behaviors.

4.2.3. Polymorphism

When polymorphism exists as a result of difference in crystal packing, it is called packing polymorphism. A polymorphism can also result from the existence of different conformers of the same molecule in conformational polymorphism. In pseudopolymorphism, the different crystal types are the result of hydration or solvation; this is more correctly referred to as solvomorphism. The effect of polymorphism on the spin-crossover behavior is known since the first studies on the classical system $[\text{Fe}(\text{L})_2(\text{NCX})_2]$ (where $\text{L} = \text{phen}$ ($\text{X} = \text{S}, \text{Se}$) or 2,2'-bipy ($\text{X} = \text{S}$)) by König and co-workers in the sixties, with numerous systems reported and structurally characterized ever since.⁶⁷⁻⁶⁸ The comparison of the crystal structures of the polymorphs showed that the differences in the spin-crossover behavior are generally attributed to crystal packing effects and crystal structure-induced modifications of the complex geometry. For example, the

extensive investigation of the *SCO* behavior in the two polymorphs (1a and 1b, Figure 14) of the mononuclear iron(II) complex $[\text{Fe}(\text{bpmen})(\text{NCSe})_2]$ [bpmen = $\text{N,N'$ -dimethyl- N,N' -bis(2-pyridylmethyl)-1,2-ethanediamine] showed that 1a undergoes a cooperative two-step *SCO* with thermal hysteresis, whereas 1b remains *HS* over all temperatures (Figure 14).⁶⁹ The origin of such influence depends on the coordination orientation of the NCSe ligand, which plays an important role in stabilizing the two polymorphs in different spin states.

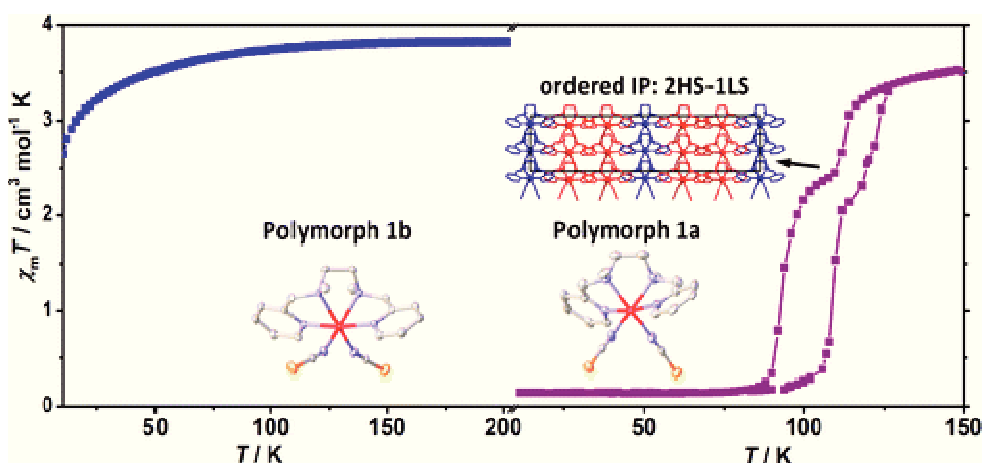


Figure 14. Variable-temperature magnetic susceptibility studies of the two polymorphs of the complex $[\text{Fe}(\text{bpmen})(\text{NCSe})_2]$: 1a and 1b. Data recorded in both cooling and heating modes at a scan rate of 2 K min^{-1} .⁶⁹

4.2.4. Lattice defects

The different synthetic procedures (crystallization techniques) as well as the mechanical treatments of the samples (e.g. ball milling, crushing in mortar) have been shown to influence strongly the spin-crossover behavior.⁷⁰ The origin of these effects stems from crystal quality considerations, in particular crystal defects (e.g. point defects, dislocations and volume defects) introduced during the crystallogenesis or the sample preparation that often increase the residual *HS* fraction in the low temperature region, and tend to make the spin transition curve more gradual.⁷¹ The size of the crystalline particle has also been reported to play a role.⁷² In any case, the sample preparation for physical characterizations of a *SCO* compound is very crucial and should be measured with great care.

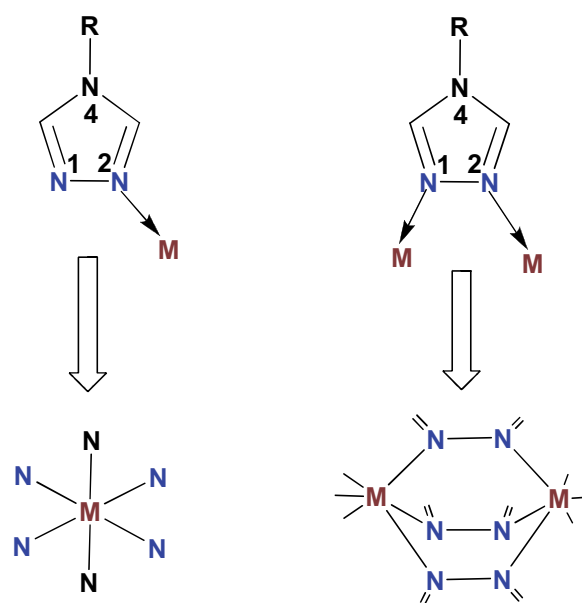
5. Aims and Strategy of the Present Work

In the perspective of the present work, the focus has been primarily defined on Fe^{II} systems based on 4-R-1,2,4-triazole ligands in combination with polynitrile anions, either organic or inorganic (e.g. [M(CN)₄]²⁻ (M=Ni, Pt and Pd)). The specifics about the corresponding precursors will be reviewed hereafter while also explaining the aims and strategy.

5.1. Selection of the ligand: 4-R-1,2,4-triazole ligands (Rtrz)

5.1.1. Impact of the substituent on the coordination mode of Rtrz ligands

As previously introduced, the 1,2,4-triazole-based systems such as [Fe(4-R-1,2,4-trz)₃][A]_x (4-R-1,2,4-trz=4-substituted-1,2,4-triazole, and A = mono- or di-valent anion) are a unique class of materials in the field of *SCO* research, with several derivatives displaying fairly abrupt spin transitions and a tendency of wide hysteresis that can be as large as 50 K around room temperature.^{2,14} The quintessence of 1,2,4-triazole systems resides in their chemical flexibility and versatility; thus, systematic variations - of the substituent on the triazole, the anions and the solvate molecules - have been investigated to ‘fine tune’ the *SCO* behaviour of the resulting materials, while the compounds usually maintain spin transition properties of relevance. Indeed, the 1,2,4-triazole (trz) entity and its derivatives are versatile ligands for transition metals as they contain two or more binding sites, can adopt various coordination modes, and can be rationally functionalised. The possible binding modes of triazole ligands, as well as their steric effects and their electronic properties, can be significantly altered by substitution/functionalization of the ligand, most notably (but not only) on the N4 position. Various substituents on the N4 position of 1,2,4-triazole have been reported to date, but it has to be noted though that most of the substituents used so far have similar compositions (e.g. either a -CH₂- or -NH- group) for the part closest to the N4 atom.⁷³ On the other hand, monodentate coordination of 4-R-trz ligands by just one nitrogen atom has been also reported in several examples, mostly involving aryl substituents and leading to discrete derivatives (Scheme 3).⁷⁴ In this regard, the influence of the functionalisation of the trz ligands on their coordination modes is of paramount magnitude to fine-tune the *SCO* properties, but remains surprisingly unaddressed in a systematic way, with the present work looking to tackle the issue.



Scheme 3. Coordination modes of 4R-1,2,4-triazole ligands.

5.1.2. The “quest” for single crystals with highly refined crystallographic data: 1D and discrete systems.

In many cases, the structural backbone is constructed through the bridging ability of the N1,N2-1,2,4-triazole ligand donors usually forming highly stable complexes, typically oligo- or polynuclear compounds in the powdered form, with crystalline samples involving triple-triazole bridged μ -N1,N2 (FeN_6) coordination environments notoriously difficult to form.⁷⁵ In fact, isolated single crystals (of 1D $[\text{Fe}(\text{4-R-1,2,4-trz})_3][\text{A}]_x$ complexes suitable for X-ray diffraction was not reported until 2011 by Guionneau *et al.* (Figure 15);⁷⁶ while the quality of the data does not meet typical diffraction standards, the structure of the 1D $[\text{Fe}^{\text{II}}(\text{NH}_2\text{trz})_3](\text{NO}_3)_2 \cdot 2\text{H}_2\text{O}$ derivative remains nevertheless the first unambiguous evidence of the chain-like polymeric nature. The *SCO* behaviour of the compound shows a highly cooperative transition with a thermal hysteresis of 32 K ($T_{1/2\uparrow} = 342$ K and $T_{1/2\downarrow} = 310$ K). The structure of the complex was only collected at one temperature, 120 K, where the complex is in the *LS* state; structural data at higher temperature were not reported, possibly as a result of the rather poor quality of the crystalline sample as mentioned by the authors. The structure tends to reveal the likely source of

the highly cooperative nature of the spin transition, whereby the chains interact *via* direct hydrogen bonds of the amino groups with an adjacent chain, and through a network of hydrogen bonds involving both the lattice nitrate ions and water molecules. However, the low refinement is further requiring the access of highly refined crystallographic data in order to assess accurately all the structural factors implicitly correlated to the *SCO* properties, more precisely to the hysteretic behavior with $T_{1/2}$ close to room temperature. This also clearly defines one of the main objectives of the present work.

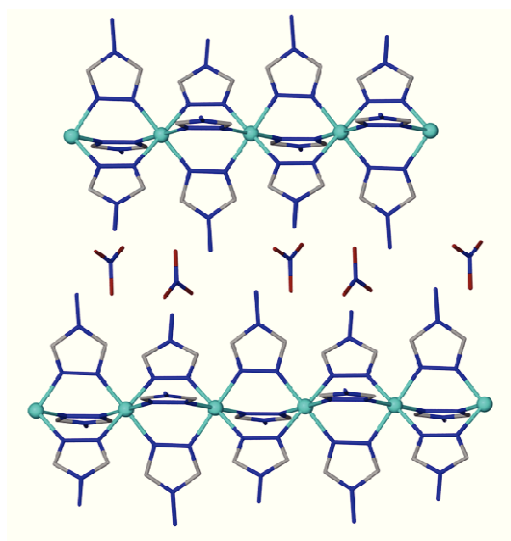


Figure 15. 1D polymeric chain of complex $[\text{Fe}(\text{NH}_2\text{trz})_3](\text{NO}_3)_2 \cdot 2\text{H}_2\text{O}$; (Right). Colour code: Fe (pale blue), N (blue); C (grey). The solvent molecules have been omitted for clarity.⁷⁶

When it comes to the *SCO* triazole based materials, the emphasis has been historically centered on the 1D compounds that tend to display more interesting *SCO* features, in comparison with the discrete derivatives such as dinuclear and trinuclear derivatives. However, this assessment and reasoning took a hit in 2015 when Galan Mascaros *et al.* reported an anionic trinuclear complex with the formula $(\text{Me}_2\text{NH}_2)_6[\text{Fe}_3(\mu\text{-L})_6(\text{H}_2\text{O})_6]$ ($\text{L} = 4\text{-(1,2,4-triazol-4-yl)ethanedisulfonate}$) which exhibits spin transition with memory effect that matches the remarkable features of triazole based coordination polymers (Figure 16).⁶⁶ Indeed, in the $[\text{Fe}_3(\mu\text{-L})_6(\text{H}_2\text{O})_6]^{6-}$ polyanionic moiety, as the dimethylammonium salt, only the central Fe^{2+} displays

spin transition as it stays in its *LS* state at room temperature, and cooperative thermally induced spin transition occurs above room temperature for the central Fe position in the trimer with the appearance of memory effect, a large hysteresis cycle (>85 K), and remarkably slow dynamics. This allows easy quenching of the metastable *HS* state *via* gradual cooling ($5 \text{ K}\cdot\text{min}^{-1}$). Once it is trapped, the *HS* state remains metastable. The thermal energy is not able to promote relaxation into the low-spin ground state below 215 K, with a characteristic $T(\text{TIESST}) = 250 \text{ K}$ (Where TIESST is temperature-induced excited spinstate trapping), i.e. the highest temperature ever observed for a thermal trapping of an excited spin state in a switchable molecular material.

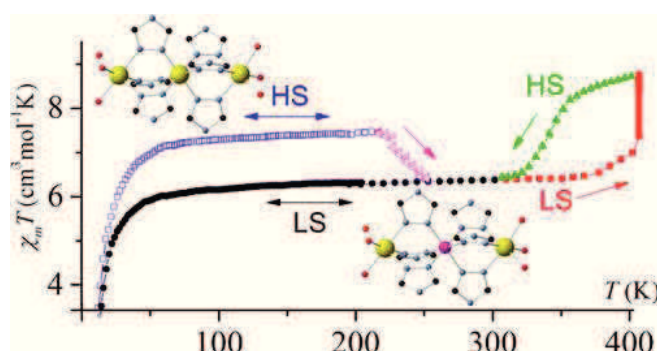


Figure 16. $\chi_m T$ vs. T plots illustrating the easy excited-state trapping and record high $T(\text{TIESST})$ in a spin crossover polyanionic Fe^{II} trimer of the material $(\text{Me}_2\text{NH}_2)_6[\text{Fe}_3(\mu\text{-L})_6(\text{H}_2\text{O})_6]$.⁶⁶

Although involving anionic sulfonated 1,2,4-triazole ligand as building block instead of the usual neutral Rtrz ligands reported to date, this derivative and its striking properties is positioned in contradiction with the “empirical” consensual belief that the chain structure is implicitly required to access hysteretic behavior at high temperature in triazole based *SCO* materials; indeed, this derivative remains hitherto the only example of trinuclear entity which displays such remarkable *SCO* properties, with most of the trinuclear^{66,77} and dinuclear⁷⁸ derivatives typically exhibiting lower degree of cooperativity (e.g. gradual transitions) at low temperatures. Thus, the limited number of triazole based trinuclear systems reported to date typically suffer a lack of refined crystallographic data, with usually only the central metal center displaying spin equilibrium and gradual transitions at low temperatures.⁷⁷ Although with usually more abrupt transition implying two metal centers, the same applies to the not many dinuclear

derivatives.⁷⁸ Ultimately, based on the results obtained with the material $(\text{Me}_2\text{NH}_2)_6[\text{Fe}_3(\mu\text{-L})_6(\text{H}_2\text{O})_6]$ and the overall manifest deficiency in unswerving structural information in triazole systems, the definite key factor(s) contributing to the hysteretic behavior close to room temperature has(have) yet to be clearly addressed, and remain(s) an open question/challenge that will shape the red line between the different chapters of the present work.

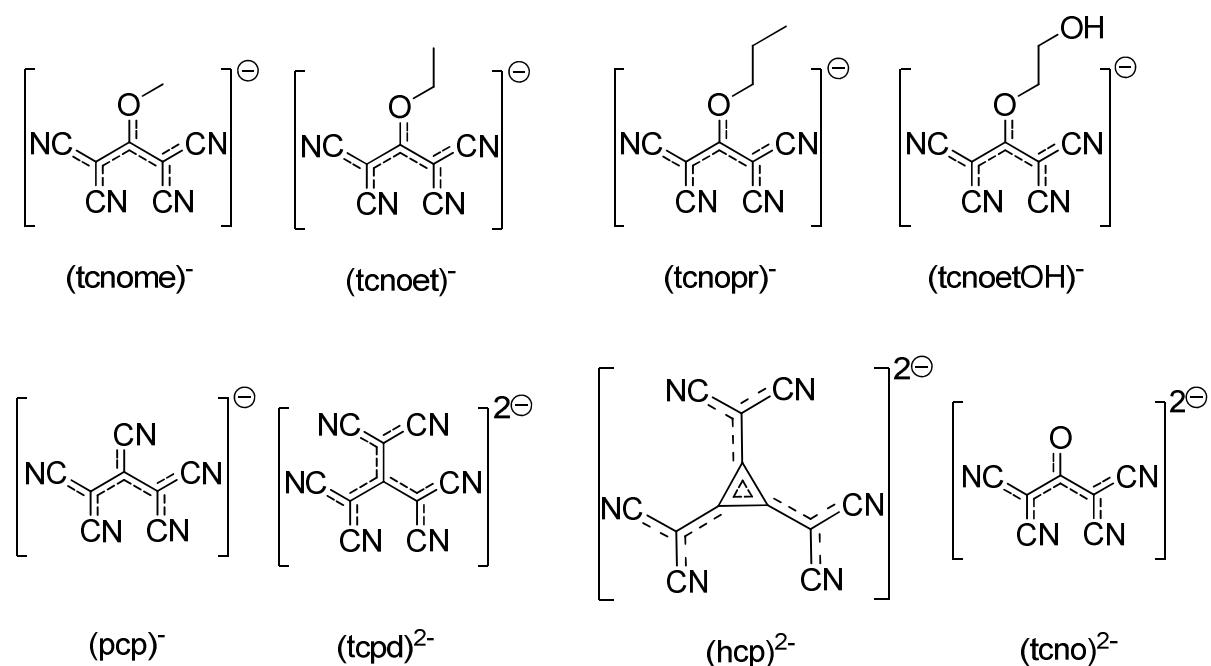
In due course, the overall “fascination” for the 1,2,4-triazole based derivatives runs beyond their relative chemical stability, robustness and the display of molecular-scale magnetic and thermochromic switching capabilities around room temperature, and the subsequent applied potential (e.g. early optical devices prototypes,^{56,79} contrast agents for Magnetic Resonance Imaging,⁸⁰ as well as the electrical addressing of *SCO* or the use of plasmons to detect *SCO*⁸¹), with the elaboration of multifunctional materials in various types such as nanoparticles,⁸² supramolecular gels,⁸³ thin films,⁸⁴ dendrimers,⁸⁵ and liquid crystals.⁸⁶ Indeed, the first methods to craft *SCO* nanoparticles involved the reverse micelle technique, which leads notably to the synthesis of $[\text{Fe}^{\text{II}}(4\text{-NH}_2\text{-trz})_3](\text{Br})_2 \cdot 3\text{H}_2\text{O} \cdot 0.03(\text{surfactant})$ derivatives with Lauropal used as surfactant.⁸⁷ About the latter, the study showed the occurrence of spin crossover in 69 nm spherical nanoparticles that exhibited room temperature thermal hysteresis. The nanoparticles size could be controlled depending on the water/surfactant ratio, and ranged from 30-120 nm. This work was later patented by Létard⁸⁸ and co-workers, while the research groups of Mallah⁸⁹ and Coronado⁹⁰ have also developed similar nanoparticles with modifications and distinct observations.

5.2. Selection of the anion: Organic and inorganic polycyano anions

5.2.1. Atypical organic cyanocarbanions: Impact on *SCO* behavior

The *SCO* derivatives with FeN_6 coordination environments frequently fall within one of the two most common types: (i) $[\text{FeL}_x]\text{A}_y$ compounds with cationic complexes $[\text{FeL}_x]^{2+}$, where L is a neutral N-donating ligand that can be mono-, bi- or tridentate (the denticity x would accordingly vary from 6 to 3 and 2, respectively), and A^{n-} is a non-coordinated anion, and (ii) $[\text{FeL}_x\text{A}_y]$, where L is a neutral ligand that can be mono-, bi- or tetra-dentate (the denticities x and y would vary accordingly), and A^{m-} is a N-donor ligand such as NCS^- , NCSe^- , dca^- (dicyanamide anion), and tcnq^- (tetracyanoquinodimethane radical anion). In this context, previous work from

Triki *et al.* has shown that the atypical polynitrile ligands are very efficient building blocks to access magnetic architectures ranging from discrete complexes to 1D, 2D and even 3D structures.⁹¹ In most of the compounds, they have displayed a high flexibility and versatility with the ability to act as multi-bridging N-donor ligands between two or more metal ions, leading to a rich variety of geometries (and symmetries).⁹¹⁻⁹⁴ Since the cyanocarbanion ligands (Scheme 4) can be easily tuned by chemical substitution or electrochemical reduction/oxidation, the coordination attributes of the polynitrile anions have been considered for investigations in the present contribution to tune the ligand field strength, and so to evaluate their influence on the *SCO* behavior in a new series of Fe^{II} derivatives based on Rtrz ligands. Besides their ability to directly link to metal centers, those anions can also be involved in supramolecular interactions in the resulting materials. As will be further explained in the next chapters, the combinations of polynitrile anionic N-donor ligands (Scheme 4) with the Rtrz ligands have proved to favor novel *SCO* complexes of type (ii).



Scheme 4. Examples of organic polynitrile anionic ligands.⁹¹

5.2.2. Extension to inorganic polycyanometallate anions: Planar tetracyanometallate anions

Certain Hofmann-type frameworks incorporating Fe^{II} with polyanionic $[\text{M}(\text{CN})_4]^{2-}$ (with $\text{M} = \text{Ni}, \text{Pt}$ and Pd) moieties have already been shown to display cooperative *SCO* behaviour,⁹⁵ with the first such framework incorporating axially-bound pyridine coordinated to the Fe centres.⁹⁶ Moreover, the first *SCO* pillared Hofmann framework that has been reported is incorporating pyrazine as the pillar between adjacent Fe centres in the metal cyanide layers (Figure 17), and has also been the major subject of research into the dynamic interplay between the *SCO* and host-guest function.⁹⁷⁻⁹⁸

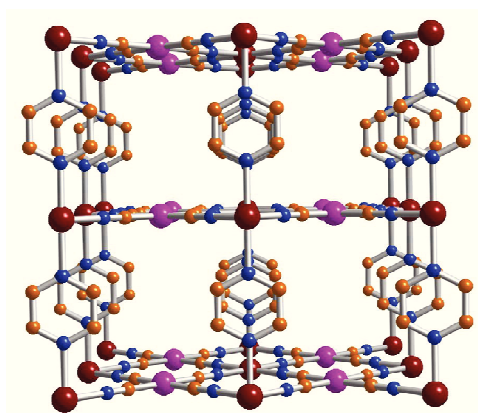


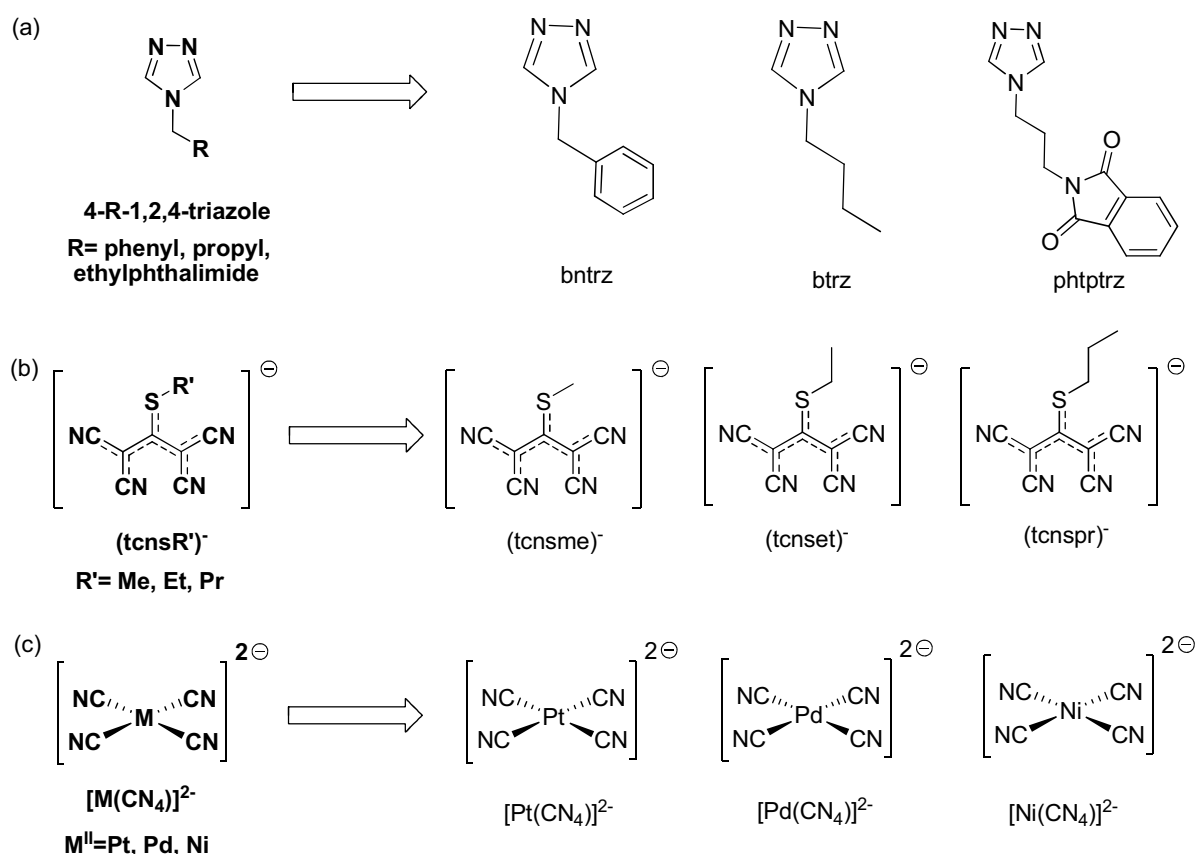
Figure 17. The 3D porous structure of $\{\text{Fe}(\text{pz})[\text{Pt}(\text{CN})_4]\}$. Atom codes: Fe (red), Pt (pink), N (orange), and C (blue).⁹⁵

These Hofmann-type frameworks have a variety of desirable structural features for the study of *SCO*. The metal cyanide layer has a high degree of structural integrity, and with a suitably rigid choice of pillar ligand would produce a framework that is robust to de-solvation and re-solvation with minimal impact on the underlying structure. The FeN_6 coordination sphere is appropriate to create *SCO* behavior for Fe^{II} , and the co-metal and pillar ligand provide means to directly modify the ligand field strength. The choice of pillar ligand can also alter the shape and size of the framework pores, which combined with a guest-dependent effect, could give rise to new and interesting *SCO* behaviours. Consequently, and as an extension to the more flexible organic polynitrile N -donor anions, the more rigid polycyanometallates anions, most notably the tetracyanometallates anions, have been considered for the design of the *SCO* materials reported here. It is also noteworthy to clearly distinguish the difference in geometry

(symmetry, bulkiness, size, volume), and eventually in charge (monoanions for some polynitrile anions, and dianions for the tetracyanometallates) that will be addressed in the discussion of the resulting materials.

5.3. Aims and Strategy

While wittingly conceding the prospect to subtly fine-tune the *SCO* behaviour of triazole based materials by varying the nature of the 4-substituent on the triazole ligand, and also the choice of the anion, the present work has focused primarily on the design, synthesis and physical properties of new Fe^{II} *SCO* systems using carefully selected 4-R-1,2,4-triazole ligands, with either specific flexible polynitrile or rigid tetracyanometallates anionic ligands (Scheme 5).



Scheme 5. Selective examples of (a) 4-R-1,2,4-triazole derivatives, (b) Polynitrile anions (tcnsR)[−], and (c) Tetracyanometallate(II) anions [M(CN)₄]^{2−} selected for the present work.

The preliminary and time-consuming step of this project included the development and optimization syntheses of the starting precursors, more precisely the synthesis of the 4-R-1,2,4-triazole ligands (with R = phenyl, alkyl, phthalimide), and the sulfur based organic cyanocarbanion ligands (tcnsR with R = methyl, ethyl, propyl) (Scheme 5). Regarding the 4-R-1,2,4-triazole ligands, the choices of the N4 substituents in the present work have been determined based on the recent developments in 1,2,4-triazole research (e.g. the 1D, di- and tri-nuclear trz *SCO* materials, as well as the first reported 1D Fe^{II} crystal structure) dedicated to the systematic evaluation of the incorporation of different substituents at the 4th position onto 1,2,4-triazole (using notably the modified Bayer synthesis), with variations in the length, the aromaticity, the nature of the functional groups, the bulkiness, the charge, and also the bonding ability (e.g. hydrogen bondings) of the substituent(s).¹⁵ As examples, previous studies performed on 4-substituted-1,2,4-triazole derivatives have noticeably included the 4-amino-1,2,4-triazole (atrz), 4-*n*-alkyl-1,2,4-triazoles (C_n-trz),⁵ 4-(2'-hydroxyethyl)-1,2,4-triazole (hyetrz) and 4-(3'-hydroxypropyl)-1,2,4-triazole (hyptrz),⁹⁹ 4-(1,2,4-triazol-4-yl)ethanesulfonate (settrz) and 4-(1,2,4-triazol-4-yl)ethanedisulfonate (dsettrz),⁶⁶ and N-(4H-1,2,4-triazol-4-yl)benzamide (tba),¹⁰⁰ which lead to a broad range of *SCO* materials, but with a customary lack of refined structural data rendering the studies of the properties rather incomplete. In the strategy from the group, all the selected 4-R-1,2,4-triazole ligands for the present work are systematically including an alkyl spacer at the 4th position between the triazole moiety and the terminal functional group of the substituent. This decision has been initially motivated by careful comparison of the *SCO* properties of 4-R-1,2,4-triazole systems, and also by a previous work from Garcia *et al.* suggesting the influence of the alkyl spacer in *SCO* materials composed of either 4H-1,2,4-triazol-4-yl-propionate (βAlatrz) or ethyl-4H-1,2,4-triazol-4-yl-acetate (αGlytrz), with one carbon difference between the two.¹⁰¹ After meticulous compilation of all those studies, we came to the conclusion/suggestion that it could be preferable to incorporate an alkyl spacer in the nature of the substituent on the 4th position of the triazole in order to (i) maintain as much as possible the electronic “integrity” of the triazole moiety, and so (ii) to limit the possible alteration of the terminal group of the substituent on both the coordination mode (and the ligand field strength) and the *SCO* characteristics of the triazole moiety. On the other hand, the choice of the organic cyanocarbanion has been driven by the extended local expertise in the synthesis and the use of such flexible ligands, with the more rigid tetracyanomellates intervening as a

comparative tool to evaluate the impact of the charge, the rigidity and the geometry of the anion on the resulting materials. Moreover, due to their chemical flexibility, the polynitrile anions can be functionalized with the possibility to rationally modulate and evaluate different functional groups in the efficient development of *SCO* covalent networks. In the end, the selected 4-R-1,2,4-triazole ligands have been combined with either anionic organic polynitrile derivatives or tetracyanomethylates to design new Fe^{II} *SCO* complexes with various dimensions ranging from polynuclear, 1D up to 3D crystalline lattices, with the establishment of correlations between the crystal structures, the *SCO* characteristics, and the nature of the substituents for the triazole ligands as well as the nature of the polynitrile anions. The novel *SCO* materials have been classified in the upcoming chapters based on the nature of the building blocks and the subsequent dimensionality of the structures. Thus, the second chapter concerns the first accurate single crystal investigations, at both *LS* and *HS* states, of a novel 1D polymeric triazole-based system.¹⁰² The third chapter focuses on trinuclear systems where the intermolecular interactions between the building units are of critical significance for the *SCO* properties, while the fourth chapter will refer to 3D derivatives. It is noteworthy to specify the ‘breakthrough’ of the present work from a structural aspect, as all the *SCO* materials presented hereafter have been obtained as single crystals and fully characterized by X-ray diffraction. Thus, with very limited structural data currently available about the triazole based materials, the systematic access to extensive structure/properties studies could expand the knowledge about *SCO* behaviours, and allow some rationalization in a consistent way.

6. Experimental approach of spin crossover materials

6.1. Crystallogenesis of *SCO* derivatives: The “royal” synthetic pathway

In order to rationally investigate spin crossover materials, the crystallogenesis represents the keystone for the establishment of structure/properties correlations, as many structural studies of *SCO* systems are thwarted by a lack of apposite crystals. In order to have refined structural information *via* X-ray diffraction techniques, suitable crystals - notably in “quality” and in “size” - must be produced reproducibly from the synthetic route. In this context, the aim consists in defining crystallization conditions that could favour the growth of single crystals (*i*) of good “quality”, i.e. single domain with limited defects (point defects, line defects, 2D or 3D defects), (*ii*) of suitable “size” for single crystal X-ray diffraction studies, i.e. with minimum requirements of ca. 0.2 - 0.4 mm in at least two of the three dimensions of the crystal, and (*iii*) ultimately, with enough mechanical resilience upon repeated *SCO* switching cycles to allow for refined crystallographic investigations of both *LS* and *HS* states, as the latter remains an actual challenge for most of the *SCO* systems. Besides the influence of the “*Chemicals factors*” previously enlightened (see section 4.1), the targeted characteristics of the crystals can be influenced by a number of factors during the crystallogenesis. Indeed, as briefly exposed hereafter, the crystals can be notably subjective to the nature of the crystallization solvent(s), the number of nucleation sites, the mechanical disturbances, and time.

- **Solvent.** If possible, the solute should be moderately soluble in the chosen crystallization solvent(s). If the solute is too soluble, and/or in the eventuality of supersaturated solutions, this will often result in small crystal size.
- **Nucleation.** A smaller number of nucleation sites, i.e. sites at which crystals begin to grow, will usually result in fewer crystals, each of larger size. Conversely, many nucleation sites will result in a smaller average crystal size, which is not favourable. In many recrystallizations, the ambient dust in the laboratory provides numerous nucleation sites and may initiate interfering crystal growth. Consequently, it is important to minimize dust or other extraneous particulate matter in the crystal growing vessel (cleaning procedure).

- **Mechanics.** Mechanical disturbances - such as vibration(s) or frequent movement(s) - of the crystal growing vessel may lead to smaller and/or poor quality crystals. Thus, the minimum of disturbance is required during the crystal growth; the latter implies to not grow crystals next to a vacuum pump for example, nor to move the vessel everyday to check if/how the crystals are growing. Preferentially, the set up should be in a “quiet” place for most of the time.
- **Temperature and Light.** The choice of the temperature (e.g. low temperature or ambient temperature) and the temperature stability during the crystallogensis may impact radically the crystal growth, while the absence of light could help the reproducibility of experiments for some systems.
- **Time.** The time of crystal growth is implicitly related to the system, but also to mechanical parameters such as the type of crystallization technique and vessel (size and shape). The concentration of the starting precursors will impact the time of growth as well. Last but not least, multiple phases can be obtain in the same system (e.g. polymorphs) within the same set up, with thermodynamics and kinetics involved, but also pH evolution or redox processes which could favor one phase or another; in that context, time could be a decisive factor in the selectivity between the phases.

Distinctly from the “*Chemicals factors*”, if a sample is not of sufficient quality, it may be necessary to use a different crystallization technique. The commonly used crystallogensis techniques include notably solvent evaporation, slow cooling of the solution, solvent/non-solvent diffusion, vapour diffusion and sublimation, and many variations on these themes (e.g. gels, different shapes of diffusion tubes). The choice of technique may be also driven by the amount of sample required, or the amount of starting materials available. Among those techniques, the most popular is arguably the solvent diffusion (Layering Technique).

- **Solvent Diffusion (Layering Technique).** This method is applicable to mg amounts of materials which are sensitive to ambient laboratory conditions (air, moisture). Typically, a solution of dissolved solute(s) (e.g. Fe(II) salt and a co-ligand) in a solvent S1 is placed in a sample tube, and then a second less dense solvent S2 - miscible with S1 and containing another solute(s) (e.g. counter-anion building block) - is carefully dripped

down the side of the tube using either a pipette or a syringe, so that S1 and S2 form discreet layers. This usually implies a difference of the density of the solvents ($S2 < S1$), and a great care in creating the solvent layers. At this stage, the choice to put one of the solute either in S1 or S2 (bottom layer or top layer, if the solute is soluble in S1 and S2) can be critical in the obtention and/or the quality of the crystals. The narrower the tube, the easier it is to build up the layer (with the involvement of capillary forces), with three to five millimeter glass tube an excellent vessel to use for this crystal growing technique. Ultimately, the single crystals form at the boundary where the solvents slowly diffuse over a period of time that could be minutes or hours up to weeks or months depending on the systems and conditions.

In the present work, multiple crystallization techniques have been deeply investigated, with the solvent diffusion (Layering Technique) providing the most suitable crystals for X-ray studies. In order to rationalize the crystallogenesi s of a specific system, the investigations have been conducted systematically and methodically with careful variations of the conditions - i.e. choices of crystallization technique and vessel, the combinations of solutes and solvents S1 and S2, the nature and concentrations of the building blocks (e.g. counter-anions) - in order to quickly converge to the optimum conditions. Taking into account the well reported difficulty to obtain single crystals in triazole based *SCO* derivatives, it is noteworthy that all the systems presented in this manuscript have been systematically and successfully obtained as single crystals suitable for X-ray studies, and that the crystallogenesi s of these systems has been significantly time-consuming. In perspective, it has been observed that the crystallogenesi s conditions are extremely system dependant; in other words, the crystallization conditions for two similar systems can be radically different as no obvious trend could be defined from one system to another.

N.B.: As previously described in section 4.2, the “*Chemical factors*” such as the nature of the Fe(II) salt and the nature of the counter-anion can have a dramatic impact on the success of the crystallogenesi s procedure. Consequently, if the compound is ionic, and is not giving suitable crystals with a given counterion or Fe(II) salt, a metathesis reaction to change the counterion or the Fe(II) salt can be considered (after verification that the ion used for the metathesis does not react with the ion of interest). The crystal quality can be habitually improved upon the use of a

different counterion. The ions of similar size tend to pack together better and subsequently give better crystals, with eventual impact on the physical properties of the crystal. For example, the sodium salt of a compound might be hygroscopic, but the tetramethyl ammonium salt might not be or at least, less so. When selecting possible counterions, the avoidance of ions which contain large non-rigid groups (like tetrabutyl ammonium), and the use of ions which have very limited conformational flexibility, is often suggested, but again these parameters are highly system dependant.

6.2 Detection and Characterization techniques of the *SCO* Behaviour: A Multi-tool approach

As previously mentioned the spin transitions are associated with profound changes, predominantly in the optical, vibrational, structural and magnetic properties. These molecular changes allow to detect the occurrence of thermal *SCO* and monitor the temperature dependence of a *SCO* via various physical methods, primarily magnetic susceptibility measurements, X-ray crystallographic studies, optical and vibrational spectroscopy, and heat-capacity measurements.^{1c,103} These experimental techniques are typically combined as a “Multi-tool” platform/approach to detect, investigate and quantitatively characterize the occurrence of spin state conversions for Fe^{II} complexes. A brief description of these techniques, in the context of *SCO* materials, is provided hereafter.

6.2.1 Vibrational spectroscopy

The Infrared absorption spectroscopy is actively used for *SCO* materials since the bond strength between the Fe^{II} center and its ligands change significantly from one spin state to the other. Indeed, the thermal spin transition from *HS* to *LS* states is associated with depletion of charge in the anti-bonding e_g* orbitals, and simultaneous increase of charge in the lower lying slightly bonding t_{2g} orbitals upon lowering of the temperature. This results in strengthening the metal-donor atom bonds and can be observed in the vibrational spectrum recorded in the far-infrared (FIR) region between ~50 and ~500 cm⁻¹, i.e. where the central metal-donor atom stretching frequencies of transition metal compounds generally appear.¹⁰⁴ With temperature-

dependent FIR or Raman spectroscopy, the vibrational bands characteristic of the *HS* and the *LS* species can be readily recognized as those with decreasing and increasing intensity, respectively, on cooling of the sample.¹⁰⁵ Although little used, the spin state conversion curve γ_{HS} vs T can be also derived by plotting the normalized area fractions of characteristic *HS* or *LS* bands as a function of temperature. Thus, the typical systems $[\text{Fe}(\text{phen})_2(\text{NCS})_2]$ and $[\text{Fe}(\text{phen})_2(\text{NCSe})_2]$ in which the C-N stretching bands of NCS^- and NCSe^- are seen as a strong doublet near 2060-2070 cm^{-1} in the *HS* state; upon cooling of $[\text{Fe}(\text{phen})_2(\text{NCS})_2]$ below the transition temperature (175 K), this doublet decreases in intensity, favoring the appearance of a new doublet at 2100-2110 cm^{-1} , which obviously stems from the *LS* state.¹⁰⁴ One has also found that certain vibrational modes of lattice constituents, such as non-coordinating anions or solvent molecules, interconnecting the spin state changing metal complexes *via* hydrogen bonds, van der Waals or other interactions, can influence spin state changes at the metal centers and can therefore be used to study *SCO* phenomena; as an example, it has been established for the *SCO* compound $[\text{Fe}(\text{ptz})_6](\text{BF}_4)_2$ that certain B-F vibrations of the tetrafluoroborate anion show temperature-dependent intensity in agreement with results from magnetic measurements.¹⁰⁶

6.2.2. Crystallography: X-ray diffraction techniques

Thermally induced *SCO* is usually accompanied by a change in the magnetic moment and color.⁶ This thermochromism is generally attributed to d-d electronic transitions and/or charge transfer transitions (Metal to ligand or ligand to metal charge transfer (MLCT/LMCT) depending on the configuration and nature of the coordination complexes). As a result, this thermochromism defines a convenient preliminary characterization method to eventually detect a spin transition; in context, the camera of the X-ray diffractometer is typically used to collect crystal images upon repeated switching cycles (cooling and warming cycles). The latter also allows estimating the $T_{1/2}$, and easily evaluating the mechanical resilience of the crystal in the eventuality to study the crystal in both *LS* and *HS* states.

The single crystal structure determination of *SCO* compounds is of paramount importance in the resolve of structure-properties correlations, and has been a salient research challenge in the field of *SCO* materials. The correlations between structural features and the *SCO*

characteristics may aid the design of materials with specific physical properties such as abrupt spin transitions near room temperature. Therefore, studies for which single crystal X-ray diffraction data could not be obtained - such as the highly studied 1D-1,2,4-triazole Fe^{II} systems - are frequently found to be at a disadvantage and rather incomplete when assessing the properties from a structural perspective. In that context, X-ray diffraction technique can be engaged to deduce the structural evolution of the compounds upon the *SCO* by notably accessing the evolution of the metal-ligand distances and bond angles, the cell parameters, and implicitly the overall structural deformations/distorsions with temperature. Indeed, a spin transition from *HS* to *LS* is accompanied by a contraction in metal-donor bond lengths. These changes in bond lengths are the results of de-population of the anti-bonding e_g orbitals (into non-bonding t_{2g}), as such the bonding orbitals of the incoming ligand can approach the metal ion more closely, and correspondingly the metal-donor bond length contracts.^{1b} Consequently, X-ray diffraction can be used to confirm the existence of a spin transition through the determination of bond lengths and angles above and below the transition temperature, and define whether the transition is associated with a change in crystallographic space group. As examples, the compiled crystallographic data on $[\text{Fe}^{\text{II}}(\text{NCS})_2(\text{L})_n]$ -type systems confirmed the changes in metal-donor bond distances with spin crossover, going from an average Fe^{II} *HS* Fe-N length of ~ 2.1 Å to Fe^{II} *LS* length of ~ 1.9 Å, with changes in N-Fe-N angles that have also been found to correlate with the spin state of a *SCO* complex;¹⁰⁷ this implies modifications (distorsion parameters) in the octahedral coordination geometry surrounding the metal centre, and a change in cell volume can be detected. This means that variable temperature X-ray crystallography may be used, not only to determine or confirm the spin state of a complex, but also to potentially map the *SCO* behaviour *via* single crystal structures or unit cell parameters at variable temperature, in order to notably evaluate the effects on the cooperativity. By detecting the *SCO* behaviour using variable temperature X-ray crystallography, a number of distorsion parameters associated with *SCO* has been defined and determined, some examples of which include the trigonal twist angle (θ_{NCS}) developed by Marchivie *et al.*,¹⁰⁸ and the “angular Jahn-Teller parameters θ vs. ϕ ” developed by Halcrow for *HS* Fe^{II} forms;¹⁰⁹ for the octahedral distorsion parameters Σ and Θ ,^{107b} Σ corresponds to the sum of the deviation from 90° of the 12 cis-angles of the FeN_6 octahedron while Θ is the sum of the deviation from 60° of the 24 trigonal angles of the projection of the

FeN6 octahedron onto its trigonal faces.^{107b} Beside the development of these various parameters obtained from crystal structure data that have created a better and more systematic understanding of *SCO* from a semi-quantitative point of view (with the possibility to rationally compare different systems), there are also a number of more qualitative analyses which can be obtained from a crystal structure that have provided insightful information into the origins of *SCO* behaviours. For instance, crystallography studies have revealed supramolecular networks of hydrogen bonding or specific orderings of π -stacking with information about how the intermolecular interactions in a structure can influence its magnetic properties; this has been particularly useful in the case of polymorphism in which minor structural variations within the complex can induce drastic changes in the magnetic behaviour. Furthermore, structural analyses have been found to shed light on the mechanisms of multiple-step spin crossovers, with variable temperature structural data being collected above, below and at the intermediate plateau(s).

When referring to the present work, single crystal X-ray data have been systematically collected for all the original compounds reported in this manuscript, with *LS* and *HS* studies thoroughly undergone for the resilient enough crystals.

For complexes in which single crystal structural data cannot be successfully collected and solved, the alternative often resides in powder X-ray diffraction (PXRD) technique. A common method, particularly used for 1,2,4-triazole based complexes, consists then in collecting single crystal structural data on analogous complexes and use these to simulate and compare with the PXRD data of the studied material;¹¹⁰ while these comparisons are usually only qualitative, they often provide a good indication of the cell parameters and packing arrangements of the *SCO* material. A similar approach can sometimes be used for complexes in which a very small change to the ligand is made; as examples, the comparison between PXRD patterns of complexes $[\text{Fe}^{\text{II}}(\text{L})_2(\text{NCX})_2]$ (where $\text{X} = \text{S}, \text{Se}, \text{BH}_3$) - obtained at different temperatures - provided plots of cell axes lengths or volume *vs.* T , as these revealed the spin transition in a similar way than susceptibility *vs.* T plots. Such data can also confirm the occurrence of structural phase changes.¹¹¹

In summary, both single crystal and powder X-ray diffraction techniques can yield detailed structural insights into the *SCO* phenomenon and have been extensively used within the field.

6.2.3. Magnetic and Photo-Magnetic Measurements

From the beginning of *SCO* research, the *SCO* behaviour has been mostly and primarily investigated using the magnetic susceptibility measurements. Indeed, the magnetic susceptibility of a compound is measured as a function of temperature, $\chi_M T$, and has been the most specific characterization method for *SCO* materials. The magnetic susceptibility ($\chi_M T$) is a value that represents the degree of magnetisation of a sample in an applied magnetic field. As the spin transition occurs from *HS* to *LS*, with decreasing temperature, the evolution of the magnetic susceptibility is measured. The different number of unpaired electrons in the *HS* and *LS* states - e.g. with four unpaired electrons in the strongly paramagnetic *HS* state and no unpaired electrons in the diamagnetic *LS* state in the case of Fe^{II} - is readily signaled by a drastic change in the $\chi_M T$ product; the latter can be then calculated by using the following equations:

$$\chi_M T = \gamma_{\text{HS}} T \cdot \chi_{\text{HS}} + \gamma_{\text{LS}} (1-T) \cdot \chi_{\text{LS}} = g^2 \cdot [S(S+1)/7.997] \quad (3)$$

Where γ_{HS} is the molar fraction of *HS* molecules, and χ_{HS} and χ_{LS} refer to the magnetic susceptibilities of the sample in the pure *HS* and *LS* states, which can be measured at sufficiently high and low temperatures, respectively, in the case of a complete spin state transition. This equation (3) can be also converted to the magnetic moment (μ_{eff}) via the equation (4).

$$\begin{aligned} \mu_{\text{eff}} &= 2.828 \cdot \sqrt{\chi_M T} && \text{in Bohr magneton, } \mu_B \text{ units} && (4) \\ \text{also, } \mu_{\text{eff}}^2 &= g^2 \cdot S(S+1) && \text{where for 'spin only' } g = 2.0 \end{aligned}$$

The *SCO* curve γ_{HS} vs T can be readily obtained with these quantities. One can also derive the effective magnetic moment $\mu_{\text{eff}} = 2.83 \cdot \sqrt{\chi_M T}$ and plot it as a function of temperature T .^{1a,112} However, because of certain complications, e.g. orbital contributions and zero-field splitting effects, it has become rather common to study the *SCO* behavior by plotting the γ_{HS} vs T function rather than the magnetic moment μ_{eff} vs T .

As a result, the expected spin-only value of $HS\text{ Fe}^{\text{II}}$, with $S = 2$, $g = 2.0$, corresponds to a $\chi_M T$ of $3.01\text{ cm}^3\cdot\text{K}\cdot\text{mol}^{-1}$. Accordingly, the $LS\text{ Fe}^{\text{II}}$ which should have no contribution to paramagnetism, and should present a $\chi_M T$ value equal or close to $0.0\text{ cm}^3\cdot\text{mol}^{-1}\cdot\text{K}$; however, in reality, the $LS\text{ Fe}^{\text{II}}$ shows a small positive $\chi_M T$ value due to second order spin-orbit coupling which induces temperature independent paramagnetism.¹⁶ The magnetic susceptibility measurements for this project have been performed at ICMCB (Institut de Chimie de la Matière Condensée de Bordeaux) with the use of a Superconducting Quantum Interference Device (or SQUID), a sensitive instrument which may be used to measure magnetic susceptibility values between 400-2 K. The preparation of dry, stable samples for magnetic susceptibility measurements involves placing the sample in a small plastic capsule, often in a small amount of paraffin mull to avoid “torquing” of the sample in a magnetic field, which can give rise to anomalous results for the anisotropic $\text{Fe}^{\text{II}}\text{ HS}$ state. The samples which contain solvent in their crystal lattice need to be measured with care, so as to ensure samples are measured in their solvated state.

Referring to photo-magnetic studies (LIESST or reverse-LIESST effects), the characteristic T_{LIESST} is commonly determined *via* the following procedure: after slow cooling at low temperature (e.g. 10 K), the sample ion in the LS state is then irradiated with a green laser (514nm, $^1A_1 \rightarrow ^1T_{1g}$ absorption band); as a result, the $\chi_M T$ value is found to increase rapidly, and usually after a delay of approx. one hour, a photo-stationary limit is reached. The light irradiation is then switched off, and the temperature is increased at a typical rate of $0.3\text{ K}\cdot\text{min}^{-1}$ while the magnetic susceptibility is measured. At low temperatures, the $HS \rightarrow LS$ relaxation is controlled by the tunneling process up to *ca.* 40 K, and therefore the kinetics is very slow with respect to the time scale of the experiment. Indeed, the time required to record the data up to 40K is approximately three hours. Above *ca.* 40 K, the system reaches the thermally activated domain, and the $HS \rightarrow LS$ relaxation becomes increasingly more rapid. As a result of this behavior, $\chi_M T$ remains nearly constant as T increases from 10 K up to 40 K, and then drops rapidly. In fact, a slight increase of $\chi_M T$ is usually observed between 10 to *ca.* 20 K, owing to the zero-field splitting within the spin quintet HS state. The $d\chi_M T/dT$ vs. T plot shows a minimum at a temperature that is defined as the T_{LIESST} value; at this temperature, the light-induced information is erased in the SQUID setup.

6.2.4. Differential Scanning Calorimetry (DSC)

The Differential Scanning Calorimetry (DSC) is a very sensitive technique to probe the molecular motions and intermolecular interactions in the degree of short-range or long-range order in the condensed states of matter. Consequently, it is a very powerful tool to detect and study phase transitions, and to further characterize and better understand *SCO* materials.¹¹³ The *SCO* derivatives as solids are molecular-based materials experiencing thermally induced phase transitions in which a change in the electronic state is strongly coupled with lattice transformations.^{1b,1c,1e} Thermodynamical parameters of the *SCO* materials such as the changes of enthalpy $\Delta H = H_{HS} - H_{LS}$ and entropy $\Delta S = S_{HS} - S_{LS}$ provide valuable information regarding the *SCO* properties, in particular cooperative interactions and the order of the spin transition. For *SCO* materials, the enthalpy changes $\Delta H = H_{HS} - H_{LS}$ are typically 10 to 20 kJ.mol⁻¹, while entropy changes $\Delta S = S_{HS} - S_{LS}$ are on the order of 50 to 80 J.mol⁻¹.K⁻¹.¹¹³ The thermally induced *SCO* phenomenon is an entropy driven process because the degree of freedom is much higher in the *HS* state than in the *LS* state, which reveals the lower distances between the vibrational levels in the *HS* state as compared to the *LS* state. Relatively 25% of the total entropy loss when going from *HS* to *LS* is of magnetic origin, viz. it results from the switch in spin states, $\Delta S = R[\ln(2S + 1)_{HS} - \ln(2S + 1)_{LS}] \approx 13.4 \text{ J.K}^{-1}.\text{mol}^{-1}$, and the extensive part originates from the variations in the intramolecular, and to a much lesser extent, intermolecular vibrations.^{8b,8c}

The first detailed calorimetric study by Sorai and Seki on [Fe(phen)₂(NCX)₂] (X = S, Se) in 1972 proved the presence of strong cooperative intermolecular interactions with the observation of sharp heat capacity peaks.^{8c} For qualitative information regarding the enthalpy change ΔH , the entropy change ΔS , the transition temperature $T_{1/2}$, and the occurrence of hysteresis, DSC measurements performed down to liquid-nitrogen temperatures are sufficient in most cases.¹¹⁴

6.2.5 Other techniques

There are various other methods and techniques to characterize a spin transition. Among those additional techniques can be mentioned the Extended X-ray Absorption Fine Structure

(EXAFS) that is used to obtain structural information of *SCO* systems, particularly when it is not possible to obtain appropriate crystals for X-ray diffraction. Also, the X-ray absorption near edge structure (XANES) is employed to infer geometry and oxidation states of *SCO* samples. The X-ray emission spectroscopy (XES) provides a detailed element-specific picture of the local electronic structure around a given atomic site. The emitted radiation is dominated by the decay of valence electrons of the excited atomic center; in the case of highly oriented systems, angular-dependent XES enables the separation of states of different symmetry of the involved orbitals. The Nuclear Forward Scattering (NFS) is a powerful technique that is capable of assessing hyperfine interactions in condensed matter. The Inelastic Neutron Scattering (INS) is used to study atomic and molecular motion as well as magnetic and crystal field excitations; it distinguishes itself from other neutron scattering techniques by resolving the change in kinetic energy that occurs when the collision between neutrons and the sample is inelastic.

Moreover, paramagnetic temperature-dependent NMR spectroscopy can be used to determine the magnetic susceptibility of a compound, especially in solution. However, the temperature range of this method is limited to the cold and boiling point of the solvent. The experimental NMR setup is known as the Evans-method,¹¹⁵ which compares the absolute shifting of the nuclei in a paramagnetic solution with a diamagnetic reference by using an external reference signal. For some complexes, the *SCO* in solution can be directly evaluated by interpretation of the temperature-dependence of their ¹H NMR chemical shifts, rather than interpreting the susceptibility.¹¹⁶

Finally, the Mössbauer spectroscopy is a useful spectroscopic analysis for iron containing compounds due to its abilities to provide information on the spin state and oxidation state, as well as providing information which may help to indicate the molecular structure of a material.^{1b,117} The two most important parameters obtained from Mössbauer spectroscopy are the isomer shift δ , and the quadrupole splitting ΔEQ as those two values differ significantly between Fe^{II} *HS* and Fe^{II} *LS* states.¹¹⁸ Because ⁵⁷Fe Mössbauer spectroscopy for iron compounds gives information on the respective mole fractions of the different spin states, and oxidation states in a system (from peak areas), it can be used, for example, in determining whether a compound which shows a reduction in susceptibility with temperature is undergoing *SCO* or if exchange coupling is occurring.¹¹⁸

Bibliography

1. (a) O. Kahn, *Molecular Magnetism*, WILEY-VCH, New York, **1993**; (b) P. Gütlich, H. A. Goodwin, in *Spin Crossover in Transition Metal Compounds*, Springer-Verlag, Berlin/Heidelberg, **2004**, 233, 234, 235; (c) P. Gütlich, A. Hauser, H. Spiering, *Angew. Chem. Int. Ed. Engl.*, **1994**, 33, 2024-2054; (d) P. Gütlich, Y. Garcia, H. Spiering, *Spin Transition Phenomenon in Magnetism: Molecules to Materials IV*; J. S. Miller, M. Drillon, Eds.; Wiley-CH Verlag: Weinheim, Germany, **2003**, 271-344; (e) P. Gütlich, Y. Garcia, H. A. Goodwin, *Chem. Soc. Rev.*, **2000**, 29, 419-427; (f) F. A. Cotton, G. Wilkinson, C. A. Murillo, M. Bochmann, *Advanced Inorganic Chemistry 6th Ed.*, John Wiley & Sons, New York, **1999**; (g) J. A. Kitchen, S. Brooker, *Coord. Chem. Rev.*, **2008**, 252, 2072; (h) K. S. Murray, *Eur. J. Inorg. Chem.*, **2008**, 3101; (i) M. A. Halcrow, *Coord. Chem. Rev.*, **2009**, 2059.
2. (a) O. Kahn, C. Kröber, C. Jay, *Adv. Mater.*, **1992**, 4, 718-728; (b) O. Kahn, C. J. Martinez, *Science*, **1998**, 279, 44; (c) O. Kahn, C. Jay Martinez, J. Kröber, R. Claude, F. Grolière, *Patent* EP0666561, **1995**; (d) J.-F. Létard, O. Nguyen, N. Daro, *Patent* FR0512476, **2005**; (e) A. Galet, A. B. Gaspar, M. C. Munoz, G. V. Bukin, G. Levchenko, J. A. Real, *Adv. Mater.*, **2005**, 17, 2949; (f) Y. Garcia, V. Kseofontov, S. Mentior, M. M. Dîrtu, C. Gieck, A. Bhatthacharjee, P. Gütlich, *Chem. Eur. J.*, **2008**, 14, 3745.
3. (a) M. Paez-Espejo, M. Sy, K. Boukheddaden, *J. Am. Chem. Soc.*, **2016**, 138, 9, 3202; (b) M. Sy, D. Garrot, A. Slimani, M. Paez-Espejo, F. Varret, K. Boukheddaden, *Angew. chem. Int. Ed.*, **2016**, 55, 5, 1755; (c) N. Willenbacher, H. Spiering, *J. Phys. C.: Solid State Phys.*, **1988**, 21, 1423.
4. (a) L. Cambi, L. Szegö, *Ber. Deutsch. Chem. Ges.*, **1931**, 64, 2591-2598; (b) L. Cambi, L. Szegö, *Ber. Deutsch. Chem. Ges.*, **1933**, 66, 656-661; (c) L. Cambi, L. Malatesta, *Ber. Deutsch. Chem. Ges.*, **1937**, 70, 2067-2078; (d) L. Cambi, L. Szego, A. Cagnasso, *Atti accad. Lincei.*, **1931**, 13, 168; (e) L. Cambi, L. Szego, *Atti accad. Lincei.*, **1931**, 15, 329.
5. R. C. Stouffer, D. H. Busch, W. B. Hadley, *J. Am. Chem. Soc.*, **1961**, 83, 3732.

6. K. Madeja, E. König, *Inorg. Nucl. Chem.*, **1963**, 25, 377.
7. (a) E. K. Barefield, D. H. Busch, S. M. Nelson, *Quart. Rev. Chem. Soc.*, **1968**, 22, 457; (b) L. Sacconi, *Coord. Chem. Rev.*, **1972**, 8, 351; (c) E. König, *Coord. Chem. Rev.*, **1968**, 3, 471; (d) R. L. Martin, A. H. White, *Trans. Met. Chem.*, **1968**, 4, 113.
8. (a) M. Sorai, J. Ensling, P. Gülich, *Chem. Phys.*, **1976**, 18, 199-209; (b) M. Sorai, S. Seki, *J. Phys. Soc. Jpn.*, **1972**, 33, 575; (c) M. Sorai, S. Seki, *J. Phys. Chem. Solids*, **1974**, 35, 555-570; (d) H. Spiering, E. Meissner, H. Köpen, E. W. Müller, P. Gülich, *Chem. Phys.*, **1982**, 68, 65; (e) H. A. Goodwin, *Coord. Chem. Rev.*, **1976**, 18, 293; (f) P. Gülich, *Struct. Bonding (Berlin)*, **1981**, 44, 83; (g) E. König, G. Ritter, S. K. Kulshreshtha, *Chem. Rev.*, **1985**, 85, 219; (h) J. K. Beattie, *Adv. Inorg. Chem.*, **1988**, 32, 1.
9. (a) E. König, *Struct. Bonding (Berlin)*, **1991**, 76, 5; (b) P. Gülich, A. Hauser, *Coord. Chem. Rev.*, **1990**, 97, 1; (c) J. Zarembovitch, O. Kahn, *New J. Chem.*, **1991**, 15, 181; (d) P. Gülich, *Nucl. Instrum. Methods Phys. Res. B*, **1993**, 76, 387.
10. (a) S. Decurtins, P. Gülich, C. P. Köhler, H. Spiering, A. Hauser, *Chem. Phys. Lett.*, **1984**, 104, 1; (b) S. Decurtins, P. Gülich, K. M. Hasselbach, A. Hauser, H. Spiering, *Inorg. Chem.*, **1985**, 24, 2174.
11. (a) J. J. McGarvey, I. Lawthers, *J. Chem. Soc. Chem. Commun.*, **1982**, 16, 906; (b) I. Lawthers, J. J. McGarvey, *J. Am. Chem. Soc.*, **1984**, 106, 4280; (c) See also: C. Brady, J. J. McGarvey, J. K. McCusker, H. Toftlund, D. N. Hendrickson, *Top. Curr. Chem.*, **2004**, 235, 1.
12. (a) P. L. Franke, J. G. Haasnoot, A. P. Zuur, *Inorg. Chim. Acta.*, **1982**, 59, 5-9; (b) E. W. Müller, J. Ensling, Spiering, H.; Gülich, P. *Inorg. Chem.*, **1983**, 22, 2074-2078.
13. A. Hauser, *Chem. Phys. Lett.*, **1986**, 124, 543-548.
14. O. Roubeau, *Chem. Eur. J.*, **2012**, 18, 15230-5244 and references therein.

15. (a) A. Hauser, *Adv Polym Sci.*, **2004**, 233, 49.; (b) N. Figgis, M. A. Hitchman, "Ligand Field Theory and its Applications", Wiley, **1966**.
16. N. Bridonneau, J. Long, J.-L. Cantin, J. von Bardeleben, S. Pillet, E.-E. Bendeif, D. Aravena, E. Ruizd and V. Marvaud, *Chem. Commun.*, **2015**, 51, 8229-8232.
17. (a) P. Gütlich, Y. Garcia, H. A. Goodwin, *Chem. Soc. Rev.*, **2000**, 29, 419; (b) X.-H. Zhao, S.-L. Zhang, D. Shao, X.-Y. Wang, *Inorg. Chem.*, **2015**, 54, 7857-7867; (c) P. Guionneau, *Dalton Trans.*, **2014**, 43, 382-393; (d) P. Chakraborty, R. Bronisz, C. Besnard, L. Guénée, P. Pattison, A. Hauser, *J. Am. Chem. Soc.*, **2012**, 134, 4049-4052; (e) C. Atmani, F. El Hajj, S. Benmansour, M. Marchivie, S. Triki, F. Conan, V. Patinec, H. Handel, G. Dupouy, C. J. Gómez-García, *Coord. Chem. Rev.*, **2010**, 254, 1559-1569; (f) L. Capes, J.-F. Létard, O. Kahn, *Chem. Eur. J.*, **2000**, 6, 2246-2255; (g) G. Dupouy, M. Marchivie, S. Triki, J. Sala-Pala, C. J. Gómez-García, S. Pillet, C. Lecomte, J.-F. Létard, *Chem. Commun.*, **2009**, 3404-3406; (h) M. Marchivie, P. Guionneau, J. A. K. Howard, G. Chastanet, J.-F. Létard, A. E. Goeta, D. Chasseau, *J. Am. Chem. Soc.*, **2002**, 124, 194-195; (i) V. Niel, M. C. Muñoz, A. B. Gaspar, A. Galet, G. Levchenko, J.-A. Real, *Chem. Eur. J.*, **2002**, 8, 2446-2453; (j) J. P. Costes, F. Dahan, J. P. Laurent, *Inorg. Chem.*, **1990**, 29, 2448-2452; (k) Y. Garcia, V. Niel, M. C. Muñoz, J.-A. Real, *Top. Curr. Chem.*, **2004**, 233, 229; (l) S. Hayami, R. Moriyama, Y. Shigeyoshi, R. Kawajiri, T. Mitani, M. Akita, K. Inoue, Y. Maeda, *Inorg. Chem.*, **2005**, 44, 7295-7297; (m) R. Ishikawa, K. Matsumoto, K. Onishi, T. Kubo, A. Fuyuhiko, S. Hayami, K. Inoue, S. Kaizaki, S. Kawata, *Chem. Lett.*, **2009**, 38, 620-621; (n) G. G. Morgan, K. D. Murnaghan, H. Muller-Bunz, V. McKee, C. J. Harding, *Angew. Chem. Int. Ed.*, **2006**, 45, 7192-7195.
18. G. W. E. R. H. Holm, Jr., A. Chakavorty, *Prog. Inorg. Chem.*, **1966**, 7, 83.
19. (a) S. Imatomi, T. Sato, T. Hamamatsu, R. Kitashima, N. Matsumoto, *Bull. Chem. Soc. Jpn.*, **2007**, 80, 2375-2377; (b) K. S. Murray, *Eur. J. Inorg. Chem.*, **2008**, 3101-3121; (c) M. Quesada, P. de Hoog, P. Gamez, O. Roubeau, G. Aromí, B. Donnadieu, C. Massera, M. Lutz, A. L. Spek, J. Reedijk, *Eur. J. Inorg. Chem.*, **2006**, 1353-1361; (d) J. Wagner, H. Görls, H. Keutel, *Inorg. Chim. Acta.*, **2005**, 358, 808-813; (e) P. A. Anderson, T.

- Astley, M. A. Hitchman, F. R. Keene, B. Moubaraki, K. S. Murray, B. W. Skelton, E. R. T. Tiekink, H. Toftlund, A. H. White, *J. Chem Soc., Dalton Trans.*, **2000**, 3505-3512; (f) J. A. Real, H. Bolvin, A. Bousseksou, A. Dworkin, O. Kahn, F. Varret, J. zarembowitch, *J. Am. Chem. Soc.*, **1992**, *114*, 4650-4658; (g) J. A. Real, A. B. Gaspar, V. Niel, M. C. Muñoz, *Coord. Chem. Rev.*, **2003**, *236*, 121-141; (h) E. König, G. Ritter, S. K. Kulshreshtha, J. Waigel, L. Sacconi, *Inorg. Chem.*, **1984**, *23*, 1241-1246; (i) Ross W. Hogue, Humphrey L. C. Feltham, Reece G. Miller, and Sally Brooker, *Inorg. Chem.*, **2016**, *55*, 4152-4165; (j) A. Arroyave, A. Lennartson, A. Dragulescu-Andrasi, K. S. Pedersen, S. Piligkos, S. A. Stoian, S. M. Greer, C. Pak, O. Hietsoi, H. Phan, S. Hill, C. J. McKenzie, and M. Shatruk, *Inorg. Chem.*, **2016**, *55*, 5904-5913
20. (a) V. Gómez, C. Sáenz de Pipaón, P. Maldonado-Illescas, J.-C. Waerenborgh, E. Martin, J. Benet-Buchholz, J.-R. Galán-Mascarós, *J. Am. Chem. Soc.*, **2015**, *137*, 11924-11927; (b) P. Gülich, A.-B. Gaspar, Y. Garcia, *Beilstein J. Org. Chem.*, **2015**, *9*, 342-391; (c) S. Brooker, *Chem. Soc. Rev.*, **2015**, *44*, 2880-2892; (d) M. Shatruk, H. Phan, B. A. Chrisostomo, A. Suleimenova, *Coord. Chem. Rev.*, **2015**, *289-290*, 62-73; (e) M.-Y. Chen, X.-R. Chen, W.-H. Ninga, X.-M. Ren, *RSC Adv.*, **2014**, *4*, 39126-39131; (f) J. Olguin, S. Brooker, *Coord. Chem. Rev.*, **2011**, *255*, 203-240; (g) M. A. Halcrow, *Chem. Soc. Rev.*, **2011**, *40*, 4119-4142; (h) A. Bousseksou, G. Molnar, L. Salmon, W. Nicolazzi, *Chem. Soc. Rev.*, **2011**, *40*, 3313-3335; (i) Y. Garcia, F. Robert, A.-D. Naik, G. Zhou, B. Tinant, K. Robeyns, S. Michotte, L. Piraux, *J. Am. Chem. Soc.*, **2011**, *133*, 15850-15853; (j) G. Félix, K. Abdul-Kader, T. Mahfoud, I. A. Gural'skiy, W. Nicolazzi, L. Salmon, G. Molnar, A. Bousseksou, *J. Am. Chem. Soc.*, **2011**, *133*, 15342-15345; (k) P. Gamez, J. Sanchez Costa, M. Quesada, G. Aromi, *Dalton trans.*, **2009**, 7845-7853; (l) S. Titos-Padilla, J. M. Herrera, X.-W. Chen, J. J. Delgado, E. Colacio, *Angew. Chem. Int. Ed.*, **2011**, *50*, 3290-3293; (m) F. Setifi, S. Benmansour, M. Marchivie, G. Dupouy, S. Triki, J. Sala-Pala, J.-Y. Salaün, C. J. Gómez-García, S. Pillet, C. Lecomte, E. Ruiz, *Inorg. Chem.*, **2009**, *48*, 1269-1271; (n) S. M. Neville, G. J. Halder, K. W. Chapman, M. B. Duriska, P. D. Southon, J. D. John D. Cashion, J.-F. Letard, B. Moubaraki, K. S. Murray, C. J. Kepert, *J. Am. Chem. Soc.*, **2008**, *130*, 2869-2876; (o) N. Ortega-Villar, M. C. Muñoz, J. A. Real, *Magnetochem.*, **2016**, *2*, 16.

21. (a) G. Dupouy, M. Marchivie, S. Triki, J. Sala-Pala, J.-Y. Salaün, C. J. Gómez-García, P. Guionneau, *Inorg. Chem.*, **2008**, *47*, 8921-8931; (b) P. Guionneau, M. Marchivie, G. Bravic, J.-F. Létard, D. Chasseau, *Top. Curr. Chem.*, **2004**, *234*, 97-128; (c) M. Marchivie, P. Guionneau, J.-F. Létard, D. Chasseau, *Acta Cryst. B*, **2005**, *B61*, 25-28.
22. (a) L. G. Lavrenova, O. G. Shakirova, *Eur. J. Inorg. Chem.*, **2013**, 5-6, 670; (b) A. Vallée, C. Train, C. Roux, *J. Chem. Educ.*, **2013**, *90*, 1071.
23. K. Sone, Y. Fukuda, *Inorganic Thermochromism*, Springer, Berlin, **1987**.
24. (a) P. Gütllich, H. A. Goodwin (Eds.), *Spin Crossover in Transition Metal Compounds*, in: *Topics in Current Chemistry*, Springer, Berlin, **2004**, vol. *I-III*, 233-235. (b) P. Gamez, J. S. Costa, M. Quesada, G. Aromí, *Dalton Trans.*, **2009**, 7845.
25. (a) S. Kobo, G. Molnár, J. A. Real, A. Bousseksou, *Angew. Chem.*, **2006**, *118*, 5918-5921; (b) *Angew. Chem. Int. Ed.*, **2006**, *45*, 5786-5789.
26. A. Bousseksou, G. Molnar, P. Demont, J. Menegotto, *J. Mater. Chem.*, **2003**, *13*, 2069.
27. M. Matsuda, H. Tajima, *Chem. Lett.*, **2007**, *36*, 700.
28. K. S. Murray, C. J. Kepert, *Top. Curr. Chem.*, **2004**, *233*, 195.
29. (a) M. H. Klingele, B. Moubaraki, J. D. Cashion, K. S. Murray, S. Brooker, *Chem. Comm.*, **2005**, 987-989; (b) M. H. Klingele, B. Moubaraki, J. D. Cashion, K. S. Murray, S. Brooker, *Chem. Eur. J.*, **2005**, *11*, 6962.
30. (a) T. Buchen, P. Gütllich, H. Toftlun, *Chem. Eur. J.*, **1996**, *2*, 1129; (b) T. Buchen, D. Schollmeyer, P. Gütllich, *Inorg. Chem.*, **1996**, *35*, 155.
31. (a) C. Baldé, C. Desplanches, M. Grunert, Y. Wei, P. Gütllich, J. F. Létard, *Eur. J. Inorg. Chem.*, **2008**, *34*, 5382; (b) C. Baldé, C. Desplanches A. Wattiaux, P. Guionneau, P. Gütllich, J.-F. Létard, *Dalton Trans.*, **2008**, *20*, 2702; (c) M. Clemente-León, E. Coronado, M. López-Jordà, C. Desplanches, S. Asthana, H. Wang, J.-F. Létard, *Chem. Sci.*, **2011**, *2*, 1121; (d) C. Faulmann, J. Chahine, L. Valade, G. Chastanet, J. F. Létard, D.

- de Caro, *Eur. J. Inorg. Chem.*, **2013**, 1058; (e) N. Paradis, G. Chastanet, J. F. Létard, *Eur. J. Inorg. Chem.*, **2012**, 3618.
32. (a) S. Bonhommeau, G. Molnar, A. Galet, A. Zwick, J. A. Real, J. J. McGarvey, A. Bousseksou, *Angew. Chem. Int. Ed.*, **2005**, 44, 26, 4069; (b) S. Cobo, D. Ostrovskii, S. Bonhommeau, L. Vendier, G. Molnar, L. Salmon, K. Tanaka, A. Bousseksou, *J. Am. Chem. Soc.*, **2008**, 130, 9019-9024.
 33. A. Hauser, *Light-Induced Spin Crossover and the High-Spin→Low-Spin Relaxation. In Spin Crossover in Transition Metal Compounds II*; P. Gülich, H. A. Goodwin, Eds.; *Top. Curr. Chem.*; Springer-Verlag: Berlin, Heidelberg, **2004**, 234, 155-198.
 34. J. F. Létard, P. Guionneau, O. Nguyen, J. S. Costa, S. Marcén, G. Chastanet, M. Marchivie, L. Goux-Capes, *Chem. Eur. J.*, **2005**, 11, 4582.
 35. (a) M. Yamada, H. Hagiwara, H. Torigoe, N. Matsumoto, M. Kojima, F. Dahan, J. P. Tuchagues, N. Re, S. Iijima, *Chem. Eur. J.*, **2006**, 12, 4536; (b) H. S. Scott, T. M. Ross, B. Moubaraki, S. M. Neville, K. S. Murray, *Eur. J. Inorg. Chem.*, **2013**, 803-812; (c) B. J. Kennedy, A. C. McGrath, K. S. Murray, B. W. Skelton, A. H. White, *Inorg. Chem.*, **1987**, 26, 483; (d) M. M. Dîrtu, D. Gillard, A. D. Naik, A. Rotaru, Y. Garcia, *Hyperfine Interact.*, **2012**, 205, 75; (e) M. Tafili-Kryeziu, M. Weil, T. Muranaka, A. Bousseksou, M. Hasegawa, A. Jun, W. Linert, *Dalton Trans.*, **2013**, 42, 15796; (f) G. Lemerrier, N. Brefuel, S. Shova, J. A. Wolny, F. Dahan, M. Verelst, H. Paulsen, A. X. Trautwein, J. P. Tuchagues, *Chem. Eur. J.*, **2006**, 12, 7421.
 36. (a) M. Enamullah, M. N. Uddin, D. Hossain, M. Kabir, A. Awwal, W. Linert, *J. Coord. Chem.*, **2000**, 49, 171; (b) C. Rajadurai, Z. Qu, O. Fuhr, B. Gopalan, R. Kruk, M. Ghafari, M. Ruben, *Dalton Trans.*, **2007**, 32, 3531; (c) Y. Garcia, P. J. van Koningsbruggen, R. Lapouyade, L. Fournés, L. Rabardel, O. Kahn, V. Ksenofontov, G. Levchenko, P. Gülich, *Chem. Mater.*, **1998**, 10, 2426.
 37. (a) J. F. Létard, L. Capes, G. Chastanet, N. Moliner, S. Létard, J. A. Real, O. Kahn, *Chem. Phys. Lett.*, **1990**, 313, 115; (b) J. F. Létard, *J. Mater. Chem.*, **2006**, 16, 2550; (c) L. Capes, J. F. Létard, O. Kahn, *Chem. Eur. J.*, **2000**, 6, 2246; (d) D. J. Harding, W.

- Phonsri, P. Harding, I. A. Gass, K. S. Murray, B. Moubaraki, J. D. Cashion, L. Liu, S. G. Telfer, *Chem. Commun.*, **2013**, 49, 634; (e) N. Wannarit, O. Roubeau, S. Youngme, P. Gamez, *Eur. J. Inorg. Chem.*, **2013**, 730.
38. A. Grosjean, *Matériaux Polymériques 1D à Transition de Spin : Investigations Structurales Multiechelles*, Thesis, Université de Bordeaux, **2013**.
39. H. L. Schläfer, G. Gliemann, *Einführung in die Ligandfeldtheorie*, Akademische Verlagsgesellschaft, Frankfurt/Main, **1967**.
40. (a) R. Claude, J. A. Real, J. Zarembowitch, O. Kahn, L. Ouahab, D. Grandjean, K. Boukheddaden, F. Varret, A. Dworkin, *Inorg. Chem.*, **1990**, 29, 4442-4448; (b) P. Spacu, M. Teodorescu, G. Filotti, P. Telniceanu, *Z. Anorg. Allg. Chem.*, **1972**, 392, 88-92.
41. (a) K. Madeja, E. König, *J. Inorg. Nucl. Chem.*, **1963**, 25, 377-385; (b) E. W. Müller, H. Spiering, P. Gülich, *Chem. Phys. Lett.*, **1982**, 93, 567-571; (c) J. A. Real, B. Gallois, T. Granier, F. Suez-Panama, J. Zarembowitch, *Inorg. Chem.*, **1992**, 31, 4972-4979.
42. J. Fleisch, P. Gülich, K. M. Hasselbach, W. Müller, *J. Phys., Colloq.*, **1974**, 6, 659-662.
43. (a) P. J. van Koningsbruggen, Y. Maeda, H. Oshio, *Top. Curr. Chem.*, **2004**, 233, 259-324; (b) S. Hayami, Y. Komatsu, T. Shimizu, H. Kamihata, Y. H. Lee, *Coord. Chem. Rev.*, **2011**, 255, 1981-1990; (c) R. W. Hogue, H. L. C. Feltham, R. G. Miller, Sally Brooker, *Inorg. Chem.*, **2016**, 55 (9), 4152-4165; (d) J. Olguin, S. Brooker, *Coord. Chem. Rev.*, **2011**, 255, 203-240; (e) G. Aromia, L. A. Barriosa, O. Roubeaub, P. Gamez, *Coord. Chem. Rev.*, **2011**, 255, 485-546; (f) M. A. Halcrow, *Polyhedron*, **2007**, 26, 3523-3576.
44. X. -H. Zhao, S. -L. Zhang, D. Shao, X. -Y. Wang, *Inorg. Chem.*, **2015**, 54 (16), 7857-7867.
45. M. Sorai, J. Ensling, K. M. Hasselbach, P. Gülich, *Chem. Phys.*, **1977**, 20, 197-208.
46. L. G. Lavrenova, E. V. Kirillova, V. N. Ikorskii, Yu. G. Shvedenkov, V. A. Varnek, L. A. Sheludyakova, S. V. Larionov, *Russ. J. Coord. Chem.*, **2001**, 27, 46 (Engl. Transl.).

47. (a) S. Bonhommeau, G. Molnar, A. Galet, A. Zwick, J. A. Real, J. J. McGarvey, A. Bousseksou, *Angew. Chem., Int. Ed. Engl.*, **2005**, *44*, 4069-4073; (b) G. Ritter, E. König, W. Irlner, H. A. Goodwin, *Inorg. Chem.*, **1978**, *17*, 224-228; (c) S. Hayami, R. Moriyama, Y. Shigeyoshi, R. Kawajiri, T. Mitani, M. Akita, K. Inoue, Y. Maeda, *Inorg. Chem.*, **2005**, *44*, 7295-7297; (d) J. Kröber, E. Codjovi, O. Kahn, F. Groliere, C. Jay, *J. Am. Chem. Soc.*, **1993**, *115*, 9810-9811; (e) J. A. Real, M. C. Muñoz, E. Andres, T. Granier, B. Gallois, *Inorg. Chem.*, **1994**, *33*, 3587-3594; (f) X. Solans, F. Lloret, J. A. Real, *Inorg. Chem.*, **1998**, *37*, 5102-5108; (g) W. Vreugdenhil, J. H. Van Diemen, R. A. G. De Graaff, J. G. Haasnoot, J. Reedijk, A. M. Van der Kraan, O. Kahn, J. Zarembowitch, *Polyhedron*, **1990**, *9*, 2971-2979.
48. (a) P. Gütlich, H. A. Goodwin, *Top. Curr. Chem.* **2004**, *233*, 1-47; (b) E. Milin, B. Benaicha, F. El Hajj, V. Patinec, S. Triki, M. Marchivie, C. J. Gómez-García, S. Pillet, *Eur. J. Inorg. Chem.*, **2016**; DOI: 10.1002/ejic.201600660.
49. (a) P. J. van Koningsbruggen, Y. Garcia, E. Codjovi, R. Lapouyade, O. Kahn, L. Fournès, L. Rabardel, *J. Mater. Chem.*, **1997**, *7*, 2069-2075; (b) F. J. Munoz-Lara, A. B. Gaspar, M. C. Munoz, A. B. Lysenko, K. V. Domasevitch, J. A. Real, *Inorg. Chem.*, **2012**, *51*, 13078.
50. (a) P. Chakraborty, C. Enachescu, C. Walder, R. Bronisz, A. Hauser, *Inorg. Chem.*, **2012**, *51*, 9714-9722.
51. (a) S. Zheng, M. A. Siegler, J. S. Costa, W. -T. Fu, S. Bonnet, *Eur. J. Inorg. Chem.*, **2013**, 1033-1042; (b) C. Baldé, C. Desplanches, F. Le Gac, P. Guionneau, J. -F. Létard, *Dalton Trans.*, **2014**, *43*, 7820-7829
52. (a) O. Kahn, E. Codjovi, *Phil. Trans. R. Soc. Lond. A*, **1996**, *354*, 359; (b) J. G. Hasnoot, *Coord. Chem. Rev.*, **2000**, *131*, 200.
53. (a) Y. Sunatsuki, H. Ohta, M. Kojima, Y. Ikuta, Y. Goto, N. Matsumoto, S. Iijima, H. Akashi, S. Kaizaki, F. Dahan, J. P. Tuchagues, *Inorg. Chem.*, **2004**, *43*, 4154; (b) B. Weber, W. Bauer, J. Obel, *Angew. Chem. Int. Ed.*, **2008**, *47*, 10098; (c) C. Rajadurai, F.

- Schramm, S. Brink, O. Fuhr, M. Ghafari, R. Kruk, M. Ruben, *Inorg. Chem.*, **2006**, *45*, 10019.
54. S. Hayami, K. Hiki, T. Kawahara, Y. Maeda, D. Urakami, K. Inoue, M. Ohama, S. Kawata, O. Sato, *Chem. Eur. J.*, **2009**, *15*, 3497.
 55. P. Gütllich, H. Köppen, H. G. Steinhäuser, *Chem. Phys. Lett.*, **1980**, *74*, 475-480.
 56. (a) O. Kahn, J. Martinez, *Science*, **1998**, *279*, 44-48; (b) J. Kröber, E. Codjovi, O. Kahn, F. Groliere, C. Jay, *J. Am. Chem. Soc.*, **1993**, *115*, 9810-9811.
 57. (a) B. Gallois, J. A. Real, C. Hauw, J. Zarembowitch, *Inorg. Chem.*, **1990**, *29*, 1152-1158; (b) Z. J. Zhong, J. Q. Tao, Z. Yu, C. Y. Dun, Y. J. Liu, X. Z. You, *J. Chem. Soc., Dalton Trans.*, **1998**, *3*, 327-328.
 58. J. A. Real, B. Gallois, T. Granier, F. Suez-Panama, J. Zarembowitch, *Inorg. Chem.*, **1992**, *31*, 4972-4979.
 59. L. Salmon, A. Bousseksou, B. Donnadieu, J. P. Tuchagues, *Inorg. Chem.*, **2005**, *44*, 1763-1773.
 60. (a) P. Gütllich, *Struct. Bonding (Berlin)*, **1981**, *44*, 83-195; (b) D. Chernyshov, M. Hostettler, K. W. Törnroos, H. B. Bürgi, *Angew. Chem., Int. Ed. Engl.*, **2003**, *42*, 3825-3830; (c) M. Hostettler, K. W. Törnroos, D. Chernyshov, B. Vangdal, H. B. Bürgi, *Angew. Chem., Int. Ed. Engl.*, **2004**, *43*, 4589-4594.
 61. (a) Y. Garcia, P. Guionneau, G. Bravic, D. Chasseau, J. A. K. Howard, O. Kahn, V. Ksenofontov, S. Reiman, P. Gütllich, *Eur. J. Inorg. Chem.*, **2000**, *7*, 1531-1538; (b) M. Thomann, O. Kahn, J. Guilhem, F. Varret, *Inorg. Chem.*, **1994**, *33*, 6029-6037; (c) J. J. A. Kolnaar, G. van Dijk, H. Kooijman, A. L. Spek, V. G. Ksenofontov, P. Gütllich, J. G. Haasnoot, J. Reedijk, *Inorg. Chem.*, **1997**, *36*, 2433-2440.
 62. (a) C. Jay, F. Groliere, O. Kahn, J. Kröber, *Mol. Cryst. Liq. Cryst.*, **1993**, *234*, 255-262; (b) J. Kröber, R. Audière, R. Claude, E. Codjovi, O. Kahn, J. G. Haasnoot, F. Crolière, C. Jay, A. Bousseksou, J. Linares, F. Varret, A. Gonthier-Vassal, *Chem. Mater.*, **1994**, *6*,

- 1404-1412; (c) F. Armand, C. Badoux, P. Bonville, A. Ruaudel-Teixier, O. Kahn, *Langmuir*, **1995**, *11*, 3467-3472; (d) A. Michalowicz, J. Moscovici, B. Ducourant, D. Cracco, O. Kahn, *Chem. Mater.*, **1995**, *7*, 1833-1842.
63. K. Nakano, N. Suemura, S. Kawata, A. Fuyuhiko, T. Yagi, S. Nasu, S. Morimoto, S. Kaizaki, *Dalton Trans.*, **2004**, 982-988.
 64. K. Yoneda, K. Adachi, S. Hayami, Y. Maeda, M. Katada, A. Fuyuhiko, S. Kawata, S. Kaizaki, *Chem. Commun.*, **2006**, 45-47.
 65. Y. Garcia, O. Kahn, L. Rabardel, B. Chansou, L. Salmon, J. P. Tuchagues, *Inorg. Chem.*, **38**, 4663-4670.
 66. V. Gómez, C. Saenz de Pipaon, P. Maldonado-Illescas, J.C. Waerenborgh, E. Martin, J. Benet-Buchholz, J.R. Galan-Mascaros, *J. Am. Chem. Soc.*, **2015**, *137*(37), 11924-11927.
 67. (a) E. König, K. Madeja, J. K. Watson, *J. Am. Chem. Soc.*, **1968**, *90*, 1146-1153; (b) E. König, K. Madeja, *Inorg. Chem.*, **1967**, *6*, 48-57.
 68. (a) A. Ozarowski, B. R. McGarvey, A. B. Sarkar, J. E. Drake, *Inorg. Chem.*, **1988**, *27*, 628-635; (b) G. S. Matouzenko, A. Bousseksou, S. Lecocq, P. J. van Koningsbruggen, M. Perrin, O. Kahn, A. Collet, *Inorg. Chem.*, **1997**, *36*, 5869-5879; (c) P. Guionneau, J. F. Létard, D. S. Yufit, D. Chasseau, G. Bravic, A. E. Goeta, J. A. K. Howard, O. Kahn, *J. Mater. Chem.*, **1999**, *9*, 985-994; (d) M. Marchivie, P. Guionneau, J. F. Létard, D. Chasseau, *Acta Crystallogr., Sect. B: Struct. Sci.*, **2003**, *59*, 479-486; (e) A. Galet, A. B. Gaspar, M. C. Muñoz, G. Levchenko, J. A. Real, *Inorg. Chem.*, **2006**, *45*, 9670-9679; (f) N. Moliner, A. B. Gaspar, M. C. Muñoz, V. Niel, J. Cano, J. A. Real, *Inorg. Chem.*, **2001**, *40*, 3986-3991; (g) A. B. Gaspar, M. C. Muñoz, N. Moliner, V. Ksenofontov, G. Levchenko, P. Gütllich, J. A. Real, *Monatsh. Chem.*, **2003**, *134*, 285-294; (h) D. L. Reger, J. R. Gardinier, M. D. Smith, A. M. Shahin, G. J. Long, L. Rebbouh, F. Grandjean, *Inorg. Chem.*, **2005**, *44*, 1852-1866.
 69. J. Luan, J. Zhou, Z. Liu, B. Zhu, H. Wang, X. Bao, W. Liu, M. -L. Tong, G. Peng, H. Peng, L. Salmon, A. Bousseksou, *Inorg. Chem.*, **2015**, *54*, 5145-5147.

70. (a) E. W. Müller, H. Spiering, P. Gütllich, *Chem. Phys. Lett.*, **1982**, 93, 567-571; (b) J. Kröber, R. Audièrre, R. Claude, E. Codjovi, O. Kahn, J. G. Haasnoot, F. Crolière, C. Jay, A. Bousseksou, J. Linares, F. Varret, A. Gonthier-Vassal, *Chem. Mater.*, **1994**, 6, 1404-1412; (c) P. Ganguli, P. Gütllich, E. W. Mueller, W. Irlér, *J. Chem. Soc., Dalton Trans.*, **1981**, 2, 441-446; (d) E. W. Müller, H. Spiering, P. Gütllich, *Inorg. Chem.*, **1984**, 23, 119-120; (e) M. S. Haddad, W. D. Federer, M. W. Lynch, D. N. Hendrickson, *Inorg. Chem.*, **1981**, 20, 131-139; (f) M. S. Haddad, M. W. Lynch, W. D. Federer, D. N. Hendrickson, *Inorg. Chem.*, **1981**, 20, 123-131.
71. (a) M. S. Haddad, W. D. Federer, M. W. Lynch, D. N. Hendrickson, *J. Am. Chem. Soc.*, **1980**, 102, 1468-1470; (b) E. W. Müller, H. Spiering, P. Gütllich, *Inorg. Chem.*, **1984**, 23, 119-120.
72. H. H. Wei,; Y. C. Jean, *Chem. Phys. Lett.*, **1984**, 106, 523-526.
73. (a) M. M. Dîrtu, C. Neuhausen, A. D. Naik, A. Rotaru, L. Spinu, Y. Garcia, *Inorg. Chem.*, **2010**, 49, 5723; (b) E. V. Lider, E. V. Peresypkina, L. G. Lavrenova, L. A. Sheludyakova, A. I. Smolentsev, V. N. Ikorskii, T. I. Yaroshenko, V. N. Elokhina, *Russ. J. Coord. Chem.*, **2010**, 36, 337, translated from *Koord. Khim.*, **2010**, 36, 337; (c) Y. Garcia, P. J. van Koningsbruggen, G. Bravic, P. Guionneau, D. Chasseau, J. Moscovici, G. L. Cascarano, K. Lambert, A. Michalowicz, O. Kahn, *Inorg. Chem.*, **1997**, 36, 6357.
74. (a) L. R. Groeneveld, G. Vos, S. Gorter, J. G. Haasnoot, *Acta Cryst. B*, **1982**, 38, 2248; (b) Z.-S. Hu, Y.-H. Lin, S.-C. Jin, *Acta Cryst. C*, **1989**, 45, 1490.
75. (a) A. Grosjean, P. Négrier, P. Bordet, C. Etrillard, D. Mondieig, S. Pechev, E. Lebraud, J.-F. Létard, P. Guionneau, *Eur. J. Inorg. Chem.*, **2013**, 796; (b) M. M. Dîrtu, C. Neuhausen, A. D. Naik, A. Rotaru, L. Spinu, Y. Garcia, *Inorg. Chem.*, **2010**, 49, 5723.
76. A. Grosean, N. Daro, B. Kauffmann, A. Kaiba, J.-F. Létard, P. Guionneau, *Chem. Commun.*, **2011**, 47, 12382.
77. (a) M. Thomann, O. Kahn, J. Guilhem, F. Varret, *Inorg. Chem.*, **1994**, 33, 6029-6037; (b) H. Z. Scott, T. M. Ross, B. Moubaraki, K. S. Murray, S. M. Neville, *Eur. J. Inorg. Chem.*, **2013**, 803-812; (c) M. B. Bushuev, L. G. Lavrenova, Y. G. Shvedenkov, A. V.

- Virovets, L. A. Sheludyakova, S. V. Larionov, *Zh. Neorg. Khim.*, **2005**, *52*, 46-51; (d) Y. Garcia, P. Guionneau, G. Bravic, D. Chasseau, J. A. K. Howard, O. Kahn, V. Ksenofontov, S. Reiman, P. Gülich, *Eur. J. Inorg. Chem.*, **2000**, 1531-1538; (e) G. Vos, R. A. le Febre, R. A. G. de Graaff, J. G. Haasnoot, J. Reedijk, *J. Am. Chem. Soc.*, **1983**, *105*, 1682-1683; (f) J. J. A. Kolnaar, G. van Dijk, H. Koojiman, A. L. Spek, V. Ksenofontov, P. Gülich, J. G. Haasnoot, J. Reedijk, *Inorg. Chem.*, **1997**, *36*, 2433-2440; (g) A. D. Naik, J. Beck, M. M. Dirtu, C. Bebrone, B. Tinant, K. Robeyns, J. Marchand-Brynaert, Y. Garcia, *Inorg. Chim. Acta.*, **2011**, *368*, 21-28; (h) Gómez, J. Benet-Buchholz, E. Martin, J.R. Galán-Mascarós, *Chem. Eur. J.*, **2014**, *20*(18), 5369-5379.
78. (a) H. S. Scott, T. M. Ross, B. Moubaraki, K. S. Murray, S. M. Neville, *Eur. J. Inorg. Chem.*, **2013**, 803-812; (b) O. Roubeau, P. Gamez, S. J. Teat, *Eur. J. Inorg. Chem.*, **2013**, 934-942; (c) J. J. A. Kolnaar, M. I. de Heer, H. Kooijman, A. L. Spek, G. Schmitt, V. Ksenofontov, P. Gülich, J. G. Haasnoot, J. Reedijk, *Eur. J. Inorg. Chem.*, **1999**, 881-886; (d) Y. Garcia, F. Robert, A. D. Naik, G. Zhou, B. Tinant, K. Robeyns, S. Michotte, L. Piroux, *J. Am. Chem. Soc.*, **2011**, *133*, 15850-15853; (e) X. Cheng, Q. Yang, C. Gao, B. Wang, T. Shiga, H. Oshio, Z. -M. Wanga, S. Gao, *Dalton Trans.*, **2015**, *44*, 11282-11285.
79. (a) O. Kahn, E. Codjovi, *Phil. Trans. R. Soc. A*, **1996**, *354*, 359-379.
80. R. N. Muller, L. van der Elst, S. Laurent, *J. Am. Chem. Soc.*, **2003**, *125*, 8405-8407.
81. (a) F. Prins, M. Monrabal-Capilla, E. A. Osorio, E. Coronado, H. S. J. van der Zant, *Adv. Mater.*, **2011**, *23*, 1545-1549; (b) G. Félix, K. Abdul-Kader, T. Mahfoud, I. A. Gural'skiy, W. Nicolazzi, L. Salmon, G. Molnár, A. Bousseksou, *J. Am. Chem. Soc.*, **2011**, *133*, 15342-15345.
82. (a) J. F. Létard, P. Guionneau, N. Daro, *Nanoparticles of a Spin Transition Compound*, *WO 2007/065996*, **2007**; (b) T. Forestier, S. Mornet, N. Daro, T. Nishihara, S.-I. Mouri, K. Tanaka, O. Fouche, E. Freysz, J. F. Létard, *Chem. Commun.*, **2008**, 4327-4329; (c) E. Coronado, J. R. Galán-Mascarós, M. Monrabal-Capilla, J. García-Martínez, P. Pardo-Ibáñez, *Adv. Mater.*, **2007**, *19*, 1359-1361.

83. (a) O. Roubeau, A. Colin, V. Schmitt, R. Clérac, *Angew. Chem.*, **2004**, *116*, 3345-3348; *Angew. Chem. Int. Ed.*, **2004**, *43*, 3283-3286; (b) T. Fujigaya, D.-L. Jiang, T. Aida, *Chem. Asian J.*, **2007**, *2*, 106-113; (c) M. Rubio, D. López, *Eur. Polym. J.*, **2009**, *45*, 3339-3346; (d) P. Grondin, O. Roubeau, M. Castro, H. Saadaoui, A. Colin, R. Clérac, *Langmuir*, **2010**, *26*, 5184-5195.
84. (a) O. Roubeau, B. Agricole, R. Clérac, S. Ravaine, *J. Phys. Chem. B*, **2004**, *108*, 15110-15116; (b) O. Roubeau, E. Natividad, B. Agricole, S. Ravaine, *Langmuir*, **2007**, *23*, 3110-3117; (c) C. Thibault, G. Molnár, L. Salmon, A. Bousseksou, C. Vieu, *Langmuir*, **2010**, *26*, 1557-1560.
85. (a) T. Fujigaya, D.-L. Jiang, T. Aida, *J. Am. Chem. Soc.*, **2005**, *127*, 5484-5489; (b) P. Sonar, C. M. Grunert, Y.-L. Wie, J. Kusz, P. Gülich, A. D. Schlüter, *Eur. J. Inorg. Chem.*, **2008**, 1613-622; (c) Y.-L. Wie, P. Sonar, M. Grunert, J. Kusz, A. D. Schlüter, P. Gülich, *Eur. J. Inorg. Chem.*, **2010**, 3930-3941.
86. (a) P. Grondin, D. Siretanu, O. Roubeau, M.-F. Achard, R. Clérac, *Inorg. Chem.*, **2012**, *51*, 5417-5426; (b) A. B. Gaspar, M. Seredyuk, P. Gülich, *Coord. Chem. Rev.*, **2009**, *253*, 2399-2413.
87. T. Forestier, A. Kaiba, S. Pechev, D. Denux, P. Guionneau, C. Etrillard, N. Daro, E. Freysz, J.-F. Létard, *Chem. Eur. J.*, **2009**, *25*, 6122.
88. (a) J.-F. Létard, N. Daro, S. Aurrifet, *PCT Int. Appl.*, **2009**, *WO 2009007534 A2* 20090115; (b) J.-F. Létard, O. Nguyen, N. Daro, *PCT Int. Appl.*, **2007**, *WO 2007065996 A1* 20070614.
89. (a) F. Volatron, L. Catala, E. Rivière, A. Gloter, O. Stéphan, T. Mallah, *Inorg. Chem.*, **2008**, *47*, 6584; (b) Y. Raza, F. Volatron, S. Moldovan, O. Ersen, V. Huc, C. Martini, F. Brisset, A. Gloter, O. Stéphan, A. Bousseksou, L. Catala, T. Mallah, *Chem. Comm.*, **2011**, *47*, 11501.

90. (a) E. Coronado, J. R. Galán-Mascarós, M. Monrabal-Capilla, J. García-Martínez, P. Pardo-Ibáñez, *Adv. Mater.*, **2007**, *19*, 1359; (b) F. Prins, M. Monrabal-Capilla, E. A. Osorio, E. Coronado, H. S. J. van der Zant, *Adv. Mater.*, **2011**, *23*, 1545; (c) J. R. Galán-Mascarós, E. Coronado, A. Forment-Aliaga, M. Monrabal-Capilla, E. Pinilla-Cienfuegos, M. Ceolin, *Inorg. Chem.*, **2010**, *49*, 5706.
91. (a) C. Atmani, F. Setifi, S. Benmansour, S. Triki, M. Marchivie, J. -Y. Salaün, C. J. Gómez-García, *Inorg. Chem. Commun.*, **2008**, *11*, 921; (b) S. Benmansour, F. Setifi, S. Triki, J. -Y. Salaün, F. Vandavelde, J. Sala-Pala, C. J. Gómez-García, T. Roisnel, *Eur. J. Inorg. chem.*, **2007**, 186; (c) S. Triki, F. Thétiot, F. Vandavelde, J. Sala-Pala, C. J. Gómez-García, *Inorg. Chem.*, **2005**, *44*, 4086; (d) F. Thétiot, S. Triki, J. Sala-Pala, J. -R. Galan-Mascaros, J. M. Martinez-Agudo, K. R. Dunbar, *Eur. J. Inorg. Chem.*, **2004**, 3783.
92. (a) E. Lefebvre, F. Conan, N. Cosquer, J. -M. Kerbaol, M. Marchivie, J. Sala-Pala, M. M. Kubicki, E. Vigier, C. J. Gómez-García, *New J. Chem.*, **2006**, *30*, 1197; (b) J. -R. Galan-Mascaros, F. Thétiot, S. Triki, J. Sala-Pala, K. R. Dunbar, *J. Phys. IV; France*, **2004**, *114*, 625; (c) W. Kaim, M. Moscherosch, *Coord. Chem. Rev.*, **1994**, *129*, 157; (d) F. Thétiot, S. Triki, J. Sala-Pala, C. J. Gómez-García, *Dalton Trans.*, **2002**, 1687; (e) F. Thétiot, S. Triki, J. Sala-Pala, S. Golhen, *Inorg. Chim. Acta.*, **2003**, *350*, 314; (f) F. Thétiot, S. Triki, J. Sala-Pala, *Polyhedron*, **2003**, *22*, 1837; (g) S. Triki, J. Sala-Pala, A. Riou, P. Molinié, *Synth. Met.*, **1999**, *102*, 1472; (h) S. Triki, J. Sala-Pala, M. Decoster, P. Molinié, L. Toupet, *Angew. Chem. Int. Ed.*, **1999**, *38*, 113; (i) S. Triki, F. Thétiot, J. -R. Galan-Mascaros, J. Sala-Pala, K. R. Dunbar, *New J. Chem.*, **2001**, *25*, 954; (j) S. Triki, F. Thétiot, J. Sala-Pala, S. Golhen, J. M. Clemente-Juan, C. J. Gómez-García, E. Coronado, *Chem. Commun.*, **2001**, 2172.
93. G. Dupouy, M. Marchivie, S. Triki, J. Sala-Pala, C. J. Gómez-García, S. Pillet, C. Lecomte, J. -F. Létard, *Chem. Commun.*, **2009**, 3404.
94. P. J. Kunkeler, P. J. v. Koningsbruggen, J. P. Cornelissen, A. N. Van der Horst, A. M. Van der Kraan, A. L. Spek, J. G. Haasnoot, J. Reedijk, *J. Am. Chem. Soc.*, **1996**, *118*, 2190.

95. (a) A. Galet, A. B. Gaspar, M. C. Muñoz, G. V. Bukin, G. Levchenko, J. A. Real, *Adv. Mater.*, **2005**, *17*, 2949; (b) V. Niel, A. Galet, A. B. Gaspar, M. C. Muñoz, J. A. Real, *Chem. Commun.*, **2003**, 1248; (c) G. Agustí, A. B. Gaspar, M. C. Muñoz, J. A. Real, *Inorg. Chem.*, **2007**, *46*, 9646; (d) K. Nakao, S. Hayami, M. Akita, I. Katsuya, *Chem. Lett.*, **2008**, *37*, 292; (e) G. Agustí, S. Cobo, A. B. Gaspar, G. Molnár, N. O. Moussa, P. Szilágyi, Á. V. Pálfi, C. Vieu, C. M. Muñoz, J. A. Real, A. Bousseksou, *Chem. Mater.*, **2008**, *20*, 6721.
96. T. Kitazawa, Y. Gomi, M. Takahashi, M. Takeda, M. Enomoto, A. Miyazaki, T. Enoki, *J. Mater. Chem.*, **1996**, *6*, 119.
97. (a) S. Cobo, D. Ostrovskii, S. Bonhommeau, L. Vendier, G. Molnár, L. Salmon, K. Tanaka, A. Bousseksou, *J. Am. Chem. Soc.*, **2008**, *130*, 9019; (b) F. Volatron, L. Catala, E. Riviere, A. Gloter, O. Stephan, T. Mallah, *Inorg. Chem.*, **2008**, *47*, 6584; (c) I. Boldog, A. B. Gaspar, V. Martinez, P. Pardo-Ibanez, V. Ksenofontov, A. Bhattacharjee, P. Gütllich, J. A. Real, *Angew. Chem. Int. Ed.*, **2008**, *47*, 6433; (d) R. Ohtani, K. Yoneda, S. Furukawa, N. Horike, S. Kitagawa, A. B. Gaspar, M. C. Muñoz, J. A. Real, M. Ohba, *J. Am. Chem. Soc.*, **2011**, *133*, 8600; (e) F. J. Muñoz Lara, A. B. Gaspar, D. Aravena, E. Ruiz, M. C. Muñoz, M. Ohba, R. Ohtani, S. Kitagawa, J. A. Real, *Chem. Comm.*, **2012**, *48*, 4686.
98. P. D. Southon, L. Liu, E. A. Fellows, D. J. Price, G. J. Halder, K. W. Chapman, B. Moubaraki, K. S. Murray, J. F. Létard, C. J. Kepert, *J. Am. Chem. Soc.*, **2009**, *131*, 10998.
99. (a) Y. Garcia, P. J. van Koningsbruggen, E. Codjovi, R. Lapouyade, O. Kahn, L. Rabardel, *J. Mater. Chem.*, **1997**, *7*, 875; (b) Y. Garcia, J. Moscovici, A. Michalowicz, V. Ksenofontov, G. Levchenko, G. Bravic, D. Chasseau, P. Gütllich, *Chem. Eur. J.*, **2002**, *8*, 4992.
100. M. Seredyuk, A. B. Gaspar, M. C. Muñoz, M. Verdaguer, F. Villain, P. Gütllich, *Eur. J. Inorg. Chem.*, **2007**, 4481.
101. M. M. Dîrtu, F. Schmit, A. D. Naik, A. Rotaru, J. Marchand-Brynaert, Y. Garcia, *Hyperfine Interact.*, **2012**, *205*, 69.

102. N. Pittala, F. Thétiot, S. Triki, K. Boukheddaden, G. Chastanet, and M. Marchivie, *Chem. Mater.*, **2016**; DOI: 10.1021/acs.chemmater.6b04118.
103. P. Gütllich, Y. Garcia, H. Spiering, *Spin Transition Phenomenon in Magnetism: Molecules to Materials IV*; J. S. Miller, M. Drillon, Eds.; Wiley-VCH Verlag: Weinheim, Germany, **2003**, 271-344
104. (a) J. H. Takemoto, B. Hutchinson, *Inorg. Nucl. Chem. Lett.*, **1972**, *8*, 769-772; (b) J. H. Takemoto, B. Hutchinson, *Inorg. Chem.*, **1973**, *12*, 705-708; (c) J. H. Takemoto, B. Streusand, B. Hutchinson, *Spectrochim. Acta, Part A*, **1974**, *30*, 827-834.
105. (a) W. A. Baker, Jr., G. J. Long, *Chem. Commun.*, **1965**, 368-369; (b) E. König, K. Madeja, *Inorg. Chem.*, **1967**, *6*, 48-55; (c) E. König, K. Madeja, *Spectrochim. Acta, Part A*, **1967**, *23*, 45-54; (d) R. Herber, L. M. Casson, *Inorg. Chem.* **1986**, *25*, 847-852; (e) R. H. Herber, *Inorg. Chem.*, **1987**, *26*, 173-178; (f) D. C. Figg, R. H. Herber, *Inorg. Chem.* **1990**, *29*, 2170-2173; (g) A. Bousseksou, J. J. McGarvey, F. Varret, J. A. Real, J.-P. Tuchagues, A. C. Dennis, M. L. Boillot, *Chem. Phys. Lett.* **2000**, *318*, 409-416.
106. E. W. Müller, J. Ensling, H. Spiering, P. Gütllich, *Inorg. Chem.*, **1983**, *22*, 2074-2078.
107. (a) P. Guionneau, M. Marchivie, G. Bravic, J.-F. Létard and D. Chasseau, *Top. Curr. Chem.*, **2004**, *234*, 97-128; (b) M. Marchivie, P. Guionneau, J.-F. Létard and D. Chasseau, *Acta Cryst. B*, **2005**, *B61*, 25-28.
108. M. Marchivie, P. Guionneau, J.-F. Létard, D. Chasseau, *Acta Cryst. Sect. B*, **2003**, *B59*, 479.
109. M. A. Halcrow, *Coord. Chem. Rev.*, **2009**, *253*, 2493.
110. M. M. Dirtu, C. Neuhausen, A. D. Naik, A. Rotaru, L. Spinu, Y. Garcia, *Inorg. Chem.*, **2010**, *49*, 5723.
111. G. J. Halder, K. W. Chapman, S. M. Neville, B. Moubaraki, K. S. Murray, J. F. Létard, C. J. Kepert, *J. Am. Chem. Soc.*, **2008**, *130*, 17552.

112. (a) H. L. Schläfer, G. Gliemann, *Einführung in die Ligandenfeldtheorie*; Akademische Verlagsgesellschaft: Wiesbaden, Germany, **1980**; (b) R. L. Carlin, A. J. van Duyneveldt, *Magnetic Properties of Transition Metal Compounds*; Springer: New York, **1977**.
113. (a) R. L. Carlin, *Magnetochemistry*; Springer-Verlag: Berlin, **1986**; (b) M. Sorai, M. Nakano, Y. Miyazaki, *Chem. Rev.*, **2006**, *106*, 976-1031; (c) E. König, *Struct. Bonding*, **1991**, *76*, 51.
114. E. König, G. Ritter, S. K. Kulshreshta, J. Waigel, H. A. Goodwin, *Inorg. Chem.*, **1984**, *23*, 1896-1902; (b) S. K. Kulshreshta, R. M. Iyer, E. König, G. Ritter, *Chem. Phys. Lett.*, **1984**, *110*, 201-204; (c) S. K. Kulshreshta, R. Sasikala, E. König, *Chem. Phys. Lett.*, **1986**, *123*, 215-217; (d) S. K. Kulshreshta, R. M. Iyer, *Chem. Phys. Lett.*, **1987**, *134*, 239-244.
115. (a) D.F.J. Evans, *J. Chem. Soc.*, **1959**, 2003; (b) E.M. Schubert, *J. Chem. Educ.*, **1992**, *69*, 62.
116. (a) B. Weber, F.A. Walker, *Inorg. Chem.*, **2007**, *46*, 6794; (b) B. Weber, C. Carbonera, C. Desplanches, J. F. Létard, *Eur. J. Inorg. Chem.*, **2008**, 1589.
117. P. Gütlich, A. Bhattacharjee, M. Seredyuk, A. B. Gaspar, *Hyperfine Interact.*, **2009**, *189*, 3.
118. (a) P. Gütlich, *Z. Anorg. Allg. Chem.*, **2012**, *638*, 15-43; (b) N. N. Greenwood, T. C. Gibb, *Mössbauer Spectroscopy*; Chapman and Hall: London, **1971**; (c) P. Gütlich, E. Bill, A. X. Trautwein, Eds. *Mössbauer Spectroscopy and Transition Metal Chemistry-Fundamentals and Applications*; Springer-Verlag: Berlin, Heidelberg, **2011**; (d) P. Gütlich, Spin Transition in Iron Compounds. In *Chemical Mössbauer Spectroscopy*; R. H. Herber, Ed.; Plenum: New York, **1984**; 27-64; (e) P. Gütlich, Spin Transition in Iron Complexes. In *Mössbauer Spectroscopy Applied to Inorganic Chemistry*; G. J. Long, Ed.; Plenum: New York, **1984**, *1*, 287-338; (f) P. Gütlich, Y. Garcia, *J. Phys.: Conf. Ser.*, **2010**, *217*, 012001.

Chapter II

New Synthetic Strategy for the Design of New One-Dimensional Fe(II) *SCO* Coordination Polymers based on Functionalized Triazole Ligands: Reliable Structural Investigations including the First Structural Studies of the High and Low Spin States

Table of Contents

Introduction	82
Results and discussion	85
1. Syntheses and infrared spectroscopy of $[\text{Fe}(\text{bntrz})_3][\text{Pt}(\text{CN})_4]\cdot\text{H}_2\text{O}$ (1)	85
2. Magnetic properties	87
3. Differential scanning calorimetry	88
4. Structural investigations in both high spin (<i>HS</i>) and low spin (<i>LS</i>) states	90
Conclusion	99
Experimental section	101
Bibliography	107

New Synthetic Strategy for the Design of New One-Dimensional Fe(II) *SCO* Coordination Polymers based on Functionalized Triazole Ligands: Reliable Structural Investigations including the First Structural Studies of the High and Low Spin States

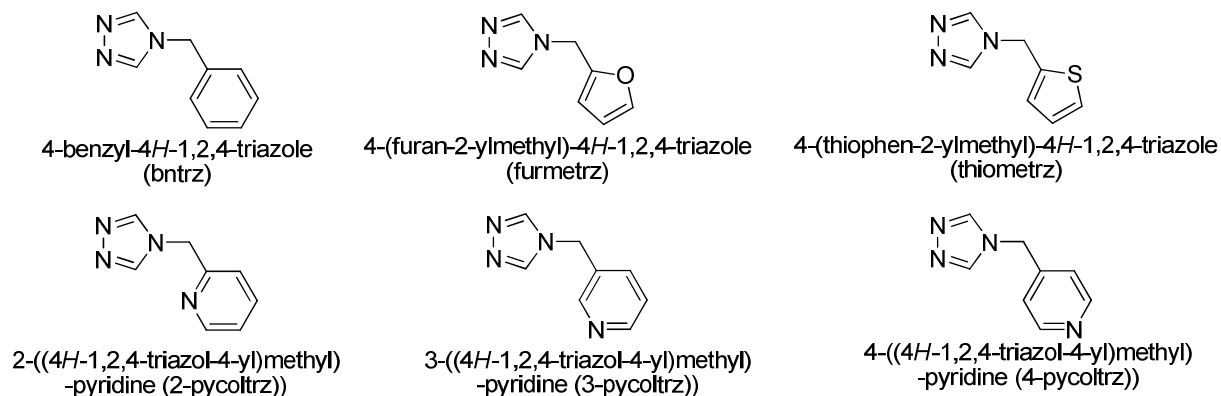
Introduction

The magnetic spin change associated to the spin-crossover (*SCO*) phenomenon represents a paradigm of bistability at the molecular level which is of current interest because of potential applications in the development of new generations of electronic devices such as non-volatile memory, molecular sensing and displays.¹⁻⁵ The *SCO* phenomenon is especially observed in Fe^{II} complexes in which the paramagnetic high spin state (*HS*, $S = 2$) can be switched reversibly to the low spin state (*LS*, $S = 0$) by several external stimuli such as temperature, pressure or light irradiation.⁶ A huge effort has been devoted to the understanding of the transition mechanisms using inter alia crystallographic tools.⁷⁻⁸ The minimum requirements for the latter involve the determination of the crystal structures in both *LS* and *HS* states to comprehend the structural parameters at the molecular and inter-molecular scales. While some systems were deeply investigated due to their remarkable switching properties, the absence of any detailed and punctilious structural information has precluded the definite understanding of these exciting properties. This is particularly the case of the so-called “triazole family”, more specifically coordination polymer chains of general formula $[\text{Fe}(\text{4-R-trz})_2(\text{trz})](\text{X})$, where 4-R-trz is a functionalized 1,2,4-triazole ligand and X a counter-anion, which display bistability with wide hysteresis loops around or above room temperature.⁹⁻¹¹ Although known for few decades, the major lack of high quality single crystals with complete structural data for those materials prevent any deep magneto-structural correlations which are of paramount importance for (i) the understanding of the origin of the thermal hysteresis loop, and (ii) the control of the transition temperature. Indeed, a deep knowledge of the structural data is required to evaluate notably the effects of the rigid triple 1,2-trz bridges and/or the characteristics of the intramolecular contacts on the propagation of the elastic interactions. Owing to the great and intensifying attention given

to these materials, scarce crystallographic investigations have been recently attempted. Among them, the structural characterizations of the *HS* and *LS* states of the $[\text{Fe}(\text{Htrz})_2(\text{trz})](\text{BF}_4)$ derivative, using distinctively high-resolution synchrotron X-ray powder diffraction combined with Raman spectroscopy¹² or X-ray diffraction data from high-quality crystalline powder,¹³ have been reported. While the 1D chain structure was proven for both *HS* and *LS* states, the rather limited quality of the diffraction patterns could not provide highly precise structural data suitable for deep magneto-structural correlations. In the same time, a single crystal of the parent Cu^{II} compound $[\text{Cu}(\text{NH}_2\text{trz})_3](\text{NO}_3)_2 \cdot 3\text{H}_2\text{O}$ has been finely investigated by Garcia *et al.* to parallel with the crystal structure of the $[\text{Fe}(\text{NH}_2\text{trz})_3](\text{NO}_3)_2$ for which only nano-sized thin crystallite needles (120-330 nm) could be prepared. However, the powder diffraction pattern of the latter did not fully fit to the diffraction pattern observed for the single crystals of the Cu^{II} compound.¹⁰ Besides, the lone single crystal structural study proving the presumably 1-D character of $[\text{Fe}(\text{NH}_2\text{trz})_3](\text{NO}_3)_2 \cdot 2\text{H}_2\text{O}$ was only reported in 2011 by Guionneau *et al.*¹⁴ However, as clearly stated by the authors, the very low diffraction pattern induced essentially by the sub-micrometric size ($> 20 \times 1 \times 1 \text{ nm}^3$) of the crystals and the damages due to the X-ray beam during the data collection led to a rather low quality of the structural data which did not allow an accurate detailed discussion of the polymeric chain structure. In addition, the study, performed at 120 K, concerned only the *LS* state of the sample since the damages caused on the crystals when warming over room temperature have hindered data collection for the *HS* state. Ultimately, those recent examples clearly expose the challenge to access refined structural data in both spin states in order to fully apprehend and rationalize the conspicuous *SCO* properties in the $\text{Fe}^{\text{II}}/\text{trz}$ systems.

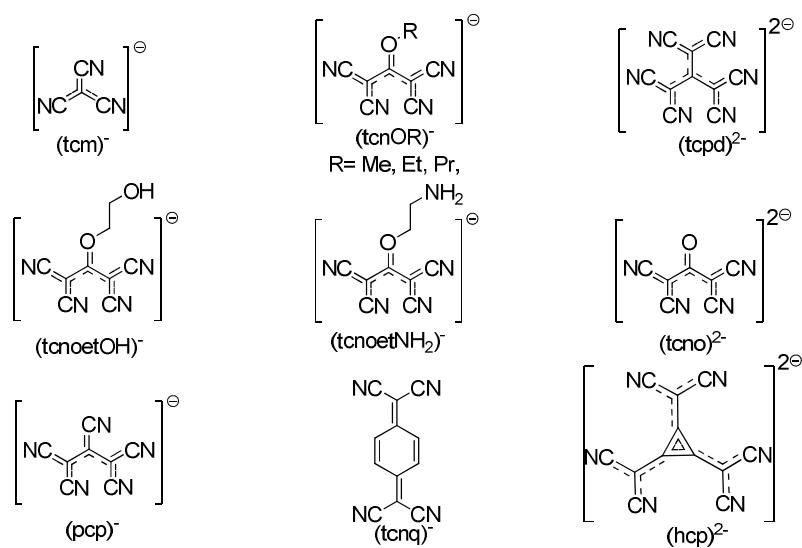
In the last few years, some Fe^{II} systems based on functionalized triazole ligands (4-R-trz) and different counter-anions have been reported.⁷ However, the majority of the involved counter-ions are rather standard monoanions, while the functional groups (R) of the triazole molecules are essentially narrowed to linear or branched alkyl or alkoxylated chains.⁷ Recently, we have extended this synthetic approach to combinations of triazole ligands and anions which were not used so far within the “triazole family”. Among them, triazole ligands involving rigid aryl groups with an alkyl spacer (Scheme 1), assuring the electronic integrity of the triazole motif, coupled

with more sophisticated anions such as polycyanometallates or organic cyanocarbanions which display very diverse sizes, geometries and charges, have been investigated (Scheme 2).¹⁵⁻¹⁶

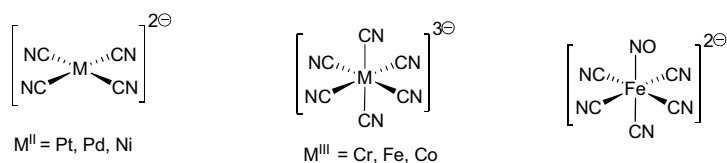


Scheme 1. Triazole ligands involving rigid aryl groups with an alkyl spacer.

Cyanocarbanions



Polycyanometallates



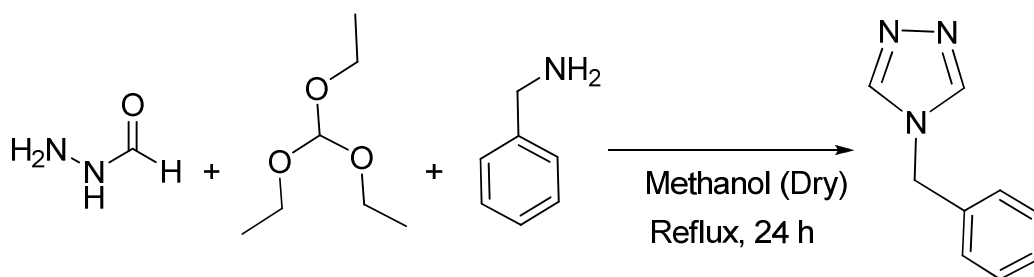
Scheme 2. Examples of the organic cyanocarbanion and polycyanometallate ligands.

In this ongoing work, we have realized at an early stage that this chemical approach tends to improve unprecedentedly the size, the quality and the robustness of the single crystals of the resulting original $\text{Fe}^{\text{II}}/\text{R-trz}$ systems. Ultimately, this synthetic strategy should allow the access to single crystals of novel *SCO* cooperative materials, which is essential to understand the origin of the unparalleled cooperativity observed in those 1D coordination polymers. In combination with the selected bntrz ligand (see Scheme 1), the initial choice of the rigid tetracyanoplatinate (II) anion has been carefully defined based on (i) the ability of the anion to form covalent linkage or ionic bonding to the neighboring units (e.g. metal complex) in the structural arrangement of a *SCO* material, and (ii) the bias to obtain single crystals with this anionic moiety. Thus, the present work reports the synthesis, structural and magnetic characterizations, as well as the first accurate single crystal investigations of both *HS* and *LS* states of the new triazole-based *SCO* Fe^{II} 1-D polymer $[\text{Fe}(\text{bntrz})_3][\text{Pt}(\text{CN})_4]\cdot\text{H}_2\text{O}$ (**1**).

Results and Discussion

1. Syntheses and infrared spectroscopy of $[\text{Fe}(\text{bntrz})_3][\text{Pt}(\text{CN})_4]\cdot\text{H}_2\text{O}$ (**1**)

The synthesis of the 4-(benzyl)-1,2,4-triazole (bntrz) triazole derivative was inspired from previously reported procedures, with slight but impactful modifications (Scheme 3).¹⁷⁻¹⁸ In summary, the bntrz ligand has been obtained by reaction - under reflux - of formic hydrazide and triethyl orthoformate with benzylamine (molar ratio: 1/1.2/1) in methanol solvent under nitrogen atmosphere. After removal of the solvent under reduced pressure, the resulting pale pink solid was recrystallized from methanol-ether solvent mixture. Finally, the resulting product was filtered and washed with ether to obtain a white crystalline powder in satisfactory yield (ca. 60%). When compared to the precedently reported protocols,¹⁸ the recrystallization of the product in methanol-ether or ethanol-ether as a purification step instead of a chromatography procedure, have allowed for a notable simplification of the synthesis. The resulting bntrz ligand has been characterized by ^1H and ^{13}C NMR spectroscopy (see experimental part).



Scheme 3. Synthesis of the triazole derivative 4-(benzyl)-1,2,4-triazole (bntrz).

Single crystals of the coordination polymer $[\text{Fe}(\text{bntrz})_3][\text{Pt}(\text{CN})_4]\cdot\text{H}_2\text{O}$ (**1**) have been synthesized *via* diffusion technique in a fine glass tube (3.0 mm diameter) by layering an ethanol solution of the bntrz ligand onto an aqueous solution containing both $\text{K}_2[\text{Pt}(\text{CN})_4]\cdot x\text{H}_2\text{O}$ and $\text{Fe}(\text{BF}_4)_2\cdot 6\text{H}_2\text{O}$ salts. The colorless single crystals of compound **1** were collected as needles after three weeks, and dried in air at room temperature.

The coordination polymer $[\text{Fe}(\text{bntrz})_3][\text{Pt}(\text{CN})_4]\cdot\text{H}_2\text{O}$ (**1**) has been characterized by infrared spectroscopy (IR), superconducting quantum interference device (SQUID) magnetic measurements, differential scanning calorimetry (DSC), and X-ray diffraction (XRD).

The infrared spectrum of **1**, recorded on single crystals sample at room temperature, and the ones of the initial precursors - i.e. the bntrz molecule only and the $\text{K}_2[\text{Pt}(\text{CN})_4]\cdot x\text{H}_2\text{O}$ salt - are provided in the experimental part. In the IR spectrum of the bntrz molecule only, the band assigned to the ring torsion of the 1,2,4-triazole motif is observed at $\nu = 638\text{ cm}^{-1}$, with the $\nu_{\text{C}=\text{N}}$ stretching vibration at 1534 cm^{-1} , and the N-N stretching band at $\nu_{\text{N}-\text{N}} = 1031\text{ cm}^{-1}$; in compound **1**, these characteristic bands of the bntrz moiety are all blue shifted at 644 cm^{-1} , $\nu_{\text{C}=\text{N}} = 1551\text{ cm}^{-1}$, and $\nu_{\text{N}-\text{N}} = 1026\text{ cm}^{-1}$, respectively (see experimental part).¹⁹ These latter values confirm the coordination of the iron to the 1,2,4-triazole ring of the bntrz ligand in **1**. Referring to the characteristic intense C-N stretching bands $\nu_{(\text{CN})}$ observed at 2129 and 2119 cm^{-1} in **1** assigned to the $[\text{Pt}(\text{CN})_4]^{2-}$ anionic units, they tend to suggest the presence of both uncoordinated and coordinated nitrile groups, but ultimately the values are very similar to the ones observed in $\text{K}_2[\text{Pt}(\text{CN})_4]\cdot x\text{H}_2\text{O}$ (2133 and 2122 cm^{-1}) and do not allow doubtless interpretation on the

coordination character of this organic ligand in compound **1**. In the low frequency region (200-400 cm^{-1}), the band observed at 277 cm^{-1} is attributable to the Fe-N stretching vibrations and in agreement with the frequency values reported in the literature for Fe(II) centers in *HS* state, and with the further reported structural data.²⁰

2. Magnetic properties

The magnetic susceptibility (χ_m) of **1** was measured over the temperature range 2-300 K on a set of single crystals. The $\chi_m T$ versus T plot (where T is the temperature) is displayed in Figure 1. In the high-temperature region, the $\chi_m T$ value (3.45 $\text{cm}^3 \cdot \text{K} \cdot \text{mol}^{-1}$) is consistent with a *HS* ($S = 2$) configuration of the hexacoordinated Fe^{II} ions. Upon cooling, the $\chi_m T$ remains constant down to a temperature value of *ca.* 240 K, then sharply decreases to *ca.* 0.0 $\text{cm}^3 \cdot \text{K} \cdot \text{mol}^{-1}$, indicating the presence of a complete sharp *HS* to *LS* first-order spin transition ($T_{1/2} = 242$ K). However, no significant thermal hysteresis effects were detected after the warming mode, at the value of the temperature scan rate of 0.4 $\text{K} \cdot \text{min}^{-1}$.

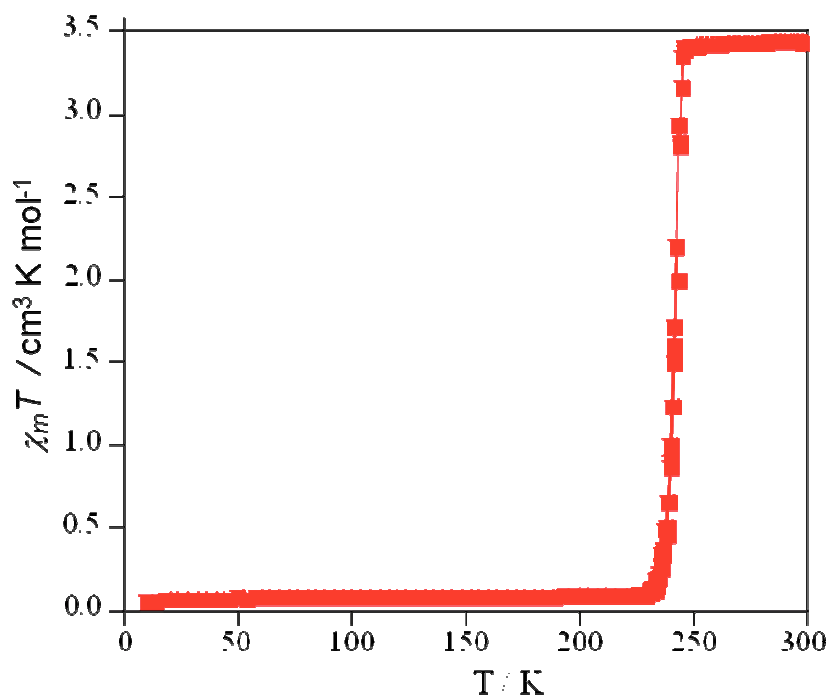


Figure 1. Thermal variation of the $\chi_m T$ product for $[\text{Fe}(\text{bntrz})_3][\text{Pt}(\text{CN})_4] \cdot \text{H}_2\text{O}$ (**1**) recorded at a scan rate of 0.4 $\text{K} \cdot \text{min}^{-1}$ in a settle mode.

As expected, this abrupt *SCO* transition is accompanied by a reversible thermochromic transition as clearly shown by the crystal images depicted in Figure 2, with an exceptional resilience of the present crystal upon repeated switching cycles without notable alteration.

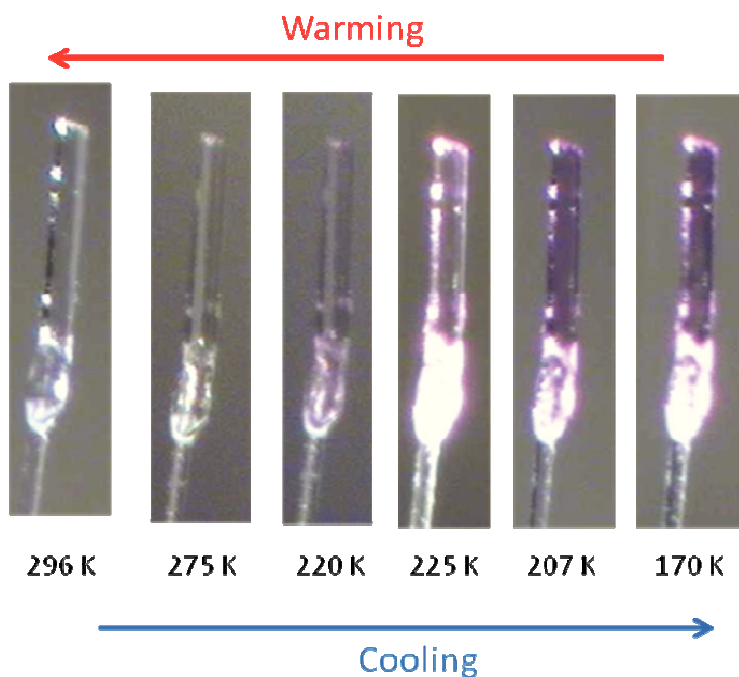


Figure 2. Crystal images of polymer **1** showing the clear thermochromism from purple to colorless for the *LS* and *HS* states, respectively.

3. Differential scanning calorimetry

In parallel to the magnetic studies, the *SCO* behavior of the 1D coordination polymer **1** has also been investigated by differential scanning calorimetry (DSC) over the temperature range of 200-260 K, on both warming and cooling modes with a temperature scan rate of 2 K.min⁻¹. The corresponding heat capacity temperature profiles are displayed in Figure 3 and the relevant thermodynamic parameters are reported in Table 1. In warming mode, an endothermic peak is observed at $T_c\uparrow = 243.5$ K, while an exothermic peak is recorded at $T_c\downarrow = 241.1$ K in cooling mode. These peaks correspond to a first-order phase transition associated with the *SCO* behavior of **1**, with a hysteresis loop width of 2.4 K.

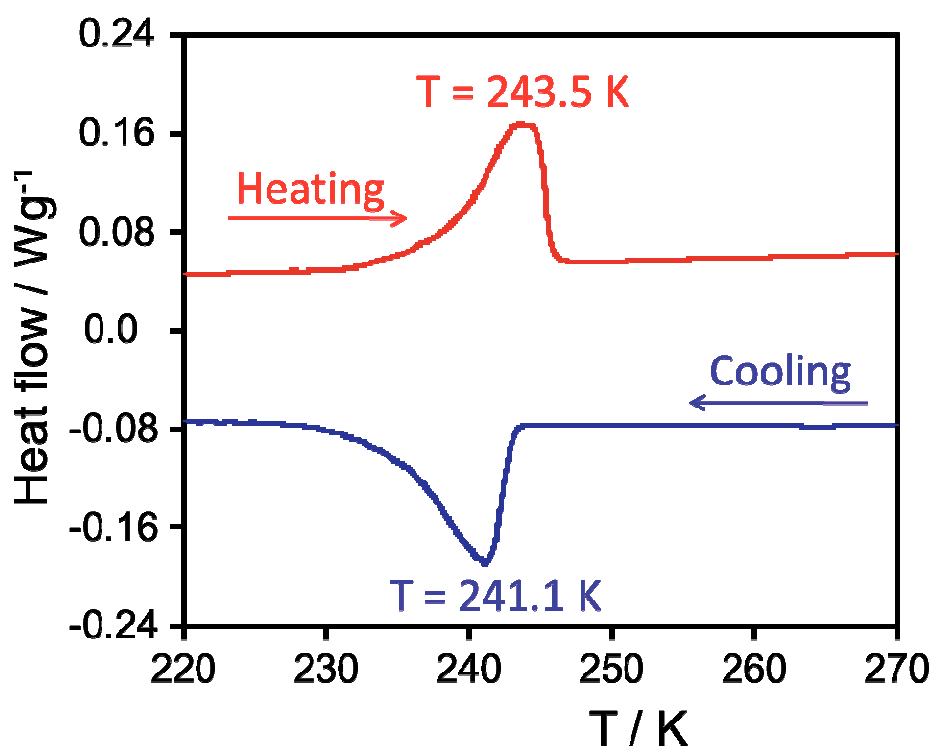


Figure 3. Differential scanning calorimetry profiles of $[\text{Fe}(\text{bntrz})_3][\text{Pt}(\text{CN})_4]\cdot\text{H}_2\text{O}$ (**1**) recorded with a temperature scan rate of $2 \text{ K}\cdot\text{min}^{-1}$; (Blue line: cooling mode; red line: heating mode).

The presence of a weak hysteresis in the DSC measurements while it was absent in magnetic measurements can be reasonably attributed to the difference of temperature scan rates ($2 \text{ K}\cdot\text{min}^{-1}$ vs. $0.4 \text{ K}\cdot\text{min}^{-1}$, respectively). Furthermore, the phase transition has been found to occur with an enthalpy and entropy changes of $\Delta H = 16.87 \text{ kJ}\cdot\text{mol}^{-1}$ and $\Delta S = 69.61 \text{ J}\cdot\text{K}^{-1}\cdot\text{mol}^{-1}$, respectively. These values are in good agreement with those reported in the literature for similar *SCO* compounds.²¹

Table 1. Thermodynamic parameters for $[\text{Fe}(\text{bntrz})_3][\text{Pt}(\text{CN})_4]\cdot\text{H}_2\text{O}$ (**1**).

T_c (K)	ΔH (kJ.mol ⁻¹)	ΔS (J.K ⁻¹ .mol ⁻¹)
241.1	16.906	70.089
243.5	16.834	69.135

4. Structural investigations in both high spin (*HS*) and low spin (*LS*) states

Based on the magnetic and calorimetric studies, the crystal structure of **1**, defined in the triclinic space group, has been determined at 296 K (*HS* state, colourless crystal), and at 120 K (*LS* state, purple crystal). The crystal data and structural refinement parameters, Fe-N bond lengths (Å) and N-Fe-N bond angles (°), and average Fe-N distances and distortion parameters of [Fe(bntrz)₃][Pt(CN)₄].H₂O (**1**), at 296 K and 120 K, are depicted in tables 2-4, respectively. An in-depth examination of the unit cell parameters, at these two temperatures, indicates the absence of any structural phase transition within the studied temperature range. The molecular structure of the cationic Fe^{II} complex [Fe(bntrz)₃]²⁺ is depicted in Figure 4.

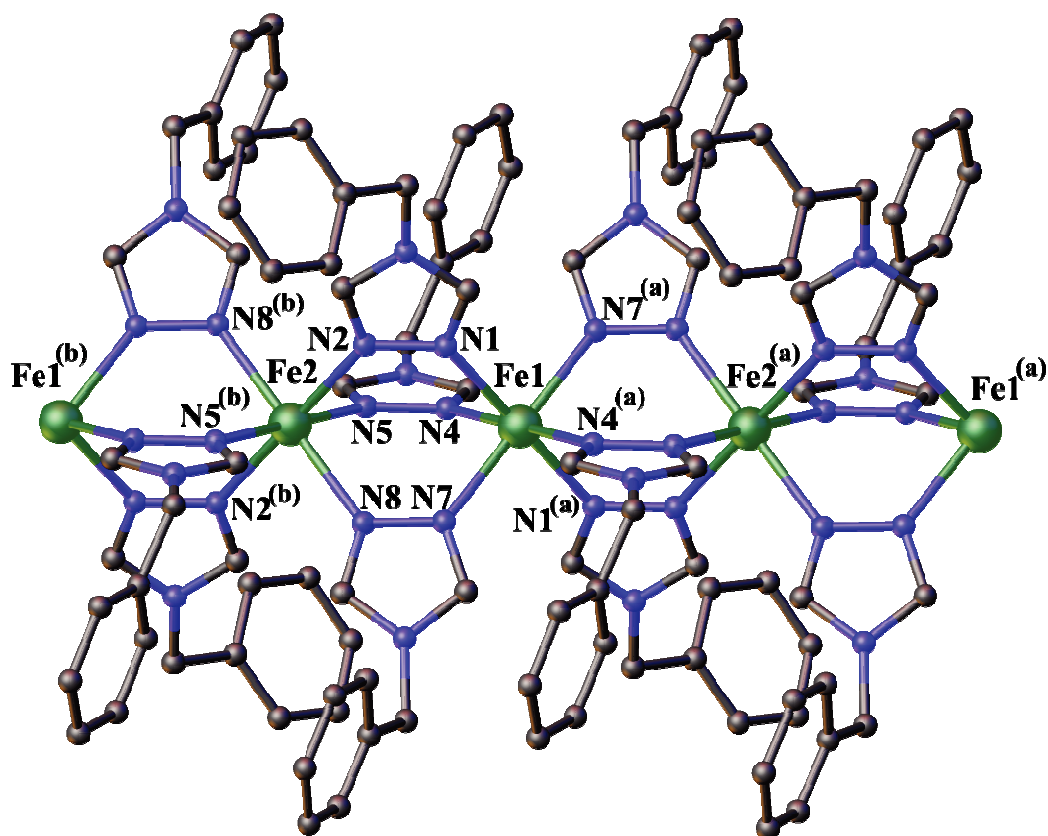


Figure 4. View of the cationic chain [Fe(bntrz)₃]²⁺ in **1**: linear chain running along the *a* axis. Codes of equivalent positions: (a) 1-*x*, -*y*, 1-*z*; (b) = -*x*, -*y*, 1-*z*. Colour code: Fe (green), N (blue) and C (grey); (Hydrogen atoms have been omitted for clarity).

Table 2. Crystal data and structural refinement parameters for compound **1**.

Colour	Colorless	purple
Temperature / K	296(2)	120(2)
Empirical formula	C ₃₁ H ₂₉ FeN ₁₃ OPt	C ₃₁ H ₂₉ FeN ₁₃ OPt
Formula weight / g.mol ⁻¹	850.61	850.61
Wavelength / Å	0.71073 Å	0.71073 Å
Crystal system	Triclinic	Triclinic
Space group	<i>P</i> -1	<i>P</i> -1
a / Å	7.8931(2)	7.4945(2)
b / Å	14.5363(4)	14.2896(4)
c / Å	14.6867(4)	14.8234(4)
α / °	94.860(2)	95.640(2)
β / °	103.461(2)	101.855(2)
γ / °	94.187(2)	92.943(2)
Volume / Å ³	1625.42(8)	1541.93(7)
Z	2	2
D _{calc} / g.cm ⁻³	1.738	1.832
Abs. Coef. / cm ⁻¹	6.20	5.052
F(000)	836	836
Crystal size / mm ³	0.27 × 0.03 × 0.03	0.27 × 0.03 × 0.03
2θ range / °	6.82 - 54.00	6.62 - 54.00
Refl. collected	20278	19471
Unique refl. / Rint	6993 / 0.0640	6654 / 0.0672
Data / restr. / N _v	5345 / 0 / 432	5305 / 432
^a R1/ ^b wR2	0.0367 / 0.0832	0.0342 / 0.1010
^c GooF	1.035	1.100
Δρ _{max/min} / eÅ ⁻³	1.270 / -0.992	1.507 / -1.899
CCDC No.	1492971	1492972

$$^aR1 = \sum |F_o - F_c| / F_o. \quad ^b wR2 = \{ \sum [w(F_o^2 - F_c^2)^2] / \sum [w(F_o^2)^2] \}^{1/2}. \quad ^c \text{GooF} = \{ \sum [w(F_o^2 - F_c^2)^2] / (N_{\text{obs}} - N_{\text{var}}) \}^{1/2}$$

The structure of **1** is built from two crystallographically independent Fe^{II} sites, Fe1 and Fe2, and two [Pt(CN)₄]²⁻ anions located on inversion centers, and three bntz ligands and one solvent water molecule located on general positions. The three bntz ligands act as μ_2 -bridging mode ($\mu_{1,2}$ -bntz bridges) leading to the regular chain structure running along the [100] direction (Figures 4 and 5).

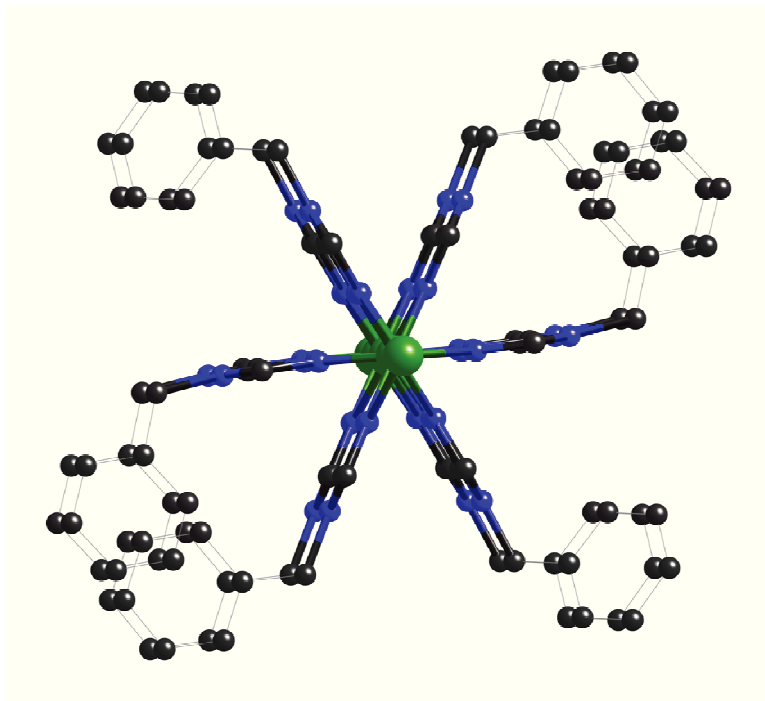


Figure 5. View of the cationic chain [Fe(bntz)₃]²⁺ in **1**: projection of the chain along the [100] direction. Colour code: Fe (green), N (blue) and C (black); (Hydrogen atoms have been omitted for clarity).

The Fe-N bond lengths and N-Fe-N bond angles, at 296 K and 120 K, are gathered in Table 3. The average Fe-N distances and distortion parameters for both spin states are listed in Table 4.²² The two crystallographically distinct Fe^{II} ions (Fe1 and Fe2) adopt similar and very regular FeN₆ octahedral geometries, as demonstrated by the unusually low values of Σ and Θ parameters (Table 4).²² Thus, it is worth noting that the distortion of the octahedrons is higher in the *LS* state than in the *HS* state, conversely to what is generally observed. While more pronounced for Fe1 compared to Fe2, this unusual effect confirms that 1-D triazole systems tend

to adopt rigid and regular coordination spheres,¹³ but also indicates that the Fe^{II} environment is more constrained in the *LS* state. The average values of the Fe-N distances for Fe1 and Fe2, at 296 K (2.190(3), 2.189(3) Å) and 120 K (1.991(4), 1.998(4) Å) (Table 4), are in agreement with the presence of *HS* and *LS* states, respectively. The latter observation is consistent with the presence of a complete *HS/LS SCO* transition, as revealed by the magnetic and the calorimetry (DSC) studies.

Table 3. Fe-N bond lengths (Å) and N-Fe-N bond angles (°) of [Fe(bntrz)₃][Pt(CN)₄].H₂O (**1**), at 296 K and 120 K.

<i>T</i> (K)	296 (<i>HS</i> state)	120 (<i>LS</i> state)
Fe1-N1	2.179(3)	1.988(3)
Fe1-N4	2.210(3)	2.000(4)
Fe1-N7	2.182(3)	1.985(3)
Fe2-N2	2.176(3)	1.998(3)
Fe2-N5	2.195(3)	2.001(4)
Fe2-N8 ^(a)	2.195(3)	1.994 (4)
N1-Fe1-N7	91.08(12)	91.30(14)
N1-Fe1-N7 ^(a)	88.92(12)	88.70(14)
N1-Fe1-N4	89.28(12)	88.32(14)
N1-Fe1-N4 ^(a)	90.72(12)	91.68(14)
N7-Fe1-N4	90.57(12)	91.09(14)
N7 ^(a) -Fe1-N4	89.43(12)	88.91(14)
N2-Fe2-N8	89.50 (12)	89.47(15)
N2-Fe2-N8 ^(b)	90.50(12)	90.53(15)
N2-Fe2-N5 ^(b)	91.04(12)	91.58(15)
N2-Fe2-N5	88.96(12)	88.42(15)
N8-Fe2-N5	90.99(12)	89.01(16)
N8 ^(b) -Fe2-N5	89.01(12)	90.99(16)

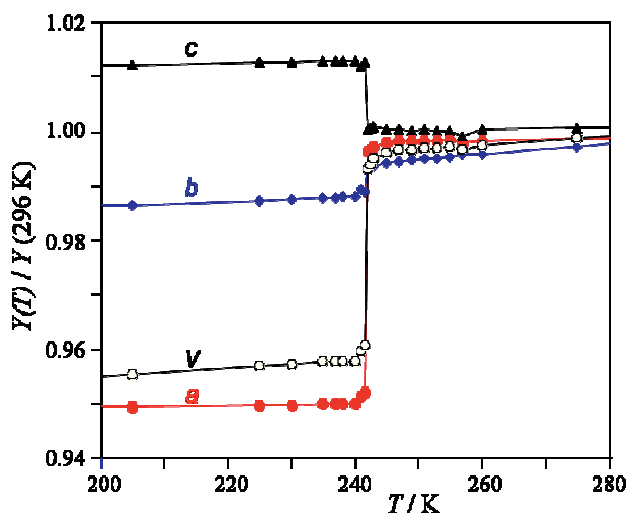
Symmetry transformations used to generate equivalent atoms: (a) 1-x, -y, 1-z; (b) = -x, -y, 1-z.

Table 4. Average Fe-N distances and distortion parameters of [Fe(bntrz)₃][Pt(CN)₄].H₂O (**1**).

<i>T</i> (K)	296 (<i>LS</i> state)		120 (<i>HS</i> state)	
Fe ^{II}	Fe1	Fe2	Fe1	Fe2
$\langle d_{\text{Fe-N}} \rangle / \text{\AA}$	2.190(3)	2.189(3)	1.991(4)	1.998(4)
$\Sigma / \Theta / ^\circ$	10 / 23	10 / 26	16 / 40	13 / 33
Spin state	<i>HS</i>	<i>HS</i>	<i>LS</i>	<i>LS</i>

^a Σ^{22} is the sum of the deviation from 90° of the 12 cis-angles of the FeN₆ octahedron; ^b Θ^{22} is the sum of the deviation from 60° of the 24 trigonal angles of the projection of the FeN₆ octahedron onto its trigonal faces.

In order to understand how the crystal structure is affected by the *SCO* transition, the temperature dependence of the lattice parameters of a single crystal of **1** was measured in the range 200–280 K. As clearly depicted in Figure 6, the evolution of the unit cell parameters (*a*, *b*, *c*) reveals significant anisotropic changes at the transition temperature (*ca.* 242 K), more precisely a contraction upon heating for the *c* parameter paralleled with positive expansions occurring simultaneously in the *ab* plane. The amplitude of the anisotropic expansion is much more pronounced along the *a* axis, proving that the major structural change accompanying the *SCO* transition in the overall structure arises along the 1D chain.

**Figure 6.** Thermal evolutions of the lattice parameters (*a*, *b*, *c*) and unit cell volume for **1**, showing the anisotropic changes (expansion along *a*, *b* and contraction along *c* axis) upon *SCO* transition.

Unlike what has been observed for the parent compound $[\text{Fe}(\text{Htrz})_2(\text{trz})](\text{BF}_4)$,¹⁴ the careful examination of the shortest inter-chain contacts (π -stacking, hydrogen bonding and Van der Waals contacts) in **1** reveals that direct interchain interactions are quasi inexistent. However, the presence of significant hydrogen bonding occurring along the $[102]$ and $[-111]$ directions connects the chains in the c and b directions respectively, leading to an overall 3D packing (Figures 7-8).

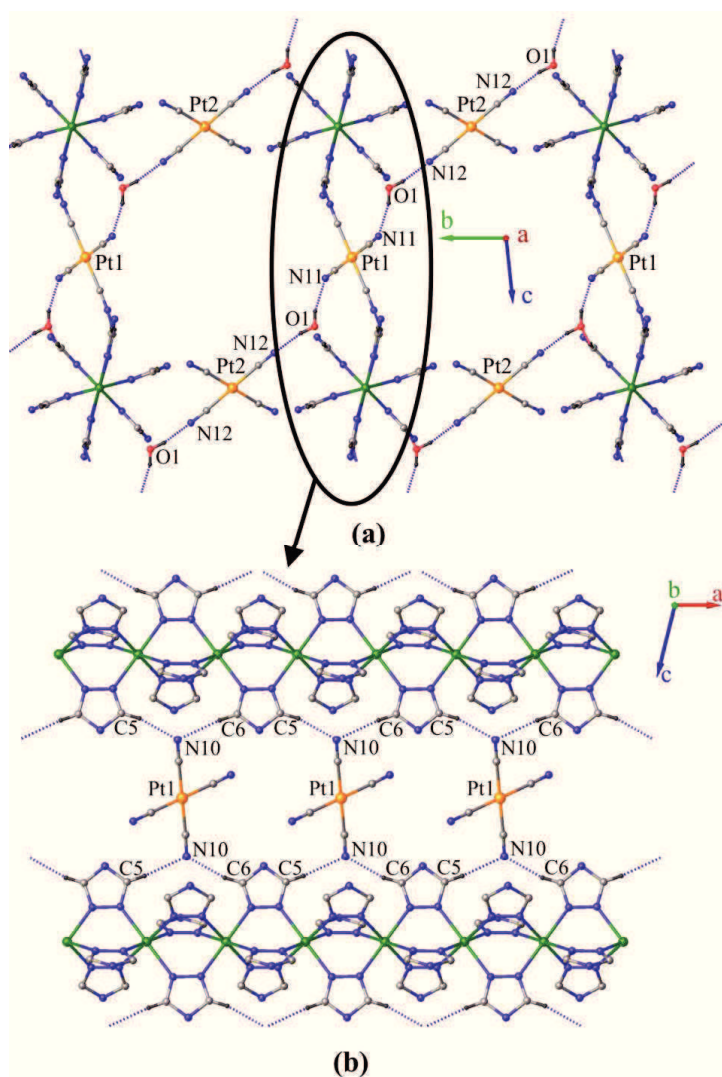


Figure 7. Intermolecular hydrogen bonding contacts in **1** (a) along the a direction and (b) along the b direction. (Hydrogen atoms and benzyl groups of the triazole have been omitted for clarity).

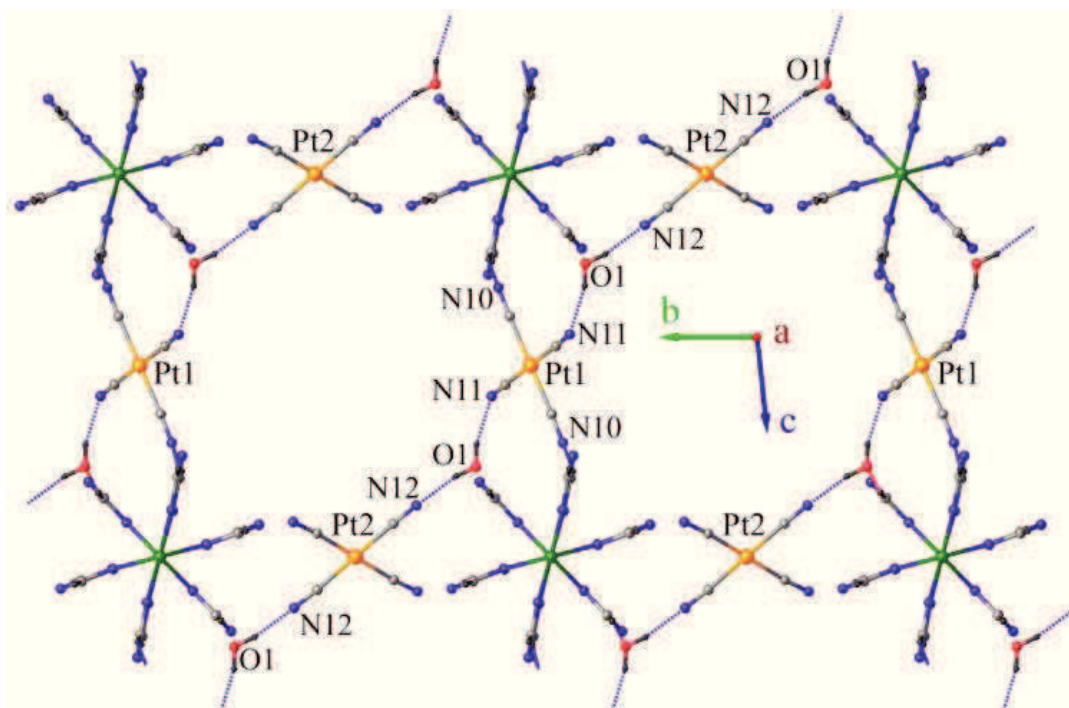


Figure 8. Intermolecular hydrogen bonding contacts in **1** (a) along the *a* direction. Shortest contacts (Å): N11...O1 = 2.944, O1...N12 = 2.995 at 296 K; N11...O1 = 2.888, O1...N12 = 2.883 at 120 K. (Hydrogen atoms, side chains of the triazole have been omitted for clarity).

These interactions are more pronounced in the *LS* state than in the *HS* state. This observation may explain the more constrained iron geometry along the chain in the *LS* state. Due to the triclinic symmetry of the crystal lattice, the inter-chain distances do not exactly match the Fe-Fe intermolecular distances, but are shorter because the chains are slightly shifted from each other in the *a* direction (Figure 9). It follows that the inter-chain distances are different along the *b* and *c* directions. Thus, in the *LS* state, they are shorter in the *b* direction (14.2708(4) Å) compared to the *c* direction (14.5072(4) Å), while in the *HS* state, we observe the opposite tendency, since the inter-chain distances along the *b* direction (14.4975(4) Å) are bigger than those observed along the *c* axis (14.2832(4) Å), leading finally to very similar distances in the *LS* and the *HS* states but inverted with respect to *a* and *b* parameters (Figures 10-11).

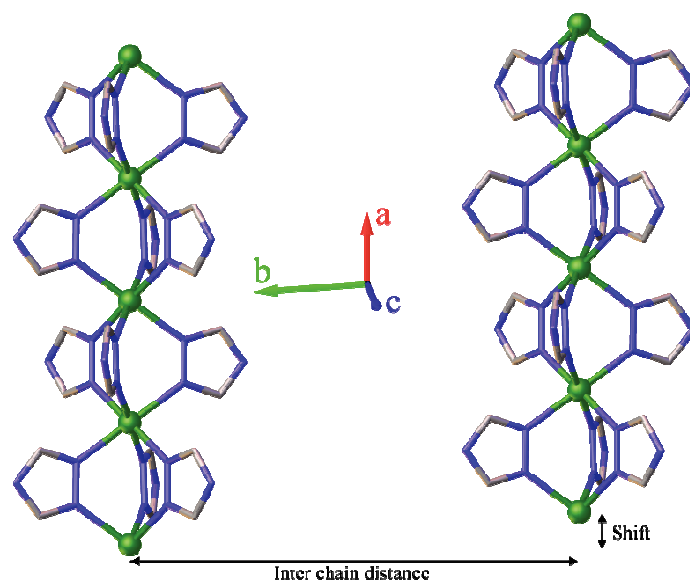


Figure 9. View of **1** showing the inter-chains distance along the *b* direction and the shift of the chain in the *a* direction (Hydrogen atoms, side chains of the triazole and anions have been omitted for clarity).

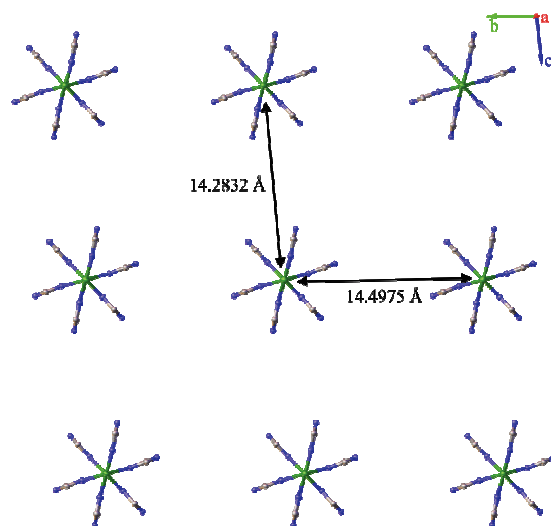


Figure 10. View of **1** along the (100) direction showing the inter-chains distances in the *b* and *c* direction at 296 K in the *HS* state (Hydrogen atoms, side chains of the triazole and anions have been omitted for clarity).

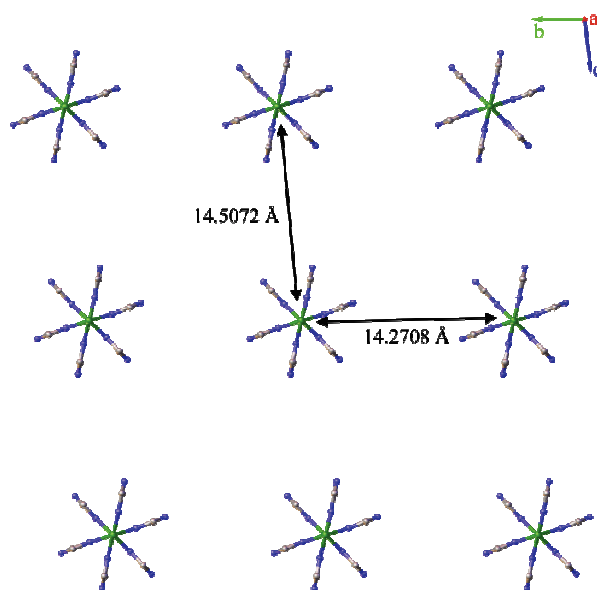


Figure 11. View of **1** along the (100) direction showing the inter-chains distances in the *b* and *c* direction at 120 K in the *LS* state (Hydrogen atoms, side chains of the triazole and anions have been omitted for clarity).

These observations indicate a significant motion of the chains that corresponds to a gliding along the *a* direction as the chains shifts increase during the *LS* to *HS* transition ($0.3287(4)$ Å and $0.3736(4)$ Å for *b* and *c* directions, respectively). This structural rearrangement of the chains may be responsible of the smaller unit cell volume change at the transition than the parent compound $[\text{Fe}(\text{Htrz})_2(\text{trz})](\text{BF}_4)$ (5.4% vs 11.5%).¹³ Such capability of structural breathing was not observed in $[\text{Fe}(\text{Htrz})_2(\text{trz})](\text{BF}_4)$ and may explain the (*i*) unusual crystal quality of compound **1** and its (*ii*) exceptional reliability and mechanical robustness to repeated *LS* to *HS* transition cycles.

Conclusion

In conclusion, we have prepared and characterized a new triazole-based $[\text{Fe}(\text{bntrz})_3][\text{Pt}(\text{CN})_4]\cdot\text{H}_2\text{O}$ (**1**) salt exhibiting an abrupt spin transition with a transition temperature of *ca.* 242 K. The cationic $[\text{Fe}(\text{bntrz})_3]^{2+}$ complex displays a polymeric chain, similar to that reported for the Fe^{II} triazole-based systems exhibiting magnetic bistability around or above room temperature.¹¹⁻¹⁴ The present study clearly evidences the starring roles of the ligand substitution and counter ion changes to prevail over the implicit crystallogenesi s issue in the $\text{Fe}^{\text{II}}/\text{trz}$ systems, with the association of bntrz ligand and $[\text{Pt}(\text{CN})_4]^{2-}$ anion leading for the first time to robust single crystals of high quality and relatively considerable size (up to $0.45 \times 0.04 \times 0.04 \text{ mm}^3$) that withstand the *LS/HS* first-order spin transition. Distinctively from other 1D $\text{Fe}^{\text{II}}/\text{trz}$ systems for which the origin of the strong cooperativity remains strictly indefinite because of the lack of structural information, the characteristics of complex **1** led us to single crystal X-ray data collections of high-quality, allowing highly refined structural characterizations of both high and low spin states, and the thermal evolution of the lattice parameters.

The polymeric chain structure of **1**, crystallographically determined at 296 K and 120 K, is built from two different Fe^{II} centers for which the average values of the Fe-N distances are in agreement with the complete *HS/LS* spin transition revealed by the magnetic data. The thermal variation of the lattice parameters shows anisotropic changes at the transition temperature, and proves that the most pronounced structural changes occur along the 1D covalent chain. The intermolecular inter-chain contacts occur through hydrogen bonding *via* the $[\text{Pt}(\text{CN})_4]^{2-}$ anions leading to an overall 3D arrangement. The absence of a wide hysteresis loop in **1** clearly reveals that the strong short-range " $\text{Fe}^{\text{II}}-(\text{Rtrz})_3-\text{Fe}^{\text{II}}$ " interactions along the chain are not sufficient to drive the existence of the metastable states at the origin of thermal hysteresis, and confirms that the overall long-range interactions should play a crucial role to promote significant elastic strains which stabilizes the spin state changes. The exceptional resilience of the present crystals upon repeated switching cycles is most likely due to the anisotropic expansion/contraction of the unit cell upon *SCO* transition, which allows the existence of a mismatch free *HS/LS* interface resulting from the capability of the " $\text{Fe}^{\text{II}}-(\text{Rtrz})$ " chains to glide from each other and

accommodate the structural modifications despite the sharp transition. This observation is similar to that of the spin-crossover single crystals [$\{\text{Fe}(\text{NCSe})(\text{py})_2\}_2(\text{m-bpypz})$] (with py = pyridine and bpypz = 3,5-bis(2-pyridyl)pyrazolate) recently reported by K. Boukheddaden *et al.*²³ In this context, we are currently investigating by optical microscopy the response of a single crystal of **1** upon thermal *SCO* transition in order to visualize the nucleation, the growth, and the propagation of *HS* and *LS* domains accompanying the first-order transition.²⁴ The observation of the orientation and the dynamics of the *HS/LS* interface should allow for a better understanding of the role of the anisotropic changes of the lattice parameters on the exceptional resilience of this material. On the other hand, we are also currently exploring other systems exhibiting similar chain, but with different crystal packing to enhance/control the interchain interactions and produce hysteretic features. *In fine*, the aim is to establish thorough and systematic magneto-structural correlations which are essential to understand the physicochemical origin of the strong cooperativity in such striking materials, but also to rationalize the tuning of the *SCO* properties.

Experimental section

1. General considerations

All the starting reagents were purchased from commercial sources (Sigma-Aldrich, Across, Fisher Scientific, Alfa Aesar and Merck) and used without further purification unless otherwise stated. Deuterated solvents were purchased from Sigma-Aldrich and Cambridge Isotope Laboratories. Dried solvents were prepared by refluxing for one day under dinitrogen over the appropriate drying agents (calcium hydride for acetonitrile, dichloromethane, hexane; magnesium and iodine for methanol; sodium for ethanol, and molecular sieves for DMF), and then degassed before use. Solvents were stored in glass ampoules under argon. Alternatively, they could be obtained from a solvent purification device (MBRAUN). All glassware and cannula were stored in an oven (>373 K). When appropriate, the reactions were carried out under argon or nitrogen by using a dual manifold vacuum/argon line and standard Schlenk techniques.

2. Synthesis of triazole ligand: 4-(Benzyl)-1,2,4-triazole (bntrz)

The 4-(benzyl)-1,2,4-triazole (bntrz) ligand was synthesized by modifying a previously reported method (see scheme 1).¹⁷ A solution of triethyl orthoformate (12 mL, 72 mmol) and formylhydrazine (3.6 g; 60 mmol) in 50 mL of freshly distilled anhydrous methanol was refluxed for 4 hours. Then, the benzylamine (6.6 mL, 60 mmol) was added to the solution under nitrogen atmosphere, and the mixture was further refluxed for 24 hours. After removal of the solvent under reduced pressure, the resulting white solid was dissolved in 100 mL of methanol and ether in 2:8 volume ratios. The resulting solution was kept in a freezer for 2 days. Finally, the product was filtered and washed with ether to obtain a white crystalline powder (Yield: 5.7 g, 60 %).

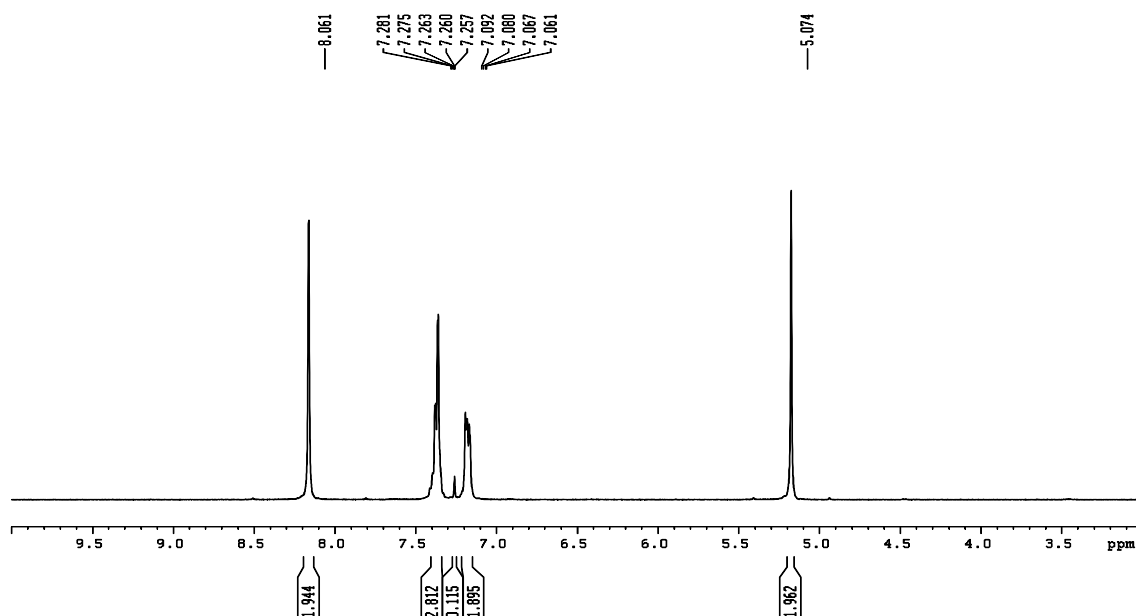


Figure 12. ^1H NMR (300 MHz, CDCl_3 , 298 K) of bntz. ^1H NMR: δ , 5.07 (s, 2H, CH_2), 7.06-7.09(m, 2H, CH), 7.25-7.28 (m, 3H, CH), 8.06 (s, 2H, $\text{CH}=\text{N}$).

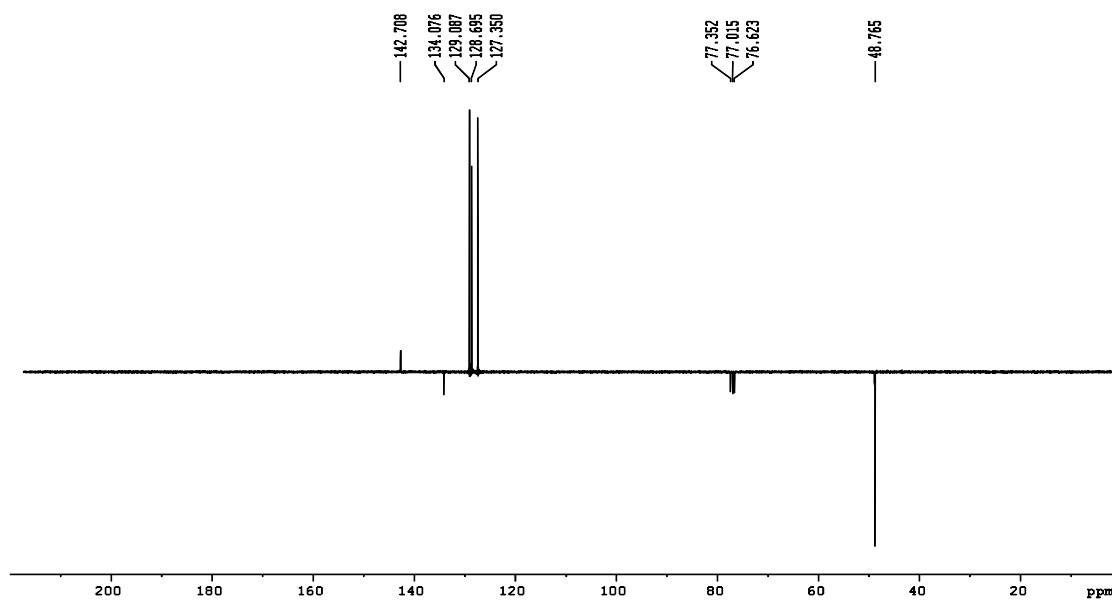


Figure 13. ^{13}C NMR (300 MHz, CDCl_3 , 298 K) of bntz. ^{13}C NMR : δ , 48.8 (Ar-C-N), 127.4 (Ar-C), 128.7 (Ar-C), 129.1(Ar-C), 134.1 (Ar-C), 142.7(N-C=N).

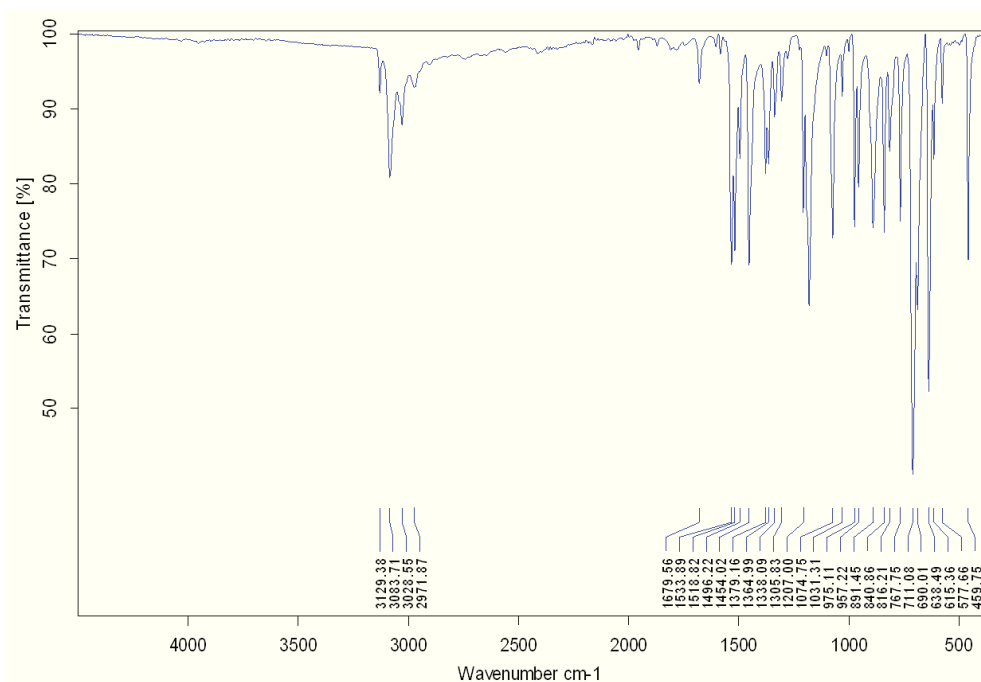


Figure 14. Infrared Spectrum of bntrz. IR data (ν , cm^{-1}): 3129w, 3084w, 3029w, 2972w, 1679w, 1534w, 1519w, 1496w, 1454w, 1379w, 1365w, 1338w, 1207w, 1181m, 1074w, 1031w, 1001w, 975w, 957w, 891w, 841w, 816w, 768w, 711s, 690m, 638m, 615w, 578w, 460w.

3. Single-crystals preparation of complex $[\text{Fe}(\text{bntrz})_3][\text{Pt}(\text{CN})_4]\cdot\text{H}_2\text{O}$ (**1**)

Single-crystals of **1** were prepared by slow diffusion, in a fine glass tube (3.0 mm diameter). An aqueous solution (5 mL) of $\text{K}_2[\text{Pt}(\text{CN})_4]\cdot x\text{H}_2\text{O}$ (0.1 mmol, 37.7 mg) and an aqueous solution (5 mL) of $\text{Fe}(\text{BF}_4)_2\cdot 6\text{H}_2\text{O}$ (0.1 mmol, 33.7mg) were mixed with stirring; the white turbid was formed from the resulting solution after 1 hour. Then, an ethanol solution (3 mL) of triazole ligand (0.3 mmol, 47.7 mg) was carefully layered onto the above solution with addition of a small amount of solvent between the two solutions to slowdown the diffusion. White needle colorless crystals of **1**, suitable for X-ray analysis, were formed and collected after three weeks (Yield 53 %, 45.1 mg). Anal. Calcd for $\text{C}_{31}\text{H}_{29}\text{FeN}_{13}\text{OPt}$: C, 43.7; H, 3.4; N, 21.4 %. Found: C, 44.1; H, 3.4; N, 21.7 %.

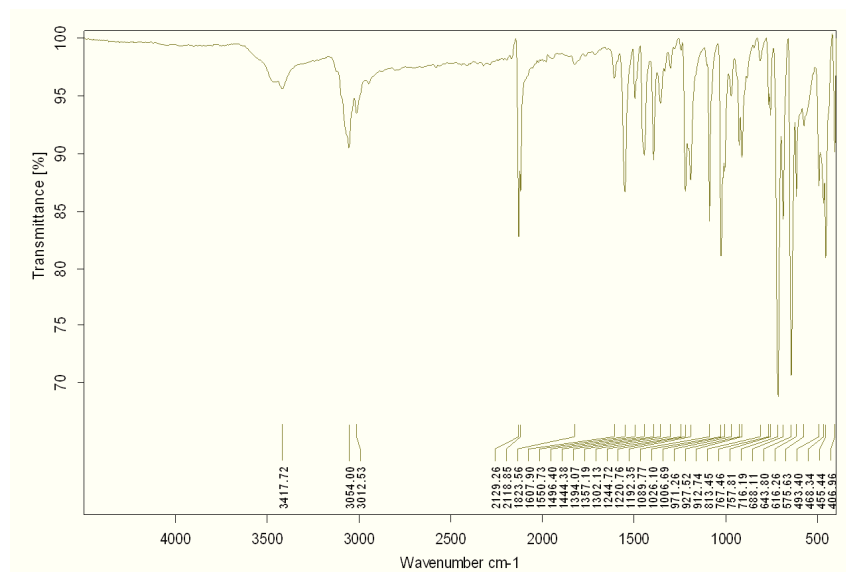


Figure 15. IR Spectrum of the single crystals of $[\text{Fe}(\text{bntrz})_3][\text{Pt}(\text{CN})_4]\cdot\text{H}_2\text{O}$ (**1**) ($4000\text{--}400\text{ cm}^{-1}$). IR data (ν , cm^{-1}): 3418br, 3054w, 3013w, 2119m, 1608w, 1551m, 1496w, 1496w, 1444w, 1394w, 1221w, 1192w, 1090m, 1026m, 716s, 688w, 644s.

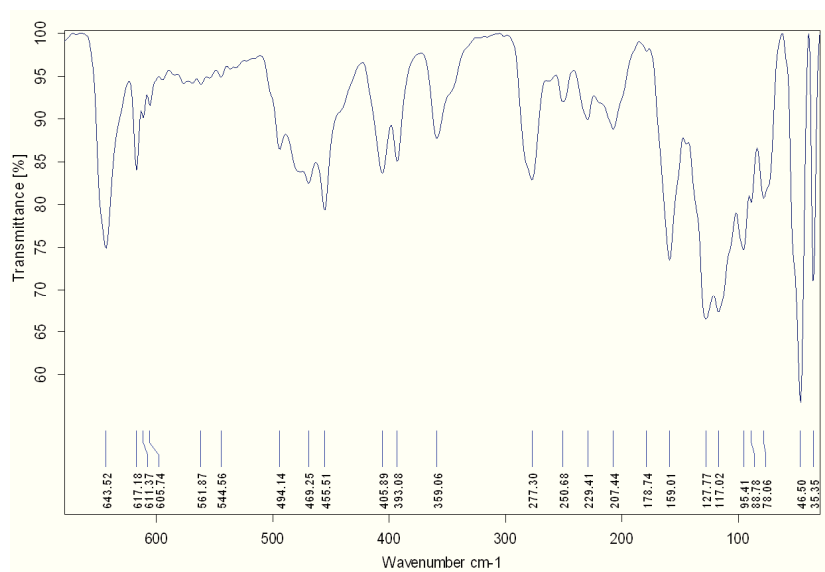


Figure 16. IR Spectrum of the single crystals of $[\text{Fe}(\text{bntrz})_3][\text{Pt}(\text{CN})_4]\cdot\text{H}_2\text{O}$ (**1**) ($650\text{ to }35\text{ cm}^{-1}$). IR data (ν , cm^{-1}): 644s, 617w, 494w, 469w, 405w, 393w, 359w, 277m, 250m, 229w, 207w, 159s, 128s, 117s, 95m, 78w, 46s, 35m.

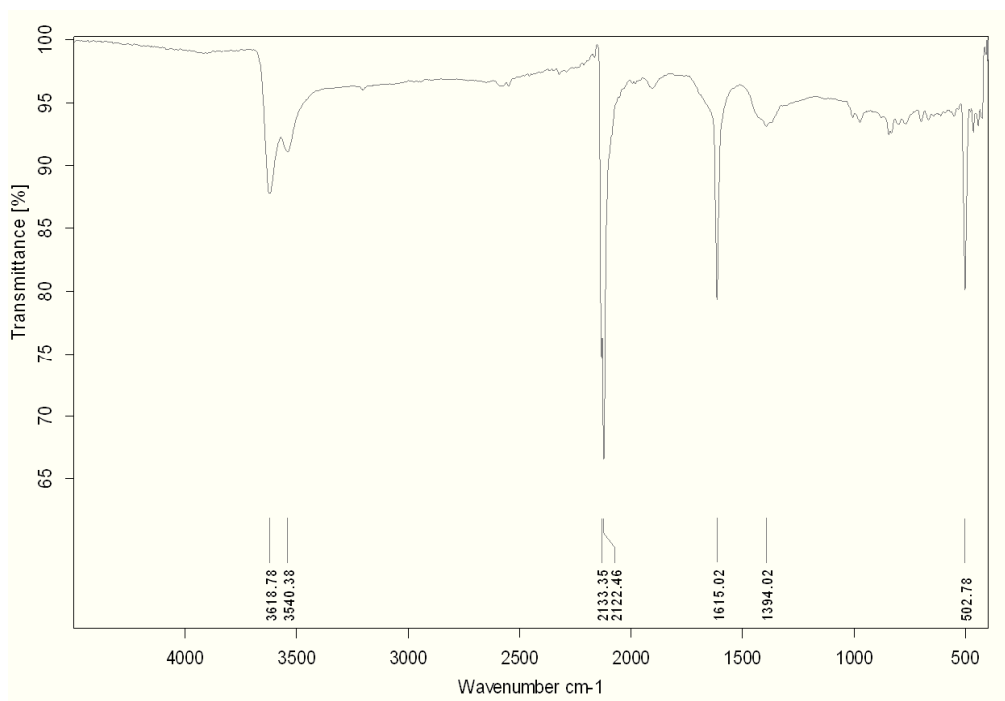


Figure 17. IR spectrum of $K_2[Pt(CN)_4] \cdot xH_2O$. IR data (ν , cm^{-1}): 2133m, 2122s.

4. X-ray Crystallography studies

Crystallographic studies of the single crystals of **1** were performed at 296 K and 120 K, using an Oxford Diffraction Xcalibur κ -CCD diffractometer equipped with a graphite monochromated Mo $K\alpha$ radiation ($\lambda = 0.71073 \text{ \AA}$). The full sphere data collections were performed using 1.0° ω -scans with an exposure time of 150 and 200 s per frame, and 60 and 80 s per frame for **1** at 296 K and 120 K, respectively. The corresponding structures were solved by direct methods with the SHELXS program and refined on F^2 by weighted full matrix least-squares methods using the SHELXL program.²⁵ All non-hydrogen atoms were refined anisotropically, while the hydrogen atoms were calculated and therefore included as isotropic fixed contributors to F_c . All other calculations were performed with standard procedures (WINGX).²⁶ Crystallographic data and structural refinement details are provided in Table 2.

5. Physical measurements and characterizations: spectroscopy, DSC and magnetic studies

$^1\text{H}/^{13}\text{C}$ - NMR spectra were recorded on Bruker AMX-300 spectrometer, and the spectra were referenced internally using residual proton solvent resonances relative to tetramethylsilane ($\delta = 0$ ppm). Infrared (IR) spectra were collected in the range $4000\text{--}35\text{ cm}^{-1}$ on a FT-IR BRUKER ATR VERTEX70 Spectrometer. DSC measurements were performed on a DSC-1/LN2 Mettler Toledo calorimeter setting the heat flow scan rate at $s = 2\text{ K}\cdot\text{min}^{-1}$. Magnetic measurements were performed with a Quantum Design MPMS-XL-5 SQUID magnetometer in the $2\text{--}300\text{ K}$ temperature range with an applied magnetic field of 2 Tesla and scan rate of $0.4\text{ K}\cdot\text{min}^{-1}$ on single crystals of compound **1**. Elemental analyses were performed at the “Service de microanalyse”, CNRS, 91198 Gif-sur-Yvette, France.

Bibliography

1. H. Phan, S. M. Benjamin, E. Steven, J. S. Brooks, M. Shatruk, *Angew. Chem. Int. Ed.*, **2015**, *54*, 823-827.
2. S.-I. Ohkoshi, H. Tokoro, *Acc. Chem. Res.*, **2012**, *45*, 1749-1758.
3. E. Coronado, J. R. Galán-Mascarós, M. Monrabal-Capilla, J. García-Martínez, P. Pardo-Ibáñez, *Adv. Mater.*, **2007**, *19*, 1359-1361.
4. O. Kahn, C. J. Martinez, *Science*, **1998**, *279*, 44-48.
5. P. Güthlich, A. Hauser, H. Spiering, *Angew. Chem. Int. Ed. Engl.*, **1994**, *33*, 2024-2054
6. M. A. Halcrow, *Spin-Crossover Materials: Properties and Applications*, John Wiley & Sons (Eds.), **2013**.
7. M. A. Halcrow, *Chem. Soc. Rev.*, **2011**, *40*, 4119-4142.
8. P. Guionneau, *Dalton Trans.*, **2014**, *43*, 382-393.
9. L. G. Lavrenova, V. N. Ikorskii, V. A. Varnek, I. M. Oglezneva, S. V. Larionov, *Koord. Khim.*, **1986**, *12*, 207.
10. M. M. Dîrtu, C. Neuhausen, A. D. Naik, A. Rotaru, L. Spinu, Y. Garcia, *Inorg. Chem.*, **2010**, *49*, 5723-5736.
11. O. Roubeau, *Chem. Eur. J.*, **2012**, *18*, 15230-15244.
12. A. Urakawa, W. Van Beek, M. Monrabal-Capilla, J.-R. Galán-Mascarós, L. Palin, M. Milanesio, *J. Phys. Chem. C*, **2011**, *115*, 1323-1329.
13. A. Grosjean, P. Négrier, P. Bordet, C. Etrillard, D. Mondieig, S. Pechev, E. Lebraud, J.-F. Létard, P. Guionneau, *Eur. J. Inorg. Chem.*, **2013**, 796-802.

14. A. Grosjean, N. Daro, B. Kauffann, A. Kaiba, J.-F. Létard, P. Guionneau, *Chem. Commun.*, **2011**, 47, 12382-12384.
15. C. Atmani, F. El Hajj, S. Benmansour, M. Marchivie, S. Triki, F. Conan, V. Patinec, H. Handel, G. Dupouy, C. J. Gómez-García, *Coord. Chem. Rev.*, **2010**, 254, 1559-1569.
16. E. Milin, V. Patinec, S. Triki, E.-E. Bendeif, S. Pillet, M. Marchivie, G. Chastanet, K. Boukheddaden, *Inorg. Chem.*, **2016** (DOI:10.1021/acs.inorgchem.6b01081).
17. (a) H. O. Bayer, R. S. Cook, W. C. von Mayer, *US Pat.*, **1974**, 3,821,376; (b) H. O. Bayer, R. S. Cook, W. C. von Mayer, *US Pat.*, **1972**, 3,647,810
18. (a) R. K. Bartlett, I. R. Humphrey, *J. Chem. Soc. (C)*, **1967**, 1664-1666; (b) A. Horvath, *Synthesis*, **1995**, 1183-1189.
19. (a) J. G. Haasnoot, G. Vos, W. L. Groeneveld, *Z. Naturforsch.*, **1977**, 32 b, 1421-1430; (b) V. P. Sinditskii, V. I. Sokol, A. E. Fogelzang, M. D. Dutov, V. Serushkin, M. A. Poraikoshits, B. S. Svetlov, *Russ. J. Inorg. Chem.*, **1987**, 32, 1950.
20. (a) K. L. Ronayne, H. Paulsen, A. Höfer, A. C. Dennis, J. A. Wolny, A. I. Chumakov, V. Schünemann, H. Winkler, H. Spiering, A. Bousseksou, P. Gülich, A. X. Trautwein, J. J. McGarvey, *Phys. Chem. Chem. Phys.*, **2006**, 8, 4685-4693; (b) J. P. Tuchagues, A. Bousseksou, G. Molnar, J. J. McGarvey, F. Varret, *Top. Curr. Chem.*, **2004**, 235, 85-103.
21. M. Sorai, S. Seki, *J. Phys. Chem. Solids*, **1974**, 35, 555-570.
22. M. Marchivie, P. Guionneau, J.-F. Létard, D. Chasseau, *Acta Cryst. B*, **2005**, 61, 25-28.
23. M. Sy, F. Varret, K. Boukheddaden, G. Bouchez, J. Marrot, S. Kawata, S. Kaizaki, *Angew. Chem. Int. Ed.*, **2014**, 139, 7539-7542.
24. M. Sy, D. Garrot, A. Slimani, M. Paez-Espejo, F. Varret, K. Boukheddaden, *Angew. Chem. Int. Ed.*, **2016**, 55, 1755-1759.

25. G. M. Sheldrick, *Acta Cryst.*, **2008**, *A64*, 112.
26. L. J. Farrugia, *J. Appl. Crystallogr.*, **1999**, *32*, 837-838.

Chapter III

Trinuclear Fe(II) Complexes Based on Functionalised Triazole and Cyanocarbanion Ligands with Unique Complete *SCO* Behaviour

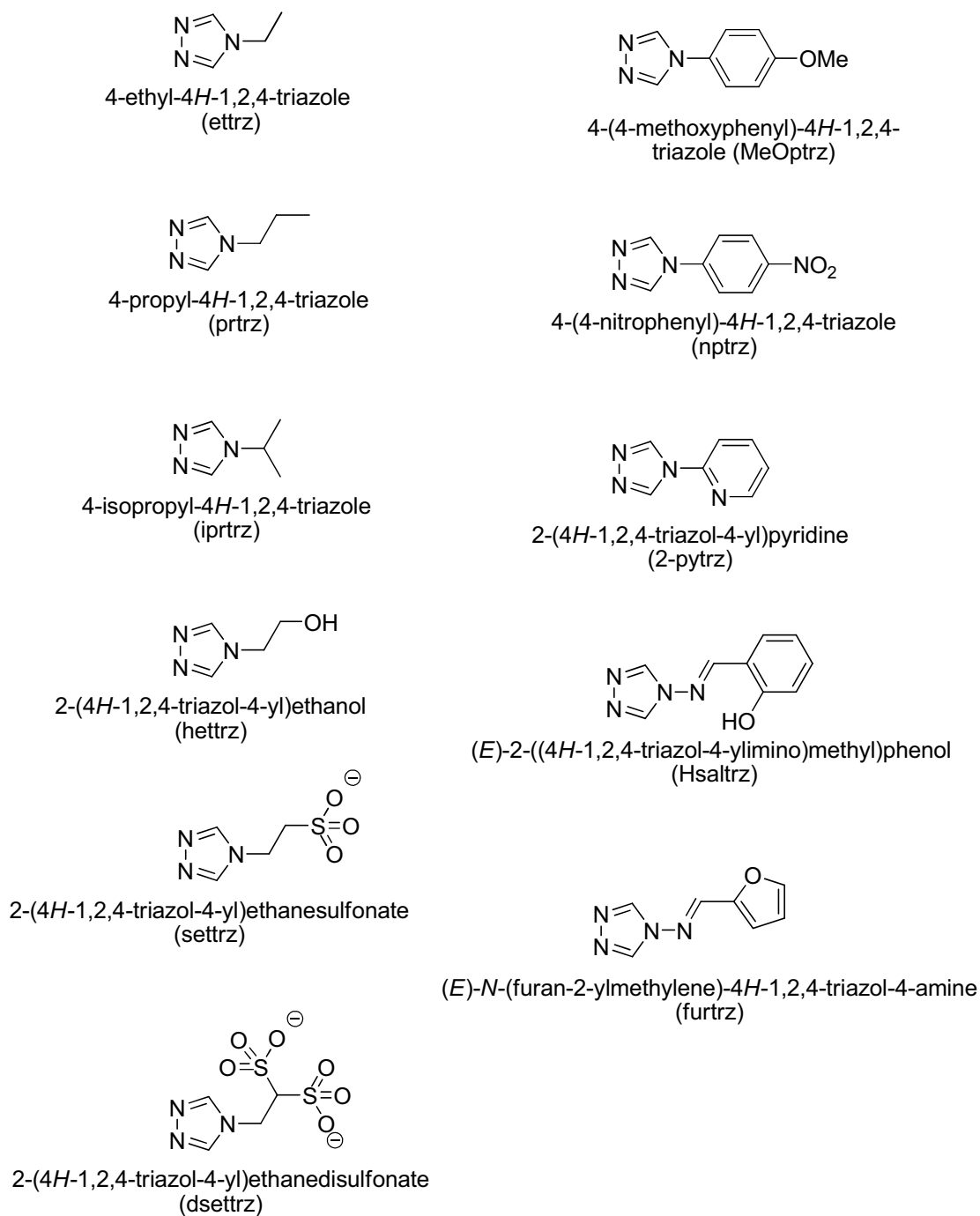
Table of Contents

Introduction	112
Results and discussion	116
1. Syntheses and spectroscopic characterizations of $[\text{Fe}_3(\text{bntrz})_6(\text{tcnset})_6]$ (2)	116
2. Magnetic properties	119
3. Calorimetric studies	120
4. Crystal structure analyses	121
Conclusion	127
Experimental section	128
Bibliography	136

Trinuclear Fe(II) Complexes Based on Functionalised Triazole and Cyanocarbanion Ligands with Unique Complete *SCO* Behaviour

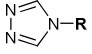
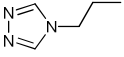
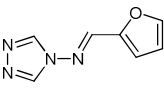
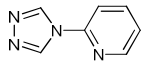
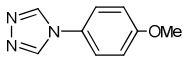
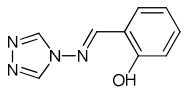
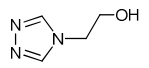
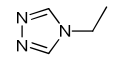
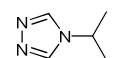
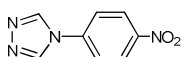
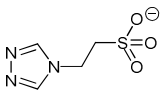
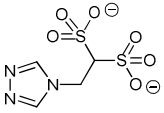
Introduction

Among the molecular switchable materials, the spin crossover (*SCO*) materials are particularly of interest, notably because of their potential applications in the development of new generations of electronic devices such as memory, molecular sensing and displays.¹ When the spin pairing energy is close to the splitting energy,^{1,2} a *SCO* transition between the high-spin state (*HS*, $S = 2$, ${}^5T_{2g}$) and low-spin state (*LS*, $S = 0$, ${}^1A_{1g}$) can be induced by different external solicitations such as temperature, pressure, magnetic field and light irradiation.^{2,3} To date, Iron (II) metal complexes involving $[FeN_6]$ octahedron coordination spheres have been the most studied *SCO* compounds. Among the few systems exhibiting remarkable *SCO* behavior, the binary systems based on the 1,2,4-triazole ligands still remain among the most promising materials for future electronic devices since some of them, such as the coordination polymer chains of general formulae $[Fe((NH_2-trz)_3)(X)_2]$ and $[Fe(Htrz)_2(trz)](X)$ (NH_2-trz = 4-amino-1,2,4-triazole, $Htrz$ = 4-H-1,2,4-triazole, trz^- = 1,2,4-triazolato, X^- = standard monoanions), display wide hysteresis loops around room temperature.⁴ However, the current and longstanding challenge to obtain single crystals of such coordination polymers make difficult to access structural data at the molecular and inter-molecular scales which are essential to understand and fine tune their *SCO* characteristics such as the origin of their strong cooperativity (see Chapter II). Alternatively, new polynuclear triazole-based *SCO* complexes, involving similar structural features - i.e. triple N1,N2-triazole bridges based on functionalized 1,2,4-triazole, similar Fe(II) environments, and/or chain sections - are currently extensively studied.⁵⁻⁸ Such polynuclear systems could assist the modeling of the *SCO* characteristics of the 1D chain polymers. In this context, several trinuclear triazole-based *SCO* complexes have been reported, with an archetypal linear molecular structure in which the Fe(II) centers are bridged by substituted 1,2,4-triazole ligands (see Scheme 1 and Table 1).⁵⁻⁸



Scheme 1. Examples of functionalized 1,2,4-triazole ligands reported in the literature for trinuclear Fe(II) *SCO* complexes.⁵⁻⁸

Table 1. Trinuclear Fe(II) *SCO* complexes with triple N1,N2-triazole bridges based on functionalized triazole ligands reported in the literature.⁵⁻⁸

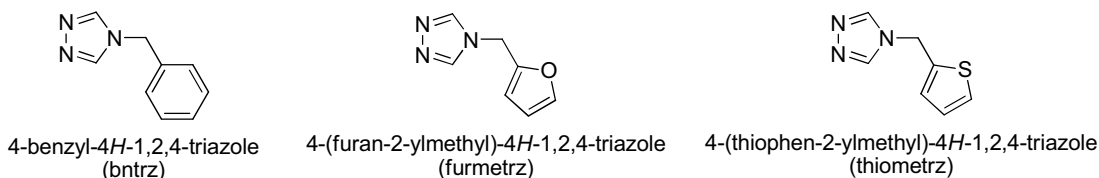
	Trinuclear complex	<i>SCO</i> behavior / $T_{1/2}$	Ref.
	$[\text{Fe}_3(\text{ptrz})_6(\text{ReO}_4)_4(\text{H}_2\text{O})_2](\text{ReO}_4)_2 \cdot \text{H}_2\text{O}$	gradual / $T_{1/2}=185$ K	5a
	$[\text{Fe}_3(\text{furtrz})_6(\text{ptol})_2(\text{MeOH})_4](\text{ptol})_4 \cdot 4(\text{MeOH})$	gradual / $T_{1/2}=170$ K	5b
	$[\text{Fe}_3(\text{pytrz})_8(\text{H}_2\text{O})_4](\text{NO}_3)_6$	Gradual / $T_{1/2}=208$ K	6a
	$[\text{Fe}_3(\text{pytrz})_8(\text{H}_2\text{O})_4](\text{ClO}_4)_6$	<i>HS</i>	6a
	$[\text{Fe}_3(\text{pytrz})_8(\text{H}_2\text{O})_4](\text{Br})_6$	<i>HS</i>	6a
	$[\text{Fe}_3(\text{meoptrz})_8(\text{H}_2\text{O})_4](\text{BF}_4)_6 \cdot 2\text{H}_2\text{O}$	<i>HS</i>	6b
	$[\text{Fe}_3(\text{meoptrz})_6(\text{H}_2\text{O})_6](\text{Tos})_6 \cdot 4\text{H}_2\text{O}$	gradual / $T_{1/2}=245$ K	6b
	$[\text{Fe}_3(\text{meoptrz})_6(\text{H}_2\text{O})_6](\text{Tos})_6$	gradual / $T_{1/2}=330$ K	6b
	$[\text{Fe}_3(\text{hsaltrz})_6(\text{H}_2\text{O})_2(\text{EtOH})_4](\text{ClO}_4)_6 \cdot 2\text{EtOH}$	<i>HS</i>	7a
	$[\text{Fe}_3(\text{hetrz})_6(\text{H}_2\text{O})_6](\text{CF}_3\text{SO}_3)_6$	gradual / $T_{1/2}=290$ K	7b
	$[\text{Fe}_3(\text{ettrz})_6(\text{H}_2\text{O})_6](\text{CF}_3\text{SO}_3)_6$	abrupt / $T_{1/2}=205$ K	7c
	$[\text{Fe}_3(\text{iptrz})_6(\text{H}_2\text{O})_6](\text{Tos})_6 \cdot 2\text{H}_2\text{O}$	gradual / $T_{1/2}=242$ K	7d
	$[\text{Fe}_3(\text{iptrz})_6(\text{H}_2\text{O})_6](\text{CF}_3\text{SO}_3)_6$	gradual / $T_{1/2}=185$ K	7d
	$[\text{Fe}_3(\text{nptrz})_6(\text{H}_2\text{O})_2(\text{EtOH})_4](\text{ptol})_6 \cdot 4\text{EtOH}$	gradual / $T_{1/2}=148$ K	7e
	$[\text{Fe}_3(\text{settrz})_6(\text{H}_2\text{O})_6] \cdot 5\text{H}_2\text{O}$	spin transition with $T_{1/2}(\uparrow)=357$ K, $T_{1/2}(\downarrow)=343$ K	8a
	$(\text{Me}_2\text{NH}_2)_6[\text{Fe}_3(\text{dsettrz})_6(\text{H}_2\text{O})_6]$	spin transition with $T_{1/2}(\uparrow)=400$ K, $T_{1/2}(\downarrow)=310$ K	8b

Tos = p-toluenesulfonate; ptol = p-tolylsulfonate.

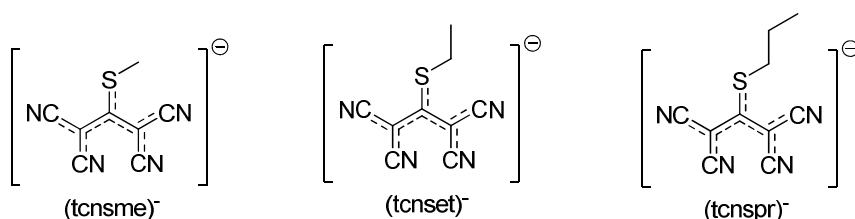
The polynuclear triazole-based systems can be categorized in two different families: (i) the complexes involving neutral functionalized 1,2,4-triazole ligands, which typically display a gradual *SCO* behavior with a transition temperature in the range 150-330 K (Table 1);⁵⁻⁷ and (ii) the second family composed of few recent examples based on anionic triazole ligands such as the 4-(1,2,4-triazol-4-yl)ethanesulfonate (settrz⁻), and the 4-(1,2,4-triazol-4-yl)ethanedisulfonate substituted triazole molecules (dsettrz²⁻) (Table 1).⁸ Referring to the latter, two series have been reported; the first one concerns complexes of formula [Fe₃(settrz)₆(H₂O)₆] \cdot nH₂O (n = 8) based on the monoanionic ligand settrz⁻, with the derivative displaying a gradual *SCO* behavior at 150 K, and a hysteretic transition above room temperature ($T_{1/2}(\uparrow) = 357$ K, $T_{1/2}(\downarrow) = 343$ K) when partially dehydrated (n = 5).^{8a} The second series is composed from the unique *SCO* trinuclear anionic complex (Me₂NH₂)₆[Fe₃(dsettrz)₆(H₂O)₆] that exhibits a large hysteretic cycle above room temperature ($T_{1/2}(\uparrow) = 400$ K, $T_{1/2}(\downarrow) = 310$ K) and a temperature of relaxation, T_{TIESST} , of 240 K which is the highest temperature observed in a switchable molecular material.^{8b}

However, in all those complexes, only the central Fe(II) ion shows a *SCO* behavior, while the two terminal ones coordinated to two or three water molecules (or other oxygenated solvent molecules and/or anions) remain in the *HS* state (Table 1).⁵⁻⁸ Thus, such complexes can be viewed as mononuclear *SCO* complexes in which the single active center displays similar environment than that described for the 1D chain polymers. In addition to deepen the knowledge of the local environment of the Fe(II) active center, the investigations of larger *SCO* molecular discrete complexes, such as “true” trinuclear systems with three *SCO* Fe(II) centers, could be critical to better understand the origin of the cooperativity in such striking 1D systems. In this context, we have extended this polynuclear synthetic approach to combinations of new functionalized triazole ligands such as those depicted in Scheme 2, and cyanocarbanions (Scheme 3) which can act as co-ligands through their N-donor nitrile groups. The strategic use of the latter N-donating based-ligands resides in preventing or limiting the formation of “Fe(II)/1,2,4-triazole” polymeric chains while favoring the coordination of the terminal sites of the polynuclear species by nitrogen groups which are more appropriate for the *SCO* activity. The present work reports the synthesis and full structural and magnetic characterizations of the first

example of triazole-based *SCO* Fe^{II} trinuclear neutral complex [Fe₃(bntrz)₆(tcnset)₆] (**2**) exhibiting a complete one-step spin transition above room temperature.



Scheme 2. Molecular structures of the triazole ligands bntrz, furmetrz and thiometrz.

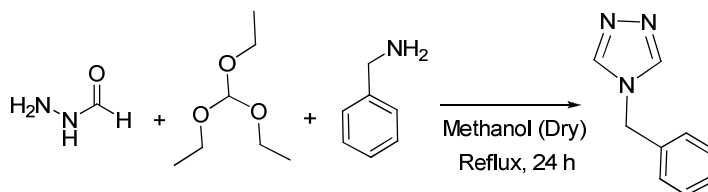


Scheme 3. Examples of functionalized cyanocarabanions of general formula (tcnsR')[−], with R' = -CH₃, -CH₂-CH₃ and -CH₂-CH₂-CH₃.

Results and Discussion

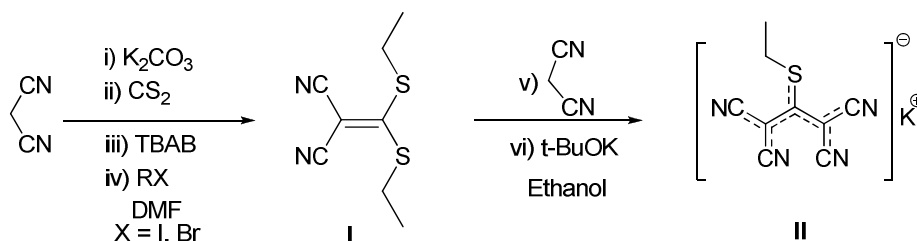
1. Syntheses and spectroscopic characterizations

The 4-(benzyl)-1,2,4-triazole (bntrz) molecule has been prepared as discussed in chapter II, i.e. by the reaction of formic hydrazide and triethyl orthoformate with benzylamine in methanol solvent under nitrogen atmosphere (see Scheme 4).⁹ The resulting pale pink solid was purified using recrystallisation from methanol-ether solvent mixture to obtain a white crystalline powder of bntrz with a yield of 60% (see details in Chapter II).

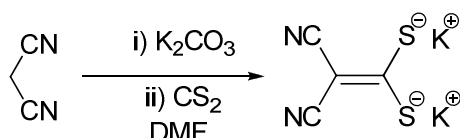


Scheme 4. Synthesis of the triazole based ligand 4-(benzyl)-1,2,4-triazole (bntrz).

The two step synthesis of the potassium [1,1,3,3-tetracyano-2-thioethylpropenide] salt K(tcnset) (**II**, Scheme 5)) has been inspired from previous work from our group, and further developed and optimized in the context of the present study which involves notably the systematic variation of different alkyl substituents on the sulphur atom (see Scheme 5).¹⁰ In the first step, the intermediate molecule 2-[bis(ethylthio)methylene]malononitrile (**I**) has been synthesized by the reaction of alkyl halide and potassium 2,2-dicyanoethene-1,1-bis(thiolate), with the latter formed *in situ* by mixing malononitrile, potassium carbonate and carbondisulphide (see Scheme 6).^{10a,b} Then, the resulting yellow oil has been purified by using flash column chromatography to obtain a pale green solid of (**I**). In the second step, the potassium [1,1,3,3-tetracyano-2-thioethylpropenide] salt K(tcnset) (**II**) has been prepared in ethanol by the reaction of the corresponding 2-[bis(ethylthio)methylene]malononitrile (**I**) with malononitrile in the presence of potassium tertiary butoxide.^{10c} After refluxing the reaction mixture for 1 hour, the final solution has been cooled down to 4 °C, which lead to the formation of a white crystalline powder of potassium [1,1,3,3-tetracyano-2-thioethylpropenide] K(tcnset) (**II**), without further purification needed. Finally, the resulting salt has been characterized by ¹H and ¹³C NMR spectroscopy (see experimental part).



Scheme 5. Synthesis of the potassium salt of [1,1,3,3-tetracyano-2-thioethylpropenide] K(tcnset).



Scheme 6. Synthesis of the potassium 2,2-dicyanoethene-1,1-bis(thiolate) *in situ*.

The single crystals of the complex $[\text{Fe}_3(\text{bntrz})_6(\text{tcnset})_6]$ (**2**) have been synthesized using diffusion technique in a fine glass tube of 3.0 mm diameter by layering a methanol solution of the bntrz ligand onto an aqueous solution containing both $\text{K}(\text{tcnset})$ and $\text{Fe}(\text{BF}_4)_2 \cdot 6\text{H}_2\text{O}$ salts. The pink colored single crystals of the complex **2** were collected and dried in air at room temperature, and successfully characterized by infrared spectroscopy (IR), magnetic studies, differential scanning calorimetry (DSC), and single crystal X-ray diffraction (XRD).

The infrared data analyses have been performed on single crystals of **2** at room temperature to ascertain the coordination modes of $(\text{tcnset})^-$ anion and triazole ligand to the Fe^{II} metal centers in complex **2**. The infrared spectra of the bntrz molecule only and the $\text{K}(\text{tcnset})$ salt are provided in the experimental section as references (Figures 8 and 14, respectively). In the IR spectra of complex **2** (Figures 15-16), the absorption bands observed at 2233 and 2191 cm^{-1} are assigned to the $\nu_{\text{C}=\text{N}}$ stretching vibrations from the $(\text{tcnset})^-$ anion. Those absorption bands are distinct from the stretching vibration modes observed for the potassium salt $\text{K}(\text{tcnset})$ (2189 cm^{-1}), which indicates the presence of both coordinated and uncoordinated nitrile groups in the complex **2**, in agreement with the further single crystal structure determination (see crystal structure analysis).

For the triazole based ligand bntrz, the band assigned to the ring torsion of 1,2,4-triazole at $\nu = 638 \text{ cm}^{-1}$, and the $\nu_{\text{C}=\text{N}}$ stretching vibration at 1534 cm^{-1} , are all shifted upon complexation to 640 cm^{-1} and 1550 cm^{-1} , respectively. Those values confirm the coordination of the triazole to the Fe^{II} centers.¹¹ Finally, the bands observed at 212, 239, 300 and 366 cm^{-1} are assigned to the Fe-N stretching frequencies, and reveal the presence of $\text{Fe}(\text{II})$ metal centers in both high spin (*HS*) state and low spin (*LS*) state at room temperature.¹¹

2. Magnetic properties

The magnetic susceptibility (χ_m) for **2** was measured over the temperature (T) range 2-380 K on a single crystal sample. The thermal variation of the $\chi_m T$ product is displayed in Figure 1. At 380 K, the $\chi_m T$ value ($9.48 \text{ cm}^3 \cdot \text{K} \cdot \text{mol}^{-1}$) is consistent with three isolated HS ($S = 2$) hexacoordinated Fe(II) ions. Upon cooling, the $\chi_m T$ decreases gradually down to a temperature value of *ca.* 320 K. Below this temperature; it sharply decreases to *ca.* $0 \text{ cm}^3 \cdot \text{K} \cdot \text{mol}^{-1}$ around *ca.* 250 K, indicating the presence of a sharp and complete HS to LS SCO first-order phase transition at *ca.* 318 K. Upon warming and cooling at a scan rate of $1 \text{ K} \cdot \text{min}^{-1}$ in settle mode, no thermal hysteresis effects were detected.

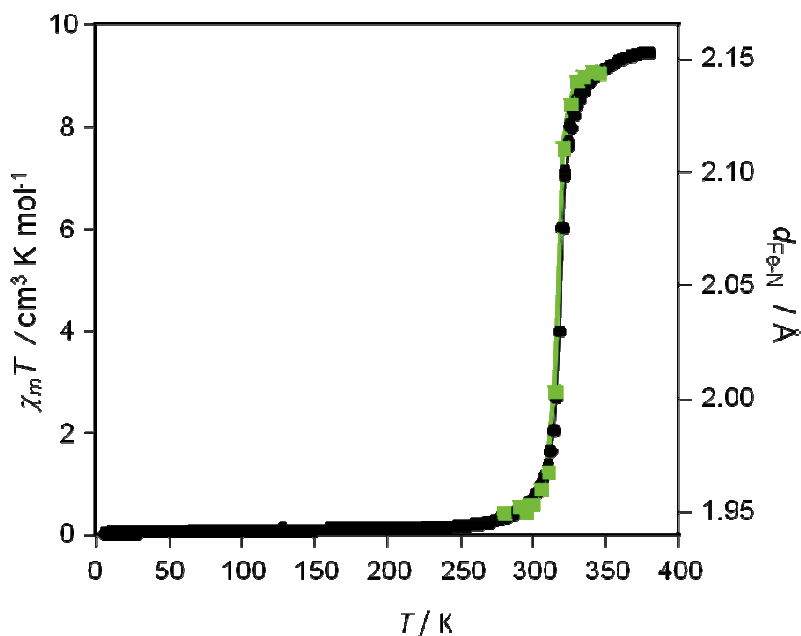


Figure 1. Thermal evolutions of the $\chi_m T$ product in the 2-380 K range (●), and of the average Fe-N distances (■) around the critical region (280-345 K, $T_{1/2} \approx 318 \text{ K}$) for $[\text{Fe}_3(\text{bntrz})_6(\text{tcnsset})_6]$ (**2**).

3. Calorimetric studies

The *SCO* properties of the complex $[\text{Fe}_3(\text{bntrz})_6(\text{tcnset})_6]$ (**2**) has been also investigated by differential scanning calorimetry (DSC) over the temperature range 290-340 K, on both warming and cooling modes with a temperature scan rate of $2 \text{ K}\cdot\text{min}^{-1}$ at ambient pressure. The heat capacity profile for **2** shows symmetrical and well-separated peaks associated with a complete spin transition (Figure 2). An endothermic peak is observed on warming at $T_c\uparrow = 318.7 \text{ K}$ while an exothermic peak is recorded on cooling at $T_c\downarrow = 317.5 \text{ K}$. Those peaks correspond to a first-order phase transition with a hysteresis loop width of 1.2 K . This phase transition occurs with values of enthalpy and entropy changes in agreement with three Fe(II) metal centres, i.e. $\Delta H = 54.08 \text{ kJ}\cdot\text{mol}^{-1}$ and $\Delta S = 170.00 \text{ J}\cdot\text{K}^{-1}\cdot\text{mol}^{-1}$, respectively. These values are in the same range with those reported in the literature for *SCO* compounds.¹²

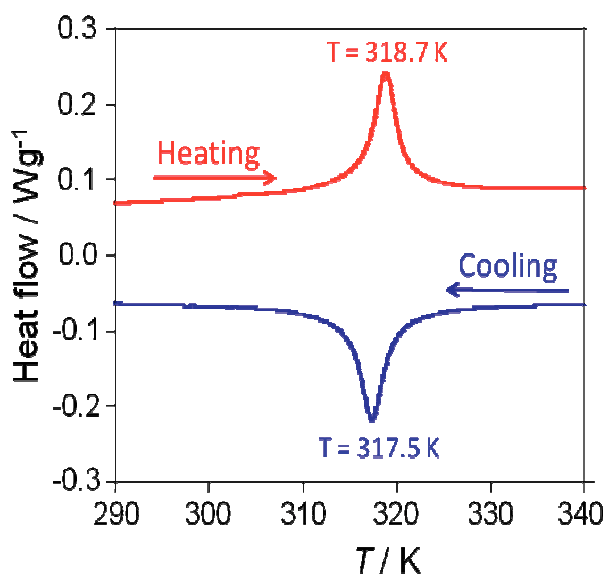


Figure 2. DSC profiles of the complex $[\text{Fe}_3(\text{bntrz})_6(\text{tcnset})_6]$ (**2**) at a scan rate of $2 \text{ K}\cdot\text{min}^{-1}$ upon heating (red) and cooling (blue), respectively.

4. Crystal structure analyses

Based on the magnetic and calorimetric observations, the crystal structure of **2** has been determined at 360 K (*HS* state, colorless crystal), and 170 K (*LS* state, pink crystal). At both temperatures, compound **2** crystallizes in the trigonal *R*-3 space group. The crystal data and structural refinement parameters, the Fe-N bond lengths (Å) and N-Fe-N bond angles (°) of [Fe₃(bntrz)₆(tcnset)₆] (**2**), at 360 K and 170 K, are gathered in Tables 2 and 4, respectively. The average Fe-N distances and distortion parameters, for both metal centers (Fe1 and Fe2), are listed in Table 3 for the two spin states. The unit cell parameters, which are similar at both temperatures, indicate the absence of any structural transition within the studied temperature range (170-360 K). The structure of **2** is built from two crystallographically independent Fe(II) ions (Fe1 and Fe2), located on (2/3 1/3 5/6) and (2/3 1/3 *z*) special positions, respectively, and one bntrz molecule and one (tcnset)[−] anion both located on general positions (Figure 3).

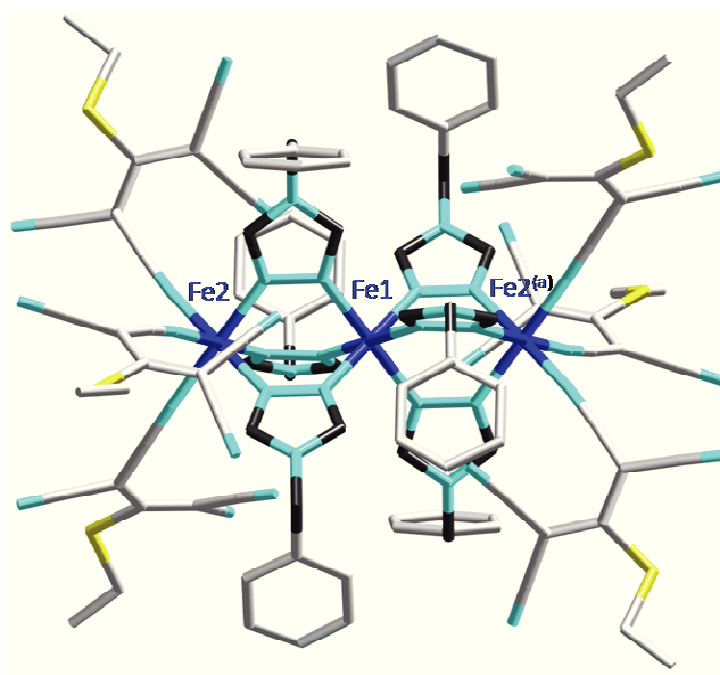


Figure 3. View of the centrosymmetric trinuclear complex [Fe₃(bntrz)₆(tcnset)₆] (**2**). (a) 2/3-*x*, 4/3-*y*, 1/3-*z*. [Fe (dark blue), N (pale blue), C (pale grey and black) and S (yellow)] (Hydrogen atoms have been omitted for clarity).

Table 2. Crystal data and structural refinement parameters for [Fe₃(bntrz)₆(tcnset)₆] (**2**).

Compound	2	
Temperature / K	360(2)	170(2)
Color	Yellow	Pink
Empirical formula	C ₁₀₈ H ₈₄ Fe ₃ N ₄₂ S ₆	C ₁₀₈ H ₈₄ Fe ₃ N ₄₂ S ₆
Formula weight / g.mol ⁻¹	2330.08	2330.08
Wavelength / Å	0.71073 Å	0.71073 Å
Crystal system	Trigonal	Trigonal
Space group	<i>R</i> -3	<i>R</i> -3
a / Å	26.055(3)	26.164(11)
c / Å	14.8240(13)	14.267(6)
Volume / Å ³	8715(2)	8458(8)
Z	3	3
D _{calc} / g.cm ⁻³	1.332	1.372
Abs. coef. / cm ⁻¹	5.43	5.60
F(000)	3600.0	3600.0
Crystal size / mm ³	0.25 × 0.02 × 0.02	0.25 × 0.02 × 0.02
2θ range / °	5.51 to 50.738	5.988 to 50.482
Refl. collected	24948	21573
Unique refl. / Rint	3544 / 0.0922	3393 / 0.0951
Data / restr. / N _v	2092 / 0 / 241	2251 / 0 / 241
Final R indexes [I ≥ 2σ (I)]	R ₁ = 0.0554, wR ₂ = 0.0958	R ₁ = 0.0506, wR ₂ = 0.0917
Final R indexes [all data]	R ₁ = 0.1214, wR ₂ = 0.1129	R ₁ = 0.1002, wR ₂ = 0.1048
°GooF	1.006	1.016
Δρ _{max/min} / eÅ ⁻³	+0.342 / -0.381	0.527 / -0.471
CCDC No.	1500725	1500724
	280 K-345 K, every 5K (CCDC numbers 1500728-1500740).	

$$^a R_1 = \sum |F_o - F_c| / F_o, \quad ^b wR_2 = \{\sum [w(F_o^2 - F_c^2)^2] / \sum [w(F_o^2)^2]\}^{1/2}, \quad ^c \text{GooF} = \{\sum [w(F_o^2 - F_c^2)^2] / (N_{\text{obs}} - N_{\text{var}})\}^{1/2}$$

The molecular structure of **2** consists of a neutral trinuclear complex of formula $[\text{Fe}_3(\text{bntrz})_6(\text{tcnset})_6]$ which can be viewed as a $[\text{Fe}_2(\text{bntrz})_3\text{Fe}(\text{bntrz})_3\text{Fe}_2]$ linear and centrosymmetric fragment in which the central metal ion (Fe1) is bound on both sides to two other Fe(II) centers (Fe2) through three μ_2 -bridging bntrz ligands (Figure 3). The central metal ion (Fe1) is surrounded by six nitrogen atoms from six equivalent μ_2 -bntrz ligands, while each external Fe2 ion adopts FeN_3N_3 octahedral environments arising from three equivalent bridging bntrz ligands and three unidentate (tcnset)[−] anions.

Examination of the Fe-N bonds and N-Fe-N bond angles, for both Fe^{II} environments (Fe1 and Fe2), reveals that the central Fe1 ion adopts a regular FeN_6 octahedral geometry which is defined by six equivalent nitrogen atoms ($[\text{Fe}1(\text{N}1)_6]$); while the two equivalent external Fe2 centers, surrounded by two different nitrogen atoms ($[\text{Fe}2(\text{N}2)_3(\text{N}4)_3]$), display a more distorted octahedron geometry, as demonstrated by the values of Σ and Θ parameters (Table 3) which are relatively low but significantly higher than those observed for the Fe1 environment.¹³ The average values of the Fe-N distances at 360 K ($\langle d_{\text{Fe}1-\text{N}} \rangle = 2.175(2)$ Å and $\langle d_{\text{Fe}2-\text{N}} \rangle = 2.158(3)$ Å), and 170 K ($\langle d_{\text{Fe}1-\text{N}} \rangle = 1.975(3)$ and $\langle d_{\text{Fe}2-\text{N}} \rangle = 1.953(3)$ Å) (Table 3), are in agreement with the presence of *HS* and *LS* state, respectively. This observation is consistent with the presence of a complete $[\text{HS}-\text{HS}-\text{HS}] \leftrightarrow [\text{LS}-\text{LS}-\text{LS}]$ *SCO* transition as initially revealed by the magnetic and the calorimetric data.

Table 3. Average Fe-N distances ($\langle d_{\text{Fe-N}} \rangle$) and distortion parameters for **2**.

<i>T</i> (K)	170		360	
*Fe ^{II} center	Fe1	Fe2	Fe1	Fe2
Fe1-N1	1.970(3)		2.175(2)	
Fe2-N2		1.962(2)		2.170(2)
Fe2-N4		1.943(3)		2.146(3)
$\langle d_{\text{Fe-N}} \rangle$ (Å)	1.970(3)	1.953(3)	2.175(2)	2.158(3)
[§] Σ / Θ (°)	4(1) / 5(2)	8(1) / 14(2)	8(1) / 9(2)	24(1) / 39(2)
Spin state	<i>LS</i>	<i>LS</i>	<i>HS</i>	<i>HS</i>

*The two Fe(II) environments are defined by N1 ($[\text{Fe}1(\text{N}1)_6]$) and by N2 and N4 ($[\text{Fe}2(\text{N}2)_3(\text{N}4)_3]$) nitrogen atoms.

[§] Σ is the sum of the deviation from 90° of the 12 cis-angles of the FeN_6 octahedron; Θ is the sum of the deviation from 60° of the 24 trigonal angles of the projection of the FeN_6 octahedron onto its trigonal faces.¹³

Table 4. Selected bond lengths (Å) and bond angles (°) in **2**.

T / K	360 (<i>HS</i> State)	170 (<i>LS</i> State)
Fe1-N1 ^(b)	2.175(2)	1.970(2)
Fe1-N1 ^(a)	2.175(2)	1.970(2)
Fe1-N1 ^(d)	2.175(2)	1.970(3)
Fe1-N1 ^(e)	2.175(2)	1.970(2)
Fe1-N1	2.175(2)	1.970(2)
Fe1-N1 ^(c)	2.175(2)	1.970(3)
Fe2-N2	2.170(2)	1.962(2)
Fe2-N2 ^(b)	2.170(2)	1.962(2)
Fe2-N2 ^(c)	2.170(2)	1.962(2)
Fe2-N4 ^(c)	2.146(3)	1.943(3)
Fe2-N4	2.146(3)	1.943(3)
Fe2-N4 ^(b)	2.146(3)	1.943(3)
N1 ^(b) -Fe1-N1 ^(d)	89.34(8)	89.63(10)
N1 ^(b) -Fe1-N1 ^(d)	89.34(8)	89.63(10)
N1-Fe1-N1 ^(e)	89.34(8)	89.64(10)
N1 ^(b) -Fe1-N1 ^(e)	180.0	180.00(10)
N1 ^(a) -Fe1-N1 ^(e)	90.67(8)	90.37(9)
N1 ^(d) -Fe1-N1 ^(c)	180.0	180.0
N1-Fe1-N1 ^(c)	90.66(8)	90.37(9)
N1 ^(b) -Fe1-N1	90.66(8)	90.37(10)
N1 ^(b) -Fe1-N1 ^(a)	89.33(8)	89.63(10)
N1 ^(d) -Fe1-N1	89.34(8)	89.63(10)
N1 ^(b) -Fe1-N1 ^(c)	90.66(8)	90.37(10)
N1 ^(a) -Fe1-N1	180.0	180.0
N1 ^(d) -Fe1-N1 ^(a)	90.66(8)	90.37(9)
N1 ^(a) -Fe1-N1 ^(c)	89.34(8)	89.63(10)
N1 ^(d) -Fe1-N1 ^(e)	90.66(8)	90.37(9)
N1 ^(e) -Fe1-N1 ^(c)	89.33(8)	89.63(9)
N2-Fe2-N2 ^(c)	90.27(9)	90.07(10)
N2 ^(b) -Fe2-N2 ^(c)	90.27(9)	90.06(10)
N2 ^(b) -Fe2-N2	90.27(9)	90.07(10)
N4 ^(c) -Fe2-N2	177.19(9)	178.95(11)
N4-Fe2-N2	87.01(9)	88.89(10)
N4-Fe2-N2 ^(b)	177.19(9)	178.94(11)
N4-Fe2-N2 ^(c)	89.03(9)	89.78(10)
N4 ^(b) -Fe2-N2	89.03(9)	89.78(10)
N4 ^(b) -Fe2-N2 ^(c)	177.19(9)	178.95(11)
N4 ^(c) -Fe2-N2 ^(c)	87.01(9)	88.89(10)
N4 ^(c) -Fe2-N2 ^(b)	89.03(9)	89.78(10)
N4 ^(b) -Fe2-N2 ^(b)	87.01(9)	88.89(10)
N4 ^(c) -Fe2-N4	93.65(9)	91.26(10)
N4 ^(b) -Fe2-N4	93.65(9)	91.26(10)
N4 ^(b) -Fe2-N4 ^(c)	93.65(9)	91.26(10)

*The two Fe(II) environments are defined by N1 ([Fe1(N1)₆]) and by N2 and N4 Fe2(N2)₃(N4)₃) nitrogen atoms.

Symmetry transformations used to generate equivalent atoms: (a) = 2/3-x, 4/3-y, 1/3-z; (b) = 1-y, 1+x-y, +z; (c) = +y-x, 1-x, +z; (d) = 2/3-y+x, 1/3+x, 1/3-z; (e) = -1/3+y, 1/3-x+y, 1/3-z.

The most intriguing and atypical characteristic in the *SCO* behavior of compound **2** concerns the presence of a one-step transition despite the presence of two chemically different metal centers (Fe2-Fe1-Fe2), as revealed by the crystal data for the two spin states. Thus, in order to undoubtedly confirm the absence of a two-step transition, and to further understand the evolution of each Fe(II) environment (Fe1 and Fe2) during the transition, the crystal structure of **2** has been solved every 5 K between 280 K and 345 K (see CCDC numbers 1500728-1500740). These additional structural investigations have not revealed any change of symmetry on the whole temperature range, but have shown similar thermal evolution of the average Fe-N distances ($\langle d_{\text{Fe-N}} \rangle$) for the two Fe(II) centers, fitting utterly the thermal magnetic behavior (see Figure 4). This latter observation clearly suggests that both iron centers of the trinuclear complex, although in different crystallographic environments, are similarly affected by the spin transition, which is consistent with the observed one-step transition from $[LS-LS-LS]$ to $[HS-HS-HS]$ states.

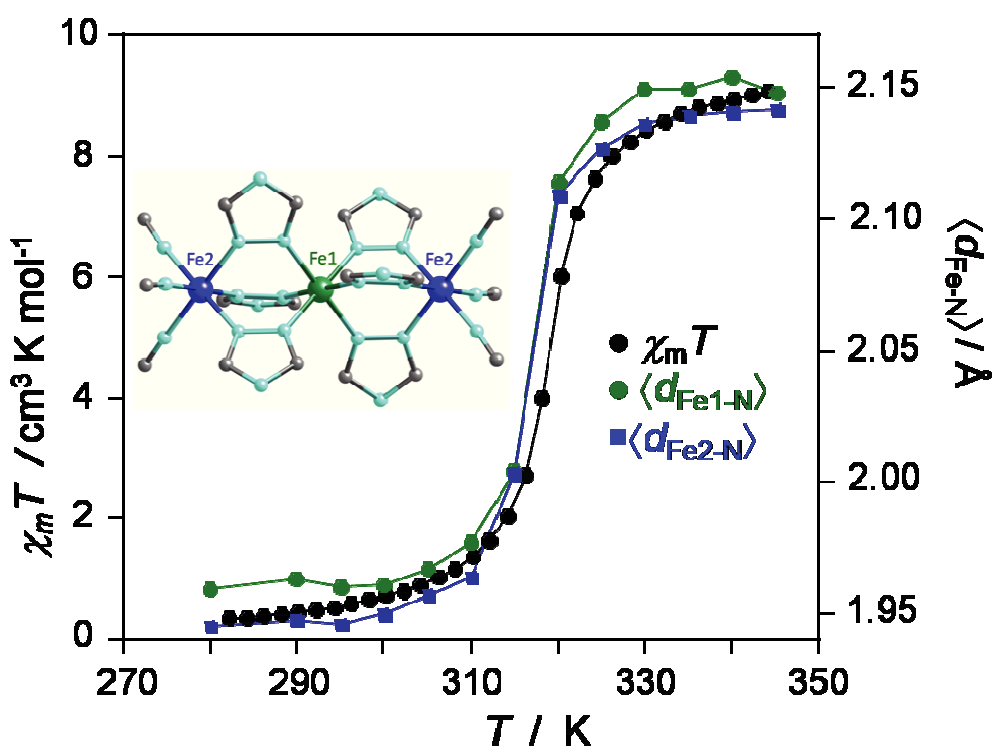


Figure 4. Thermal evolutions of the average Fe-N distances of each Fe(II) center (Fe1 and Fe2) in the trinuclear units of **2** ([Fe2-Fe1-Fe2]), and of the $\chi_m T$ product in the 280-340 K range.

The careful examination of the shortest inter-molecular contacts (π -stacking, hydrogen bonding and Van der Waals contacts) in **2** reveals that the trinuclear moieties are linked together by six hydrogen bonds involving the triazole ring, and the CN branches from the cyanocarbanions of adjacent trinuclear complexes. Such inter-trinuclear contacts lead to a supramolecular chain oriented along the c parameter (Figure 5). The corresponding chains are connected to each other through Van der Waals contacts involving the S-Et groups of the cyanocarbanions. During the HS to LS transition, the inter-trinuclear separations show a decrease of 0.124(3) Å along the c axis. This contraction induces a structural rearrangement of the cyanocarbanions and the side chains of the triazole, leading to an unexpected increase of the inter-chain distances from 15.043 Å to 15.106 Å when cooling from 360 K down to 170 K.

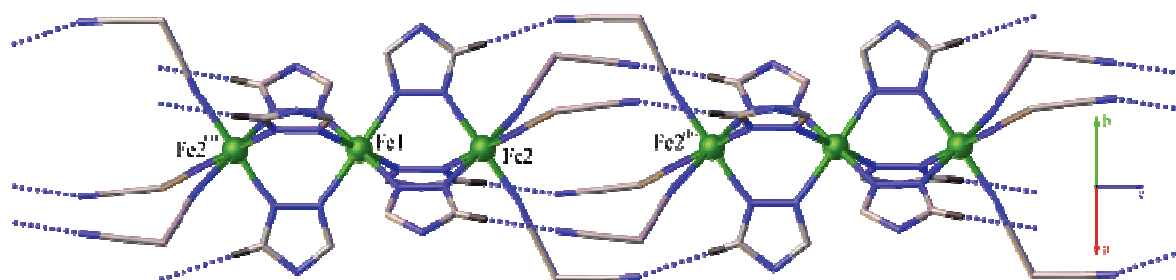


Figure 5. View of **2** along the direction axis showing the hydrogen bond contacts between trinuclear units: C2...N5 = 3.329 (4) Å at 360 K; C2...N5 = 3.151(4) Å at 170 K. (a) = $2/3-x, 4/3-y, 1/3-z$; (b) = $1-y, 1+x-y, +z$; [Fe (Green), N (blue), C (pale grey)] (Benzyl group of triazole ligand bntrz, part of the cyanocarbanion tcnset⁻, and hydrogen atoms are omitted for clarity).

Conclusion

In summary, we have prepared and fully characterized a new trinuclear $[\text{Fe}_3(\text{bntrz})_6(\text{tcnset})_6]$ (**2**) neutral complex that exhibits a one-step spin transition above room temperature ($T_{1/2} \approx 318$ K), and defined to our knowledge as the first *SCO* trinuclear complex exhibiting a complete spin transition. The one-step nature of the magnetic transition has been notably confirmed by detailed structural studies around the critical region that clearly showed that the thermal evolutions for the three Fe(II) environments are similar and fit adequately the one-step transition from $[LS-LS-LS]$ to $[HS-HS-HS]$ states. In addition, the comparison of the trinuclear structure of $[\text{Fe}_3(\text{bntrz})_6(\text{tcnset})_6]$ (**2**) with the 1D architecture of $[\text{Fe}(\text{bntrz})_3][\text{Pt}(\text{CN})_4]\cdot\text{H}_2\text{O}$ (**1**) described in the first chapter clearly emphasizes the impact of the anion in those “ $\text{Fe}^{\text{II}}/\text{bntrz}/\text{anion}$ ” systems. Indeed, the substitution of the rigid $[\text{Pt}(\text{CN})_4]^{2-}$ tetracyanometallate dianionic moiety by the more flexible $(\text{tcnset})^-$ monoanionic entity induces drastic structural modifications, and distinct dimensionality, even though both derivatives display a one-step spin transition above room temperature (with a T_{SCO} of ca. 242 K and 318 K for **1** and **2**, respectively).

Experimental section

1. General Considerations

All the starting reagents were purchased from commercial sources (Sigma-Aldrich, Across, Fisher Scientific, Alfa Aesar and Merck), and used without further purification unless otherwise stated. Deuteriated solvents were purchased from Sigma-Aldrich and Cambridge Isotope Laboratories. Dried solvents were prepared by refluxing for one day under nitrogen over the appropriate drying agents (calcium hydride for acetonitrile, dichloromethane, and hexane; magnesium and iodine for methanol; sodium for ethanol, and molecular sieves for DMF), and then degassed before use. Solvents were stored in glass ampoules under argon. All the glassware and cannula were stored in an oven (>373 K). When appropriate, the reactions were carried out under argon or nitrogen by using a dual manifold vacuum/argon line and the standard Schlenk techniques. Thin layer chromatography (TLC) was carried out on silica gel 60 with fluorescent indicator UV₂₅₄ (Silica gel 60 F₂₅₄) plates of 0.2 mm thicknesses. Flash column chromatography was performed on silica gel (230-400) mesh.

N.B.: Because of the use of organic ligands composed with cyano functional groups, all the experiments reported here have been undergone with great caution, especially considering the eventual release of the gases HCN and related derivatives that are poisonous and potentially lethal at low levels. Consequently, all those compounds should be prepared and handled behind suitable protective shields. In this context, all the waste involving polynitrile compounds were destroyed using a specific basic bath containing a saturated ethanolic solution of KOH mixed with an aqueous solution of NaOCl, while the glassware were cleaned using a basic bath consisting of a saturated ethanol/water solution of KOH (1:1 volume ratio).

2. Syntheses of the ligands

2.1. Synthesis of the triazole-based ligand: 4-(Benzyl)-1,2,4-triazole (bntrz)

The 4-(benzyl)-1,2,4-triazole (bntrz) ligand was synthesized as previously described in Chapter II (Experimental section), using a method similar to that reported by Bayer *et al.*⁹

2.2. Synthesis of the cyanocarbanion salt: potassium [1,1,3,3-tetracyano-2-thioethylpropenide] K(tcnset)

The potassium [1,1,3,3-tetracyano-2-thioethylpropenide] (K(tcnset)) has been prepared in two steps according to modified literature methods.¹⁰ In the first step, 2-[bis(ethylthio)methylene]malononitrile was synthesized from malononitrile and alkyl halide following the reported methods. Then, the potassium [1,1,3,3-tetracyano-2-thioethylpropenide] salt K(tcnset) was obtained from the corresponding 2-[bis(ethylthio)methylene]malononitrile after reaction with malononitrile in the presence of potassium tert-butoxide.

➤ First step: Synthesis of 2-[bis(ethylthio)methylene]malononitrile (I)

To a solution of malononitrile (4.0 g, 60.55 mmol) in DMF (25 mL) was added K₂CO₃ (8.37 g, 60.55 mmol). After stirring for 30 min. at room temperature, CS₂ (3.6 mL, 66.6 mmol) was added dropwise, and the reaction mixture was stirred at room temperature for an additional 10 min. before ethyl halide (121.1 mmol) and tetrabutylammonium bromide (4 g, 10 mmol) were successively added. After further stirring for 30 minutes at room temperature, then the reaction mixture was refluxed for 2 h at 50 °C. Subsequently, after stirring for 24-48 h at room temperature while monitoring the reaction status with TLC (2:98 (v/v) Ethylacetate: Hexane), the reaction mixture was diluted with water (200 mL) and extracted with Et₂O (4×200 mL). The combined organic layers were washed with Brine solution (100 mL) and dried over MgSO₄, then filtered and concentrated under reduced pressure. The crude product was purified by chromatography on silica gel [hexane/EtOAc, 10:0 to 9.5:0.5 (v/v)] to provide ketene dithioacetal as pale green solid (Yield: 60 %, 7.170 g). The ¹H, ¹³C and IR spectra are provided hereafter (Figures 9-11).

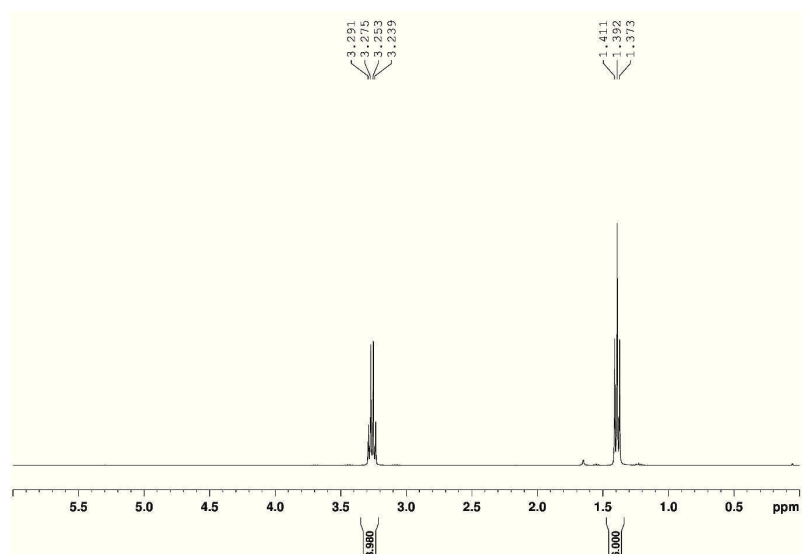


Figure 9. ^1H NMR (400 MHz, CDCl_3 , 298 K) of 2-[bis(ethylthio)methylene]malononitrile (**I**). ^1H NMR : δ , 3.27 (q, 4H, - SCH_2 -), 1.39 (t, 6H, - CH_3).

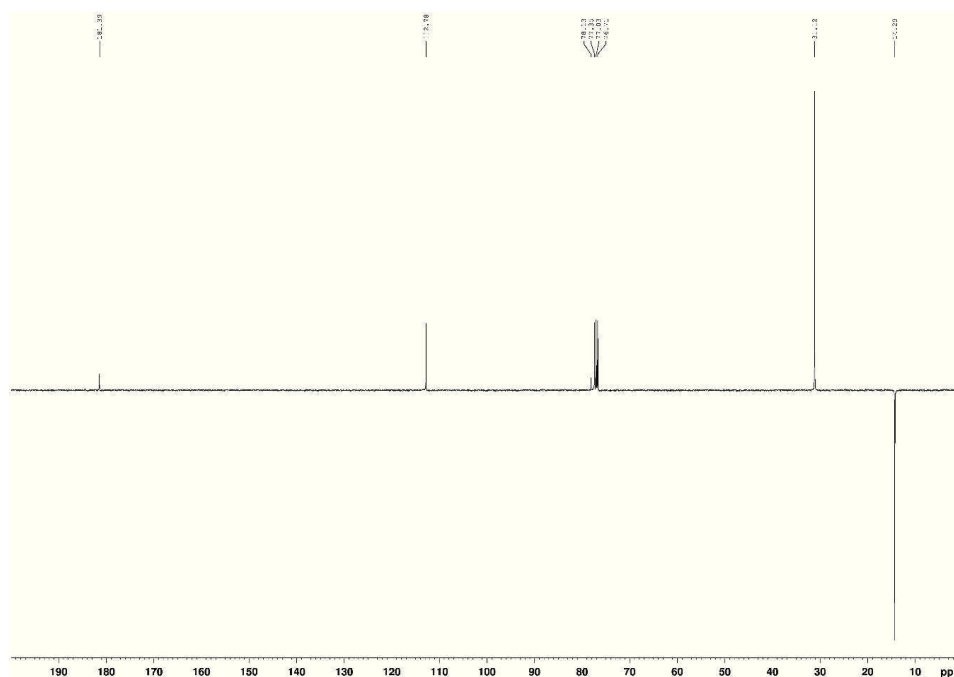


Figure 10. ^{13}C NMR (400 MHz, CDCl_3 , 298 K) of 2-[bis(ethylthio)methylene]malononitrile (**I**). ^{13}C NMR : δ , 181.4 (- $\text{C}(\text{S-Et})_2$), 112.8 (-CN), 78.1 (- $\text{C}(\text{CN})_2$), 31.1 (- SCH_2 -), 14.3 (- CH_3).

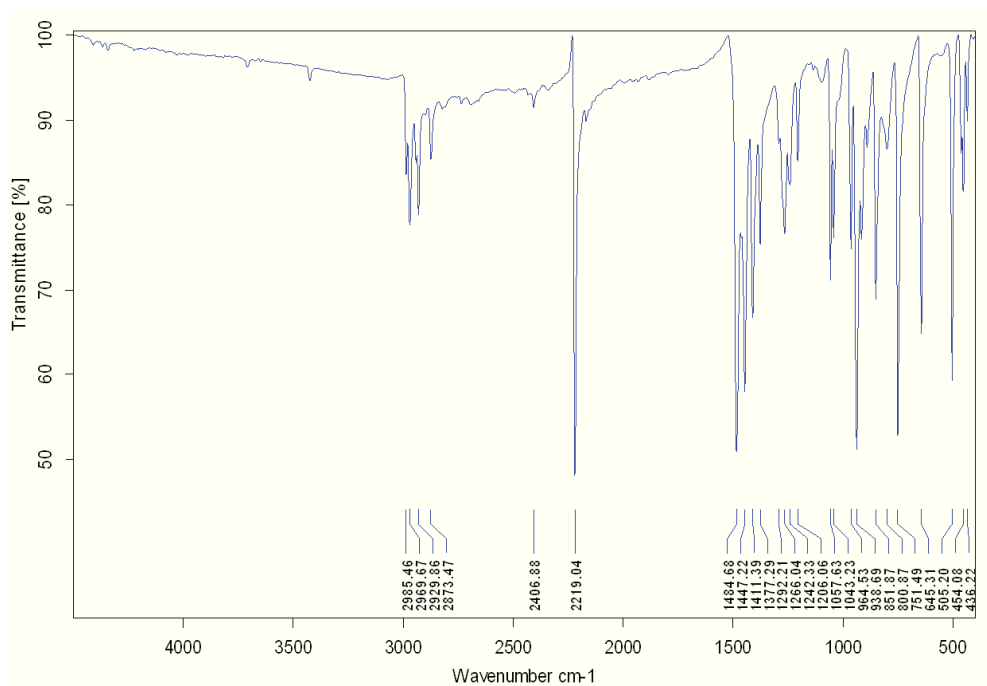


Figure 11. Infrared Spectrum of 2-[bis(ethylthio)methylene]malononitrile (**I**). IR data (ν , cm^{-1}) : 2970w, 2930w, 2874w, 2407w, 2349w, 2322w, 2219s, 1486s, 1463m, 1411w, 1377w, 1265w, 1240w, 1206w, 1057m, 1043m, 964s, 939w, 852w, 801w, 751w, 646m, 505m, 454m, 436w.

➤ Second step: Synthesis of K(tcnset) (**II**)

In this second step, a warm ethanol solution (30 mL) of the previously synthesized 2-[bis(ethylthio)methylene]malononitrile (**I**) (1.98 g, 10 mmol) was added dropwise to an ethanol solution (10 mL) of malononitrile (0.66 g, 10 mmol) and *t*-BuOK (1.12 g, 10 mmol). The resulting mixture was refluxed for 1h, then cooled to room temperature, and finally kept at 4 °C for two days. The compound was filtered on a sintered-glass funnel, washed with distilled diethyl ether, and ultimately dried under vacuum to obtain the potassium salt of [1,1,3,3-tetracyano-2-thioalkylpropenide] (K(tcnset), **II**) as a white crystalline powder (Yield: 86%, 2.076 g). The ^1H , ^{13}C and IR spectra are given hereafter (Figures 12-14).

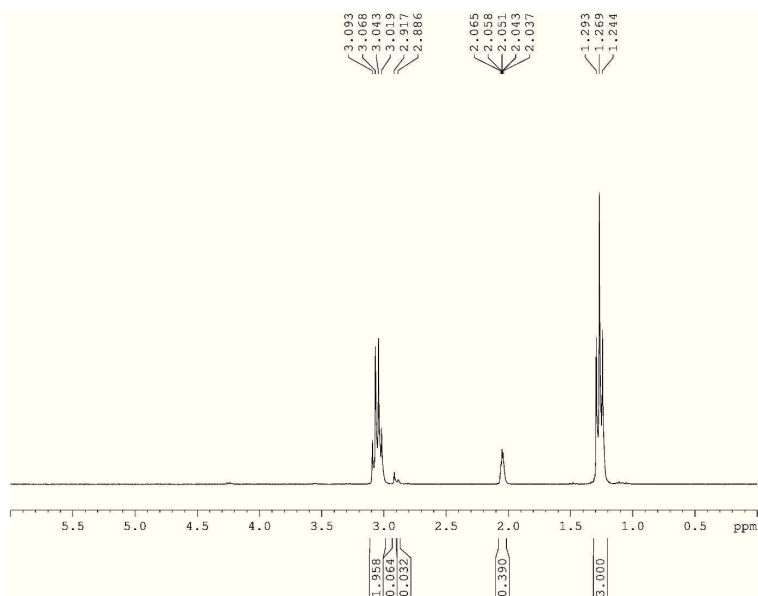


Figure 12. ^1H NMR (300 MHz, Acetone- D_6 , 298 K) of K(tcnset) (**II**). ^1H NMR : δ , 3.06 (q, 2H, -SCH₂-), 1.27 (t, 3H -CH₃).

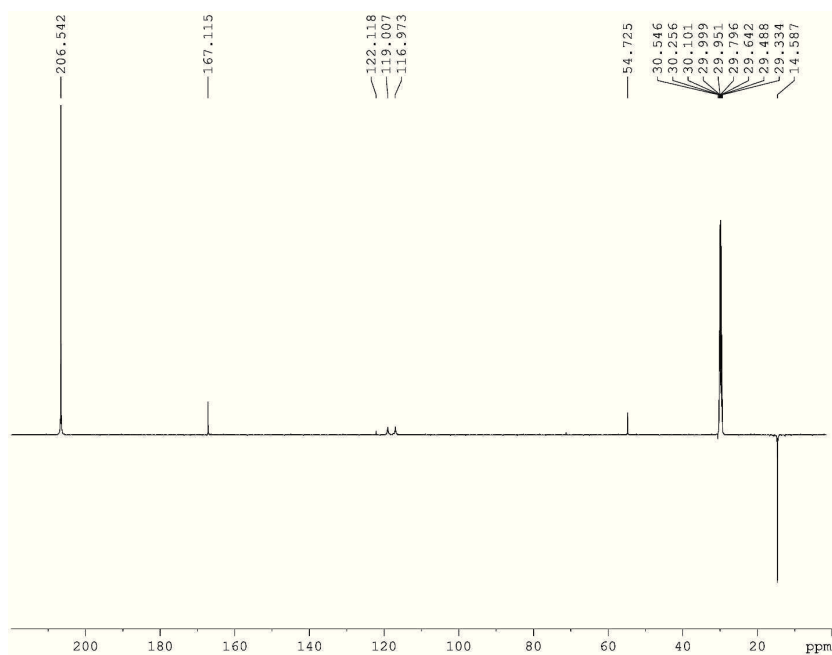


Figure 13. ^{13}C NMR (500 MHz, Acetone- D_6 , 298 K) of K(tcnset) (**II**). ^{13}C NMR : δ , 167.1 (-C(S-Pr)₂), 119.1 (-CN), 116.9 (-CN), 54.7 (-C(CN)₂), 29.8 (-SCH₂-), 14.6 (-CH₃).

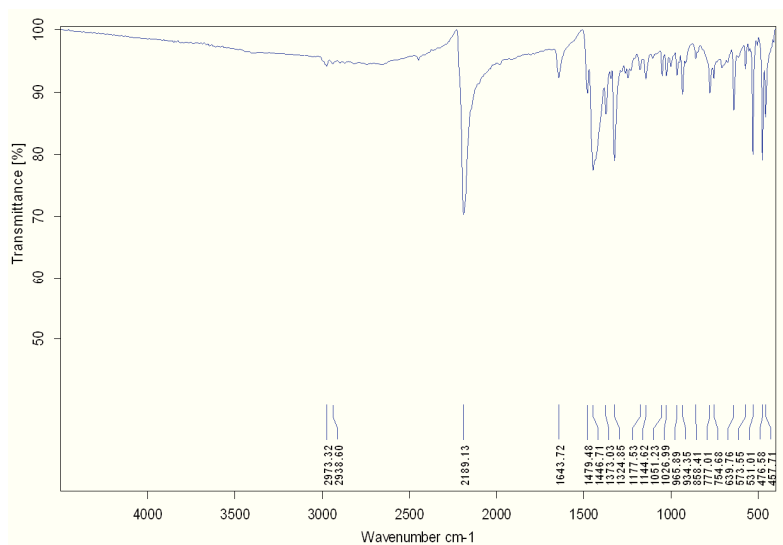


Figure 14. Infrared Spectrum of K(tcnset). IR (ν , cm^{-1}) : 2189s, 1644w, 1445s, 1373w, 1325w, 934w, 777w, 640w, 531w, 477w, 458w.

3. Single-crystals preparation of $[\text{Fe}_3(\text{bntrz})_6(\text{tcnset})_6]$ (**2**)

The single-crystals of the linear trinuclear Fe(II) *SCO* complex $[\text{Fe}_3(\text{bntrz})_6(\text{tcnset})_6]$ (**2**) were prepared by slow diffusion, in a fine glass tube (3.0 mm diameter). Typically, an aqueous solution of $\text{Fe}(\text{BF}_4)_2 \cdot 6\text{H}_2\text{O}$ (33.755 mg, 0.1 mmol) and K(tcnset) (48 mg, 0.2 mmol) in 10 mL of distilled water with a small amount of ascorbic acid, and a solution of bntrz (47.7 mg, 0.3 mmol) in 2.5 mL of methanol, were initially prepared. The aqueous solution of Fe^{II} was placed in the bottom of a fine tube of 3.0 mm, upon which a solvent mixture of water and methanol - with a ratio of 2:1 - was carefully added. Then, a methanol solution of bntrz was carefully layered on top of the buffer layer. *In fine*, pink single crystals of **1** suitable for X-ray diffraction were grown at the interface over a period of three weeks. Alternatively, an aqueous solution of $\text{Fe}(\text{BF}_4)_2 \cdot 6\text{H}_2\text{O}$ placed at the bottom of a glass tube was covered with a water ‘*buffer*’, over which an aqueous solution of the bntrz ligand and K(tcnset) salt was layered. The same pink single crystals of **1** were obtained in smaller size compared to the above-mentioned experimental conditions. Anal. Calcd for $\text{C}_{108}\text{H}_{84}\text{Fe}_3\text{N}_{42}\text{S}_6$: C, 55.6; H, 3.6; N, 25.2 %. Found: C, 56.1; H, 3.5; N, 24.8 %. IR spectra are given below (Figures 15-16).

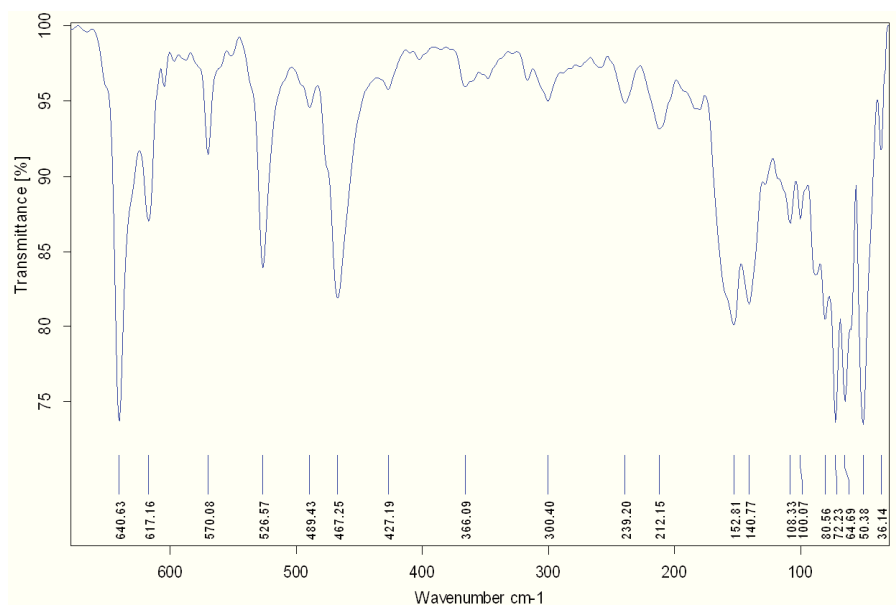


Figure 15. IR Spectrum of the Single-Crystals of $[\text{Fe}_3(\text{bntrz})_6(\text{tcnsset})_6]$ (**2**) ($650\text{--}35\text{ cm}^{-1}$).

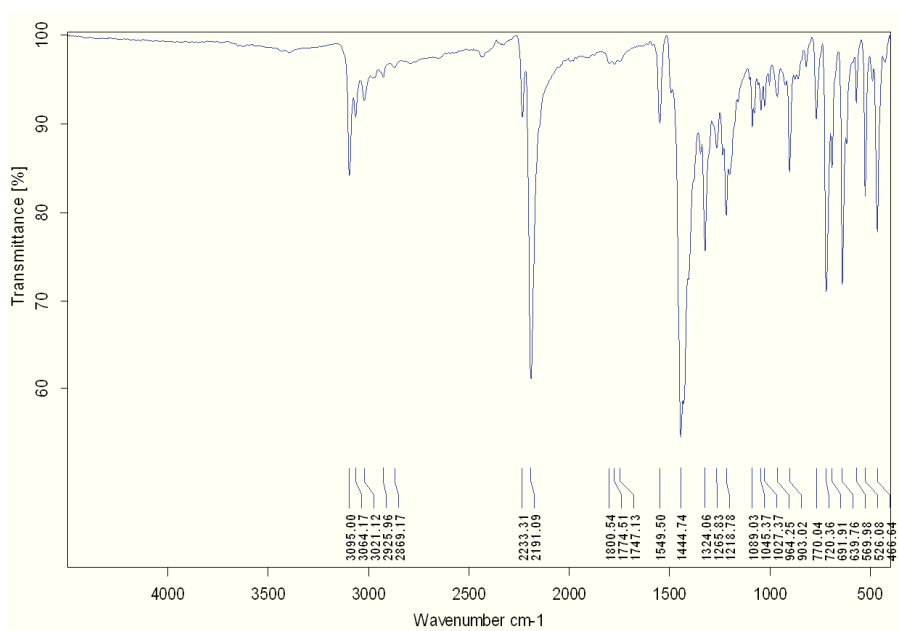


Figure 16. IR Spectrum of the Single-Crystals of $[\text{Fe}_3(\text{bntrz})_6(\text{tcnsset})_6]$ (**2**) ($4000\text{--}450\text{ cm}^{-1}$). IR (ν , cm^{-1}) : 3095w, 3064w, 3021w, 2233w, 2191s, 1549w, 1445s, 1324s, 1219m, 1089w, 1045w, 1027w, 903w, 721m, 641m, 527w, 467w, 362w, 300w, 279w, 239w, 212w, 153m, 141m, 108w, 100w, 72w, 65w, 50w.

4. Physical Measurements and characterizations

Single crystal X-ray studies were performed at 296 K and 120 K on Xcalibur 2 κ -CCD diffractometer using Mo K α radiation ($\lambda = 0.71073$ Å). The corresponding structures were solved by direct methods with the SHELXS program and refined on F^2 by weighted full matrix least-squares methods using the SHELXL program.¹⁴ All non-hydrogen atoms were refined anisotropically, hydrogen atoms were located in difference Fourier maps, and treated using a riding model. Crystallographic data and refinement details are available in Table 2. $^1\text{H}/^{13}\text{C}/^{31}\text{P}$ -NMR spectra were recorded on Bruker AMX-300, AMX-400 and AMX-500 spectrometers, and the spectra were referenced internally using residual proton solvent resonances relative to tetramethylsilane ($\delta = 0$ ppm). Magnetic measurements were performed with a Quantum Design MPMS-XL-5 SQUID magnetometer in the 2-300 K temperature range with an applied magnetic field of 2 Tesla and a scan rate of $0.4 \text{ K}\cdot\text{min}^{-1}$ on single crystals of compound **2** (mass of 4.25 mg). The DSC measurements were performed on a DSC-1/LN2 Mettler Toledo calorimeter setting the heat flow scan rate at $s = 2 \text{ K}\cdot\text{min}^{-1}$ on single crystals of **2** (mass of 4.40 mg). The infrared (IR) spectra were collected in the range $4000\text{--}35 \text{ cm}^{-1}$ on a FT-IR BRUKER ATR VERTEX70 Spectrometer. Elemental analyses were performed at the “Service de microanalyse”, CNRS, 91198 Gif-sur-Yvette, France.

Bibliography

1. (a) E. Coronado, J. R. Galán-Mascarós, M. Monrabal-Capilla, J. García-Martínez and P. Pardo-Ibáñez, *Adv. Mater.*, **2007**, *19*, 1359; (b) A. Bousseksou, G. Molnar, L. Salmon and W. Nicolazzi, *Chem. Soc. Rev.*, **2011**, *40*, 3313; (c) G. Félix, K. Abdul-Kader, T. Mahfoud, I. A. Gural'skiy, W. Nicolazzi, L. Salmon, G. Molnar and A. Bousseksou, *J. Am. Chem. Soc.*, **2011**, *133*, 15342.
2. (a) P. Gütllich, A-B. Gaspar and Y. Garcia, *Beilstein J. Org. Chem.*, **2015**, *9*, 342; (b) M. Shatruck, H. Phan, B. A. Chrisostomo and A. Suleimenova, *Coord. Chem. Rev.*, **2015**, *289-290*, 62; (c) C. Atmani, F. El Hajj, S. Benmansour, M. Marchivie, S. Triki, F. Conan, V. Patinec, H. Handel, G. Dupouy and C. J. Gómez-García, *Coord. Chem. Rev.*, **2010**, *254*, 1559.
3. (a) Y. Garcia, V. Niel, M. C. Muñoz and J.-A. Real, *Top. Curr. Chem.*, **2004**, *233*, 229-257; (b) S. Hayami, R. Moriyama, Y. Shigeyoshi, R. Kawajiri, T. Mitani, M. Akita, K. Inoue and Y. Maeda, *Inorg. Chem.*, **2005**, *44*, 7295; (c) R. Ishikawa, K. Matsumoto, K. Onishi, T. Kubo, A. Fuyuhiko, S. Hayami, K. Inoue, S. Kaizaki and S. Kawata, *Chem. Lett.*, **2009**, *38*, 620; (d) G. Morgan, K. D. Murnaghan, H. Muller-Bunz, V. McKee and C. J. Harding, *Angew. Chem. Int. Ed.*, **2006**, *45*, 7192; (e) M. A. Halcrow, *Chem. Soc. Rev.*, **2011**, *40*, 4119; (f) P. Guionneau, *Dalton Trans.*, **2014**, *43*, 382.
4. (a) M. M. Dîrtu, C. Neuhausen, A. D. Naik, A. Rotaru, L. Spinu and Y. Garcia, *Inorg. Chem.*, **2010**, *49*, 5723; (b) O. Rubeau, *Chem. Eur. J.*, **2012**, *18*, 15230.
5. (a) M. B. Bushuev, L. G. Lavrenova, Yu. G. Shvedenkov, A. V. Virovets, L. A. Sheludyakova, and S. V. Larionov, *Russ. J. Inorg. Chem.*, **2007**, *52*, 46-51; (b) Y. M. Klein, N. F. Sciortino, C. E. Housecroft, C. J. Kepert and S. M. Neville, *Magnetochemistry*, **2016**, *2*.
6. (a) O. G. Shakirova, L. G. Lavrenova, Y. G. Shvedenkov, G. A. Berezovskii, D. Y. Naumanov, L. A. Sheludyakova, G. V. Dolgushin and S. V. Larionov, *Russ. J. Coord.*

- Chem.*, **2004**, *30*, 473; (b) M. Thomann, O. Kahn, J. Guilhem and F. Varret, *Inorg. Chem.*, **1994**, *33*, 6029.
7. (a) H. Z. Scott, T. M. Ross, B. Moubaraki, K. S. Murray and S. M. Neville, *Eur. J. Inorg. Chem.*, **2013**, 803; (b) Y. Garcia, P. Guionneau, G. Bravic, D. Chasseau, J. A. K. Howard, O. Kahn, V. Ksenofontov, S. Reiman and P. Gütllich, *Eur. J. Inorg. Chem.*, **2000**, *7*, 1531-1538; (c) G. Vos, R. A. le Febre, R. A. G. de Graaff, J. G. Haasnoot and J. Reedijk, *J. Am. Chem. Soc.*, **1983**, *105*, 1682; (d) J. J. A. Kolnaar, G. van Dijk, H. Koojiman, A. L. Spek, V. Ksenofontov, P. Gütllich, J. G. Haasnoot and J. Reedijk, *Inorg. Chem.*, **1997**, *36*, 2433; (e) D. Savard, C. Cook, G. D. Enright, I. Korobkov, T. J. Burchell and M. Murugesu, *CrystEngComm.*, **2011**, *13*, 5190.
 8. (a) V. Gómez, J. Benet-Buchholz, E. Martin and J. R. Galan-Máscaros, *Chem. Eur. J.*, **2014**, *20*, 5369; (b) V. Gómez, C. S. de Pipaón, P. Maldonado-Illescas, J. C. Waerenborgh, E. Martin, J. Benet-Buchholz and J. R. Galan-Máscaros, *J. Am. Chem. Soc.*, **2015**, *137*, 11924.
 9. (a) H. O. Bayer, R.S. Cook, W. C. von Mayer, *United States Patent*, **1974**, 3,821,376; (b) H. O. Bayer, R.S. Cook, W. C. von Mayer, *United States Patent*. **1972**, 3,647,810.
 10. (a) S. Lethu and J. Dubois, *Eur. J. Org. Chem.*, **2011**, 3920; (b) P. G. Baraldi, F. Fruttarolo, M. A. Tabrizi, D. Preti, R. Romagnoli, H. El-Kashef, A. Moorman, K. Varani, S. Stefania Gessi, S. Merighi and P. A. Borea, *J. Med. Chem.*, **2003**, *46*, 1229; (c) G. Dupouy, M. Marchivie, S. Triki, J. Sala-Pala, J.-Y. Salaün, C. J. Gómez-García and P. Guionneau, *Inorg. Chem.*, **2008**, *47*, 8921.
 11. (a) J. G. Haasnoot, G. Vos, W. L. Groeneveld, *Z. Naturforsch. B*, **1977**, *32*, 1421; (b) J. H. Adriaanse, S. H. C. Askes, Y. van Bree, S. van Oudheusden, E. D. van den Bos, E. Gunay, I. Mutikainen, U. Turpeinen, G. A. van Albada, J. G. Haasnoot, J. Reedijk, *Polyhedron*, **2009**, *28*, 3143.
 12. P. Gütllich and H. A. Goodwin, *Top. Curr. Chem.*, **2004**, *233*, 1-47.

13. (a) P. Guionneau, M. Marchivie, G. Bravic, J.-F. Létard and D. Chasseau, *Top. Curr. Chem.*, **2004**, 234, 97-128; (b) M. Marchivie, P. Guionneau, J.-F. Létard and D. Chasseau, *Acta Cryst. B*, **2005**, B61, 25-28.
14. G. M. Sheldrick, *Acta Cryst.*, **2008**, A64, 112.

Appendix I

Effect of the Functional Group of the Cyanocarbanion on Magneto-Structural Properties in Triazole based Fe(II) Systems: Preliminary Results.

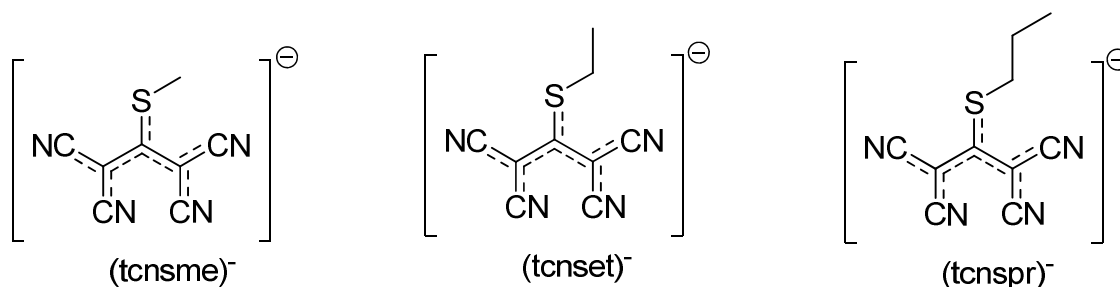
N.B.: This appendix is related to very recent results in line with Chapter III. Although preliminary, these results have been considered of relevance to be included as an appendix in this manuscript in the perspective of chapter III.

Table of Contents

1. Syntheses and characterizations of functionalized cyanocarbanions ligand (tcnsR') ⁻	140
2. Synthesis, structure and magnetic properties of complex [Fe ₃ (bntrz) ₆ (tcnspr) ₆] (3): Preliminary results	151
2.1. Synthesis and characterizations	151
2.2. Structural studies	153
2.3. Magnetic properties	156
2.4. Differential scanning calorimetry	157
3. Synthesis, structure and magnetic properties of the complex [Fe ₃ (bntz) ₈ (tcnsme) ₂][tcnsme] ₂ .4H ₂ O (4): Preliminary results	159
3.1. Synthesis	159
3.2. Preliminary structural characterizations and magnetic properties	159
Conclusion	163

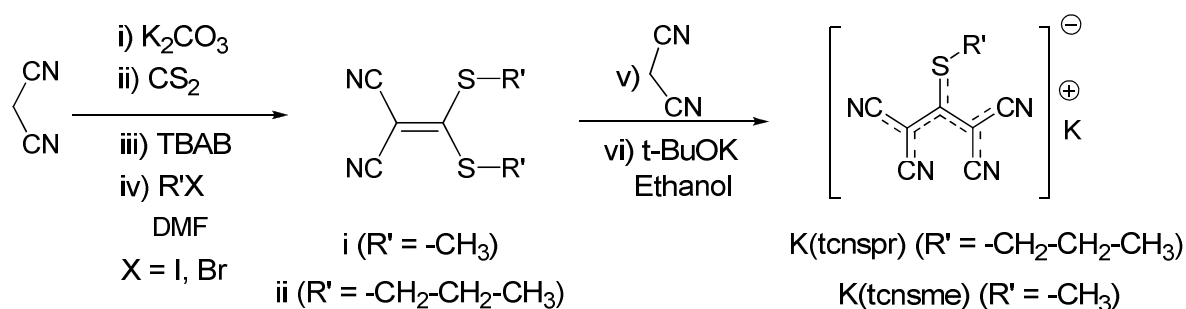
1. Syntheses and characterizations of functionalized cyanocarbanions ligand (tcnsR')⁻

As previously conferred in chapters II and III, the studies of the “Fe^{II}/bntrz/anion” systems - i.e. the 1D polymer [Fe(bntrz)₃][Pt(CN)₄].H₂O (**1**) and the discrete trinuclear complex [Fe₃(bntrz)₆(tcnset)₆] (**2**) - have clearly evidenced that the structural features and ensuing *SCO* behaviour of the material can be tuned not only by the functionalization of the triazole ligand, but also by the characteristics of the selected anionic ligand, notably the rigidity, the charge and the size of the anion. Those results led us to further extend the synthetic strategy defined with compound **2** to other new systems based at first on the same triazole ligand bntrz, but involving the systematic variation of the R' substituent from the functionalized organic polycyanocarbanion (tcnsR')⁻, with notably methyl and propyl groups; thus, the substitution reaction lead to the synthesis of the corresponding functionalized organic cyanocarbanions (tcnspr)⁻ and (tcnsme)⁻ (Schemes 1 and 2). Now the question is “what is (are) the effect(s) of the anions on the resulting magneto-structural behavior of the material?”, more precisely “what is the influence of those functional groups (R') of the organic polycyano anionic ligands?”.



Scheme 1. Functionalized cyanocarbanions of general formula (tcnsR')⁻, with R' = -CH₃, -CH₂-CH₃, and -CH₂-CH₂-CH₃.

In this regard, we initially developed the syntheses of those novel polycyano anionic ligands (tcnsme)⁻ and (tcnspr)⁻ as potassium salts following the similar two step procedure previously described for (tcnset)⁻ ligand (Scheme 2). These anionic ligands were both obtained as pale yellow polycrystalline powders in good yields (67% and 70.5%, respectively).

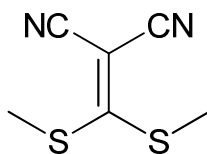


Scheme 2. General protocol for the synthesis of the carbon analogous sulphur polynitrile derivatives $\text{K}(\text{tcnsme})$ (i), and $\text{K}(\text{tcnspr})$ (ii).

■ **Syntheses of 2-[bis(methylthio)methylene]malononitrile (i) and 2-[bis(propylthio)-methylene]malononitrile (ii).**

A suspension of K_2CO_3 (8.37 g, 60.55 mmol) in DMF (25 mL) was treated with the addition of malononitrile (4.0 g, 60.55 mmol). The mixture was cooled down to 0°C , and CS_2 (3.6 mL, 66.6 mmol) was added dropwise. The resulting yellow suspension was stirred at 20°C for 10 minutes, after which alkylhalide (121.1 mmol) and tetrabutylammonium bromide (4 g, 10 mmol) were added over 30 minutes. The reaction mixture was stirred for 2 hours at 50°C , and subsequently for an additional 24 to 48 hours at room temperature while monitoring the reaction status with TLC (2:98 ethylacetate: hexane). The final mixture was diluted with water (200 mL) and extracted with Et_2O (4×200 mL); the combined organic layers were washed with Brine solution (100 mL) and dried over MgSO_4 , then filtered and concentrated under reduced pressure. The crude product was purified by chromatography on silica gel [hexane/ EtOAc , 10:0 to 9.5:0.5 (v/v)] to provide 2-[(bis-methylthio)methylene]malononitrile (i) and 2-[bis(propylthio)-methylene]malononitrile (ii) with reasonable yields (75% (7.725 g) and 46% (6.205 g), respectively). The infrared and NMR data for each derivative are detailed hereafter.

➤ 2-[Bis(methylthio)methylene]malononitrile (i):



Yield : 75% (7.725 g); ^1H NMR (300 MHz, CDCl_3) : δ , 2.76 (s, 6H, -SCH₃) (Figure 1); ^{13}C NMR (300 MHz, CDCl_3) : δ , 184.0 (-C(S-Me)₂), 112.8 (-C \equiv N), 76.3 (-C(CN)₂) 19.3 (-SCH₃) (Figure 2); IR data (ν , cm^{-1}) : 3003w, 2926w, 2827w, 2417w, 2351w, 2308w, 2209s, 1489w, 1442s, 1417s, 1316m, 1211w, 983w, 960w, 922m, 869s, 708w, 610w, 475w, 457w (Figure 3).

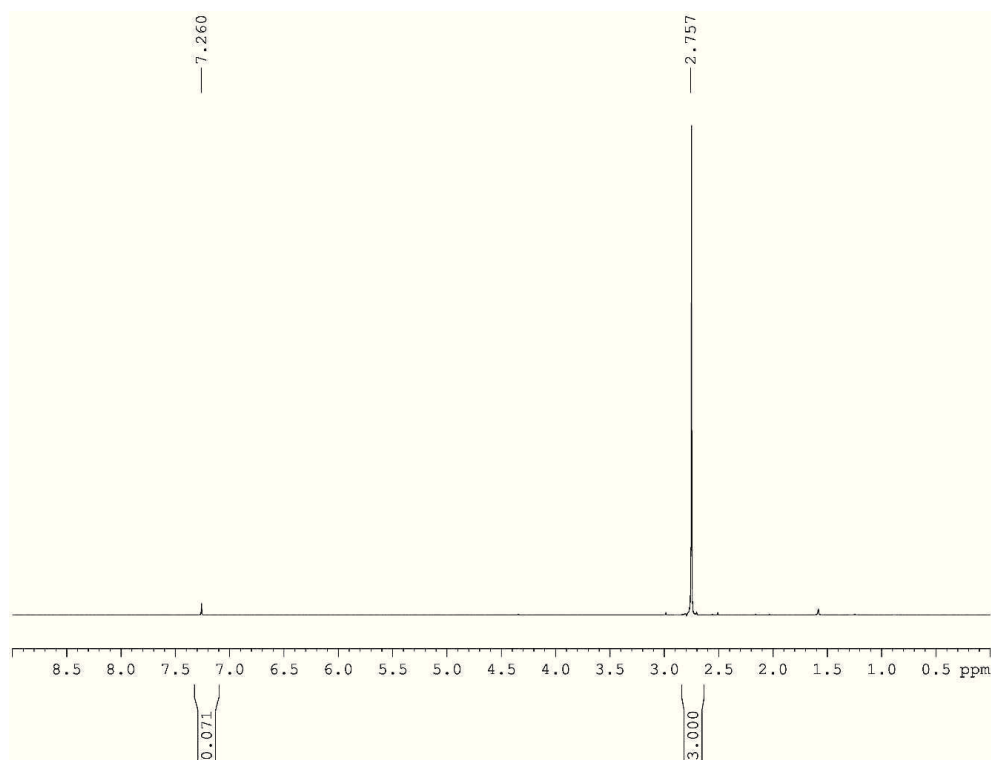


Figure 1. ^1H NMR (300 MHz, CDCl_3 , 298 K) of 2-[bis(methylthio)methylene]malononitrile (i).

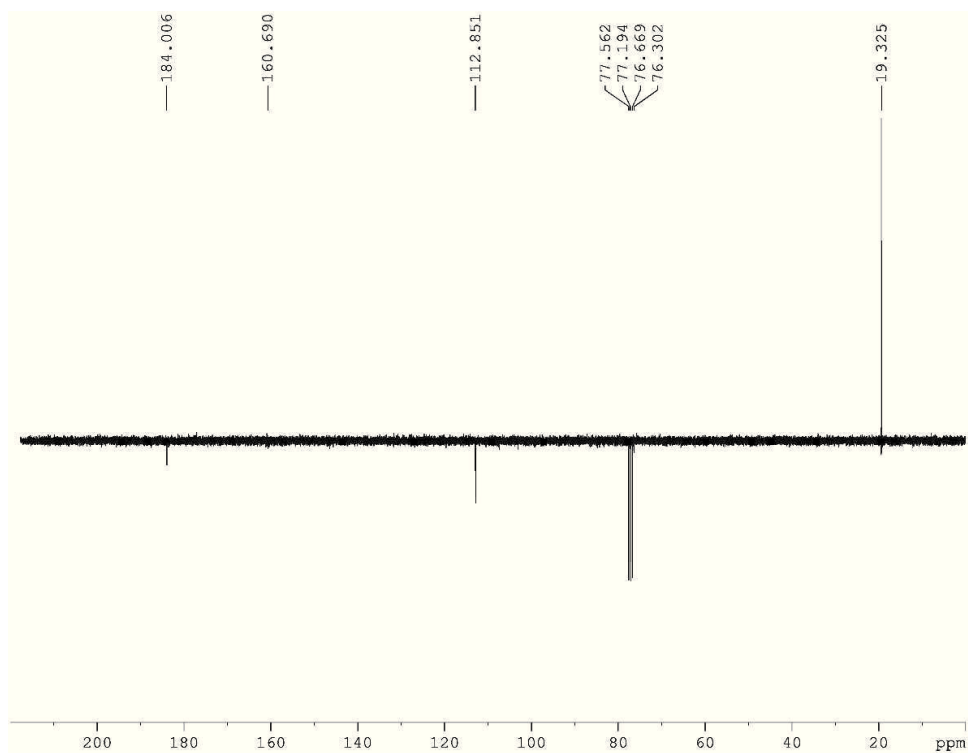


Figure 2. ¹³C NMR (300 MHz, CDCl₃, 298 K) of 2-[bis(methylthio)methylene]malononitrile (i).

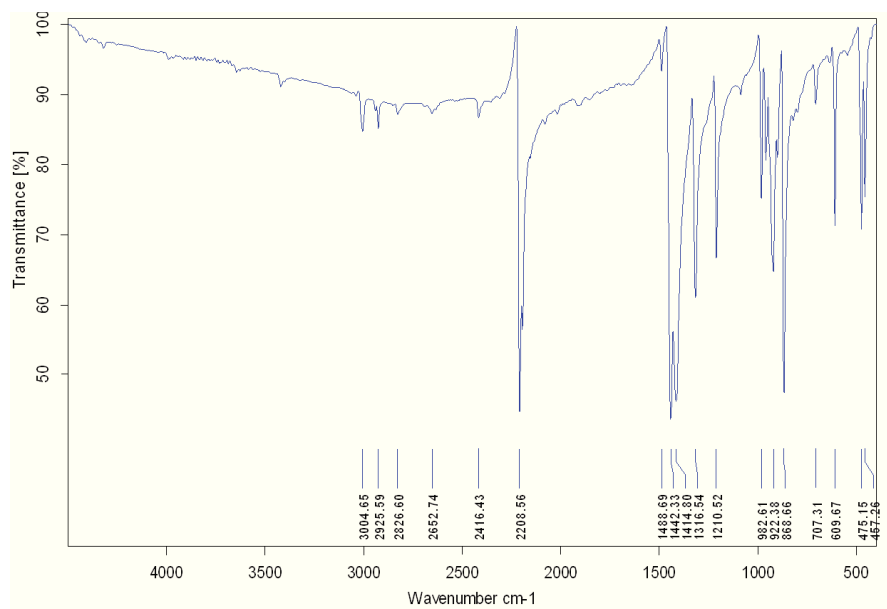
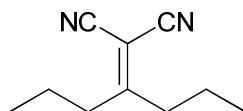


Figure 3. IR Spectrum of 2-[bis(methylthio)methylene]malononitrile (i).

➤ 2-[Bis(propylthio)methylene]malononitrile (ii):



Yield: 46% (6.205 g); ^1H NMR (300 MHz, CDCl_3) : δ , 3.19 (t, 4H, $-\text{SCH}_2-$), 1.73 (m, 4H, $-\text{CH}_2-\text{CH}_3$), 1.03 (t, 6H, $-\text{CH}_3$) (Figure 4); ^{13}C NMR (300 MHz, CDCl_3) : δ , 182.2 ($-\text{C}(\text{S-Pr})_2$), 112.7 ($-\text{CN}$), 78.2 ($-\text{C}(\text{CN})_2$), 38.5 ($-\text{SCH}_2-$), 22.4 ($-\text{CH}_2-\text{CH}_3$), 12.8 ($-\text{CH}_3$) (Figure 5); IR data (ν , cm^{-1}) : 2966w, 2933w, 2874w, 2407w, 2360w, 2349w, 2216s, 1454s, 1380w, 1339w, 1292w, 1240w, 1208w, 1091w, 1052w, 944m, 896w, 872w, 854w, 780w, 730w, 705w, 665w, 617w, 507m, 452w (Figure 6).

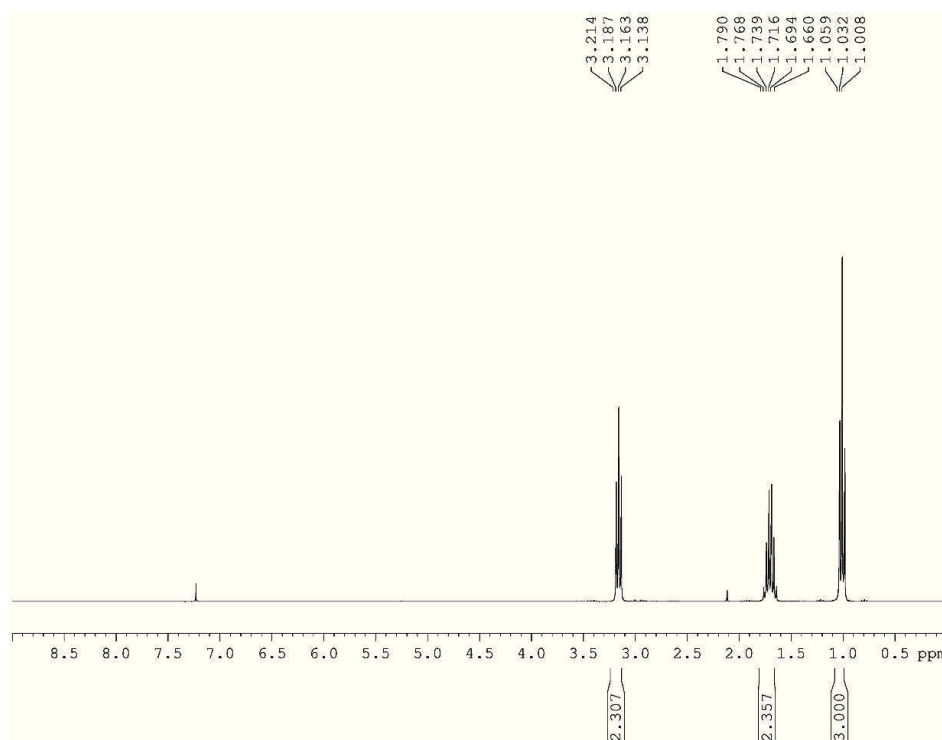


Figure 4. ^1H NMR (300 MHz, CDCl_3 , 298 K) of 2-[bis(propylthio)methylene]malononitrile (ii).

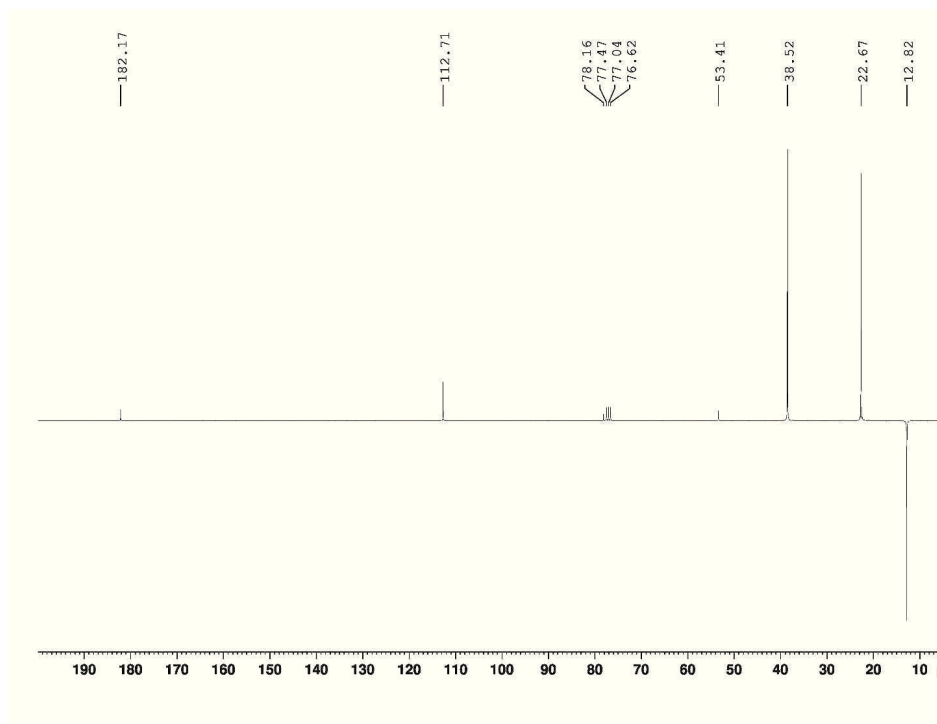


Figure 5. ¹³C NMR (300 MHz, CDCl₃, 298 K) of 2-[bis(propylthio)methylene]malononitrile (ii).

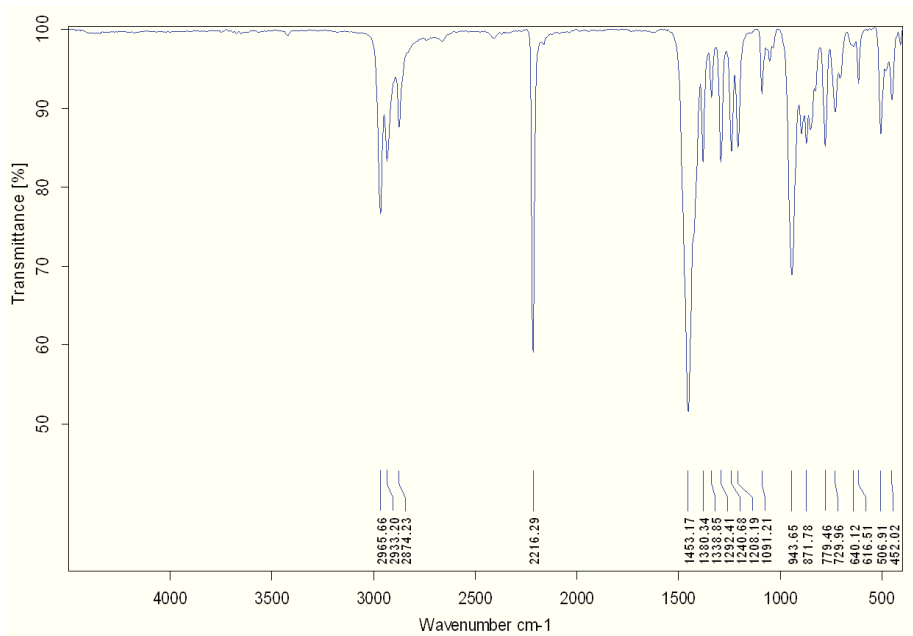
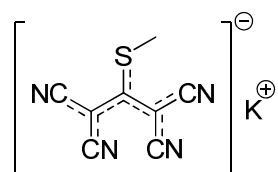


Figure 6. IR Spectrum of 2-[bis(propylthio)methylene]malononitrile (ii).

■ **Syntheses of potassium [1,1,3,3-tetracyano-2-thioalkylpropenide] salts: K(tcnsmc) and K(tcnspr).**

In this second step, a warm solution of the previously synthesized thioacetal, i.e. 2-[bis(alkylthio)methylene]malononitrile (10 mmol) in EtOH (30 mL), was added dropwise to an ethanol solution (10 mL) of malononitrile (0.66 g, 10 mmol) and t-BuOK (1.12 g, 10 mmol). The resulting solution was refluxed for 1h, and then the reaction mixture was cooled down to room temperature, and finally kept at 4 °C for two days. The resulting compound was filtered on a sintered-glass funnel and washed with distilled diethyl ether, and ultimately dried under vacuum to obtain yellow crystalline powders of K(tcnsmc) and K(tcnspr) salts in good yields (67% (1.516 g) and 70.5% (1.605 g), respectively).

➤ Potassium [1,1,3,3-tetracyano-2-thiomethylpropenide] K(tcnsmc):



Yield : 67% (1.516 g); ¹H NMR (300 MHz, Acetone-D₆) : δ, 2.54 (s, 3H -CH₃) (Figure 7); ¹³C NMR (500 MHz, Acetone-D₆) : δ, 170.2 (-C(S-Me)₂), 119.0 (-CN), 117.0 (-CN), 53.6 (-C(CN)₂), 18.4 (-SCH₃) (Figure 8); IR data (ν, cm⁻¹) : 2188s, 1450s, 1426m, 1329w, 1248w, 955w, 928w, 857w, 642w, 576w, 529w, 470w (Figure 9).

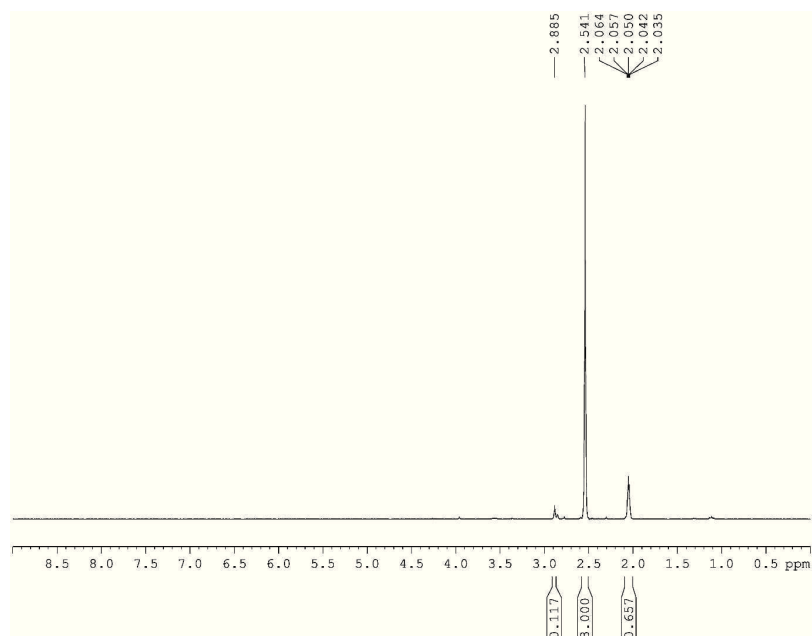


Figure 7. ¹H (300 MHz, Acetone-D₆) of K(tnsme) at 298 K.

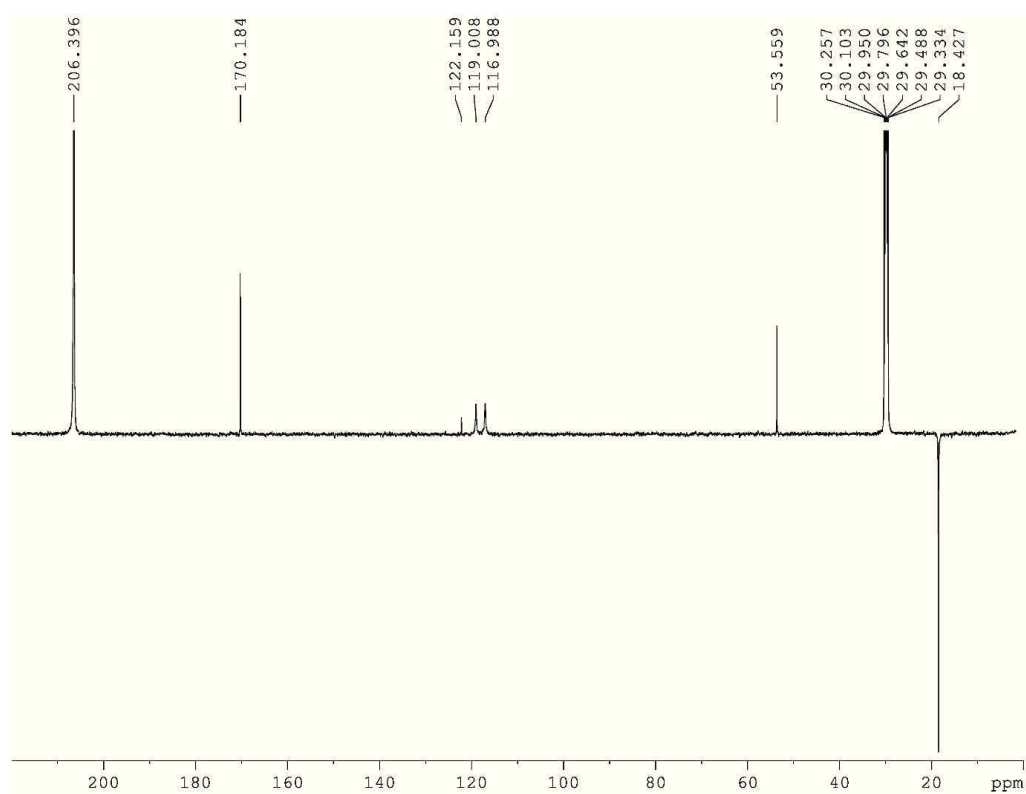


Figure 8. ¹³C NMR (500 MHz, Acetone-D₆) of K(tnsme) at 298 K.

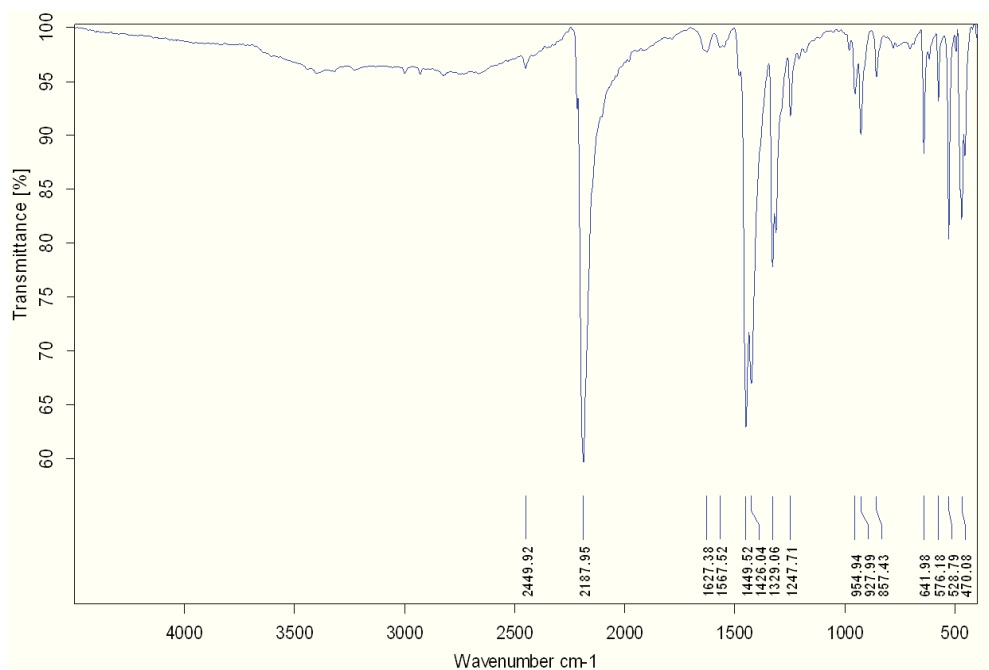
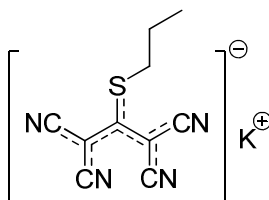


Figure 9. IR Spectrum of K(tcmsme).

➤ Potassium [1,1,3,3-tetracyano-2-thiopropylpropenide] K(tcmspr):



Yield : 70.5% (1.605 g); ^1H NMR (300 MHz, Acetone- D_6) : δ , 3.02 (t, 2H, $-\text{SCH}_2-$), 1.64 (hx, 2H, $-\text{CH}_2-\text{CH}_3$), 1.01 (t, 3H, $-\text{CH}_3$) (Figure 10); ^{13}C NMR (500 MHz, Acetone- D_6) : δ , 167.7 ($-\text{C}(\text{S-Pr})_2$), 118.9 ($-\text{CN}$), 117.0 ($-\text{CN}$), 54.7 ($-\text{C}(\text{CN})_2$), 37.8 ($-\text{SCH}_2-$), 23.4 ($-\text{CH}_2-\text{CH}_3$), 13.2 ($-\text{CH}_3$) (Figure 11); IR data (ν , cm^{-1}) : 2967w, 2933w, 2874w, 2440w, 2218w, 2199s, 2186s, 1445s, 1423s, 1328w, 1239w, 929w, 841w, 723w, 650w, 574w, 525w (Figure 12).

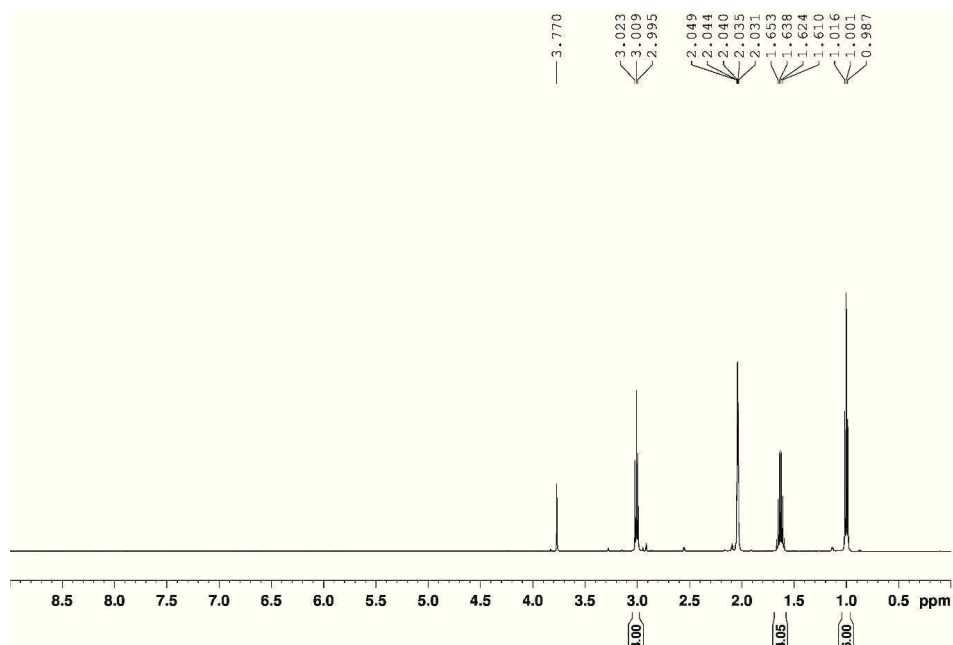


Figure 10. ^1H (300 MHz, Acetone- D_6) of K(tnspr) at 298 K.

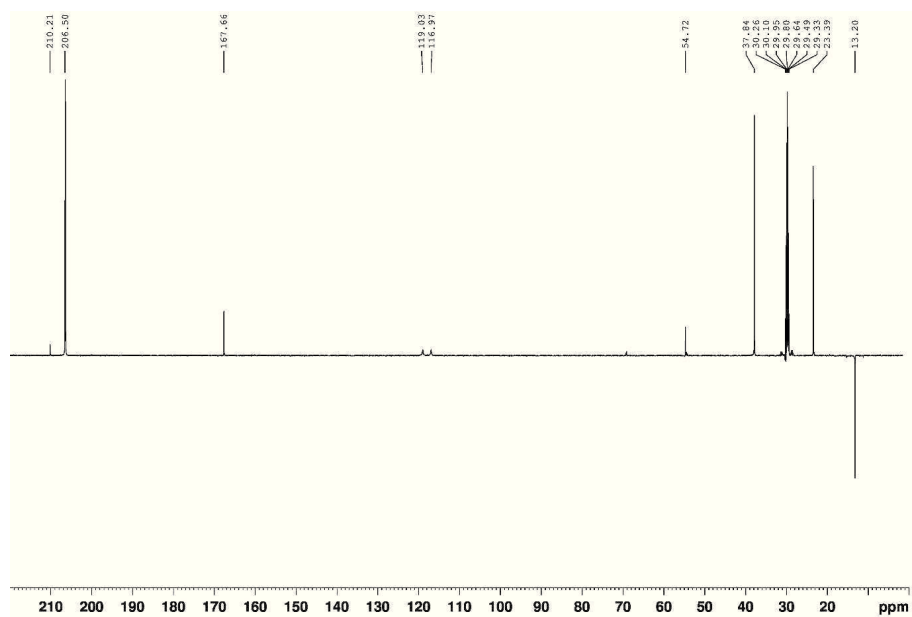


Figure 11. ^{13}C NMR (500 MHz, Acetone- D_6) of K(tnspr) at 298 K.

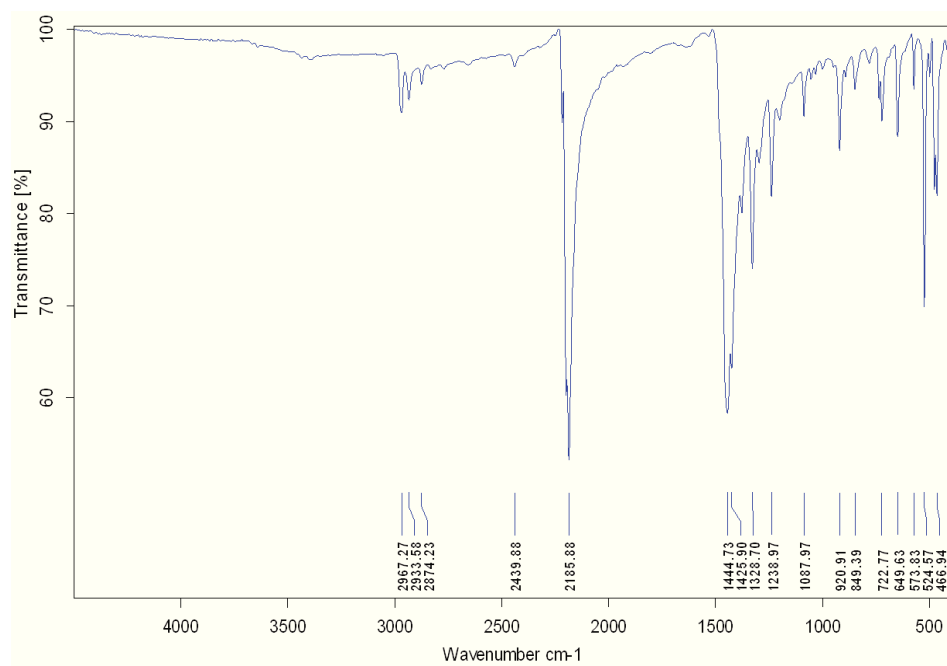


Figure 12. Infrared spectrum of K(tnspr).

2. Synthesis, structure and magnetic properties of the complex [Fe₃(bntrz)₆(tcnspr)₆] (**3**): Preliminary results

We describe here a new trinuclear Fe^{II} compound [Fe₃(bntrz)₆(tcnspr)₆] (**3**) resulting from the combination of the 4-R-1,2,4-triazole ligand (bntrz) with the functionalized thio-polynitrile anionic ligand 1,1,3,3-tetracyano-2-thiopropylpropenide (tcnspr)⁻ anion. This compound has been characterized by single crystal X-ray diffraction associated with magnetic and DSC studies, which revealed a neutral trinuclear structure exhibiting a one-step first-order [HS-HS-HS] ↔ [LS-LS-LS] transition around room temperature.

2.1. Syntheses and characterizations

Single crystals of the complex [Fe₃(bntrz)₆(tcnspr)₆] (**3**) have been obtained using diffusion technique in a fine glass tube (3.0 mm diameter) by addition of an aqueous solution of the bntrz ligand onto a water-acetone solution containing both K(tcnspr) and Fe(BF₄)₂·6H₂O salts. Single crystals of pink color suitable for single crystal X-ray diffraction were collected after one week, and dried in air at room temperature.

Infrared data analyses were undertaken as preliminary studies to ascertain the coordination mode(s) of the (tcnspr)⁻ anion and bntrz triazole ligand to the Fe^{II} metal centers in the complex **3** (Figure 13). In the corresponding IR spectra, absorption bands assigned to the ν_{CN} stretching vibrations of the (tcnspr)⁻ anion are observed at 2232 and 2193 cm⁻¹. These values, distinct from the corresponding one observed for the potassium salt K(tcnspr) (2186 cm⁻¹), are indicative of the presence of both coordinated and uncoordinated nitrile groups in **3**, and in agreement with the subsequent single crystal structure determination. About the triazole based ligand bntrz in **3**, the band assigned to the ring torsion of 1,2,4-triazole at ν = 638 cm⁻¹, and the ν_{C=N} stretching vibration at 1534 cm⁻¹, are all shifted upon complexation in **3** to 639 cm⁻¹ and 1547 cm⁻¹, respectively; these values implicitly confirm the coordination of the iron atom to the 1,2,4-triazole ring.¹² In the low frequency region (Figure 13), the bands observed at 206, 212, 242, 279, 315 and 350 cm⁻¹ are assigned to the Fe-N stretching vibrations, and reveal the

presence of Fe(II) metal centers in both high spin (*HS*) state and low spin (*LS*) state at room temperature, as further confirmed with the magnetic measurements.

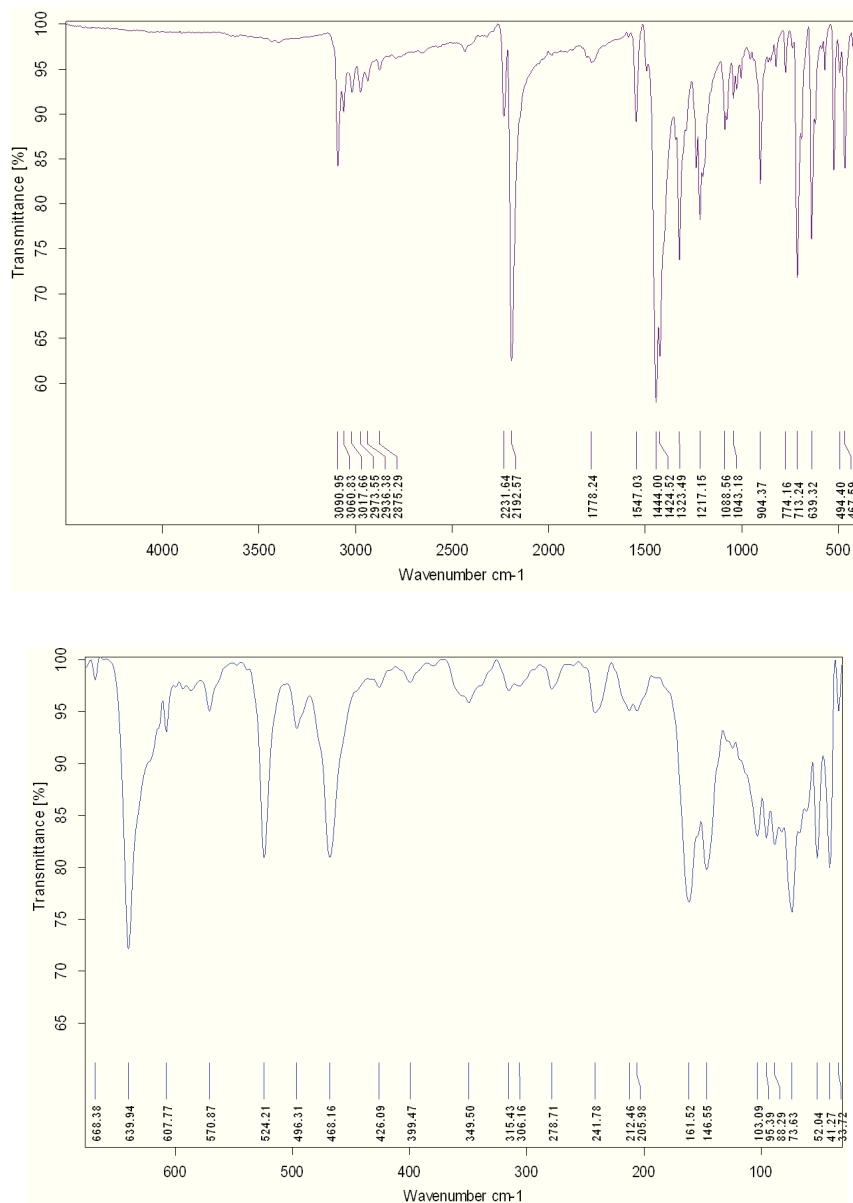


Figure 13. Infrared spectra of the single-crystals of $[\text{Fe}_3(\text{bntrz})_6(\text{tcnsp})_6]$ (**3**). IR data (ν , cm^{-1}): 3091w, 3061w, 3018w, 2974w, 2936w, 2232w, 2193s, 1547w, 1444s, 142s, 1323m, 1217m, 1089w, 1043w, 904w, 713m, 640m, 524w, 468w, 350w, 315w, 279w, 242w, 212w, 206w, 162m, 147m, 103w, 15w, 73m, 52w, 41w.

2.2. Structural studies

The compound $[\text{Fe}_3(\text{bntrz})_6(\text{tcnspr})_6]$ (**3**) has been structurally characterized at 295 K (pink crystal, Figure 14). The crystal data and structural refinement parameters of **3** at 295 K are listed in Table 1. The Fe-N bond lengths, N-Fe-N bond angles, and the average Fe-N bond distances are listed in Table 2. This compound crystallizes in the trigonal *R*-3 space group at 295 K. These crystallographic data reveal that compound **3** displays a neutral discrete trinuclear structure with similar structural features than the compound **2** previously discussed in Chapter III (Figure 14).

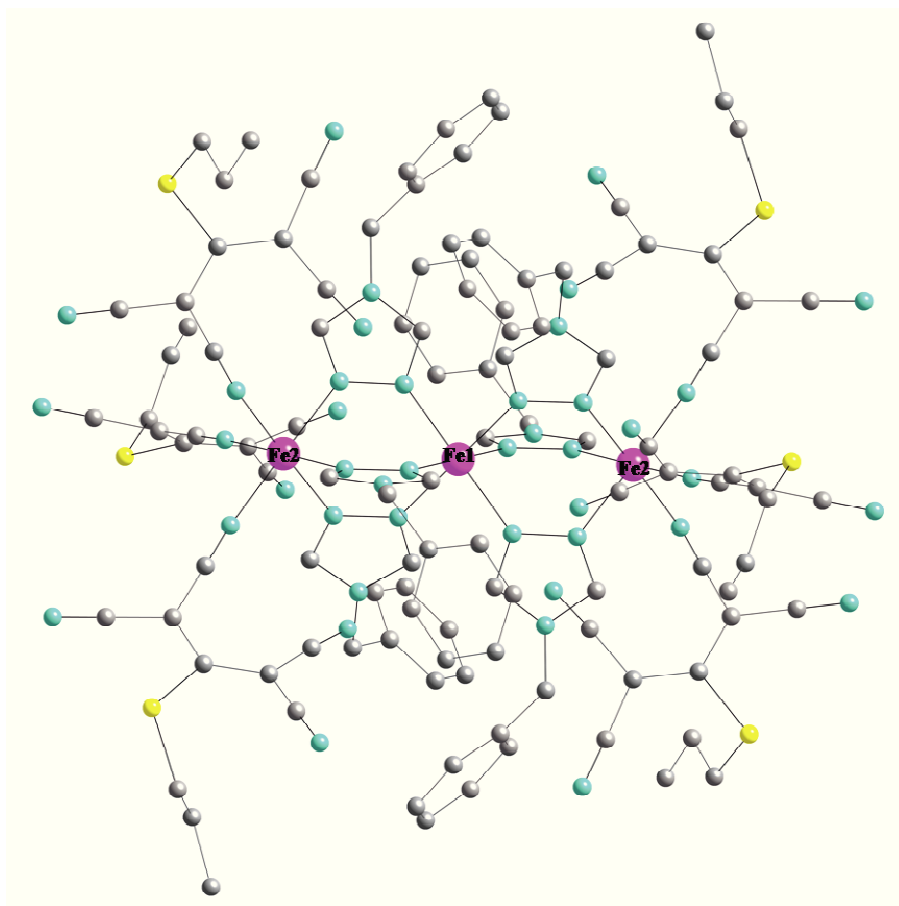


Figure 14. View of the centrosymmetric trinuclear complex of $[\text{Fe}_3(\text{bntrz})_6(\text{tcnspr})_6]$ (**3**) at 295 K. [Fe (pink), N (pale blue), C (pale grey) and S (yellow)] (Hydrogen atoms have been omitted for clarity).

Table 1. Crystal data and structural refinement parameters for [Fe₃(bntrz)₆(tcnspr)₆] (**3**).

Temperature / K	295
Color	Colorless
Empirical formula	C ₁₁₄ H ₉₆ Fe ₃ N ₄₂ S ₆
Formula weight / g.mol ⁻¹	2414.24
Wavelength / Å	0.71073 Å
Crystal system	Trigonal
Space group	<i>R</i> -3
a / Å	26.033(5)
c / Å	14.750(3)
Volume / Å ³	8657(3)
Z	3
D _{calc} / g.cm ⁻³	1.389
Abs. coef. / cm ⁻¹	5.49
F(000)	3744
Crystal size / mm ³	0.18 × 0.07 × 0.06
2θ range / °	6.60 to 57.86
Refl. collected	6557
Unique refl. / Rint	4108 / 0.1078
Data / restr. / N _v	1151 / 0 / 249
Final R indexes [all data]	R1 = 0.0846, wR2 = 0.1696
^c GooF	0.925
Δρ _{max/min} / eÅ ⁻³	0.901 / -0.502

$$^a R1 = \sum |F_o - F_c| / F_o. \quad ^b wR2 = \{ \sum [w(F_o^2 - F_c^2)^2] / \sum [w(F_o^2)^2] \}^{1/2}. \quad ^c \text{GooF} = \{ \sum [w(F_o^2 - F_c^2)^2] / (N_{\text{obs}} - N_{\text{var}}) \}^{1/2}$$

Table 2. Selected Fe-N bond lengths (Å), average Fe-N bond lengths (Å), and N-Fe-N bond angles (°) for **3** at 295 K.

295 K	
N(1)-Fe(1)	2.017(7)
Fe(1)-N(1)#1	2.017(7)
Fe(1)-N(1)#2	2.017(7)
Fe(1)-N(1)#3	2.017(7)
Fe(1)-N(1)#4	2.017(7)
Fe(1)-N(1)#5	2.017(7)
<Fe1-N>	2.017(7)
N(2)-Fe(2)	2.047(7)
N(3)-Fe(2)	2.021(9)
Fe(2)-N(3)#2	2.021(9)
Fe(2)-N(3)#4	2.021(9)
Fe(2)-N(2)#2	2.047(7)
Fe(2)-N(2)#4	2.047(7)
<Fe2-N>	2.034(9)
N(1)#1-Fe(1)-N(1)	180.0(8)
N(1)#1-Fe(1)-N(1)#2	89.6(3)
N(1)-Fe(1)-N(1)#2	90.4(3)
N(1)#1-Fe(1)-N(1)#3	90.4(3)
N(1)-Fe(1)-N(1)#3	89.6(3)
N(1)#2-Fe(1)-N(1)#3	89.6(3)
N(1)#1-Fe(1)-N(1)#4	89.6(3)
N(1)-Fe(1)-N(1)#4	90.4(3)
N(1)#2-Fe(1)-N(1)#4	90.4(3)
N(1)#3-Fe(1)-N(1)#4	180.0(4)
N(1)#1-Fe(1)-N(1)#5	90.4(3)
N(1)-Fe(1)-N(1)#5	89.6(3)
N(1)#2-Fe(1)-N(1)#5	180.0(4)
N(1)#3-Fe(1)-N(1)#5	90.4(3)
N(1)#4-Fe(1)-N(1)#5	89.6(3)
N(3)-Fe(2)-N(3)#2	91.8(3)
N(3)-Fe(2)-N(3)#4	91.8(3)
N(3)#2-Fe(2)-N(3)#4	91.8(3)
N(3)-Fe(2)-N(2)#2	178.4(3)
N(3)#2-Fe(2)-N(2)#2	89.8(3)
N(3)#4-Fe(2)-N(2)#2	88.4(3)
N(3)-Fe(2)-N(2)#4	88.4(3)
N(3)#2-Fe(2)-N(2)#4	178.4(3)
N(3)#4-Fe(2)-N(2)#4	89.8(3)
N(2)#2-Fe(2)-N(2)#4	90.0(3)
N(3)-Fe(2)-N(2)	89.8(3)
N(3)#2-Fe(2)-N(2)	88.4(3)
N(3)#4-Fe(2)-N(2)	178.4(3)
N(2)#2-Fe(2)-N(2)	90.0(3)
N(2)#4-Fe(2)-N(2)	90.0(3)

*The two Fe(II) environments are defined by N8 ([Fe1(N1)₆]) and by N9 and N5 Fe2(N2)₃(N4)₃) nitrogen atoms.

Symmetry transformations used to generate equivalent atoms: #1 -x,-y,-z #2 -x+y,-x,z #3 y,-x+y,-z #4 -y,x-y,z

#5 x-y,x,-z.

2.3. Magnetic properties

The temperature-dependent measurements of the magnetic susceptibility of the crystalline sample of complex **3** were carried out in the temperature range 2-350 K (Figure 15). Similar to what has been observed for the derivative $[\text{Fe}_3(\text{bntrz})_6(\text{tcnset})_6]$ (**2**), this investigation elucidated a very abrupt *SCO* behaviour around room temperature for $[\text{Fe}_3(\text{bntrz})_6(\text{tcnspr})_6]$ (**3**). Thus, in the temperature range 2-200 K, the $\chi_m T$ product presents a value of ca. $0 \text{ cm}^3 \cdot \text{K} \cdot \text{mol}^{-1}$ typically observed for a diamagnetic low spin ($S = 0$) compound. However, above this temperature, the $\chi_m T$ product rises dramatically to a saturated *HS* value of $9.48 \text{ cm}^3 \cdot \text{K} \cdot \text{mol}^{-1}$ at ca. 300 K, which is indicative of the presence of a sharp and complete *HS* to *LS SCO* first-order phase transition. In comparison with compound **2** ($T_{1/2} \approx 318 \text{ K}$), the one-step spin transition occurs at a significantly lower temperature for **3**. As in complex **2**, no thermal hysteresis effects were detected upon warming and cooling modes at a scan rate of $1 \text{ K} \cdot \text{min}^{-1}$ in settle mode.

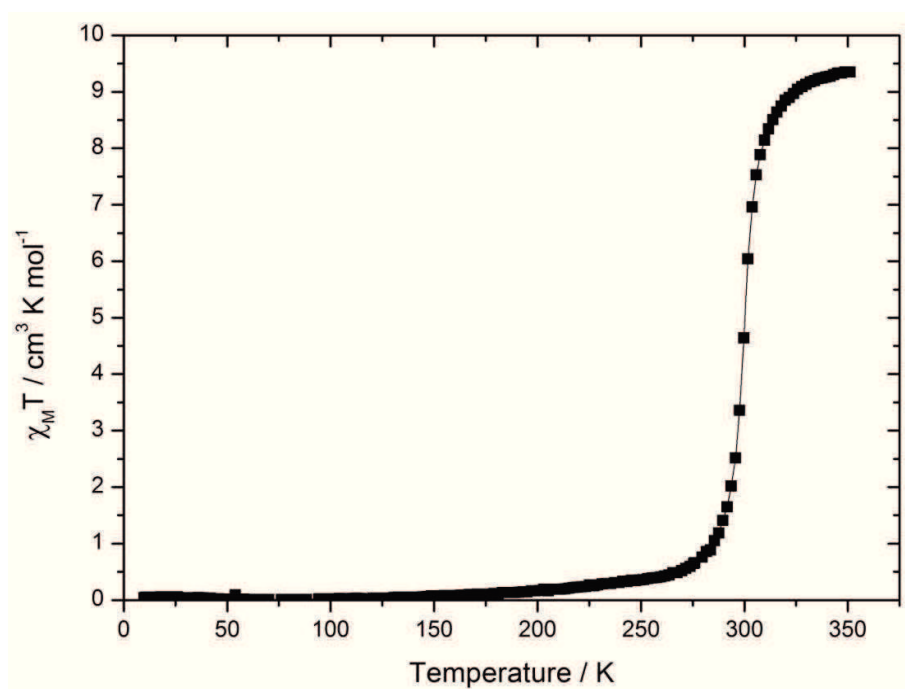


Figure 15. Thermal evolution of the $\chi_m T$ product in the 2-350 K range for $[\text{Fe}_3(\text{bntrz})_6(\text{tcnspr})_6]$ (**3**).

2.4. Differential scanning calorimetry (DSC)

The *SCO* behaviour of **3** was also investigated by calorimetric measurements. The DSC study for **3** was performed in the temperature range 170–400 K at ambient pressure, with a temperature scan rate of 2 K.min⁻¹ in both heating and cooling modes. The heat capacity curves of **3** obtained by DSC show symmetrical and well-separated peaks associated with the abrupt spin transition (Figure 16). Thus, an endothermic peak is observed at $T_{c\uparrow} = 300.10$ K upon warming while an exothermic peak has been recorded at $T_{c\downarrow} = 299.27$ K on cooling. This phase transition occurs with an average enthalpy and entropy changes of $\Delta H = 34.75$ kJ.mol⁻¹ and $\Delta S = 115.80$ J.K⁻¹.mol⁻¹, respectively, for the three Fe(II) metal centres in compound **3**; although significantly lower in comparison with compound **2** ($\Delta H = 54.08$ kJ.mol⁻¹ and $\Delta S = 170.00$ J.K⁻¹.mol⁻¹, respectively), the two values remain in the same range with those reported in the literature for *SCO* compounds.¹²

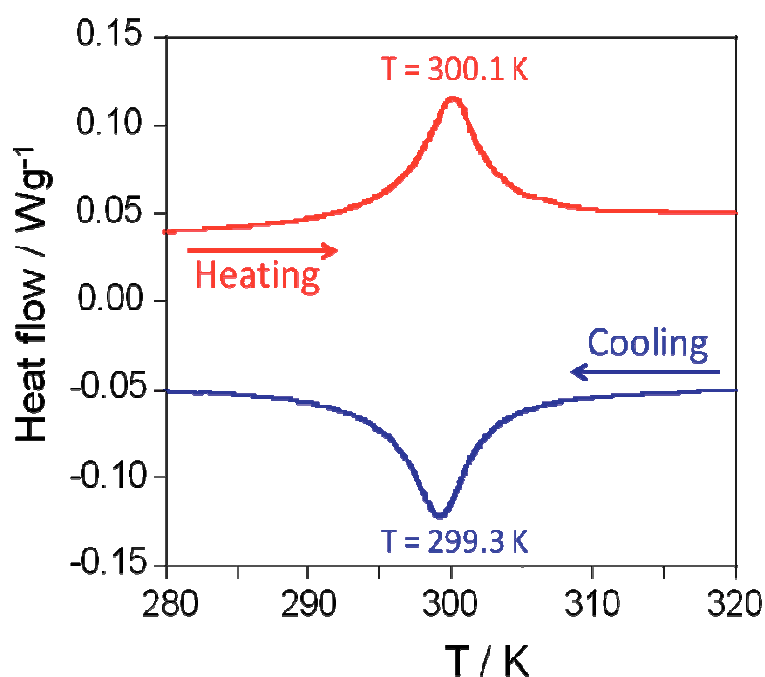


Figure 16. DSC profiles of the coordination polymer **3** at 2 K.min⁻¹ upon heating (red) and cooling (blue), respectively.

Finally, as evidenced by the structural and magnetic/DSC studies, the compound **3** - built from the (tcnspr)⁻ anion instead of the (tcnset)⁻ moiety for **2** - present structural features and a *SCO* behavior very similar to what has been observed in **2**, but the *SCO* temperature is significantly lowered by ca. 18K ($T_{SCO} \approx 318$ K for **2**, and ca. 300 K for **3**). Thus, the present results proved that the nature of the functional group in the cyanocarbanion can significantly impact the *SCO* temperature, which suggests the possibility to further exploit this “*Chemical factor*” to fine tune the *SCO* Characteristics - such as the *SCO* temperature - in these triazole based Fe(II) systems.

3. Synthesis, structure and magnetic properties of the complex $[\text{Fe}_3(\text{bntz})_8(\text{tcnsme})_2][\text{tcnsme}]_2 \cdot 4\text{H}_2\text{O}$ (**4**)

3.1. Synthesis

The single crystals of the complex $[\text{Fe}_3(\text{bntz})_8(\text{tcnsme})_2][\text{tcnsme}]_2 \cdot 4\text{H}_2\text{O}$ (**4**) have been synthesized using diffusion technique in a fine glass tube (3.0 mm diameter) by carefully layering an aqueous solution of the bntz ligand onto a water-acetone solution containing both $\text{K}(\text{tcnsme})$ and $\text{Fe}(\text{BF}_4)_2 \cdot 6\text{H}_2\text{O}$ salts. The resulting pale pink single crystals of **4**, suitable for X-ray diffraction, have been obtained in one to two weeks, and dried in air at ambient conditions.

3.2. Preliminary structural characterizations and magnetic properties

The crystal structure of **4** has been solved at 170 K. The unit cell parameters and refinement data are given in Table 3. The asymmetric unit contains two Fe(II) centers Fe1 and Fe2, located respectively on the inversion center ($\frac{1}{2} \frac{1}{2} \frac{1}{2}$) and on a general position, four bntz ligands, three $(\text{tcnsme})^-$ anions and two water molecules, all located on general positions, giving the general formula of $[\text{Fe}_3(\text{bntz})_8(\text{tcnsme})_2][\text{tcnsme}]_2 \cdot 4\text{H}_2\text{O}$ (**4**) (Figures 17 and 18).

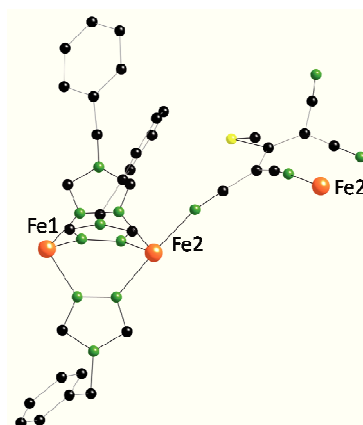


Figure 17. Asymmetric unit of $[\text{Fe}_3(\text{bntz})_8(\text{tcnsme})_2][\text{tcnsme}]_2 \cdot 4\text{H}_2\text{O}$ (**4**) (Fe, orange; N, green; C, black). Hydrogen atoms, benzyl groups, and part of $(\text{tcnsme})^-$ anions have been omitted for clarity.

Table 3. Crystal data and structural refinement parameters for **4**.

Compound	4
Temperature / K	170
Color	Pink
Empirical formula	C ₁₂₀ H ₉₈ Fe ₃ N ₄₈ O ₄ S ₆
Formula weight / g.mol ⁻¹	2636.37
Wavelength / Å	0.71073 Å
Crystal system	Monoclinic
Space group	<i>P</i> 21/ <i>n</i>
<i>a</i> / Å	14.061(4)
<i>b</i> / Å	22.362(8)
<i>c</i> / Å	21.005(7)
β / °	106.54(4)
Volume / Å ³	6332(4)
<i>Z</i>	2
<i>D</i> _{calc} / g.cm ⁻³	1.383
Abs. coef. / cm ⁻¹	5.11
F(000)	2720
Crystal size / mm ³	0.12 × 0.06 × 0.05
2 θ range / °	6.86 to 58.44
Refl. collected	9758
Unique refl. / R _{int}	7874 / 0.2135
Data / restr. / N _v	2032 / 0 / 517
Final R indexes	R ₁ = 0.1280, wR ₂ = 0.2667
^c GooF	0.973
$\Delta\rho_{\text{max/min}}$ / eÅ ⁻³	+0.506 / -0.481

$$^a R_1 = \sum |F_o - F_c| / F_o, \quad ^b wR_2 = \{ \sum [w(F_o^2 - F_c^2)^2] / \sum [w(F_o^2)^2] \}^{1/2}, \quad ^c \text{GooF} = \{ \sum [w(F_o^2 - F_c^2)^2] / (N_{\text{obs}} - N_{\text{var}}) \}^{1/2}$$

The molecular structure of **4** consists of trinuclear moieties of formula $[\text{Fe}_3(\mu_2\text{-bntrz})_6(\text{bntrz})_2]$ in which six bntrz ligands act as μ_2 -bridging coordination modes similar to that described for compounds $[\text{Fe}_3(\text{bntrz})_6(\text{tcnset})_6]$ (**2**) and $[\text{Fe}_3(\text{bntrz})_6(\text{tcnspr})_6]$ (**3**); each of the two remaining bntrz ligands is terminally coordinated to the two external Fe2 centres. These trinuclear $[\text{Fe}_3(\mu_2\text{-bntrz})_6(\text{bntrz})_2]$ fragments are connected to each other by symmetric double cyanocarbanion bridges involving 12-membered metallacycles, resulting in the alternating chain depicted in figure 18.

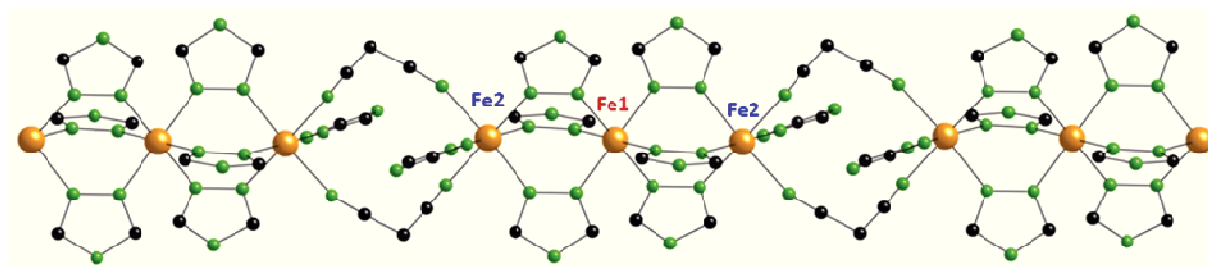


Figure 18. View of the 1-D alternating chain of $[\text{Fe}_3(\text{bntrz})_8(\text{tcnsme})_2][\text{tcnsme}]_2 \cdot 4\text{H}_2\text{O}$ (**4**) (Fe, orange; N, green; C, black). Hydrogen atoms, benzyl group and part of $(\text{tcnsme})^-$ anion have been omitted for clarity.

This molecular extended arrangement clearly involves trinuclear Fe_3 units nearly similar to those described previously for **2** and **3**, but the overall molecular structure of **4** is ultimately very different. This difference arises from the slightly modified $(\text{tcnsme})^-$ anion for which two of them act in **4** as bridging ligands through two nitrile groups from the same $-\text{C}(\text{CN})_2$ “wing”.

The preliminary magnetic studies are depicted in Figure 19 in the form of the $\chi_m T$ product vs. Temperature (T), where χ_m is the molar magnetic susceptibility. As expected, the magnetic behaviour of **4** is very different from those described for the discrete trinuclear complexes i.e. **2** and **3**. In the temperature range 2-200 K, the $\chi_m T$ product, close to zero $\text{cm}^3 \cdot \text{K} \cdot \text{mol}^{-1}$, is in

agreement with the *LS* state. Above this temperature, the $\chi_m T$ product increases markedly to reach a plateau at $8.9 \text{ cm}^3 \cdot \text{K} \cdot \text{mol}^{-1}$ at *ca.* 325 K; the latter may be attributed to a complete *LS-HS* conversion of the two external Fe2 ion centers associated to a partial *LS-HS* conversion of the central Fe ion (Fe1).

After warming further, the $\chi_m T$ product increases abruptly to reach a value of $10.9 \text{ cm}^3 \cdot \text{K} \cdot \text{mol}^{-1}$ at *ca.* 380 K, which is consistent with the presence of three isolated Fe(II) centers in a *HS* state. Upon cooling, the $\chi_m T$ product shows then a gradual decrease down to a temperature value of 290 K. Below this temperature, a sharp decrease of the $\chi_m T$ down to 250 K is observed, where the thermal behavior becomes more gradual, to reach finally the diamagnetic *LS* state below 100 K. The difference observed between the warming and the cooling scans may be attributed to the complete or partial dehydration of compound **4** at 380 K. However, additional SQUID measurements such as multiple warming and cooling cycles should be performed in order to confirm the origin and the presence of the two different magnetic behaviors.

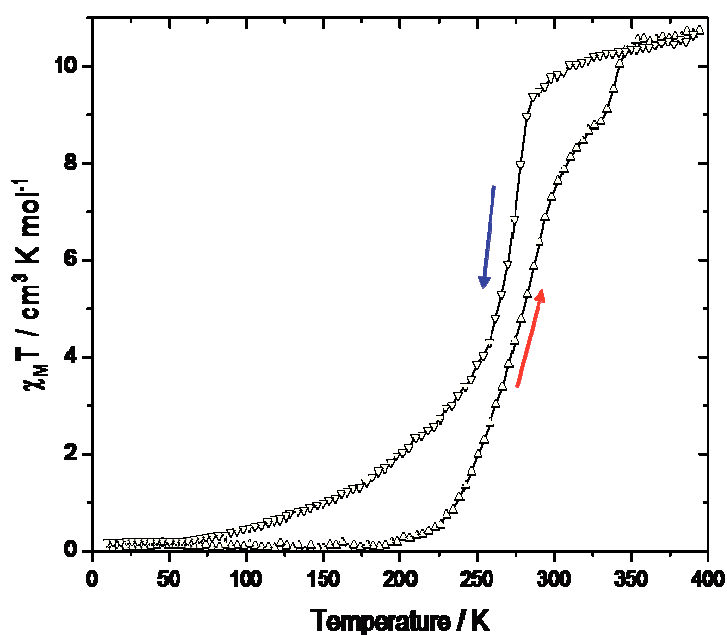


Figure 19. Thermal evolution of the $\chi_m T$ product in the 2-380 K range for **4** (Heating mode (Δ) and Cooling mode (∇)).

Conclusion

In summary, we have extended the strategy developed with the compound $[\text{Fe}_3(\text{bntrz})_6(\text{tcnset})_6]$ (**2**) in order to evaluate the influence of the nature of the substituent from the polynitrile anionic moiety on the structural and magnetic features of the resulting materials. Thus, two new Fe(II) *SCO* systems $[\text{Fe}_3(\text{bntrz})_6(\text{tcnspr})_6]$ (**3**) and $[\text{Fe}_3(\text{bntrz})_8(\text{tcnsme})_2](\text{tcnsme})_2 \cdot 4\text{H}_2\text{O}$ (**4**) - based on the combination of *bntrz* and $(\text{tcnspr})^-$ and $(\text{tcnsme})^-$ ligands, respectively - have been synthesized as single crystals, and preliminarily characterized. The neutral trinuclear complex $[\text{Fe}_3(\text{bntrz})_6(\text{tcnspr})_6]$ (**3**) exhibits similar structural and magnetic behaviours than compound $[\text{Fe}_3(\text{bntrz})_6(\text{tcnset})_6]$ (**2**), as it also displays a single step *SCO* behaviour around room temperature; even though the substitution of the $(\text{tcnset})^-$ by the $(\text{tcnspr})^-$ analogue did not modify the type of spin transition (abrupt - one step), the slight modification of the alkyl group (from ethyl to propyl) in the chemical structure of the polynitrile anion induced a significant drop of *ca.* 18 K for the transition temperature ($T_{1/2} \approx 318$ K for **2**, and *ca.* 300 K for **3**). In comparison, the compound $[\text{Fe}_3(\text{bntrz})_8(\text{tcnsme})_2](\text{tcnsme})_2 \cdot 4\text{H}_2\text{O}$ (**4**) exhibits a structure clearly distinct from **2** and **3** that is constructed through trinuclear building blocks $[\text{Fe}-(\mu_2\text{-bntrz})_3(\text{bntrz})\text{-Fe}-(\mu_2\text{-bntrz})_3(\text{bntrz})\text{-Fe}]$ and $(\mu_2\text{-tcnsme})^-$ anions, resulting in an alternating chain. Accordingly, the compound **4** displayed an expected two step *SCO* behaviour. A contrario compounds **2** and **3**, the change to a methyl group induced this time a different type of *SCO* behavior in **4**. This study proved ultimately that subtle variations of the R' substituent in the cyanocarbanion $(\text{tcnsR}')^-$ can play a vital role on the magneto-structural properties in triazole-based Fe(II) systems.

Chapter IV

Spin-Crossover (*SCO*) Behaviours of Three Dimensional Materials Based on Functionalized Triazole Ligand

Table of Contents

Introduction	166
Results and discussion	169
1. Syntheses and characterizations of $\{\text{Fe}_3(\mu_2\text{-phtptrz})_6[\mu_2\text{-Pt(CN)}_4]_3\} \cdot \text{C}_2\text{H}_5\text{OH} \cdot 5.5\text{H}_2\text{O}$ (5) and $\{\text{Fe(phtptrz)}[\text{Pt(CN)}_4] \cdot \text{H}_2\text{O}\}$ (6)	169
2. Structural characterizations	172
3. Magnetic properties	186
Conclusion and perspectives	189
Experimental section	191
Bibliography	200

Spin-Crossover (*SCO*) Behaviours of Three Dimensional Materials Based on Functionalized Triazole Ligand

In synopsis of the preceding two chapters, the swap of the organic polynitrile ligands by inorganic $[\text{Pt}(\text{CN})_4]^{2-}$ analogues in the “ Fe^{II} /bntrz/Anion systems” permitted to reach extended one dimensional (1D) networks instead of trinuclear complexes. In a rational continuance aiming to further evaluate the magneto-structural influence of the nature of the functional group at the 4th position of the triazole ligand while maintaining $[\text{Pt}(\text{CN})_4]^{2-}$ moiety as counter-anions, two new three dimensional (3D) materials $\{\text{Fe}_3(\mu_2\text{-phtptrz})_6[\mu_2\text{-Pt}(\text{CN})_4]_3\} \cdot \text{C}_2\text{H}_5\text{OH} \cdot 5.5\text{H}_2\text{O}$ (**5**) and $\{\text{Fe}(\text{phtptrz})[\text{Pt}(\text{CN})_4] \cdot \text{H}_2\text{O}\}$ (**6**), based on the functionalized triazole 2-(3-(4H-1,2,4-triazol-4-yl)propyl)isoindoline-1,3-dione (phtptrz), have been synthesized, and notably characterized by single crystal X-ray crystallography in both low spin and high spin states. In comparison with the 4-(benzyl)-4H-1,2,4-triazole (bntrz) ligand involved in the materials described in Chapters II and III, the phtptrz presents a bulkier phthalimido group, with a longer alkyl spacer (three carbons *vs.* one in bntrz) between the N4 substituent and the triazole motif which provides more flexibility. The two compounds **5** and **6** display different 3D structures and different magnetic behaviours; even so they have been synthesized from the exact same starting precursors but with different crystal engineering conditions. Consequently, a two-step *SCO* behavior is observed only in **5**, while **6** shows a characteristic paramagnetic behavior with *HS* Fe^{II} ions in the whole studied temperature range. In this respect, compound **5** can be labelled as the first three dimensional *SCO* material based on functionalized triazole-ligand (phtptrz) which has been characterized structurally in *LS* and *HS* states.

◆ Introduction

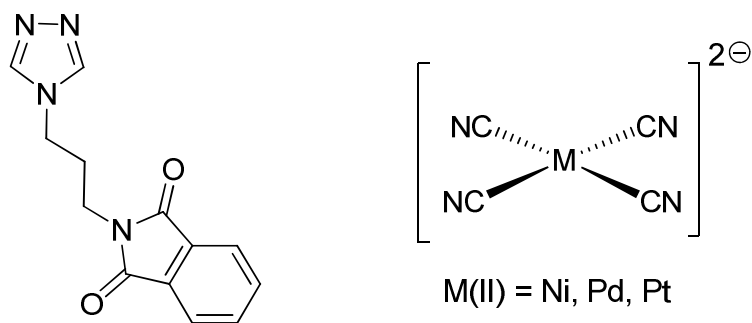
The Spin-crossover (*SCO*) materials, explicitly first-row transition metal complexes with $3d^4$ - $3d^7$ electronic configurations that can switch reversibly between high-spin (*HS*) and low-spin (*LS*) states, currently represent one of the most attractive examples of switchable molecular materials.¹ More specifically, in Fe^{II} metal derivatives involving pseudo-octahedral $[\text{FeN}_6]$ coordination spheres, the spin transition between the high-spin state (*HS*; $S=2$, $^5T_{2g}$) and low-spin state (*LS*; $S=0$, $^1A_{1g}$), and the associated optical changes, can be induced by different external stimuli such as temperature, pressure, and light irradiation. Consequently, those switchable molecular materials can be considered for various applications such as data storage, display devices, sensors, biomaterials, and multifunctional materials, to name a few.² In this regard, specifically, $[\text{Fe}^{\text{II}}/4\text{-R-1,2,4-triazole}]$ (with

R = functional group of various natures) systems proved to provide the adequate structural requirements (i.e. ligand-field strength, distortion parameters, elastic interactions) around the Fe^{II} centre for the occurrence of *SCO* behaviors with high cooperativity around and above ambient temperature.^{1d,3-5} As initiated by O. Kahn and co-workers, the *SCO* materials of general formula [Fe(4-R-1,2,4-trz)₃](A)_x (where 4-R-1,2,4-trz = 4-substituted-1,2,4-triazole and A = mono or divalent anion) have been extensively investigated as bulk sensors and opto-electronic displays.^{1d,3a,4} Ever since, the major research developments in these triazole systems, carried out notably by Y. Garcia,^{4,6} E. Coronado,⁷ J.-F. Létard,⁸ A. Bousseksou,⁹ *et al.*, have focused on (i) understanding the origin of their outstanding *SCO* properties, with the need to access single-crystals stable at both spin states, and (ii) the nanostructuration of such materials to shape applied devices such as sensors.¹⁰ Beside their dazzling properties, the main advantage of the 4-R-1,2,4-triazole derivatives, which really makes the triazole systems quite unique and explain their dominance in *SCO* materials, resides in their chemical flexibility and stability, notably with the possibility to modify the triazole ring at the 4th position to finely tune the cooperativity.⁴⁻⁶

In those *SCO* materials, the specifics about the coupling of the molecular electronic states with lattice transformations (elastic interactions) and the intermolecular interactions (which can be generated through strong or weak hydrogen bonding, π - π interactions, or simply Van der Waals forces) would ultimately define the cooperativity and the characteristics of the *SCO* behaviour.¹¹⁻¹² The key role of those intra- and inter-molecular interactions remains quite challenging to analyze and optimize the *SCO* behaviour in those Fe^{II} compounds. Among the strategies that have proven proficient to tune the *SCO* properties can be cited the modifications of the ligand coupled with the nature of the anion. Thus, the nature of the functional group at the 4th position on the triazole ring can alter the ligand field strength around the Fe^{II} centers, as well as the intra- and inter-molecular interactions occurring throughout the crystal lattice, while the covalent ability of the anionic ligands can also raise efficient propagation of cooperative interactions with extended covalent networks.⁴⁻⁶ However, the majority of the anions involved until recently are rather standard monoanions (e.g. BF₄⁻, ClO₄⁻, PF₆⁻, and NCX⁻ (X = S, Se)),^{5,13-16} while the functional groups (R) of the triazole molecules are essentially narrowed to linear or branched alkyl or alkoxyated chains. Distinctly and recently, inorganic anionic ligands, especially tetracyanometallates [M(CN)₄]²⁻ (M= Ni, Pt and Pd; Scheme 1), have drawn attention as an alternative due to their high electronic delocalization, and their geometry with multiple cyano groups allowing various bridging modes.¹⁷ These anions have been recently and covalently involved in the design of strongly cooperative polymeric networks ranging from 1D to 3D.^{12a, 17} Two distinctive classes of three-dimensional *SCO* metal-organic frameworks (MOFs) have

been reported up to now. The first class consists in frameworks where the iron(II) nodes are connected exclusively through flexible organic linkers, such as $[\text{Fe}(\text{L})(\text{NCS})_2] \cdot \text{G}$ ($\text{L} = \text{DL-1,2-bis(4'-pyridyl)-1,2-ethanediol (bped)}$),¹⁸ 1,2-di-4-pyridylethylene (dpe ; trans isomer),¹⁹ and 4,4'-azopyridine (azpy),²⁰ $\text{G} = \text{guest molecule(s)}$). Distinctly, frameworks in which rigid $[\text{M}^{\text{II}}(\text{CN})_4]^{2-}$ inorganic bridging anions and organic linkers connect the Fe^{II} centers are labelled as “Hofmann-like” *SCO* coordination polymers, and generically formulated as $\{\text{Fe}(\text{L})[\text{M}(\text{CN})_4]\} \cdot \text{G}$ ($\text{L} = \text{pyrazine (pz)}$),²¹ azpy ,²² 4,4'-bis(pyridyl)-acetylene (bpac),²³ and 1,2-di(4-pyridyl)ethylene (dpe)²⁴; $\text{M}^{\text{II}} = \text{Ni, Pd, and Pt}$; $\text{G} = \text{guest molecule(s)}$). In the latter, the equatorial positions of the $[\text{FeN}_6]$ environments are generally occupied by four CN groups from the tetracyanometalate bridging ligands, and the axial positions are linked by monodentate or bidentate ligands, resulting in 3D architectures. The *SCO* properties in all of these materials are snugly correlated to the chemical nature and size of the adsorbed guest molecules, with the $\{\text{Fe}(\text{pz})[\text{M}(\text{CN})_4]\}$ derivatives one of the most remarkable examples reported to date because the corresponding frameworks can allow reversible control of the magnetic and optical properties through chemical response at room temperature.^{17d,18,25}

In line with the previous chapters and the strategy from our group, the 4-R-1,2,4-trz ligands preferentially have to include an alkyl spacer at the 4th position (between the triazole moiety and the terminal functional group of the substituent) in order to (i) maintain as much as possible the electronic “integrity” of the triazole moiety, and so to limit the possible alteration of the terminal group of the substituent on both the coordination mode (and the ligand field strength) and the *SCO* characteristics. Another potential advantage attributable to the presence of an alkyl spacer resides in the enhancement of the overall flexibility of the 4-R-1,2,4-trz ligand which can favour the implication of the triazole ligand into H-bonding or π - π interactions of relevance for the cooperativity. Thus, the functionalized triazole ligand 2-(3-(4H-1,2,4-triazol-4-yl)propyl)isoindoline-1,3-dione (phtptrz) (scheme 1), with a propylphthalimide group (including a ‘flexible’ propyl spacer) as substituent located on the 4th position of the triazole ring, has been combined with the $[\text{M}(\text{CN})_4]^{2-}$ anionic moiety (Scheme 1) to investigate the effect of the substituent on structural and *SCO* properties in $[\text{Fe}(4\text{-R-1,2,4-trz})_3](\text{A})_x$ systems. In comparison with the benzyl substituent of the triazole ligands from the previous chapters, the phtptrz is significantly bulkier, with the presence of oxygen atoms which could favor H-bonding interactions.



Scheme 1. Molecular structures of the 2-(3-(4H-1,2,4-triazol-4-yl)propyl)isoindoline-1,3-dione (phtptrz) molecule and tetracyanometallate $[M(CN)_4]^{2-}$ dianion.

In this chapter, we report two novel three dimensional (3D) compounds - $\{Fe_3(\mu_2\text{-phtptrz})_6[\mu_2\text{-Pt(CN)}_4]_3\} \cdot C_2H_5OH, 5.5H_2O$ (**5**) and $\{Fe(\text{phtptrz})[Pt(CN)_4] \cdot H_2O\}$ (**6**) - with syntheses details, structural characterizations and magnetic studies. Obtaining of the two compounds **5** and **6** built from the same building blocks, coupled with robust single crystals, is offering a triple perspective to study simultaneously (*i*) the influence of the substituent of the triazole ligand, notably in comparison with the materials from the previous chapters, but also (*ii*) the influence of the structural properties (and implicitly the crystal engineering conditions), and finally (*iii*) the detailed single-crystal X-ray diffraction study at both *LS* and *HS* states, which is of critical importance because of the very limited crystallographic data currently available for triazole based materials.

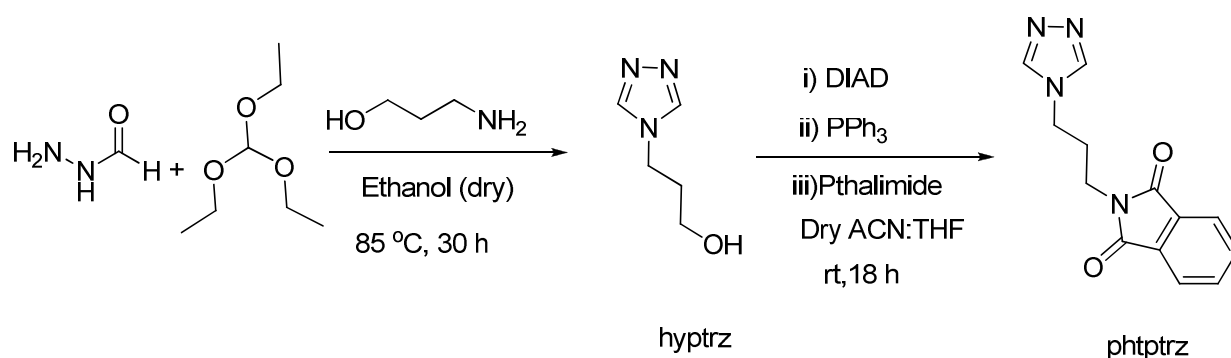
◆ Results and Discussion

1. Syntheses and characterizations

1.1. Synthesis of the ligand 2-(3-(4H-1,2,4-triazol-4-yl)propyl)isoindoline-1,3-dione (phtptrz)

The maiden synthetic step included the development and optimization syntheses of the starting precursors, more precisely the synthesis of the functionalized 4-R-1,2,4-triazole phtptrz ligand. The synthetic route has been directly inspired from previously reported protocols to access a series of triazole ligands modified with various functional groups such as hydroxyl and phthalimide at the 4th position,²⁶⁻²⁷ with slight but impactful modifications of the present work mainly aimed at (*i*) improving significantly the yields and (*ii*) facilitating the purification steps which usually define the complexity of the syntheses for the 4R-triazole molecules. Thus, the triazole ligand phtptrz has been

prepared in two steps with the implication of the 3-(4H-1,2,4-triazol-4-yl)propan-1-ol (hyptrz) as an intermediate derivative (Scheme 2).



Scheme 2. Two-step synthesis of phtptrz ligand.

In the first step, the intermediate hyptrz has been obtained following a synthetic route previously described by Bayer *et al.*²⁶ and Garcia *et al.*²⁷; the latter consists initially in refluxing under inert atmosphere a mixture of formic hydrazide, triethyl orthoformate and 3-amino-1-propanol in 1/1.1/1 stoichiometric ratio while using dry ethanol as a solvent. Distinctively from the protocols reported from Bayer *et al.* and Garcia *et al.*,²⁶⁻²⁷ the precursor hyptrz has been ultimately obtained/synthesized with a significantly improved yield through a modified and easier workup method; indeed, the resulting crude product has been recrystallized using a combination of dry ethanol and ether solvent mixture at low temperature. As a result, a white crystalline solid of hyptrz has been collected after few days, and the yield has been significantly improved from 51 % to 72 %. The second step leading to the phtptrz ligand resumes in a Mitsunobu's coupling reaction involving the precursor hyptrz and phthalimide in presence of diisopropyl azodicarboxylate (DIAD) and triphenylphosphine (PPh₃), but again with a subtle adaptation from similar protocols as regards the molar ratios of the respective reagents.²⁷ In a distinctive synthesis performed at low temperature (0-4 °C) with stirring, a suspension of the precursor hyptrz and phthalimide (1 equivalent each) in dry acetonitrile (ACN) is added to a mixture of 1.23 equivalents - instead of 1.5 usually reported - of triphenylphosphine and DIAD in dry THF.²⁷ The latter synthetic refinement proved to impact significantly the yield. Thus, after the reaction mixture is allowed to warm up to room temperature followed by an overnight stirring, the workup of the resulting white solid led to a white crystalline powder of phtptrz with a yield of 82%, up by 7% from similar reported protocols. The organic ligand was characterized inter alia by ¹H and ¹³C NMR spectroscopy, and IR spectroscopy (see experimental section).

1.2. Syntheses of single crystals of $\{\text{Fe}_3(\mu_2\text{-phtptrz})_6[\mu_2\text{-Pt(CN)}_4]_3\} \cdot \text{C}_2\text{H}_5\text{OH} \cdot 5.5\text{H}_2\text{O}$ (**5**) and $\{\text{Fe(phtptrz)}[\text{Pt(CN)}_4] \cdot \text{H}_2\text{O}\}$ (**6**)

Although the $\text{Fe}^{\text{II}}/4\text{-R-1,2,4-triazole}$ *SCO* materials have been known for few decades, the access to single crystals suitable for X-ray diffraction has remained a contemporary challenge due to the high reactivity of the triazole ligands with Fe^{II} salts which tend to favor the formation of amorphous and/or polycrystalline powders. In that matter, the crystallogensis of $\{\text{Fe}_3(\mu_2\text{-phtptrz})_6[\mu_2\text{-Pt(CN)}_4]_3\} \cdot \text{C}_2\text{H}_5\text{OH} \cdot 5.5\text{H}_2\text{O}$ (**5**) and $\{\text{Fe(phtptrz)}[\text{Pt(CN)}_4] \cdot \text{H}_2\text{O}\}$ (**6**) has been undeniably the decisive and finicky synthetic step. In order to achieve this breakthrough, different crystal engineering techniques (e.g. diffusion and slow evaporation techniques), coupled with variations of key chemical parameters (stoichiometry, concentration, nature of the salts, nature/mixture of the solvents), have been intensively investigated to define the opportune conditions. Ultimately, single crystals of $\{\text{Fe}_3(\mu_2\text{-phtptrz})_6[\mu_2\text{-Pt(CN)}_4]_3\} \cdot \text{C}_2\text{H}_5\text{OH} \cdot 5.5\text{H}_2\text{O}$ (**5**) and $\{\text{Fe(phtptrz)}[\text{Pt(CN)}_4] \cdot \text{H}_2\text{O}\}$ (**6**) - suitable for X-ray diffraction - have been distinctly synthesized using diffusion techniques in fine glass tube (3.0 mm diameter) by layering an ethanol solution of the $\text{Fe}(\text{ClO}_4)_2 \cdot x\text{H}_2\text{O}$ salt onto a water:ethanol (1:1) solution containing both $\text{K}_2[\text{Pt(CN)}_4] \cdot 3\text{H}_2\text{O}$ and phtptrz ligand, but with significant variations in the concentrations and the molar ratios (1/0.3/3 for **5** and 1/1/2 for **6**) of the precursors. An alternative diffusion technique protocol has also been defined for **6** by layering an ethanol solution of the phtptrz ligand onto an aqueous solution containing both $\text{Fe}(\text{ClO}_4)_2 \cdot x\text{H}_2\text{O}$ and $\text{K}_2[\text{Pt(CN)}_4] \cdot 3\text{H}_2\text{O}$ salts, in a 2/1/1 molar ratio, respectively (see experimental section). After a period of one to two weeks, compound **5** was obtained as rhombohedral colorless single crystals, while compound **6** resulted in orange plates. The single crystals of the two complexes were collected by filtration and dried in ambient conditions. The crystals of the two compounds **5** and **6** were further investigated using notably single-crystal IR, X-ray diffraction analysis and magnetic measurements. While referring to recent work from our group related to single crystals of $[\text{Fe}(\text{bntrz})_3][\text{Pt(CN)}_4] \cdot \text{H}_2\text{O}$ (**1**) (bntrz = 4-(benzyl)-4H-1,2,4-triazole, *Chapter I*), it is noteworthy that the crystallogensis conditions for $\text{Fe}^{\text{II}}/4\text{-R-1,2,4-triazole}$ *SCO* materials seem to be highly system-dependant, with even momentous variations in the crystallization conditions for the two derivatives **5** and **6** built from the same starting precursors.

1.3. IR Spectroscopy of **5** and **6**

The infrared spectra of **5** and **6**, recorded on single crystals samples at room temperature, and the ones of the initial precursors - i.e. the phtptrz ligand and the $K_2[Pt(CN)_4] \cdot xH_2O$ salt - are provided in Figures 18-21 (Experimental Section). The IR spectra of **5** and **6** display characteristic bands attributed to the distinctive bond vibration modes from the triazole ring of the phtptrz moiety, most notably sharp $\nu_{(C=O)}$ bands (1707 cm^{-1} for **5**, and 1720 cm^{-1} for **6**) with values clearly blue-shifted when compared to the one of the phtptrz only (1695 cm^{-1}). The stretching vibration of the triazole ring is shifted to 1555 cm^{-1} for **5** and 1547 cm^{-1} for **6**, i.e. higher frequencies with respect to those observed for free phtptrz (1520 cm^{-1}). The latter observations tend to suggest the coordination of the triazole-based ligand in **5** and **6** derivatives.^{14,28}

Moreover, with regards to the $[Pt(CN)_4]^{2-}$ anions, both compounds exhibit characteristic $\nu_{(CN)}$ bands ($2153, 2133\text{ cm}^{-1}$ for **5**, and 2157 cm^{-1} for **6**) with a distinct blue shift from the stretching vibration modes observed in $K_2[Pt(CN)_4] \cdot xH_2O$ (2133 and 2122 cm^{-1}). The two bands observed for **5** can be respectively assigned to the presence of both bridging and terminal CN groups,^{12a} while the lone band in **6** reveals a bridging coordination mode of the $[Pt(CN)_4]^{2-}$ moiety.²⁹

2. Structural characterizations of $\{Fe_3(\mu_2\text{-phtptrz})_6[\mu_2\text{-Pt(CN)}_4]_3\} \cdot C_2H_5OH, 5.5H_2O$ (**5**) and $\{Fe(\text{phtptrz})[Pt(CN)_4] \cdot H_2O\}$ (**6**)

The structural studies of **5** and **6** have been defined based on preliminary thermochromism tests and further correlated to the magnetic studies; indeed, single crystals of **5** display significant optical color change, from colorless at room temperature to pink below ca. 235 K, which suggests the occurrence of a spin transition. Distinctly, the single crystals of **6** did not exhibit any color change with temperature within the studied temperature range.

Thus, the single crystals of **5** have been investigated at 296 K (*HS* state) and 170 K (*LS* state), even though the rather petite size of the crystals required extended time for the respective data collections. However, the structural studies of **6** have been carried out only at 296 K (*HS* state) as no thermochromism was observed.

2.1. Structural studies of $\{\text{Fe}_3(\mu_2\text{-phtptrz})_6[\mu_2\text{-Pt}(\text{CN})_4]_3\} \cdot \text{C}_2\text{H}_5\text{OH} \cdot 5.5\text{H}_2\text{O}$ (**5**), at 296 K (*HS*) and 170 K (*LS*)

Compound **5** crystallizes in the triclinic space group P-1, at both temperatures 170 K and 296 K. The crystallographic data for **5** are listed in Table 1. Fe-N bond lengths and angles for the Fe^{II} coordination sphere, including average Fe-N distances, are summarized in Table 2. The crystal structure of **5** is built from two crystallographically distinct pseudo octahedral Fe^{II} centers Fe1 and Fe2, respectively located on a general position and a special position $[0\ 0\ -1/2]$, three crystallographically distinct phtptrz ligands in general positions, three crystallographically independent quasi planar $[\text{Pt}(\text{CN})_4]^{2-}$ anionic units ($[\text{Pt1}(\text{CN})_4]^{2-}$, $[\text{Pt2}(\text{CN})_4]^{2-}$, and $[\text{Pt3}(\text{CN})_4]^{2-}$ units located on special positions $[0\ 0\ 0]$, $[0\ 1/2\ -1/2]$, and $[1/2\ 0\ -1/2]$, respectively), and one non coordinated ethanol and 5.5 water molecules on general positions (Figures 1 and 2). As regards the $[\text{FeN}_6]$ distorted octahedral coordination spheres, the environment of Fe1 is composed of three nitrogen atoms (N7, N12, N15) respectively associated to the triazole rings of the three phtptrz ligands, and the other nitrogen atoms (N1, N2, N3) are from the three $[\text{Pt}(\text{CN})_4]^{2-}$ anionic units (Figures 1 and 2); distinctly, the Fe2 centre, which lies on an inversion centre, is coordinated to six nitrogen atoms (N8, N11, N16, N8^(a), N11^(a), N16^(a); symmetry code: (a) $-x, -y, -1-z$) from the triazole rings of six phtptrz ligands (Figures 1 and 2). It is worth to note that the $[\text{Pt}(\text{CN})_4]^{2-}$ anions are only coordinated to the Fe1 ions.

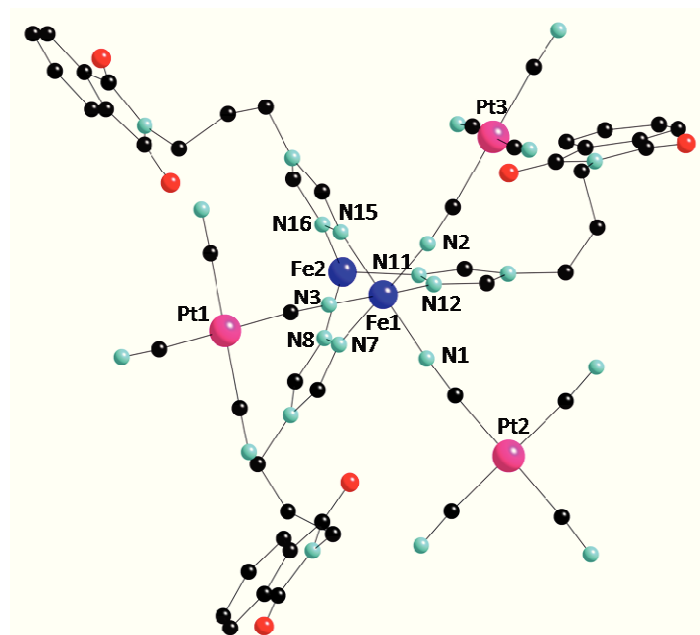


Figure 1. Asymmetric unit of **5** showing the coordination environments of the two crystallographically distinct Fe^{II} centers. Hydrogen atoms have been omitted for clarity. Colour code: Fe: dark blue, Pt: pink, N: pale blue, O: red and C: black.

Table 1. Crystallographic data for $\{\text{Fe}_3(\mu_2\text{-phtptrz})_6[\mu_2\text{-Pt}(\text{CN})_4]_3\} \cdot \text{C}_2\text{H}_5\text{OH} \cdot 5.5\text{H}_2\text{O}$ (**5**) and $\{[\text{Fe}(\text{phtptrz})][\text{Pt}(\text{CN})_4] \cdot \text{H}_2\text{O}\}$ (**6**)

Compound	5		6
T (K)	296 (<i>HS</i> state)	170 (<i>LS</i> state)	296 (<i>HS</i> state)
Colour	Colorless	Purple	Orange
Molecular formula	$\text{C}_{90}\text{H}_{78}\text{Fe}_3\text{N}_{36}\text{O}_{15}\text{Pt}_3$	$\text{C}_{90}\text{H}_{78}\text{Fe}_3\text{N}_{36}\text{O}_{15}\text{Pt}_3$	$\text{C}_{17}\text{H}_{14}\text{N}_8\text{O}_3\text{FePt}$
Formula weight / g.mol^{-1}	2656.70	2656.70	629.30
Wavelength / Å	0.71073 Å	0.71073 Å	0.71073 Å
Crystal system	Triclinic	Triclinic	Monoclinic
Space group	<i>P</i> -1	<i>P</i> -1	<i>P</i> 2 ₁ / <i>n</i>
<i>a</i> / Å	14.5060(7)	14.2876(5)	7.556(5)
<i>b</i> / Å	14.8140(6)	14.6062(5)	14.702(5)
<i>c</i> / Å	15.0984(7)	14.7848(6)	17.993(5)
α / °	67.288(4)	66.660(3)	90.000(5)
β / °	70.412(4)	69.459(3)	100.026(5)
γ / °	67.469(4)	66.767(3)	90.000(5)
Volume / Å ³	2696.9(2)	2533.00(15)	1968.3(16)
<i>Z</i>	1	1	4
<i>D</i> _{calc} / g.cm^{-3}	1.632	1.742	2.124
Abs. Coef. / cm^{-1}	43.44	46.25	78.75
<i>F</i> (000)	1302	1302	1200
2 θ range / °	7.358 - 43.22	6.76 - 50.70	6.88 - 57.6
Refl. collected	35491	29397	9603
Unique refl. / <i>R</i> _{int}	9843 / 0.1121	9250 / 0.0768	4466 / 0.0648
Data / restr. / <i>N</i> _v	6225 / 0 / 673	7669 / 0 / 673	3807 / 0 / 271
^a <i>R</i> ₁ / ^b <i>wR</i> ₂	0.0522 / 0.0908	0.0365 / 0.0703	0.0509 / 0.1267
^c GooF	0.929	0.974	1.130

$$^a\text{R1} = \sum |F_o - F_c| / F_o, \quad ^b\text{wR2} = \{ \sum [w(F_o^2 - F_c^2)^2] / \sum [w(F_o^2)^2] \}^{1/2}, \quad ^c\text{GooF} = \{ \sum [w(F_o^2 - F_c^2)^2] / (N_{\text{obs}} - N_{\text{var}}) \}^{1/2}$$

Table 2. Fe-N bond lengths (Å), bond angles (°) and average Fe-N distances of the **5**, at 296 K and 170 K.

T / K	296 (<i>HS</i> State)	170 (<i>LS</i> State)
Fe1-N1	2.093(6)	1.966(4)
Fe1-N2	2.102(6)	1.976(4)
Fe1-N3	2.107(7)	1.966(4)
Fe1-N7	2.198(5)	1.981(3)
Fe1-N12	2.177(6)	1.978(3)
Fe1-N15	2.177(6)	1.981(4)
<Fe1-N>	2.1423(6)	1.9746(4)
Fe2-N8	2.181(5)	2.005(4)
Fe2-N8 ^(a)	2.181(5)	2.005(4)
Fe2-N11	2.196(6)	2.015(3)
Fe2-N11 ^(a)	2.196(6)	2.015(3)
Fe2-N16	2.194(5)	1.998(4)
Fe2-N16 ^(a)	2.194(5)	1.998(4)
<Fe2-N>	2.1903(6)	2.006(4)
N8-N7-Fe1	128.6(4)	127.4(3)
N11-N12-Fe1	126.6(4)	126.0(3)
N16-N15-Fe1	126.7(4)	125.5(3)
N1-Fe1-N2	94.4(2)	94.19(15)
N1-Fe1-N3	94.6(3)	94.81(15)
N1-Fe1-N7	86.0(2)	86.89(15)
N1-Fe1-N12	87.8(2)	88.50(15)
N1-Fe1-N15	174.5(2)	176.12(15)
N2-Fe1-N3	93.6(2)	2 93.58(15)
N2-Fe1-N7	179.6(2)	178.50(15)
N2-Fe1-N12	91.1(2)	88.81(15)
N2-Fe1-N15	89.4(2)	88.49(16)
N3-Fe1-N7	86.3(2)	87.37(14)
N3-Fe1-N12	174.6(2)	175.76(15)
N3-Fe1-N15	89.2(2)	87.81(15)
N12-Fe1-N7	89.0(2)	90.17(14)
N12-Fe1-N15	88.1(2)	88.75(14)
N15-Fe1-N7	90.2(2)	90.38(15)
N7-N8-Fe2	121.0(4)	123.1(3)
N12-N11-Fe2	123.4(4)	124.6(3)
N15-N16-Fe2	123.5(4)	125.2(3)
N8-Fe2-N8 ^(a)	180.0(3)	180.0
N8-Fe2-N11 ^(a)	88.2(2)	89.79(14)
N8-Fe2-N11 ^(a)	91.8(2)	90.21(14)
N8 ^(a) -Fe2-N11 ^(a)	88.2(2)	89.79(14)
N8-Fe2-N11	91.8(2)	90.21(14)
N8-Fe2-N16	91.7(2)	90.00(14)
N8 ^(a) -Fe2-N16 ^(a)	91.7(2)	90.00(14)
N8 ^(a) -Fe2-N16 ^(a)	88.3(2)	90.00(14)
N8-Fe2-N16 ^(a)	88.3(2)	90.00(14)
N11-Fe2-N11 ^(a)	180.0	180.00(15)
N16 ^(a) -Fe2-N11	90.3(2)	90.44(14)
N16-Fe2-N11 ^(a)	89.7(2)	89.56(14)
N16-Fe2-N11 ^(a)	89.7(2)	90.44(14)
N16-Fe2-N11	90.3(2)	89.56(14)
N16-Fe2-N16 ^(a)	180.0	180.0

Symmetry code: (a) -x, -y, 1-z

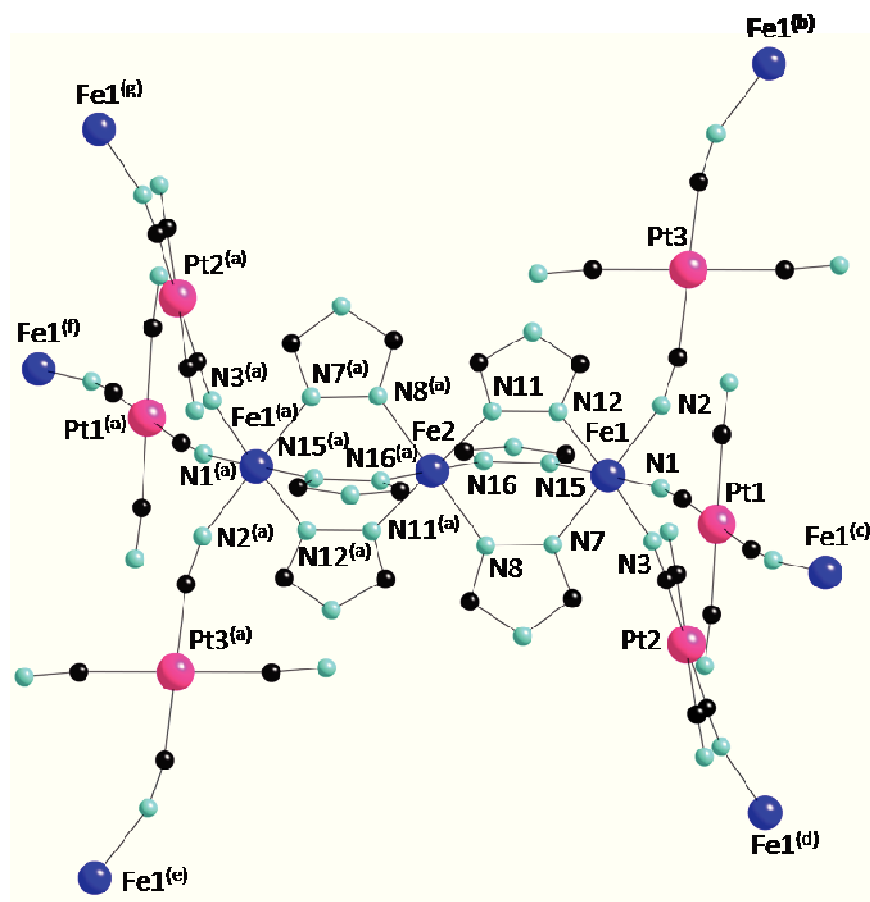


Figure 2. View of the trinuclear [Fe1-Fe2-Fe1] units in **5**, with the coordination spheres of the Fe^{II} centers and atom labelling. Symmetry codes: (a) -x, -y, 1-z; (b) = 1-x, -y, 1-z; (c) = -x, -y, 2-z; (d) = -x, 1-y, 1-z; (e) = -1+x, y, z; (f) = x, y, -1+z; (g) = x, -1+y, z. Hydrogen atoms and phtalimido propyl (phtp) groups of the phtptrz ligands have been omitted for clarity. Colour code: Fe: dark blue, Pt: pink, N: pale blue, O: red and C: black.

The Fe(II) centers Fe1 and Fe2 are connected through triple N1,N2-1,2,4-triazole bridges from the phtptrz ligands ((N7-N8), (N11-N12), and (N15-N16)), thereby forming [Fe1-Fe2-Fe1] trinuclear units running along the [100] direction (Figure 2). Moreover, the three crystallographically different [Pt(CN)₄]²⁻ anions all display a μ_2 -bridging coordination mode involving the Fe1 ions ([Fe1-NC-Pt(1,2,3)-CN-Fe1]). As a result, the trinuclear units are covalently linked, *via* the [Pt(CN)₄]²⁻ ligands, along the three directions [100], [010] and [001], to form a three dimensional covalent network depicted in Figures 3-5. The resulting three dimensional packing of {Fe₃(μ_2 -phtptrz)₆[μ_2 -Pt(CN)₄]₃}.C₂H₅OH.5.5H₂O (**5**) can be described as 2D layers based upon pseudo-lozenge motifs defined by four [Fe1-Fe2-Fe1] trimer units (tops) linked by [Pt(1,2)(CN)₄]²⁻

$[\text{Pt}(1,3)(\text{CN})_4]^{2-}$ and $[\text{Pt}(2,3)(\text{CN})_4]^{2-}$ anions (sides) in the bc, ac and ab planes, respectively (Figures 3-5); those 2D layers are interlinked through the $[\text{Pt}(1,2,3)(\text{CN})_4]^{2-}$ units along the $[001]$, $[010]$ and $[100]$ direction, respectively (Figures 3-5), and stacked in an eclipsed fashion to generate the formation of channels running along the $[100]$, $[010]$ and $[001]$ direction (Figures 3-5). Because of those structural arrangements which are nearly similar in all the three crystallographic directions, the structure of $\{\text{Fe}_3(\mu_2\text{-phtptrz})_6[\mu_2\text{-Pt}(\text{CN})_4]_3\} \cdot \text{C}_2\text{H}_5\text{OH} \cdot 5.5\text{H}_2\text{O}$ (**5**) can be viewed as a “distorted rhombohedral crystallographic system”.

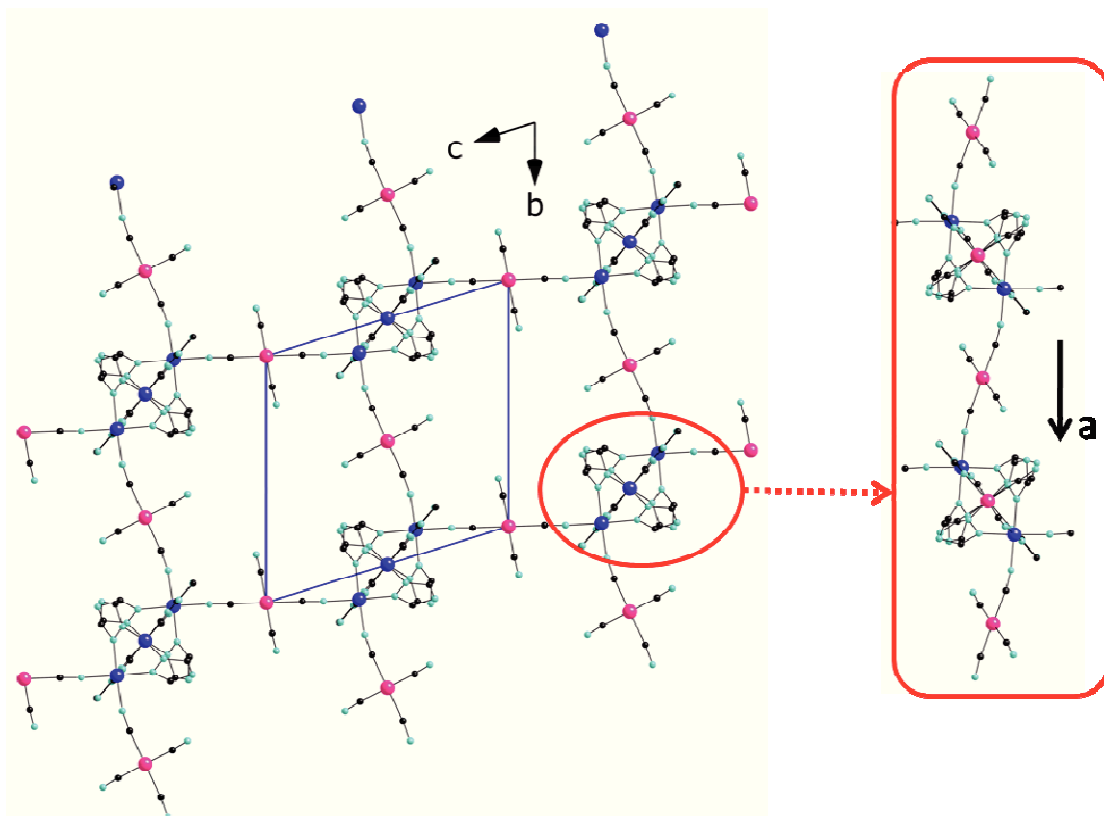


Figure 3. View of the three dimensional structure of **5** showing (i) the 2D layers based upon pseudo-lozenge motifs defined by four $[\text{Fe1-Fe2-Fe1}]$ units which are linked by $[\text{Pt1}(\text{CN})_4]^{2-}$ and $[\text{Pt2}(\text{CN})_4]^{2-}$ anions in the $[001]$ and $[010]$ directions, respectively; and (ii) the interlinks between these layers through the third $[\text{Pt3}(\text{CN})_4]^{2-}$ units in the $[100]$ direction. Hydrogen atoms and phtalimido propyl (phtp) groups of the phtptrz ligands have been omitted for clarity. Colour code: Fe: dark blue, Pt: pink, N: pale blue, O: red and C: black.

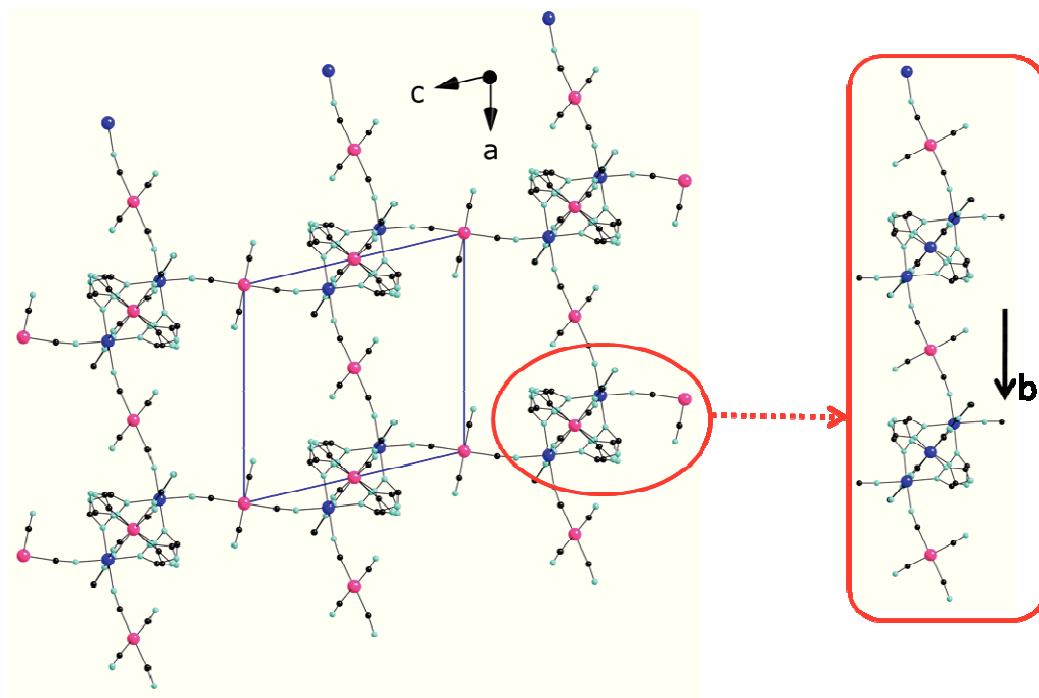


Figure 4. View of the three dimensional structure of **5** showing (i) the 2D layers based upon pseudo-lozenge motifs defined by four [Fe1-Fe2-Fe1] units which are linked by $[\text{Pt1}(\text{CN})_4]^{2-}$ and $[\text{Pt3}(\text{CN})_4]^{2-}$ anions in the [001] and [100] directions, respectively; and (ii) the interlinks between these layers through the third $[\text{Pt2}(\text{CN})_4]^{2-}$ units in the [010] direction.

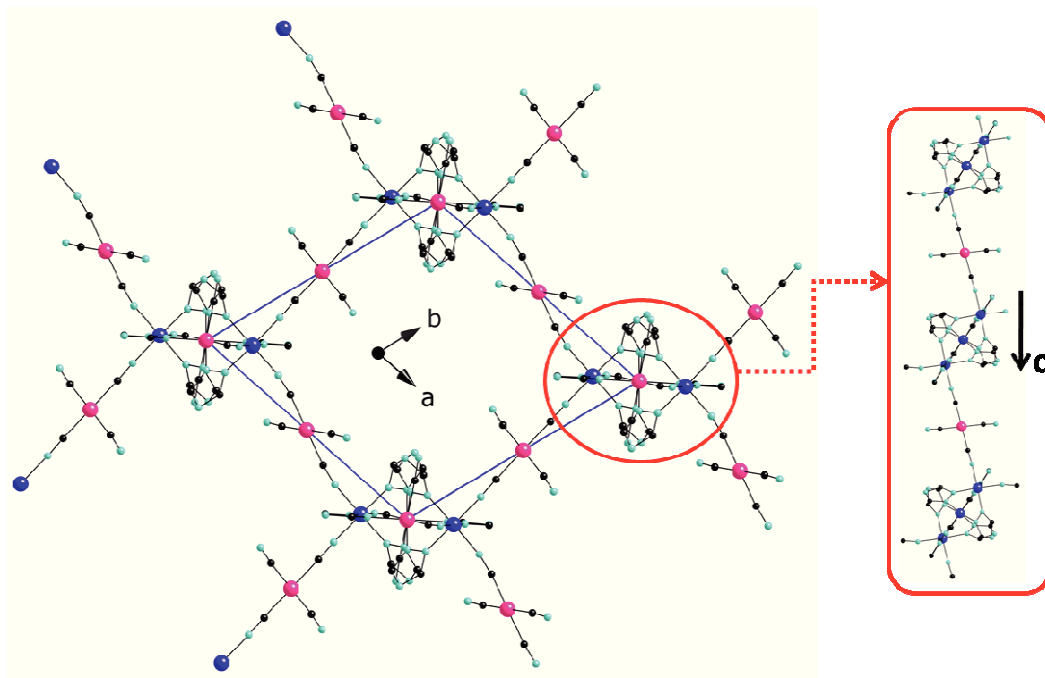
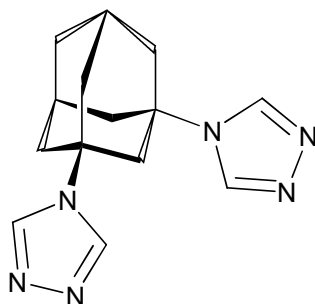


Figure 5. View of the three dimensional structure of **5** showing (i) the 2D layers based upon pseudo-lozenge motifs defined by four [Fe1-Fe2-Fe1] units which are linked by $[\text{Pt3}(\text{CN})_4]^{2-}$ and $[\text{Pt2}(\text{CN})_4]^{2-}$ anions in the [100] and [010] directions, respectively; and (ii) the interlinks between these layers through the third $[\text{Pt1}(\text{CN})_4]^{2-}$ units in the [001] direction.

This arrangement in **5** can be compared to some extent to the one observed in the three-dimensional iron(II) spin-crossover porous coordination polymer, based on the bis(1,2,4-triazol-4-yl)adamantane (tr₂ad; Scheme 3) ligand and the [Au(CN)₂][−] metalloligand anions with the formula {Fe₃(tr₂ad)₄[Au(CN)₂]₂} [Au(CN)₂]₄·8H₂O, that has been reported by J.A. Real *et al.* in 2012 (Figures 6 and 7).^{10f} Although involving distinctive ligands, the latter present similarly structured [Fe1-Fe2-Fe1] triads, with the main difference residing in the covalent connections between the trimeric motifs. Thus, the triads are connected along the [001] direction by the tr₂ad ligands, while along the [010] direction, the triads are connected through both [Au(CN)₂][−] anions and tr₂ad ligands (Figure 7), resulting in clearly different sets of Fe...Fe distances through both types of bridging ligands.^{10f} Distinctly, the inter-trimers covalent links in **5** are exclusively provided by the [Pt(CN)₄]^{2−} ligands. *Per contra* to **5**, the compound {Fe₃(tr₂ad)₄[Au(CN)₂]₂} [Au(CN)₂]₄·8H₂O displays a SCO behaviour only after complete dehydration process at 400 K.^{10f}



Scheme 3. Molecular structure of tr₂ad ligand.^{10f}

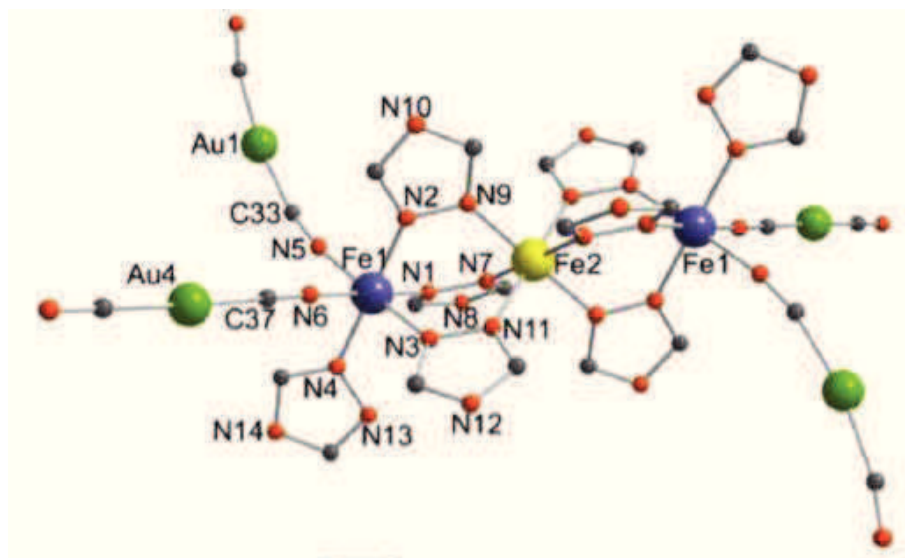


Figure 6. Simplified view of the coordination spheres around the iron(II) atoms in {Fe₃(tr₂ad)₄[Au(CN)₂]₂} [Au(CN)₂]₄·8H₂O with the corresponding atom numbering. Color code: N, orange; C, gray; Fe, yellow and blue and Au1 and Au4, green.^{10f}

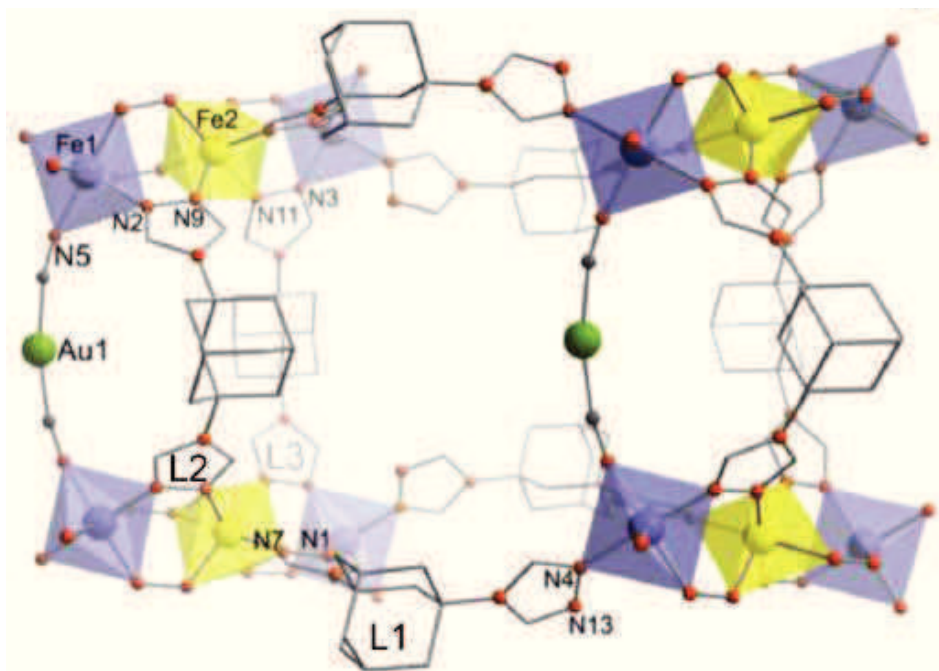


Figure 7. Projection of a fragment of $\{\text{Fe}_3(\text{tr}_2\text{ad})_4[\text{Au}(\text{CN})_2]_2\}[\text{Au}(\text{CN})_2]_4 \cdot 8\text{H}_2\text{O}$, in the xy plane. Color code: N, orange; C, gray; Fe, yellow and blue octahedra; O (H_2O), magenta tetrahedra and rhombic pseudocubic prisms; Au1 and Au4, green.^{10f}

The oxidation state (+2) of Fe(II) in compound **5** was confirmed for all the iron metal centres by charge consideration, and from the examination of the Fe-N bond lengths (Table 2). Indeed, as shown in Table 2, the mean value of the Fe1-N distances of 2.1423(6) Å is slightly shorter than the mean Fe2-N distance of 2.1903(6) Å, while both values are consistent with the *HS* state of the Fe^{II} ions at 296 K.²⁴ The Fe-N(phtptrz) distances for both Fe^{II} centres (Fe1 and Fe2) can be considered in the same range (2.177 - 2.196 Å). Thus, the difference observed in the mean Fe-N distances can be mainly attributed to the shorter Fe1-N($[\text{Pt}(\text{CN})_4]^{2-}$) bonds in **5** (Table 2). Moreover, the distance Fe1...Fe2 within the trinuclear units is 3.901 Å; as regards the Fe1...Fe1 distances in **5** between neighbouring trinuclear units, we can notice that they are significantly longer through the μ_2 - $[\text{Pt}(\text{CN})_4]^{2-}$ bridges i.e. Fe1-Pt3-Fe1, Fe1-Pt2-Fe1 and Fe1-Pt1-Fe1, with values of 10.078, 10.261 and 10.319 Å along the [100], [010] and [001] directions, respectively.

The cooling down process of the single crystal of **5** is accompanied by a color change from colorless at 296 K to pink at 170 K (Figure 8), with the quality of the crystal presenting adequate robustness to allow for x-ray studies at both temperatures. Thus, with the aim to gather inclusive data about the structural evolution occurring upon the corresponding spin crossover phenomenon, the same single crystal was also analyzed by x-ray diffraction at 170 K. The average Fe-N distances for the two spin states, as well as Fe-N bond lengths and N-Fe-N bond angles are listed in Table 2, at 296 K and 170 K. An in-depth examination of the unit cell parameters, at these two temperatures, indicates the absence of any structural transition within the studied temperature range. From 296 K to 170 K, the octahedral geometries of the two non equivalent Fe^{II} centers evolve considerably. Indeed, the values and significant decreases of the mean Fe1-N and Fe2-N distances, at 296 K ($\langle\text{Fe1-N}\rangle = 2.1423(6)$; $\langle\text{Fe2-N}\rangle = 2.1903(6)$ Å) and 170 K ($\langle\text{Fe1-N}\rangle = 1.9746(4)$ Å; $\langle\text{Fe2-N}\rangle = 2.006(4)$ Å), are characteristic and in agreement with spin conversions - for both Fe1 and Fe2 centres - from *HS* states at 296 K to *LS* states at 170 K, with typical variations of the mean $\langle\text{Fe-N}\rangle$ distances of *ca.* 0.17-0.18 Å. The latter observation is consistent with the contraction associated to the occurrence of a complete *HS/LS SCO* transition within the trinuclear units, i.e. corresponds to a [Fe1(*HS*)-Fe2(*HS*)-Fe1(*HS*)] (296 K) / [Fe1(*LS*)-Fe2(*LS*)-Fe1(*LS*)] (170 K) spin crossover, as later confirmed by the magnetic studies. As a result, the intramolecular Fe1...Fe2 distances within the trinuclear units, at 296 K (Fe1...Fe2 = 3.901 Å) and 170 K (Fe1...Fe2 = 3.695 Å), are reduced by 0.206 Å, with the value at 170 K in the range of the one previously reported at 120 K in the similar three dimensional compound $\{\text{Fe}_3(\text{tr}_2\text{ad})_4[\text{Au}(\text{CN})_2]_2\}[\text{Au}(\text{CN})_2]_4 \cdot 8\text{H}_2\text{O}$ (3.6438(8) Å).^{10f}

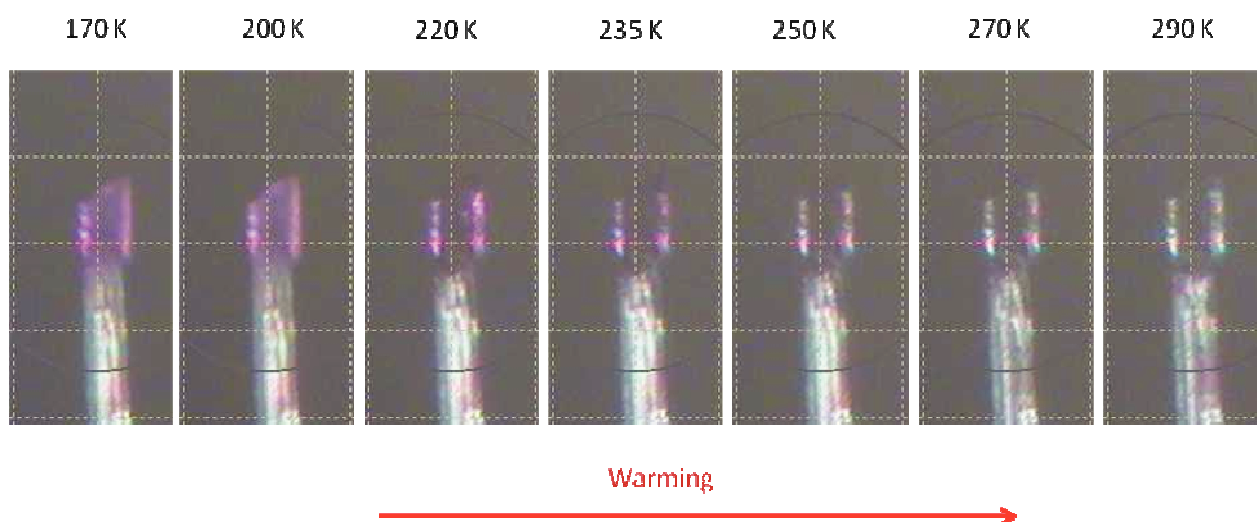


Figure 8. Thermochromism pictures for **5** taken from 170 K to 290 K with the X-ray diffraction camera.

In addition to those changes and the evolution of the intramolecular Fe1...Fe2 distances within the trinuclear units, the *SCO* phenomenon is also accompanied by the variation of the intermolecular distances between the trinuclear units. As mentioned earlier, upon spin transition, the Fe1...Fe2 intramolecular distances within the unit cell at 170 K are also slightly shortened, leading to the lower distances between the two trinuclear units through the μ_2 -[Pt(CN)₄]²⁻ bridges Fe1-Pt3-Fe1, Fe1-Pt2-Fe1 and Fe1-Pt1-Fe1, with values of 10.005, 10.118 and 10.145 Å along the [100], [010] and [001] directions, respectively. Finally, the solid-state *SCO* behaviour of **5** involves mainly an intramolecular cooperativity within the triads units, and the characteristics of this cooperativity have been further estimated *via* the magnetic measurements.

2.2. Structural studies of {Fe(phtptrz)[Pt(CN)₄].H₂O} (**6**).

Distinctly from **5**, the single crystals of **6** did not exhibit *SCO* behaviour within the studied temperature range, as defined by preliminary thermochromism tests and further correlated to the magnetic studies. Consequently, the structural studies performed on single crystals of **6** have been carried out only at 296 K. The compound **6** crystallizes in the monoclinic *P*2₁/*n* at 296 K. The crystallographic data for **6** are listed in Table 1. The Fe-N bond lengths and angles for the Fe^{II} coordination sphere, including average Fe-N distances, are summarized in Table 3. As shown in Figure 9, the crystal structure of **6** is built from one Fe^{II} ion, one phtptrz ligand, one [Pt(CN)₄]²⁻ anion, and one uncoordinated water molecule, all located on general positions. Each Fe^{II} ion adopts a trans octahedral [FeN₅O] configuration, with one nitrogen atom (N5) and one oxygen atom (O2) from two different phtptrz ligands in the axial positions, and the other four N atoms (N1, N2, N3 and N4) defining the equatorial plane and belonging to four different anionic [Pt(CN)₄]²⁻ ligands (Figure 9). This [FeN₅O] coordination sphere observed for this compound is rather atypical, especially regarding the two axial positions involving two phtptrz units distinctively coordinated through one oxygen atom from the phthalimide group (O2) and one nitrogen atom of the triazolyl group (N5). Thus, each phtptrz ligand act as a μ_2 -bridging ligand, with the involvement of both the phthalimido group and the triazole motif of the ligand, while the [Pt(CN)₄]²⁻ anions display a μ_4 -bridging coordination mode (Figures 9 and 10). It is noteworthy that the coordination modes of both phtptrz and [Pt(CN)₄]²⁻ ligands in **6** proves in drastic contrast with the ones adopted in the structural arrangement of **5**. Indeed, the μ_2 -bridging mode of the phtptrz ligands in **5** was exclusively engaged through the nitrogen atoms of the triazole group which allowed for the formation of triple bridged Fe^{II} trimers and the occurrence of spin crossover, while the tetracyanometallate units were limited to

a η^2 -coordination mode. As a result, the Fe^{II} centers in **6** are linked along the three crystallographic directions - within the [100] and [010] directions *via* the $[\text{Pt}(\text{CN})_4]^{2-}$ anions, and in the [001] direction *via* the phtptrz units - to form a rather complex three dimensional covalent network, as depicted in Figure 10.

Table 3. Fe-N and Fe-O bond lengths (Å) and angles ($^\circ$), and average Fe-N distances (Å) parameters of the Fe^{II} coordination sphere of **6** at 296 K.

T / K	296 (HS State)
Fe1-N1	2.160(8)
Fe1-N2(e)	2.177(8)
Fe1-N3(f)	2.188(7)
Fe1-N4(g)	2.148(8)
Fe1-N5	2.170(8)
<Fe1-N>	2.1686(8)
Fe1-O2(h)	2.179(7)
N4-Fe1-N1	174.3(3)
N4-Fe1-N5	94.4(3)
N1-Fe1-N5	91.2(3)
N4(g)-Fe1-N2(e)	90.3(3)
N1-Fe1-N2(e)	90.6(3)
N5-Fe1-N2(e)	94.1(3)
N4(g)-Fe1-N3(f)	91.4(3)
N1-Fe1-N3(f)	87.2(3)
N5-Fe1-N3(f)	91.5(3)
N2(e)-Fe1-N3(f)	174.0(3)
N4(g)-Fe1-O2(h)	85.5(3)
N1-Fe1-O2(h)	88.8(3)
N5-Fe1-O2(h)	175.3(3)
N2(e)-Fe1-O2(h)	90.6(3)
O2(h)-Fe1-N3(f)	83.8(3)

Symmetry codes: (e) 1+x, y, z; (f) 1-x, -1-y, -z; (g) 2-x, -1-y, -z; (h) 1/2+x, -1/2-y, 1/2+z.

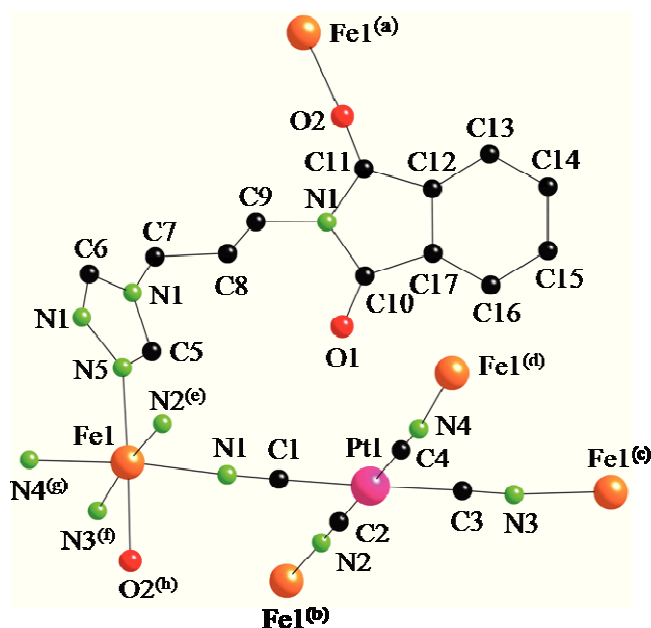


Figure 9. Asymmetric unit and atom-labeling scheme of **6** showing the coordination environment of the Fe(II) centre. Symmetry codes: (a) $-1/2+x, -1/2-y, -1/2+z$; (b) $-1+x, y, z$; (c) $1-x, -y, -z$; (d) $2-x, -y, -z$; (e) $1+x, y, z$; (f) $1-x, -1-y, -z$; (g) $2-x, -1-y, -z$; (h) $1/2+x, -1/2-y, 1/2+z$. Hydrogen atoms have been omitted for clarity. [Fe: orange, Pt: pink, N: green, O: red and C: gray].

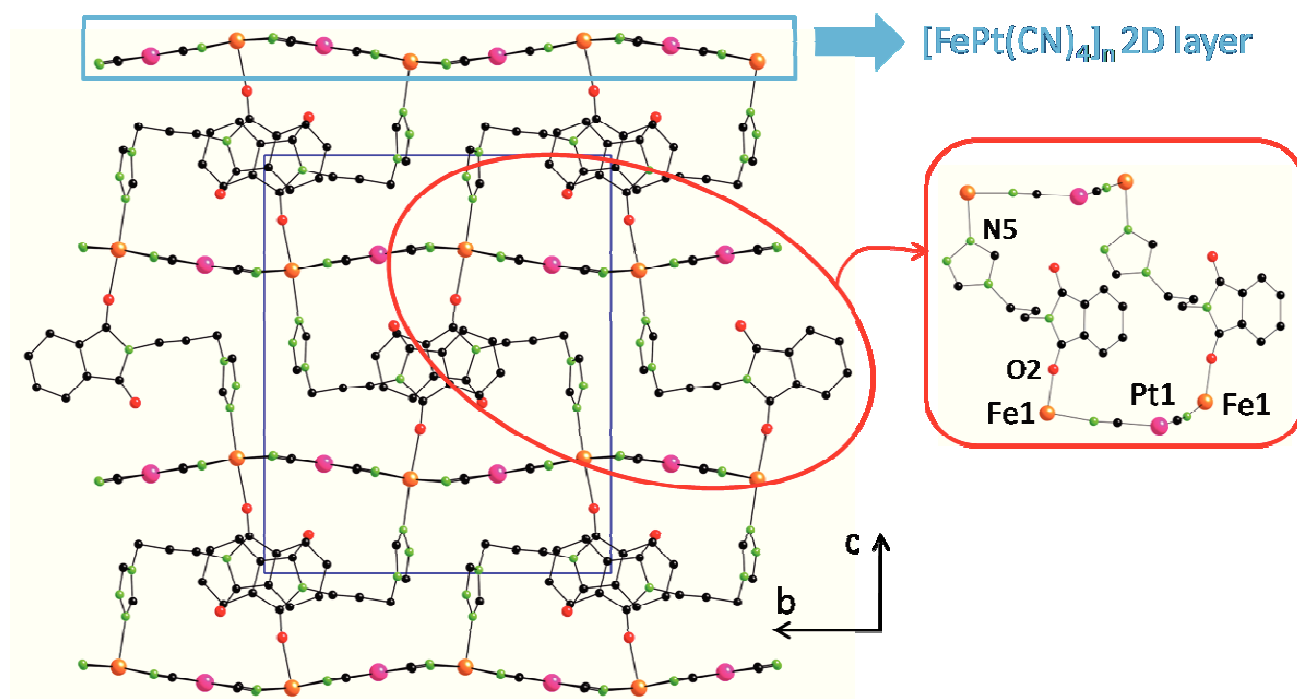


Figure 10. View of the 3D framework of **6** illustrating the respective 2_{-} -coordination modes of the phtptrz and the $[\text{Pt}(\text{CN})_4]^{2-}$ ligands, and the distribution of the Fe sites. H atoms have been omitted for clarity. [Fe: orange, Pt: pink, N: green, O: red and C: gray].

The complete 3D framework, which resembles a disrupted 3D Hofmann-type material,¹⁸⁻²¹ can be initially described as $[\text{Fe}(\text{Pt}(\text{CN})_4)]_n$ 2D corrugated layers built from the $[\text{Fe1-N(1-4)C-Pt1-CN(1-4)-Fe1}]$ linkages (Figure 10). Those undulating grids are non-planar due to the out-of-plane tilt of the Fe octahedrons likely induced by the steric restrictions of the phtptrz ligands (Figures 9 and 10). The 3D connectivity is completed by links of the 2D layers through the ${}_2\text{-phtptrz}$ ligands, with $[\text{Fe1-O2-(phtptrz)-N5-Fe1}]$ connections established along the $[001]$ direction (Figure 10); in that regard, the phtptrz units are oriented in an alternating up and down fashion with respect to adjacent Fe centers (Figure 9). Furthermore, the 2D sheets interdigitate in a staggered fashion such that the phtptrz ligands align in an offset face to face fashion, further packing into a supramolecular structure. The Fe...Fe inter-layer distance - i.e. through the phtptrz linkages between two neighbouring Fe^{II} centers of two successive layers - is 10.418 Å, while the shortest intra-layers Fe...Fe distances - i.e. within the 2D layers through the $\text{Pt}(\text{CN})_4]^{2-}$ units are 7.556 and 7.404 Å along the row.

Finally, the two compounds **5** and **6** display very different 3D structures, even so they have been synthesized from the exact same starting precursors, i.e. $\text{Fe}(\text{ClO}_4)_2 \cdot x\text{H}_2\text{O}$ and $\text{K}_2[\text{Pt}(\text{CN})_4] \cdot 3\text{H}_2\text{O}$ salts, and phtptrz ligands. As already pinpointed in the previous chapters, the latter observation emphasizes the critical and exceedingly underrated role of the crystal engineering conditions (stoichiometry, concentration, nature/mixture of the solvents, and crystallization technique), not only in obtaining single crystals suitable for X-ray diffraction, but also for the decisive input they can have in the structural arrangements and ensuing *SCO* behaviors of the resulting materials. Thus, starting from the same reagents but with meaningful (and highly system-dependant) variations in the crystallization conditions, the main difference in the 3D structures of **5** and **6** resides in the coordination mode of the phtptrz ligand, with a bridging mode through the triazole motif in **5**, and an hybrid bridging mode involving both the phtalimido and the triazol groups in **6**; consequently, a *SCO* behavior is observed only in **5**, as revealed hereafter in the magnetic studies. Those observations imply especially the eventual covalent ability of this functional group as clearly evidenced in the comparative structural study of **5** and **6**. Also in comparison with the trinuclear and 1D systems presented in *Chapters II and III*, the substitution of the bntrz for the bulkier (and more flexible) phtptrz ligand, still coupled with the use of $[\text{Pt}(\text{CN})_4]^{2-}$ anionic units able to be engaged in bridging coordination modes, allows for the access of higher dimension architectures.

3. Magnetic properties

3.1. Magnetic studies of $\{\text{Fe}_3(\text{phtptrz})_6[\text{Pt}(\text{CN})_4]_3\} \cdot \text{C}_2\text{H}_5\text{OH} \cdot 5.5\text{H}_2\text{O}$ (**5**)

The magnetic susceptibility (χ_M) of **5** and **6** were measured over the 2-350 K temperature (T) range (under an applied dc field of 20 kOe for **5**, and 10 kOe for **6**) on a set of single crystals. The $\chi_M T$ versus T plots of **5** and **6** are displayed in Figures 11 and 12, respectively. The thermochromism from pink color at low temperature to colorless color at high temperature has been observed in the sample output of **5**, while **6** remained orange over the whole temperature range.

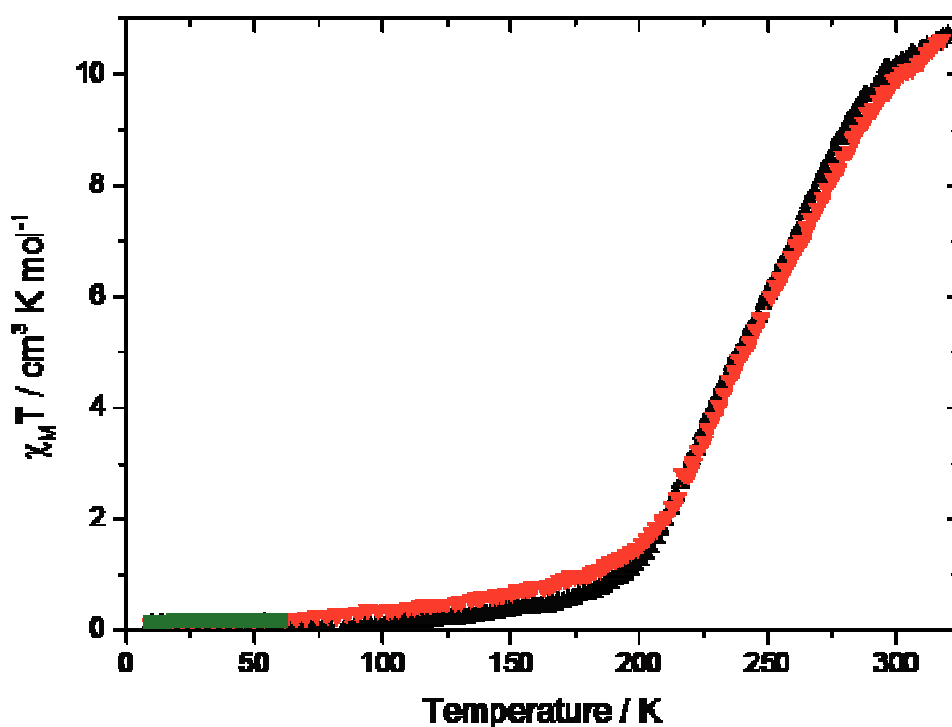


Figure 11. Magnetic properties of **5** in the form of $\chi_M T$ vs. T plots recorded in the temperature range 2-350 K, at a scan rate of 1 K.min⁻¹ and a magnetic field of 20 kOe.

In the high-temperature region, the $\chi_M T$ value of **5** (ca. 10.45 cm³.K.mol⁻¹) is consistent with the value expected for a high spin state (HS , $S = 2$) configuration of three Fe(II) ions (expected $\chi_M T$ value of ca. 3.2-3.6 cm³.K.mol⁻¹ per HS Fe^{II} center), i.e. with a $[\text{Fe1}(HS)\text{-Fe2}(HS)\text{-Fe1}(HS)]$ spin configuration within the trimeric units of the corresponding 3D structure (Figure 11). Upon cooling, the $\chi_M T$ remains constant down to ca. 350 K, and then experiences a first step decrease to ca. 7.0 cm³.K.mol⁻¹ at 260 K that can be attributed to the spin transition from the HS to the LS state of approximately one-third of the iron (II) ions. Further lowering of the temperature results in a second

step decrease of the $\chi_M T$ product to attain a value of ca. $0.0 \text{ cm}^3 \cdot \text{K} \cdot \text{mol}^{-1}$ at 120 K, indicating a complete *HS* to *LS* spin transition of the remaining two-thirds of the Fe(II) centers, i.e. with a $[\text{Fe1}(\text{LS})\text{-Fe2}(\text{LS})\text{-Fe1}(\text{LS})]$ spin configuration of the triads (Figure 11). As revealed in the structural studies of **5**, the two crystallographically different Fe1 and Fe2 centers defining the trimeric units present distinct ligand-field environments, with Fe2 coordinated to six nitrogen atoms from phtptrz ligands, and Fe1 connected to two different types of nitrogen atoms from phtptrz ligands and $[\text{Pt}(\text{CN})_4]^{2-}$ anions. Taking into account these structural data, the high- and low-temperature steps could be reasonably ascribed to the spin transition of the Fe2 and Fe1 sites, respectively; the latter assumption would then suggest a $[\text{Fe1}(\text{HS})\text{-Fe2}(\text{LS})\text{-Fe1}(\text{HS})]$ spin configuration of the triads at 260 K.

In light of these results, and in comparison to the 1D and trinuclear systems presented in the previous two *chapters II and III*, the complex **5** displays relatively moderate cooperative interactions between the Fe^{II} centers in the crystal lattice, with the temperate character imputable to the large separation between the trinuclear units in the framework which reduces the cooperativity in the crystal packing. This observation clearly reveals the magneto-structural influences of the functional groups of the R-trz ligands, coupled with the nature of the anion. Indeed, the replacement of the benzyl group (bntrz = 4-(benzyl)-4H-1,2,4-triazole) by the bulkier phtalimido group (phtptrz), in combination with $[\text{Pt}(\text{CN})_4]^{2-}$ anions, tend to favor - at least in those Fe^{II} /triazole systems - higher dimension architectures, with the preferential formation of triads instead of polymeric chains, but also to reduce the degree of cooperativity. This ascertainment can be further extended to the $\{\text{Fe}_3(\text{tr}_2\text{ad})_4[\text{Au}(\text{CN})_2]_2\}[\text{Au}(\text{CN})_2]_4 \cdot 8\text{H}_2\text{O}$ derivative that has been reported by J.A. Real *et al.* in 2012 (Figure 5);^{10f} in spite of having a 3D structure comparable to **5** and involving distant trimeric units and analogous ligands, the latter concealed any display of *SCO* behaviour while **5** presents a two-step transition. This constatation can be notably correlated to the more pronounced bulkiness of the tr_2ad ligand compared to the phtptrz moiety. Nevertheless, the multistep *SCO* profile observed in **5** is akin to the one recorded for the dehydrated analogue $\{\text{Fe}_3(\text{tr}_2\text{ad})_4[\text{Au}(\text{CN})_2]_2\}[\text{Au}(\text{CN})_2]_4$.^{10f}

As regards the *SCO* temperatures reported for the polymeric chain and trinuclear complexes (*Chapters II and III*), the values varied between 240 K and 350 K depending on the functional group at the 4th position of the triazole ring, and the nature of the counter anion. A contrario, the lower $T_{1/2}$ values recorded for **5** tend to suggest a correlation between the ligand-field strength of the 4-R-trz ligand and the value of the *SCO* temperature, with weaker ligand-field strength for the phtptrz ligand compared to the benzyl analogue (bntrz).

3.2. Magnetic studies of {Fe(phtptrz)[Pt(CN)₄].H₂O} (**6**).

In plain contrast to the *SCO* behavior of **5**, only the *HS* state is observed for **6** over the whole temperature range 2-380 K. As illustrated in Figure 12, the $\chi_M T$ value of **6** is equal to 3.55 cm³.K.mol⁻¹ at 300 K, and consistent with a *HS* (*S* = 2) configuration of the hexacoordinated Fe(II) ions. The $\chi_M T$ value remains constant down to 50 K. Below this temperature, the rapid decrease of the $\chi_M T$ is ascribed to the expected zero-field splitting (*ZFS*) of the *HS* Fe(II) ions (Figure 12).

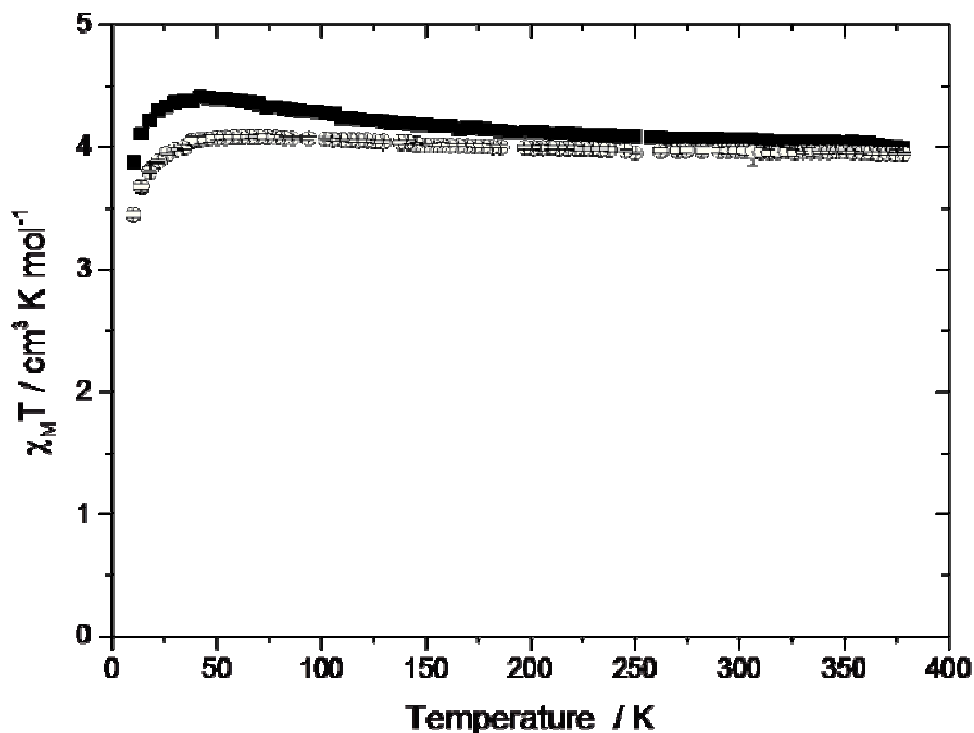


Figure 12. Magnetic properties in the form of $\chi_M T$ vs. *T* plots for **6** recorded in the temperature range 2-380 K, at a scan rate of 1 K.min⁻¹ and magnetic field of 10 KOe.

The drastic differences of the magnetic behaviors between **5** and **6** arise from the significant differences of the coordination environments of the Fe(II) centers. The Fe(II) centers (Fe1 and Fe2) in **5** involve [FeN₆] environments, while the Fe(II) centres in **6** are surrounded by five nitrogen atoms and one oxygen atom from the phthalimido group i.e. a [FeN₅O] environment. The later environment induces the lower ligand field energy. As a result of their structural specificities, the compound **6** expresses a characteristic paramagnetic behavior, while **5** manifests a *SCO* behaviour. This comparative study between **5** and **6** undoubtedly points out the key role of the bridging mode of the phtptrz ligand on the *SCO* properties, and more broadly the magneto-structural influence of the functional group of the 4-R-1,2,4-triazole ligand.

◆ Conclusion and perspectives

In a logical continuation of the previous chapters aiming to further evaluate the magneto-structural influence of the nature of the functional group at the 4th position of the 4-R-triazole ligand while maintaining $[\text{Pt}(\text{CN})_4]^{2-}$ moiety as counter-anions, two new 3D materials $\{\text{Fe}_3(\mu_2\text{-phtptrz})_6[\mu_2\text{-Pt}(\text{CN})_4]_3\} \cdot \text{C}_2\text{H}_5\text{OH} \cdot 5.5\text{H}_2\text{O}$ (**5**) and $\{\text{Fe}(\text{phtptrz})[\text{Pt}(\text{CN})_4] \cdot \text{H}_2\text{O}\}$ (**6**), based on the functionalized triazole 2-(3-(4H-1,2,4-triazol-4-yl)propyl)isoindoline-1,3-dione (phtptrz), have been synthesized, and notably characterized by single crystal X-ray crystallography - in both low spin and high spin states - and magnetic studies. In comparison with the 4-(benzyl)-4H-1,2,4-triazole (bntrz) ligand involved in the materials described in *Chapters II and III*, the phtptrz presents a bulkier phthalimido group, and a longer alkyl spacer (three carbons *vs.* one) between the N4 substituent and the triazole motif which provides more flexibility. Although conceived from the same building blocks (with different crystal engineering), the structures and magnetic behaviors of **5** and **6** significantly differ. The 3D arrangement of **5** is built from trinuclear $[\text{Fe1-Fe2-Fe1}]$ units composed of two types of metal centers in distorted octahedral $[\text{FeN}_6]$ environments: the central Fe2 ion is coordinated to six $\mu_2\text{-phtptrz}$ ligands, and the peripheral Fe1 ions of the triads are coordinated to three $\mu_2\text{-phtptrz}$ ligands and three $\mu_2\text{-}[\text{Pt}(\text{CN})_4]^{2-}$ ligands leading to Fe(II) centres with a slightly lower ligand field energy. Distinctly, the 3D structure of **6** consists of $[\text{Fe}(\text{Pt}(\text{CN})_4)]_n$ 2D corrugated layers, involving $[\text{FeN}_5\text{O}]$ spheres and $\mu_4\text{-}[\text{Pt}(\text{CN})_4]^{2-}$, linked through the $\mu_2\text{-phtptrz}$ ligands. The main difference in the 3D structures of **5** and **6** resides in the coordination mode of the phtptrz ligand, with a bridging mode through the triazole motif in **5**, and a hybrid bridging mode involving both the phthalimido and the triazol groups in **6**. This results in higher ligand field strength $[\text{FeN}_6]$ environments in **5** in contrast with the $[\text{FeN}_5\text{O}]$ coordination spheres observed in **6**. Consequently, a two-step *SCO* behavior is observed only in **5**, while **6** shows a characteristic paramagnetic behavior with *HS* Fe^{II} ions in the whole studied temperature range.

In line with the results compiled in the previous *chapters II and III*, the comparative study of **5** and **6** further evidences that the characteristics of the functionalization of the triazole at the 4th position - i.e. nature/bulkiness of the functional group, length of the alkyl spacer, and overall flexibility in the coordination modes of the 4-R-trz ligand - combined with the nature of the anion (geometry, size/volume, charge, and coordination flexibility) drastically impact the inter-metallic interactions/connectivity *via* covalent bonding, and so the genesis of a *SCO* behavior close to room temperature. In summary, the substitution of the organic polynitrile ligands by inorganic $[\text{Pt}(\text{CN})_4]^{2-}$ analogues in the “ $\text{Fe}^{\text{II}}/\text{bntrz}/\text{Anion}$ ” systems enabled the access to extended 1D networks instead of

trinuclear complexes, while the replacement of the bntrz ligand by the bulkier (and more flexible) phtptrz ligand in the “Fe^{II}/R-trz/[Pt(CN)₄]²⁻” systems led us to 3D architectures with lower degree of cooperativity. This ascertainment can be further extended to the {Fe₃(tr₂ad)₄[Au(CN)₂]₂}[Au(CN)₂]₄·8H₂O derivative,^{10f} which has a 3D structure comparable to **5**, but concealed any display of *SCO* behaviour while **5** presents a two-step spin transition. Although the rationalization of their distinct behaviors remains to be carefully acceded, this constataion can be notably correlated to the more pronounced bulkiness of the tr₂ad ligand compared to the phtptrz moiety, and also to the nature of the covalent active anions. In this respect, the compound **5** can be labelled as the first triazole-bridged Fe^{II} 3D complex which displays a *SCO* behaviour.

However, as already pinpointed in the previous chapters and univocally demonstrated with the syntheses of **5** and **6**, any approach - based exclusively on the nature of the precursors to tailor the design of materials with *SCO* behaviors of relevance - would be ultimately inappropriate, or at least incomplete. Indeed, the two compounds **5** and **6** display very different 3D arrangements and magnetic behaviors, even so they have been synthesized from the exact same starting precursors, i.e. Fe(ClO₄)₂·xH₂O and K₂[Pt(CN)₄]·3H₂O salts, and phtptrz ligands. The latter observation stresses out the decisive and remarkably underestimated role of the crystal engineering conditions (stoichiometry, concentration, nature/mixture of the solvents, and crystallization technique), not only in obtaining single crystals suitable for X-ray diffraction, but also for the decisive input they can have in the structural arrangements and ensuing *SCO* behaviors of the resulting materials. These results once again highlight the highly sensitive complexity to anticipate and predict the design of *SCO* materials with tuned properties, but also the even more pressing need for systematic and refined magneto-structural correlations, notably with access to single-crystal X-ray diffraction studies at both *HS* and *LS* states, to better understand the driving forces of the spin crossover phenomenon in the so called “triazole family”. In that regard, the convenient and flexible two-step route - that has been successfully optimized to increase the yield of the phtptrz by 20 % from previously reported protocols - has already been defined as a synthetic platform to access a wide range of 4-R-trz ligands, with functional R groups of various natures; these new ligands, in combination with selected anionic candidates with covalent ability, are already under investigations, with the aim to refine the roles of the functional group of the 4-R-trz ligands and the anion in the *SCO* behavior.

◆ Experimental section

1. General information

The iron(II) salt $\text{Fe}(\text{ClO}_4)_2 \cdot x\text{H}_2\text{O}$, the potassium tetracyanometallates $\text{K}_2[\text{M}(\text{CN})_4] \cdot x\text{H}_2\text{O}$ ($\text{M} = \text{Ni}, \text{Pd}, \text{Pt}$) and ascorbic acid were purchased from Sigma-Aldrich and Alfa Aesar, and used as received. Deuteriated solvents were purchased from Sigma-Aldrich and Cambridge Isotope Laboratories. Dried solvents were prepared by refluxing for one day under dinitrogen over the appropriate drying agents (sodium-naphthalene and benzophenone for THF; sodium-benzophenone and calcium hydride for diethyl ether; calcium hydride for acetonitrile; magnesium and iodine for methanol; sodium for ethanol and molecular sieves for DMF), and degassed before use. Solvents were stored in glass ampoules under argon. Alternatively, they could be obtained from a solvent purification device (MBRAUN). All glassware and cannula were stored in an oven ($>353 \text{ K}$). All the ligand syntheses experiments were carried out under argon or nitrogen by using a dual manifold vacuum/argon line and standard Schlenk techniques. The syntheses of single crystals of **5** and **6** were carried out in ambient conditions. Perchlorate salts are potentially explosive, only small quantities of these compounds should be prepared and handled behind suitable protective shields.

2. Synthesis of the ligand 2-(3-(4H-1,2,4-triazol-4-yl)propyl)isoindoline-1,3-dione (phtptrz): a two-step synthesis

The 4-R-1,2,4-triazole derivative 2-(3-(4H-1,2,4-triazol-4-yl)propyl)isoindoline-1,3-dione (phtptrz) was synthesized *via* a two step route inspired from previously reported protocols,²⁶⁻²⁷ but with impactful modifications to improve the purification and the yield. In the first step, the intermediate 3-(4H-1,2,4-triazol-4-yl)propan-1-ol is synthesized through a modified Bayer synthesis,²² followed in the second step by a modified Mitsunobu reaction,²⁷ as illustrated in Scheme 2, with details provided hereafter.

- Step 1: Synthesis of the intermediate 3-(4H-1,2,4-triazol-4-yl)propan-1-ol (hyptrz)

A mixture of triethyl orthoformate (18 mL, 108 mmol) and formyl hydrazine (5.4 g, 90 mmol) in dry ethanol (100 mL) is refluxed for 6 hours under nitrogen atmosphere, then 3-aminopropanol (6.9 mL, 90 mmol) is added and the resulting solution is refluxed for additional 24 h. Subsequently, the mixture is allowed to cool down to room temperature, and the resulting crude product is recrystallized from dry ethanol and ether mixture at low temperature (-32°C). Finally, the moisture sensitive white crystalline product is filtered off, washed with cold ether very rapidly, and dried under vacuum. Yield: 8.25 g (72 %).

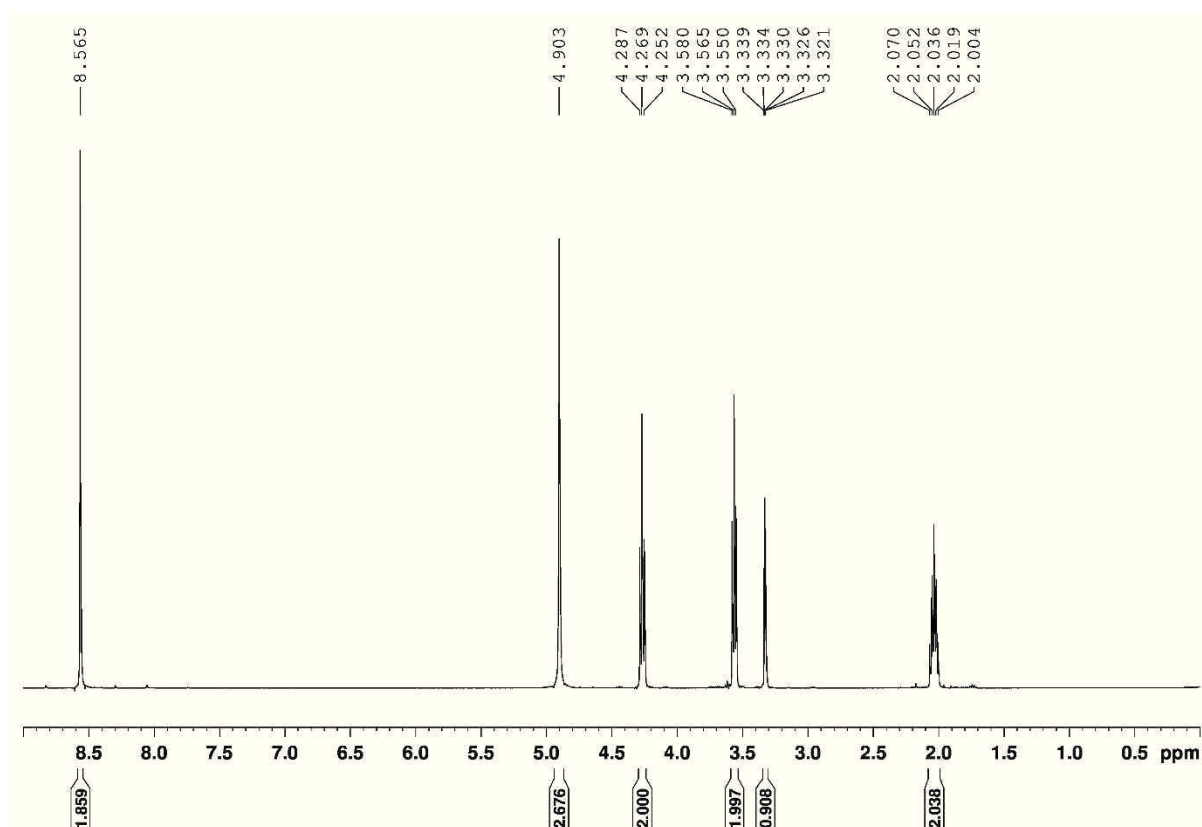


Figure 13. ^1H NMR (300 MHz, MeOD , 298 K) of 3-(4H-1,2,4-triazol-4-yl)propan-1-ol (hyptrz). ^1H NMR : δ 8.56 (s, 2H, -N-CH=N), 4.27 (t, 2H, trz- CH_2 -), 3.56 (t, 2H, - CH_2 -OH), 2.04 (m, 2H, CH_2 - CH_2 -OH).

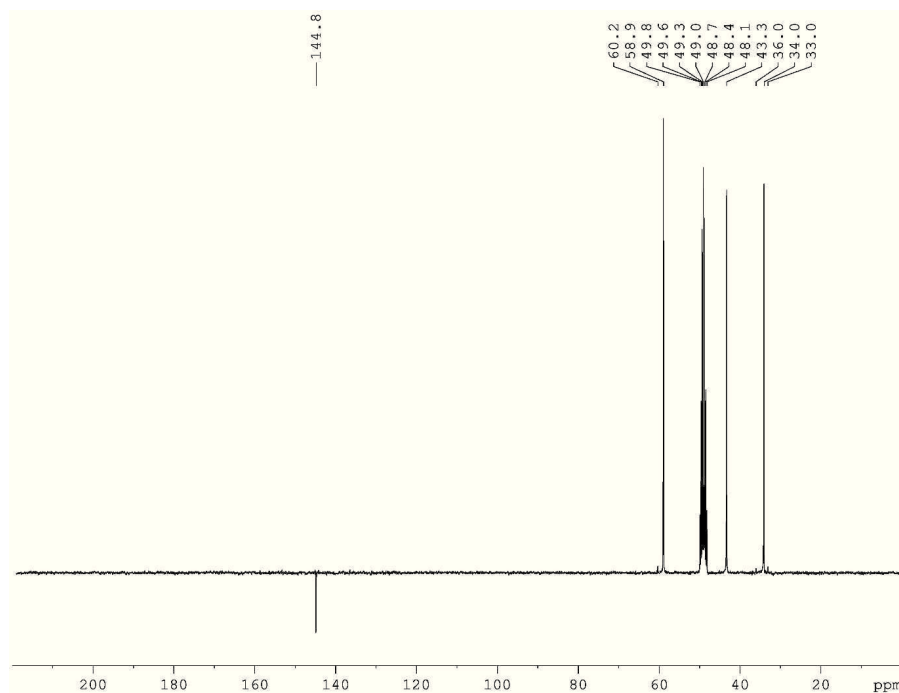


Figure 14. ^{13}C NMR (300 MHz, MeOD, 298 K) of 3-(4H-1,2,4-triazol-4-yl)propan-1-ol (hyptrz). ^{13}C NMR : δ 144.8 (-N-CH=N), 58.9 (trz-CH₂-), 43.3 (-CH₂-OH), 33.0 (-CH₂-CH₂-OH).

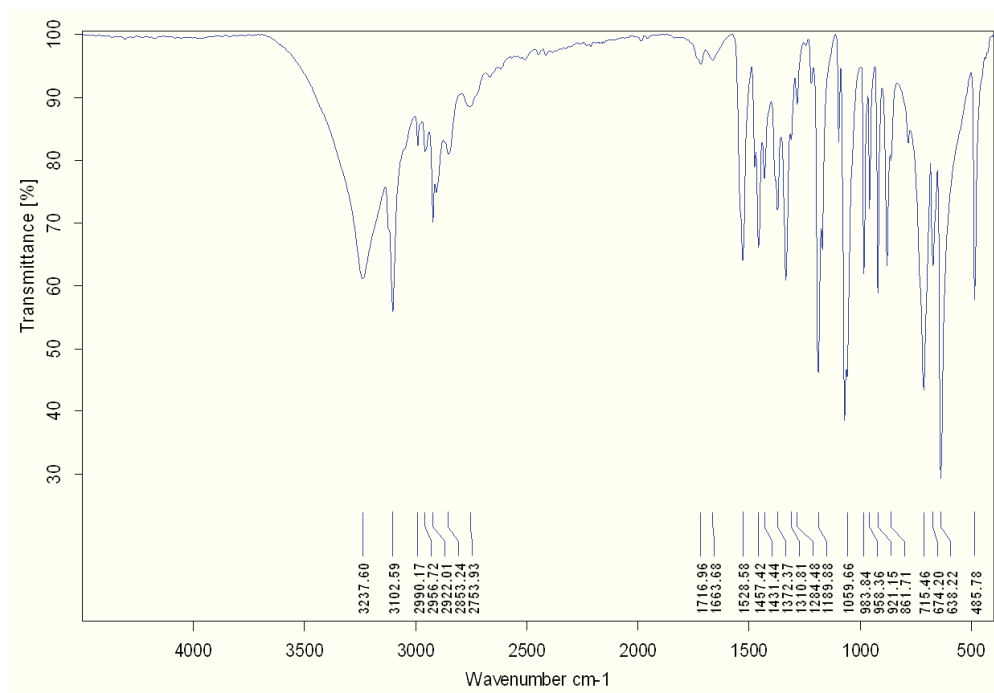


Figure 15. IR Spectra of the intermediate 3-(4H-1,2,4-triazol-4-yl)propan-1-ol (hyptrz). IR (ν , cm⁻¹) : 3328br, 3103m, 2990w, 2957w, 2855w, 2760w, 2349w, 2322w, 1657w, 1530w, 1475w, 1457w, 1432w, 1384m, 1372w, 1355w, 1310w, 1284w, 1221w, 1191m, 1171w, 1097w, 1071m, 1060m, 984w, 958m, 921w, 880w, 716m, 672w, 665w, 638s, 486w.

- Step 2: Synthesis of the 2-(3-(4H-1,2,4-triazol-4-yl)propyl)isoindoline-1,3-dione (phtptrz)

Diisopropyl azodicarboxylate (DIAD) (9.7 mL, 49.45 mmol, 1.23 equivalent) is added with stirring in small portions to a solution of triphenylphosphine (PPh₃) (12.98 g, 49.45 mmol, 1.23 equiv.) in dry THF (60 mL) at 0 °C under argon, and the mixture is stirred for 10 min. Then, a suspension of phthalimide (5.89 g, 40 mmol, 1 equiv.) and 4-(3-Hydroxypropyl)-1,2,4-triazole (5.08 g, 40 mmol, 1 equivalent) in dry acetonitrile (60 mL) is added to the reaction mixture at 0 °C, and the resulting mixture is stirred overnight at room temperature. The white precipitate formed was collected using sintered funnel, washed with cold THF and acetonitrile to obtain a white crystalline powder. Yield: 82 % (8.45 g).

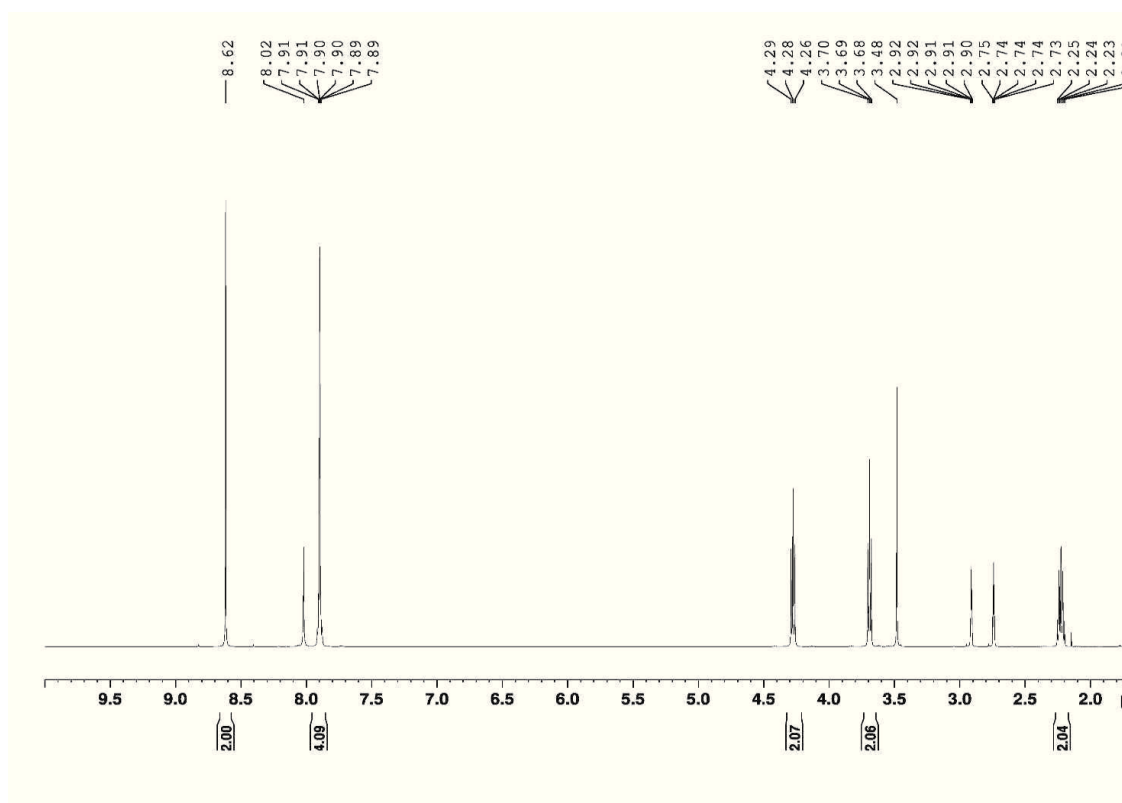


Figure 16. ¹H NMR (500 MHz, DMF-D7, 298 K) of 2-(3-(4H-1,2,4-triazol-4-yl)propyl)isoindoline-1,3-dione (phtptrz). ¹H NMR : δ 8.62 (s, 2H, -N-CH=N-), 7.91-7.89 (m, 4H, H_{Ar}), 4.27 (t, 2H, trz-CH₂-), 3.69 (t, 2H, -CH₂-Pth), 2.23 (qi, 2H, -CH₂-CH₂-Pth).

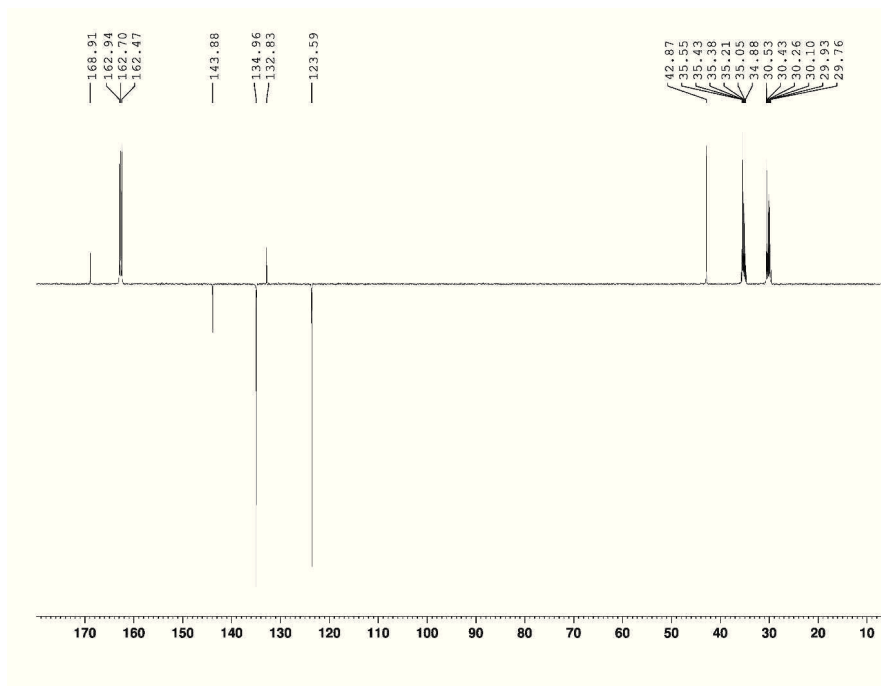


Figure 17. ^{13}C NMR (500 MHz, DMF- D_7 , 298 K, 298 K) of 2-(3-(4H-1,2,4-triazol-4-yl)propyl)isoindoline-1,3-dione (phtptrz). ^{13}C NMR : δ 168.9 (2C, $-\text{C}=\text{O}$), 143.9 (2C, $-\text{N}-\text{CH}=\text{N}-$), 134.9 (2C, C_{Ar}), 132.8 (2C, C_{Ar}), 123.5 (2C, C_{Ar}), 42.8 (trz- CH_2 -), 35.4 ($-\text{CH}_2$ -Pth), 30.5 ($-\text{CH}_2-\text{CH}_2$ -Pth)

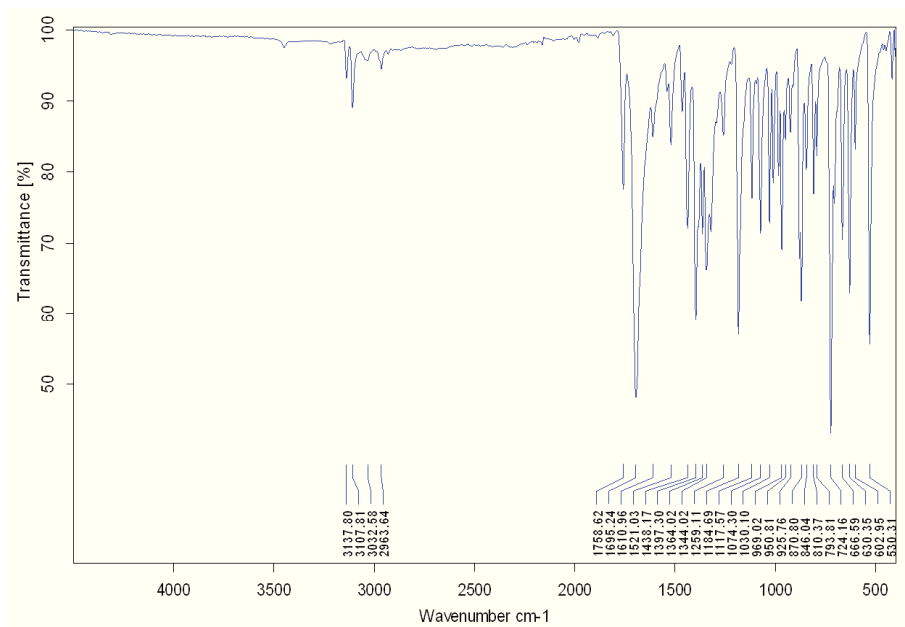


Figure 18. Infrared Spectra of 2-(3-(4H-1,2,4-triazol-4-yl)propyl)isoindoline-1,3-dione (phtptrz). IR (ν , cm^{-1}) : 3138w, 3108w, 3033w, 2964w, 1758w, 1695s, 1521w, 1438w, 1397w, 1364w, 1344w, 1259w, 1189m, 1118w, 1074w, 1030w, 969w, 951w, 925w, 871m, 846w, 810w, 793w, 724s, 667w, 630m, 603w, 530s.

3. Metal Complex Syntheses

■ Synthesis of single crystals of $\{\text{Fe}_3(\mu_2\text{-phtptrz})_6[\mu_2\text{-Pt}(\text{CN})_4]_3\} \cdot \text{C}_2\text{H}_5\text{OH} \cdot 5.5\text{H}_2\text{O}$ (**5**).

A water-ethanol (1:1) solution (6.5 mL) of phtptrz (76.89 mg, 0.3 mmol) and $\text{K}_2[\text{Pt}(\text{CN})_4] \cdot 3\text{H}_2\text{O}$ (12.95 mg, 0.03 mmol), and an ethanol solution (5 mL) of $\text{Fe}(\text{ClO}_4)_2 \cdot x\text{H}_2\text{O}$ (25.5 mg, 0.1 mmol) with a small amount of ascorbic acid, are initially prepared. A total of 1 mL of the solution containing both the phtptrz ligand and $\text{K}_2[\text{Pt}(\text{CN})_4] \cdot 3\text{H}_2\text{O}$ salt is placed at the bottom of a fine glass tube (5 mm diameter), and a water-ethanol (1:2) buffer solution (0.5 mL) is immediately layered on top. Then, a volume of 0.5 mL of the ethanol solution of Fe^{II} is delicately layered above the buffer layer. After two weeks, colorless rhombohedral crystals of **5** suitable for single-crystal X-ray diffraction are obtained by slow diffusion. However, few orange crystals of **6** are also formed at the same time, and removed manually.

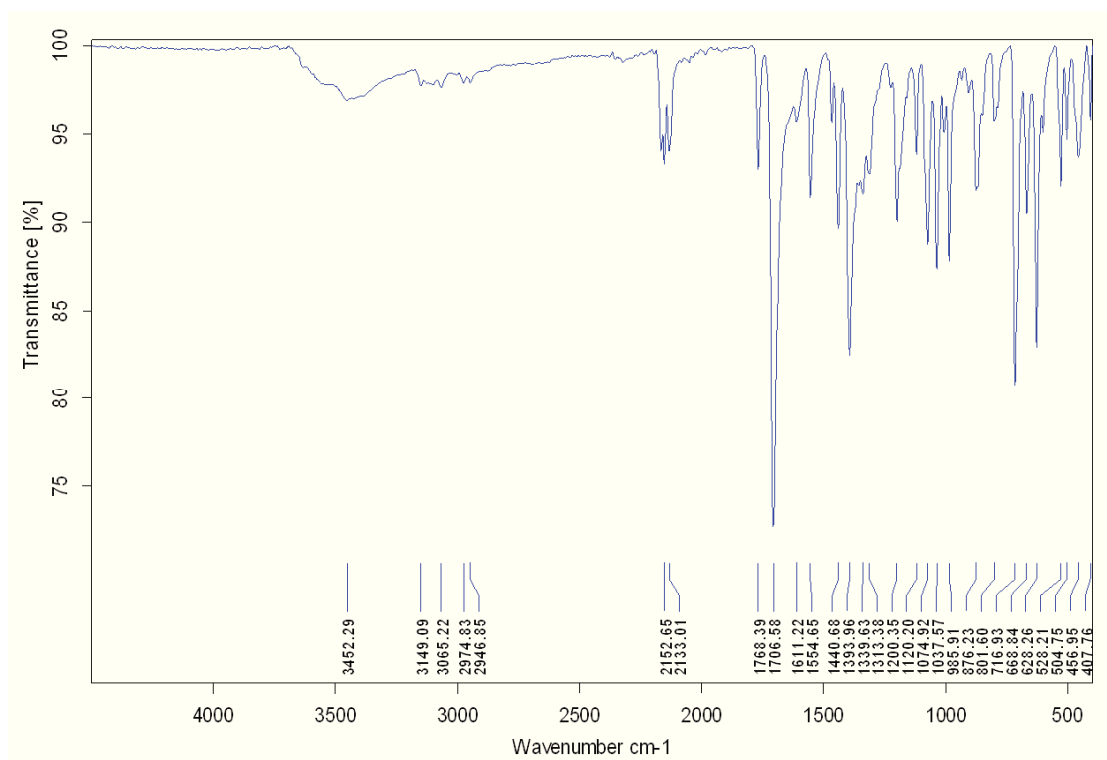


Figure 19. Infrared Spectra of single crystals of $\{\text{Fe}_3(\mu_2\text{-phtptrz})_6[\mu_2\text{-Pt}(\text{CN})_4]_3\} \cdot \text{C}_2\text{H}_5\text{OH} \cdot 5.5\text{H}_2\text{O}$ (**5**). IR (ν , cm^{-1}) : 3452br, 3149w, 3065w, 2975w, 2945w, 2153w, 2133w, 1768w, 1707s, 1555w, 1441w, 1394m, 1200w, 1120w, 1075w, 1038w, 986w, 876w, 802w, 717m, 669w, 628m, 528w, 505w, 457w, 408w.

■ Synthesis of single crystals of $\{\text{Fe}(\text{phtptrz})[\text{Pt}(\text{CN})_4]\cdot\text{H}_2\text{O}\}$ (**6**)

A water-ethanol (1:1) solution (20 mL) containing phtptrz (51.25 mg, 0.2 mmol) and $\text{K}_2[\text{Pt}(\text{CN})_4]\cdot 3\text{H}_2\text{O}$ (43.14 mg, 0.1 mmol), and an ethanol solution (1.5 mL) of $\text{Fe}(\text{ClO}_4)_2\cdot x\text{H}_2\text{O}$ (25 mg, 0.1 mmol) with few crystals of ascorbic acid are initially prepared. A volume of 1 mL of the solution of phtptrz and $\text{K}_2[\text{Pt}(\text{CN})_4]\cdot 3\text{H}_2\text{O}$ is introduced in the ground of a fine glass tube (5 mm diameter). Then, an ethanol solution (0.5 mL) of Fe^{II} was layered above the buffer layer solution (0.5 mL) of water-ethanol (1:2). Orange plate crystals of **6** are formed over a couple of weeks.

Alternatively, an aqueous solution (10 mL) containing $\text{Fe}(\text{ClO}_4)_2\cdot x\text{H}_2\text{O}$ (25.5 mg, 0.1 mmol), small quantity of ascorbic acid, and $\text{K}_2[\text{Pt}(\text{CN})_4]\cdot 3\text{H}_2\text{O}$ (43.14 mg, 0.1 mmol), and another ethanol solution of phtptrz (51.25 mg, 0.2 mmol) are initially prepared. A volume of 1 mL of the aqueous solution of $\text{Fe}(\text{ClO}_4)_2\cdot x\text{H}_2\text{O}$ and $\text{K}_2[\text{Pt}(\text{CN})_4]\cdot 3\text{H}_2\text{O}$ is then placed at the bottom of a fine glass tube (5 mm diameter), covered with an ethanol-water (1:1) buffer solution (0.5 mL), over which 0.5 mL of the ethanol solution of phtptrz is layered. Orange plate crystals of **6** are formed in 2 weeks.

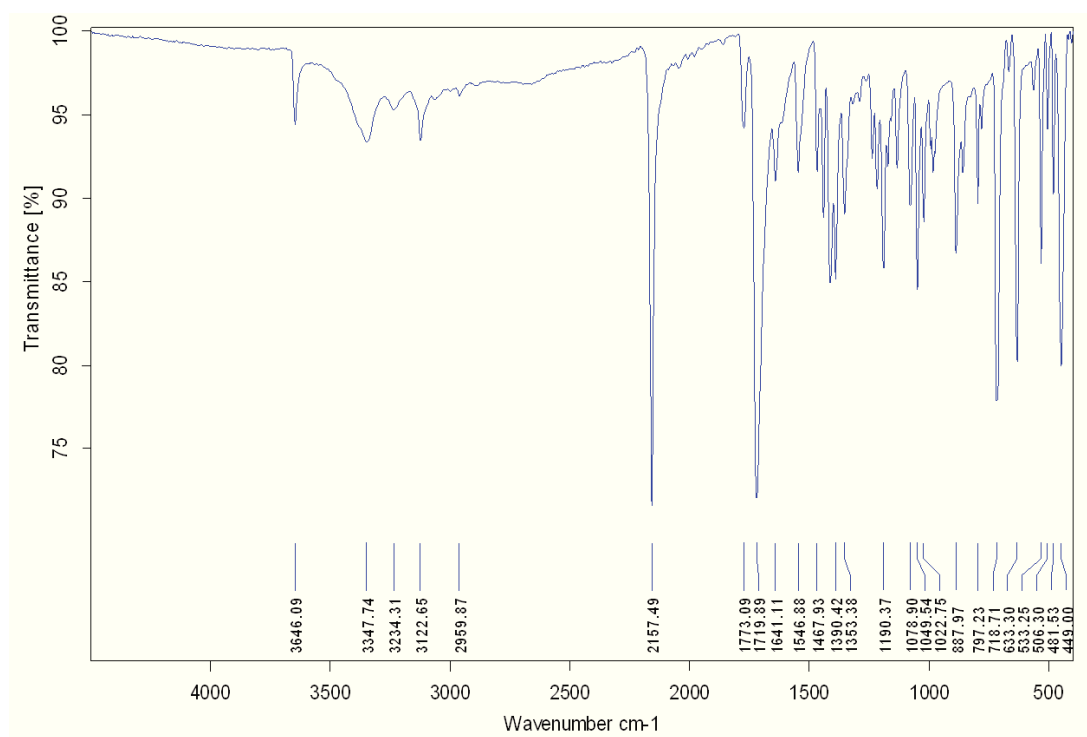


Figure 20. Infrared Spectra of single crystals of $\{\text{Fe}(\text{phtptrz})[\text{Pt}(\text{CN})_4]\cdot\text{H}_2\text{O}\}$ (**6**). IR (ν , cm^{-1}) : 3646w, 3348br, 3234w, 3123w, 2157s, 1773w, 1720s, 1641w, 1547w, 1468w, 1441w, 1413m, 1390m, 1353m, 1238w, 1218w, 1172w, 1078w, 1049m, 1022w, 888w, 719s, 633m, 533w, 481w, 448s.

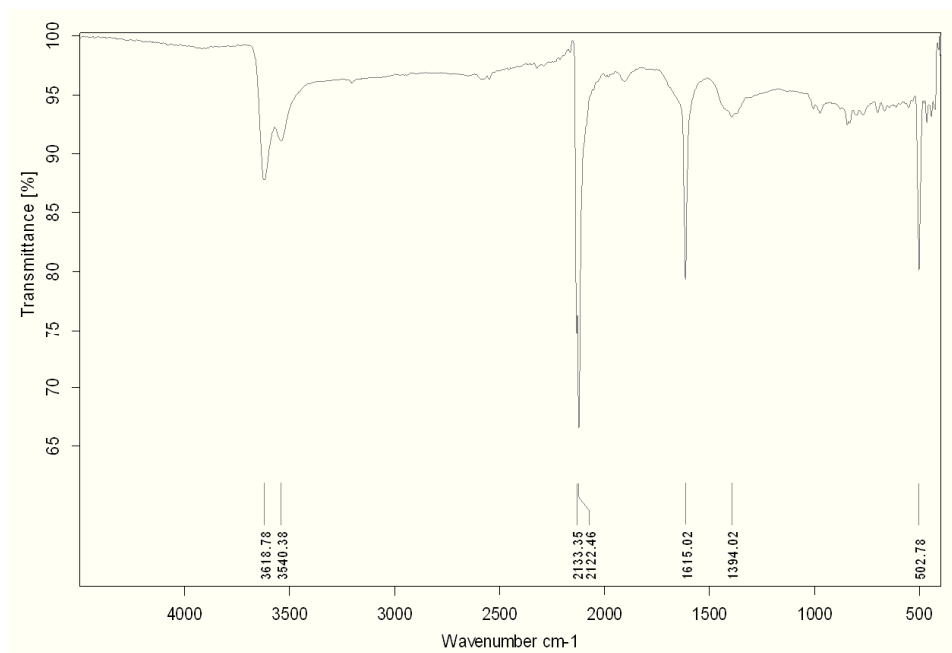


Figure 21. Infrared Spectra of $\text{K}_2[\text{Pt}(\text{CN})_4] \cdot x\text{H}_2\text{O}$. IR (ν , cm^{-1}) : 2133s, 2122m.

4. X-ray Crystallography

Crystallographic studies of the Fe^{II} complexes **5** and **6** were performed at 296 K and 170 K, using an Oxford Diffraction Xcalibur κ -CCD diffractometer equipped with a graphite monochromated Mo $K\alpha$ radiation ($\lambda = 0.71073 \text{ \AA}$). The full sphere data collections were performed using 1.0° ω -scans with an exposure time of 150 s and 200 s per frame for **5**, at 296 K and 170 K, and 150 s for **6** at 296 K, respectively. Data collection and data reduction were done with the CRYSLIS-CCD and CRYSLIS-RED programs on the full set of data.³⁰ The crystal structures were solved by direct methods and successive Fourier difference syntheses, and were refined on F2 by weighted anisotropic full-matrix least-squares methods.³¹ All non-hydrogen atoms were refined anisotropically, while the hydrogen atoms were calculated and therefore included as isotropic fixed contributors to Fc. All other calculations were performed with standard procedures (WINGX).³² Crystal data, structure refinement and collection parameters are listed in Table 1.

Due to its intrinsic relative small size, the single crystal of **5** that has been used for x-ray diffraction analysis required an extended data collection time. However, as illustrated in Figure 8, the robustness of the single crystal allowed to obtain data collections for both the *HS* (296 K) and *LS* (170 K) states. In comparison, the structural data for **6** was obtained only at 293 K (*HS*) in a short period of time, as the crystals were significantly bigger in size.

5. Physical measurements

^1H and ^{13}C NMR spectra were recorded on Bruker AMX-300 (300 MHz), AMX-400 (400 MHz) and AMX-500 (500 MHz) spectrometers, and the spectra were referenced internally using residual proton solvent resonances relative to tetramethylsilane ($\delta = 0$ ppm). Splitting patterns are designed as: s singlet, d doublet, t triplet, q quartet, m multiplet, br. Broad. Infrared spectra were recorded in the range of $4000\text{--}400\text{ cm}^{-1}$ on a FT-IR BRUKER ATR VERTEX70 spectrometer. Single crystal diffraction analyses were performed using an Oxford Diffraction Xcalibur κ -CCD diffractometer. Variable temperature magnetic susceptibility measurements were carried out in the temperature range 2–400 K, in cooling and warming scans, with an applied magnetic field of 1–2 Tesla on polycrystalline samples obtained after grinding of single crystals of compounds **5** and **6** (with masses of 0.54 mg and 5.270 mg, respectively) with a Quantum Design MPMS-XL-5 SQUID magnetometer. The susceptibility data were corrected for the sample holders previously measured under the same conditions, and for the diamagnetic contributions as deduced by using Pascal's constant tables. The magnetic measurements were performed with different cooling and warming rates in the range $0.5\text{--}5\text{ K}\cdot\text{min}^{-1}$.

■ Bibliography

1. (a) P. Gütlich, H. A. Goodwin, in *Spin Crossover in Transition Metal Compounds*, Springer-Verlag, Berlin/Heidelberg, **2004**, 233, 234, 235; *Topics in Current Chemistry*, Springer: Berlin, **2004**; Vols. 1-3; (b) J. F. Létard, P. Guionneau, L. Goux-Capes, *Top. Curr. Chem.* **2004**, 235, 221. (c) M. A. Halcrow, *Spin-crossover materials: properties and applications*, Wiley-VCH: Weinheim, John Wiley & Sons, Ltd., U.K., **2013**, Chapter 1, pp 1-54, DOI: 10.1002/9781118519301.ch1; (d) O. Kahn, C. J. Martinez, *Science*, **1998**, 279, 44-48; (e) P. Gütlich, Y. Garcia, H. A. Goodwin, *Chem. Soc. Rev.*, **2000**, 29, 419-427; (f) A. Bousseksou, G. Molnar, L. Salmon, W. Nicolazzi, *Chem. Soc. Rev.*, **2011**, 40, 3313-3335; (g) M. C. Muñoz, J. A. Real, *Coord. Chem. Rev.*, **2011**, 255, 2068-2093; (h) G. Aromí, L. A. Barrios, O. Roubeau, P. Gamez, *Coord. Chem. Rev.*, **2011**, 255, 485-546; (i) M. A. Halcrow, *Chem. Soc. Rev.*, **2011**, 40, 4119-4142; (j) P. Gütlich, A. B. Gaspar and Y. Garcia, *Beilstein J. Org. Chem.*, **2013**, 9, 342-391.
2. (a) T. Matsumoto, G. N. Newton, T. Shiga, S. Hayami, Y. Matsui, H. Okamoto, R. Kumai, Y. Murakami, H. Oshio, *Nat. Commun.*, **2014**, 5, 3865; (b) D. Aravena, E. Ruiz, *J. Am. Chem. Soc.*, **2012**, 134, 777-779; (c) G. A. Craig, O. Roubeau, G. Aromí, *Coord. Chem. Rev.*, **2014**, 269, 13-31; (d) B. Warner, J. C. Oberg, T. G. Gill, F. El Hallak, C. F. Hirjibehedin, M. Serri, S. Heutz, M. A. Arrio, P. Saintavit, M. Mannini, G. Poneti, R. Sessoli, P. J. Rosa, *J. Phys. Chem. Lett.*, **2013**, 4, 1546-1552; (e) J. Larionova, L. Salmon, Y. Guari, A. Tokarev, K. Molvinger, G. Molnár, A. Bousseksou, *Angew. Chem., Int. Ed.*, **2008**, 47, 8236-8240; (f) C. F. Wang, R. F. Li, X. Y. Chen, R. J. Wei, L. S. Zheng, J. Tao, *Angew. Chem., Int. Ed.*, **2015**, 54, 1574-1577; (g) Y.-S. Koo, J. R. Galan-Mascaros, *Adv. Mater.*, **2014**, 26, 6785-6789; (h) M. B. Duriska, S. M. Neville, B. Moubaraki, J. A. Cashion, G. J. Halder, K. W. Chapman, C. Balde, J. F. Létard, K. S. Murray, C. J. Kepert, S. R. Batten, *Angew. Chem., Int. Ed.*, **2009**, 48, 2549-2552; (i) E. M. Hernandez, C. M. Quintero, O. Kraieva, C. Thibault, C. Bergaud, L. Salmon, G. Molnár, A. Bousseksou, *Adv. Mater.*, **2014**, 26, 2889-2893; (j) H. Phan, S. M. Benjamin, E. Steven, J. S. Brooks, M. Shatruk, *Angew. Chem., Int. Ed.*, **2015**, 54, 823-827; (k) E. Ludwig, H. Naggert, M. Kalläne, S. Rohlf, E. Kröger, A. Bannwarth, A. Quer, K. Rossnagel, L. Kipp, F. Tuczek, *Angew. Chem., Int. Ed.*, **2014**, 53, 3019-3023; (l) M. Seredyuk, M. C. Muñoz, M. Castro, T. Romero-Morcillo, A. B. Gaspar, J. A. Real, *Chem. Eur. J.*, **2013**, 19, 6591-6596; (m) V. A. Money, C. Carbonera, J. Elhaik, M. A. Halcrow, J. A. K. Howard, J. F. Letard, *Chem. Eur. J.*, **2007**, 13, 5503-5514; (

- n) E. Coronado, G. Minguez Espallargas, *Chem. Soc. Rev.*, **2013**, 42, 1525-1539; (o) (b) T. Liu, H. Zheng, S. Kang, Y. Shiota, S. Hayami, M. Mito, O. Sato, K. Yoshizawa, S. Kanegawa, C. Duan, *Nat. Commun.*, **2013**, 4, 2826.
3. (a) O. Kahn, C. Kröber, C. Jay, *Adv. Mater.*, **1992**, 4, 718-728; (b) P. J. van Koningsbruggen, Y. Garcia, E. Codjovi, R. Lapouyade, O. Kahn, L. Fournès, L. Rabardel, *J. Mater. Chem.*, **1997**, 7, 2069-2075; (c) L. G. Lavrenova, V. N. Ikorskii, V. A. Varnek, I. M. Oglezneva, S. V. Larionov, *Koord. Khim.*, **1986**, 12, 207; (d) V. A. Varnek, L. G. Lavrenova, *J. Struct. Chem.*, **1995**, 36, 104; (e) E. Codjovi, L. Sommer, O. Kahn, C. Jay, *New J. Chem.*, **1996**, 20, 503-505; (f) A. Sugahara, M. Enomoto, N. Kojima, *J. Phys. Conf. Ser.*, **2010**, 217, 012128; (g) G. A. Berezovskii, O. G. Shakirova, Y. G. Shvedenkov, L. G. Lavrenova, *Russ. J. Phys. Chem. A*, **2003**, 77, 1054-1058.
 4. (a) M. M. Dîrtu, C. Neuhausen, A. D. Naik, A. Rotaru, L. Spinu, Y. Garcia, *Inorg. Chem.*, **2010**, 49, 5723-5736; (b) M. M. Dîrtu, A. Rotaru, A. Gillard, J. Linares, E. Codjovi, B. Tinant, Y. Garcia, *Inorg. Chem.*, **2009**, 48, 7838-7852 and references therein.; (c) Y. Garcia, J. Moscovici, A. Michalowicz, V. Ksenofontov, G. Levchenko, G. Bravic, D. Chasseau, P. Gütlich, *Chem. Eur. J.*, **2002**, 8, 4992-5000.
 5. O. Roubeau, *Chem. Eur. J.*, **2012**, 18, 15230-5244 and references therein.
 6. (a) M. M. Dîrtu, A. D. Naik, A. Rotaru, L. Spinu, D. Poelman, Y. Garcia, *Inorg. Chem.*, **2016**, 55, 4278-4295; (b) Y. Garcia, F. Robert, A. D. Naik, G. Zhou, B. Tinant, K. Robeyns, S. Michotte, L. Piraux, *J. Am. Chem. Soc.*, **2011**, 133, 15850-15853; (c) A. D. Naik, K. Robeyns, C. F. Meunier, A. F. Léonard, A. Rotaru, B. Tinant, Y. Filinchuk, B. L. Su, Y. Garcia, *Inorg. Chem.*, **2014**, 53, 1263-1265; (d) C. M. Jureschi, J. Linares, A. Boulmaali, P. Richard Dahoo, A. Rotaru, Y. Garcia, *Magnetochemistry*, **2016**, 16, 187.
 7. (a) E. Coronado, J. R. Galán-Mascarós, M. Monrabal-Capilla, J. Garcíá-Martínez, P. Pardo-Ibañez, *Adv. Mater.*, **2007**, 19, 1359-1361; (b) J. R. Galán-Mascarós, E. Coronado, A. Forment-Aliaga, M. Monrabal-Capilla, E. Pinilla-Cienfuegos, M. Ceolin, *Inorg. Chem.*, **2010**, 49, 5706-5714; (c) M. Gimenez-Marqués, M. L. Garcia-Sanz de Larrea, E. Coronado, *J. Mater. Chem. C*, **2015**, 3, 7946-7953; (d) A. Holovchenko, J. Dugay, M. Giménez-Marqués, R. Torres-Cavanillas, E. Coronado, H. S. J. van der Zant, *Adv. Mater.*, **2016**; DOI: 10.1002/adma.201600890.

8. (a) T. Forestier, S. Mornet, N. Daro, T. Nishihara, S. I. Mouri, K. Tanaka, O. Fouche', E. Freysz, J. F. Létard, *Chem. Commun.*, **2008**, 4327-4329; (b) O. Fouche', J. Degert, G. Jonusauskas, N. Daro, J. F. Létard, E. Freysz, *Phys. Chem. Chem. Phys.*, **2010**, *12*, 3044-3052; (c) C. Etrillard, V. Faramarzi, J. F. Dayen, J. F. Létard, B. Doudin, *Chem. Commun.*, **2011**, *47*, 9663-9665; (d) L. Moulet, N. Daro, C. Etrillard, J. F. Létard, A. Grosjean, P. Guionneau, *Magnetochemistry*, **2016**, *2*, 10; (e) J. F. Létard, N. Daro, O. Nguyen, *Nanoparticles of a spin transition compound*, **2007**, Patent **WO2007/065996**.

9. (a) H. Shepherd, C. Quintero, G. Molnár, L. Salmon, A. Bousseksou, Luminescent spin crossover materials in *Spin-Crossover Materials: Properties and Applications* (ed. M. A. Halcrow), John Wiley & Sons, **2013**, 347-374; (b) G. Molnár, I. A. Guralskiy, L. Salmon, W. Nicolazzi, C. Quintero, A. Akou, K. Abdel-kader, G. Félix, T. Mahfoud, C. Bergaud, C. Bartual, C. Thibault, C. Vieu, A. Bousseksou, Bistable photonic nanostructures based on molecular spin crossover complexes, "*Photonic Crystal Materials and Devices X*", **2012**, vol. 8425, 842513; (c) A. Rotaru, J. Dugay, R. P. Tan, I. A. Guralskiy, L. Salmon, P. Demont, J. Carrey, G. Molnár, M. Respaud, A. Bousseksou, *Adv. Mater.*, **2013**, *25*, 1745-1749; (d) T. Q. Hung, F. Terki, S. Kamara, M. Dehbaoui, S. Charar, B. Sinha, C. Kim, P. Gandit, I. A. Guralskiy, G. Molnár, L. Salmon, H. J. Shepherd, A. Bousseksou, *Angew. Chem., Int. Ed.*, **2013**, *52*, 1185-1188; (e) H. J. Shepherd; G. Molnár, W. Nicolazzi, L. Salmon, A. Bousseksou, *Eur. J. Inorg. Chem.*, **2013**, *2013*, 653-661; (f) I. A. Guralskiy, C.M. Quintero, G. Molnár, I.O. Fritsky, L. Salmon, A. Bousseksou, *Chem. Eur. J.*, **2012**, *18*, 9946-9954.

10. (a) J. M. Herrera, S. Titos-Padilla, S. J. A. Pope, I. Berlanga, F. Zamora, J. J. Delgado, K.V. Kamenev, X. Wang, A. Prescimone, E. K. Brechin, E. Colacio, *J. Mater. Chem. C*, **2015**, *3*, 7819-7829; (b) H. S. Scott, T. M. Ross, B. Moubaraki, K. S. Murray, S. M. Neville, *Eur. J. Inorg. Chem.*, **2013**, 803-812; (c) L. G. Lavrenova, O. G. Shakirova, *Eur. J. Inorg. Chem.*, **2013**, 670-682; (d) V. Gómez, J. Benet-Buchholz, E. Martin, J. R. Galán-Mascarós, *Chem. Eur. J.*, **2014**, *20*, 5369-5379; (e) V. Gómez, C. Sáenz de Pipaón, P. Maldonado-Illescas, J. C. Waerenborgh, E. Martin, J. Benet-Buchholz, J. R. Galán-Mascarós, *J. Am. Chem. Soc.*, **2015**, *137*, 11924-11927; (f) F. J. Muñoz-Lara, A. B. Gaspar, M. C. Muñoz, A. B. Lysenko, K. V. Domasevitch, J. A. Real, *Inorg. Chem.*, **2012**, *51*, 13078-13080.

11. (a) M. A. Halcrow, *Spin-Crossover Materials: Properties and Applications*; M. A. Halcrow, Ed.; Wiley: Chichester, U.K., **2013**, Chapter 5, 147-169 DOI: 10.1002/9781118519301.ch5; (b) B. Weber, W. Bauer, J. Obel, *Angew. Chem. Int. Ed.*, **2008**, *47*, 10098-10101.

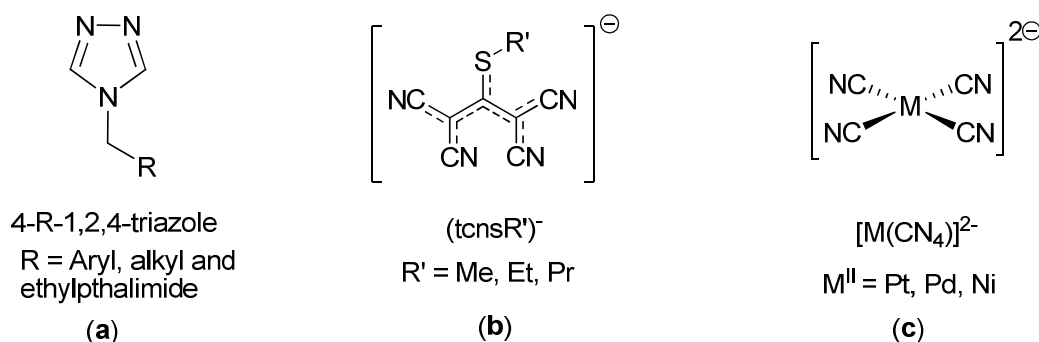
12. (a) F. Setifi, E. Milin, C. Charles, F. Thetiot, S. Triki, C. J. Gomez Garcia, *Inorg. Chem.*, **2014**, *53*, 97-104. (b) G. Agusti, A. B. Gaspar, M. C. Muñoz, J. A. Real, *Inorg. Chem.*, **2007**, *46*, 9646-9654; (c) Kosaka, W. Kosaka, K. Nomura, K. Hashimoto, S. Ohkoshi, *J. Am. Chem. Soc.*, **2005**, *127*, 8590-8591; (d) M. Arai, W. Kosaka, T. Matsuda, S. Ohkoshi, *Angew. Chem. Int. Ed.*, **2008**, *47*, 6885-6887.
13. M. M. Dîrtu, A. Rotaru, D. Gillard, J. Linares, E. Codjovi, B. Tinant and Y. Garcia, *Inorg. Chem.*, **2009**, *48*, 7838-7852.
14. M. M. Dîrtu, A. D. Naik, A. Rotaru, L. Spinu, D. Poelman and Yann Garcia, *Inorg. Chem.*, **2016**, *55*, 4278-4295.
15. L. G. Lavrenova, O. G. Shakirova, *Eur. J. Inorg. Chem.*, **2013**, 670-682
16. M. M. Dîrtu, Y. Garcia, M. Nica, A. Rotaru, J. Linares, F. Varret, *Polyhedron*, **2007**, *26*, 2259-2263
17. (a) M. C. Muñoz, J. A. Real, *Coord. Chem. Rev.*, **2011**, *255*, 2068-2093. (b) M. C. Muñoz, J. A. Real, Spin-Crossover Materials: Properties and Applications; M. A. Halcrow, Ed.; Wiley: Chichester, U.K., **2013**; Chapter 4, pp 121-146, DOI: 10.1002/9781118519301.ch4; (c) G. Molnár, S. Cobo, J. A. Real, F. Carcenac, E. Daran, C. Vieu, A. Bousseksou, *Adv. Mater.*, **2007**, *19*, 2163; (d) P. D. Southon, L. Liu, E. A. Fellows, D. J. Price, G. J. Halder, K. W. Chapman, B. Moubaraki, K. S. Murray, J. F. Létard, C. J. Kepert, *J. Am. Chem. Soc.*, **2009**, *131*, 10998; (e) R. Ohtani, K. Yoneda, S. Furukawa, N. Horike, S. Kitagawa, A. B. Gaspar, M. C. Muñoz, J. A. Real, M. Ohba, *J. Am. Chem. Soc.*, **2011**, *133*, 8600; (f) F. J. Muñoz-Lara, A. B. Gaspar, D. Aravena, E. Ruiz, M. C. Muñoz, M. Ohba, R. Ohtani, S. Kitagawa, J. A. Real, *Chem. Commun.*, **2012**, *48*, 4686; (g) N. F. Sciortino, K. R. Scherl-Gruenwald, G. Chastanet, G. J. Halder, K. W. Chapman, J. F. Létard, C. J. Kepert, *Angew. Chem. Int. Ed.*, **2012**, *51*, 10154; (h) X. Bao, H. J. Shepherd, L. Salmon, G. Molnár, M. L. Tong, A. Bousseksou, *Angew. Chem. Int. Ed.*, **2013**, *52*, 1198.
18. S. M. Neville, G. J. Halder, K. W. Chapman, M. B. Duriska, P. D. Southon, J. D. Cashion, J. F. Létard, B. Moubaraki, K. S. Murray, C. J. Kepert, *J. Am. Chem. Soc.*, **2008**, *130*, 2869.
19. J. A. Real, E. Andrés, M. C. Muñoz, M. Julve, T. Granier, A. Bousseksou, F. Varret, *Science*, **1995**, *268*, 265.

20. G. J. Halder, C. J. Kepert, B. Moubaraki, K. S. Murray, J. D. Cashion, *Science*, **2002**, 298, 1762.
21. M. Ohba, K. Yoneda, G. Agustí, M. C. Muñoz, A. B. Gaspar, J. A. Real, M. Yamasaki, H. Ando, Y. Nakao, S. Sakaki, S. Kitagawa, *Angew. Chem. Int. Ed.*, **2009**, 48, 4767.
22. G. Agustí, S. Cobo, A. B. Gaspar, G. Molnár, N. O. Moussa, P. A. Szilágyi, V. Pálfi, C. Vieu, M. C. Muñoz, J. A. Real, A. Bousseksou, *Chem. Mater.*, **2008**, 20, 6721.
23. (a) C. Bartual-Murgui, N. A. Ortega-Villar, H. J. Shepherd, M. C. Muñoz, L. Salmon, G. Molnár, A. Bousseksou, J. A. Real, *J. Mater. Chem.*, **2011**, 21, 7217; (b) C. Bartual-Murgui, L. Salmon, A. Akou, N. A. Ortega-Villar, H. J. Shepherd, M. C. Muñoz, G. Molnár, J. A. Real, A. Bousseksou, *Chem. Eur. J.*, **2012**, 18, 507.
24. F. J. Muñoz-Lara, A. B. Gaspar, M. C. Muñoz, M. Arai, S. Kitagawa, M. Ohba, J. A. Real, *Chem. Eur. J.*, **2012**, 18, 8013.
25. (a) V. Niel, J. M. Martinez-Agudo, M. C. Muñoz, A. B. Gaspar, J. A. Real, *Inorg. Chem.*, **2001**, 40, 3838; (b) M. Ohba, K. Yoneda, G. Agustí, M. C. Muñoz, A. B. Gaspar, J. A. Real, M. Yamasaki, H. Ando, Y. Nakao, S. Sakaki, S. Kitagawa, *Angew. Chem., Int. Ed.*, **2009**, 48, 4767;
26. (a) H. O. Bayer, R. S. Cook, W.C. von Mayer, *US Patent. 3821376*, **1974**; (b) L. Seidel, W. C. Von Meyer, S. Greenfield, *US Patent 4120684*, **1978**.
27. (a) O. Mitsunobu, *Synthesis* **1981**, 1; (b) Y. Boland, P. Hertsens, J. Marchand-Brynaert, Y. Garcia, *Synthesis*, **2006**, 9, 1504-1512.
28. (a) Haasnoot, J.G. and Groeneveld, N.L., *Z. Naturforsch., B: Anorg. Chem., Org. Chem.*, **1977**, 32, 1421; (b) M. B. Bushuev, L. G. Lavrenova, Yu. G. Shvedenkov, A. V. Virovets, L. A. Sheludyakova, and S. V. Larionov, *Rus. J. Inorg. Chem.*, **2007**, 52, 46-51.
29. E. Milin, V. Patinec, S. Triki, E. Bendeif, S. Pillet, M. Marchivie, G. Chastanet, and K. Boukheddaden, *Inorg. Chem.*, **2016**. DOI: 10.1021/acs.inorgchem.6b01081
30. Oxford Diffraction (**2006**). Xcalibur CCD/RED CrysAlis Software system. Oxford Diffraction Ltd, Abingdon, England.

31. A. Altomare, M. C. Burla, M. Camalli, C. Cascarano, C. Giacovazzo, A. Guagliardi, A. G. G. Moliterni, G. Polidori, R. Spagna, *J. Appl. Cryst.*, **1999**, 32, 115-119.
32. G. Sheldrick, Crystal structure refinement with SHELXL. *Acta Cryst. C*, **2015**, 71, 3-8.

General Conclusion

The present work has focused primarily on the design, synthesis and physical properties of new triazole based Fe^{II} *SCO* systems using carefully selected 4-R-1,2,4-triazole ligands, with either (i) inorganic ‘*rigid*’ tetracyanometallates $[\text{M}(\text{CN})_4]^{2-}$ or (ii) specific ‘*flexible*’ organic cyanocarbanions $(\text{tcnsR}')^-$ ($(\text{tcnsR}')^- = 1,1,3,3\text{-tetracyano-2-thioalkylpropenide}$) ligands (Scheme 1). Ultimately, the prospect consists of methodically evaluating the impact of the functionalization of precursors 4-R-1,2,4-triazole and atypical anions with the establishment of magneto-structural correlations which are essential to comprehend the physicochemical origin of the strong cooperativity in such striking materials, but also to rationalize the tuning of the *SCO* properties. Moreover, an intense exertion has been particularly committed to tackle the structural knowledge gap related to triazole-based Fe^{II} *SCO* materials by systematically seeking access to single crystals through deep crystallogeneses investigations.



Scheme 1. Selective examples of (a) 4-R-1,2,4-triazole derivatives, (b) Cyanocarbanions $\text{K}(\text{tcnsR}')$, and (c) Tetracyanometallate(II) anions $[\text{M}(\text{CN})_4]^{2-}$ used in the present work.

Based on the current developments in 1,2,4-triazole research, we have recently developed an alternative synthetic approach - explained in **Chapter I** - with combinations of triazole ligands and anions which were not used so far within the “triazole family”. In this ongoing work, we have realized at an early stage that this chemical approach tends to improve unprecedentedly the size, the quality and the robustness of the single crystals of the resulting original Fe^{II} /R-trz systems. Thus, the preliminary and time-consuming step of this project included the development and optimization syntheses of the starting precursors, more precisely the synthesis of the 4-R-1,2,4-triazole ligands (with R = Aryl, alkyl, phthalimide), and the sulfur based polynitrile organic ligands (tcnsR with R' = methyl, ethyl, propyl)

(Scheme 1). In the strategy from the group, the selected 4-R-1,2,4-triazole ligands are systematically including an alkyl spacer at the 4th position between the triazole moiety and the terminal functional group of the substituent in order to notably maintain as much as possible the electronic “integrity” of the triazole moiety. Another potential advantage attributable to the presence of an alkyl spacer resides in the enhancement of the overall flexibility of the 4-R-1,2,4-trz ligand which can favour the implication of the triazole ligand into H-bonding or short contacts (π - π and Van der Waals interactions) of relevance for the cooperativity. On the other hand, the choice of atypical organic polynitrile anions has been driven by the extended local expertise in the synthesis and the use of such flexible ligands, with the more rigid tetracyanomellates intervening as a comparative tool to evaluate the impact of the charge, the rigidity and the geometry of the anion on the resulting materials.

In **Chapter II**, we reported the synthesis, structural and magnetic characterizations, as well as the first accurate/reliable single crystal investigations of both *HS* and *LS* states, of the new triazole-based *SCO* Fe^{II} 1-D polymer [Fe(bntrz)₃][Pt(CN)₄].H₂O (**1**) salt exhibiting an abrupt *SCO* behaviour with a transition temperature of *ca.* 242 K. In combination with the selected bntrz ligand, the initial choice of the rigid tetracyanoplatinate (II) anion has been carefully defined based on (i) the ability of the anion to form covalent linkage or ionic bonding to the neighboring units (e.g. metal complex) in the structural arrangement of a *SCO* material, and (ii) the bias to obtain single crystals with this anionic moiety. The cationic [Fe(bntrz)₃]²⁺ complex displays a polymeric chain, similar to that reported for the Fe^{II} triazole-based systems exhibiting magnetic bistability around or above room temperature. Distinctively from other 1D Fe^{II}/trz systems, the present study clearly evidences the starring roles of the ligand substitution and counter ion changes to prevail over the implicit crystallogenesi s issue in the Fe^{II}/trz systems, with the association of bntrz ligand and [Pt(CN)₄]²⁻ anion leading for the first time to robust single crystals of high quality that withstand the *LS/HS* first-order spin transition. The polymeric chain structure of **1**, crystallographically determined at 296 K and 120 K, is built from two different Fe^{II} centers for which the average values of the Fe-N distances are in agreement with the complete *HS/LS* spin transition revealed by the magnetic data. The thermal variation of the lattice parameters shows anisotropic changes at the transition temperature, and proves that the most pronounced structural changes occur along the 1D covalent chain. The intermolecular inter-chain contacts occur through hydrogen bonding *via* the [Pt(CN)₄]²⁻ anions leading to an overall 3D arrangement. The absence of a wide hysteresis loop in **1** clearly confirms that the overall

long-range interactions are required to promote significant elastic strains which stabilize the spin state changes. The exceptional resilience of the present crystals upon repeated switching cycles is most likely due to the anisotropic expansion/contraction of the unit cell upon *SCO* transition, which allows the existence of a mismatch free *HS/LS* interface. In this context, we are currently investigating by optical microscopy the response of a single crystal of **1** upon thermal *SCO* transition in order to visualize the nucleation, the growth, and the propagation of *HS* and *LS* domains accompanying the first-order transition. The observation of the orientation and the dynamics of the *HS/LS* interface should allow for a better understanding of the role of the anisotropic changes of the lattice parameters on the exceptional resilience of this material. On the other hand, we are also currently exploring other systems exhibiting similar chain, but with different crystal packing to enhance/control the interchain interactions and produce hysteretic features.

Alternatively to the current and longstanding challenge to obtain single crystals of the 1D coordination polymer chains based on the 1,2,4-triazole ligands, new polynuclear triazole-based *SCO* complexes, involving similar structural features are currently extensively studied. Such polynuclear systems could assist the modeling of the *SCO* characteristics of the 1D chain polymers. In this context, several trinuclear triazole-based *SCO* complexes have been reported, with an archetypal linear molecular structure in which the Fe(II) centers are bridged by substituted 1,2,4-triazole ligands. However, in all those complexes, only the central Fe(II) ion shows a *SCO* behavior, while the two terminal ones remain in the *HS* state. Thus, such complexes can be viewed as mononuclear *SCO* complexes in which the single active center displays similar environment than that described for the 1D chain polymers. In addition to deepen the knowledge of the local environment of the Fe(II) active center, the investigations of larger *SCO* molecular discrete complexes, such as “true” trinuclear systems with three *SCO* Fe(II) centers, could be critical to better understand the origin of the cooperativity in such striking 1D systems. In this context, we discussed in **Chapter III** the synthesis and full structural and magnetic characterizations of the first example of triazole-based *SCO* Fe^{II} trinuclear neutral complex [Fe₃(bntrz)₆(tcnset)₆] (**2**) exhibiting a complete one-step spin transition above room temperature ($T_{1/2} \approx 318$ K), and defined to our knowledge as the first *SCO* trinuclear complex exhibiting a complete spin transition. The strategic use of the (tcnset)[−] N-donating based-ligand resides in preventing or limiting the formation of “Fe(II)/1,2,4-triazole” polymeric chains while favoring the coordination of the terminal sites of the polynuclear species by nitrogen groups which are more appropriate for the *SCO*

activity. The one-step nature of the magnetic transition has been notably confirmed by detailed structural studies around the critical region that clearly showed that the thermal evolutions for the three Fe(II) environments are similar and fit adequately the one-step transition from $[LS-LS-LS]$ to $[HS-HS-HS]$ states. In addition, the comparison of the trinuclear structure of $[\text{Fe}_3(\text{bntrz})_6(\text{tcnset})_6]$ (**2**) with the 1D architecture of $[\text{Fe}(\text{bntrz})_3][\text{Pt}(\text{CN})_4]\cdot\text{H}_2\text{O}$ (**1**) described in the first chapter clearly emphasizes the impact of the anion in those “Fe^{II}/bntrz/anion” systems. Indeed, the substitution of the rigid $[\text{Pt}(\text{CN})_4]^{2-}$ tetracyanometallate dianionic moiety by the more flexible $(\text{tcnset})^-$ monoanionic entity induces drastic structural modifications, and distinct dimensionality, even though both derivatives display a one-step spin transition above room temperature (with a T_{SCO} of ca. 242 K and 318 K for **1** and **2**, respectively).

The results obtained in *Chapters II and III* led us to further extend the synthetic strategy developed with compound $[\text{Fe}_3(\text{bntrz})_6(\text{tcnset})_6]$ (**2**) - to other new systems involving the systematic variation of the R' substituent from the functionalized organic polycyanocarbanion $(\text{tcnsR}')^-$ with notably shorter and longer alkyl groups - in order to assess the influence of the latter on the magneto-structural features of the resulting materials. Although preliminary, these results have been considered of relevance to be included in the **Appendix I in the perspective of Chapter III**. In this regard, we initially developed the syntheses of those novel polycyano anionic ligands $(\text{tcnsme})^-$ and $(\text{tcnspr})^-$ as potassium salts following the similar two step procedure previously described for $(\text{tcnset})^-$ ligand. Thus, two new Fe(II) *SCO* systems $[\text{Fe}_3(\text{bntrz})_6(\text{tcnspr})_6]$ (**3**) and $[\text{Fe}_3(\text{bntrz})_8(\text{tcnsme})_2](\text{tcnsme})_2\cdot 4\text{H}_2\text{O}$ (**4**) - based on the combination of bntrz and $(\text{tcnspr})^-$ and $(\text{tcnsme})^-$ ligands, respectively - have been synthesized as single crystals, and preliminarily characterized. The neutral trinuclear complex $[\text{Fe}_3(\text{bntrz})_6(\text{tcnspr})_6]$ (**3**) exhibits similar structural and magnetic behaviours than compound $[\text{Fe}_3(\text{bntrz})_6(\text{tcnset})_6]$ (**2**), as it also displays a single step *SCO* behaviour around room temperature; even though the substitution of the $(\text{tcnset})^-$ by the $(\text{tcnspr})^-$ analogue did not modify the type of spin transition (abrupt - one step), the slight modification of the alkyl group (from ethyl to propyl) in the chemical structure of the polynitrile anion induced a significant drop of ca. 18 K for the transition temperature ($T_{1/2} \approx 318$ K for **2**, and ca. 300 K for **3**). In comparison, the compound $[\text{Fe}_3(\text{bntrz})_8(\text{tcnsme})_2](\text{tcnsme})_2\cdot 4\text{H}_2\text{O}$ (**4**) exhibits a structure clearly distinct from **2** and **3** that is constructed through trinuclear building blocks $[\text{Fe}-(\mu_2\text{-bntrz})_3(\text{bntrz})-\text{Fe}-(\mu_2\text{-bntrz})_3(\text{bntrz})-\text{Fe}]$ and $(\mu_2\text{-tcnsme})^-$ anions, resulting in an alternating chain. Accordingly, the compound **4** displays an expected two step *SCO*

behaviour. A contrario compounds **2** and **3**, the change to a methyl group induced this time a different type of *SCO* behavior in **4**. These results proved ultimately that subtle variations of the R' substituent in the cyanocarbanion tcnsR'^- can play a crucial role on the magneto-structural properties, which suggests the possibility to further exploit this “*Chemical factor*” to fine tune the *SCO* Characteristics - such as the *SCO* temperature - in these triazole based Fe(II) systems.

In a logical continuance of the previous chapters aiming to further evaluate the magneto-structural influence of the nature of the functional group at the 4th position of the 4-R-triazole ligand while maintaining $[\text{Pt}(\text{CN})_4]^{2-}$ moiety as counter-anions, two new 3D materials - $\{\text{Fe}_3(\mu_2\text{-phtptrz})_6[\mu_2\text{-Pt}(\text{CN})_4]_3\} \cdot \text{C}_2\text{H}_5\text{OH}, 5.5\text{H}_2\text{O}$ (**5**) and $\{\text{Fe}(\text{phtptrz})[\text{Pt}(\text{CN})_4] \cdot \text{H}_2\text{O}\}$ (**6**), based on the functionalised triazole 2-(3-(4H-1,2,4-triazol-4-yl)propyl)isoindoline-1,3-dione (phtptrz) - are reported in **Chapter IV**. In comparison with the 4-(benzyl)-4H-1,2,4-triazole (bntrz) ligand involved in the materials described in Chapter II and III, the phtptrz presents a bulkier phtalimido group, with a longer alkyl spacer (three carbons vs. one in bntrz) between the N4 substituent and the triazole motif which provides more flexibility. Although conceived from the same building blocks (with different crystal engineering conditions), the structures and magnetic behaviors of **5** and **6** significantly differ. The 3D arrangement of **5** is built from trinuclear $[\text{Fe1-Fe2-Fe1}]$ units composed of two types of metal centers in distorted octahedral $[\text{FeN}_6]$ environments: the central Fe2 ion is coordinated to six $\mu_2\text{-phtptrz}$ ligands, and the peripheral Fe1 ions of the triads are coordinated to three $\mu_2\text{-phtptrz}$ ligands and three $\mu_2\text{-}[\text{Pt}(\text{CN})_4]^{2-}$ ligands leading to Fe(II) centres with a slightly lower ligand field energy. Distinctly, the 3D structure of **6** consists of $[\text{Fe}(\text{Pt}(\text{CN})_4)]_n$ 2D corrugated layers, involving $[\text{FeN}_5\text{O}]$ spheres and $\mu_4\text{-}[\text{Pt}(\text{CN})_4]^{2-}$, linked through the $\mu_2\text{-phtptrz}$ ligands. The main difference in the 3D structures of **5** and **6** resides in the coordination mode of the phtptrz ligand, with a bridging mode through the triazole motif in **5**, and a hybrid bridging mode involving both the phtalimido and the triazol groups in **6**. This results in higher ligand field strength $[\text{FeN}_6]$ environments in **5** in contrast with the $[\text{FeN}_5\text{O}]$ coordination spheres observed in **6**. Consequently, a two-step *SCO* behavior is observed only in **5**, while **6** shows a characteristic paramagnetic behavior with *HS* Fe^{II} ions in the whole studied temperature range. To our knowledge, compound **5** can be labelled as the first three dimensional *SCO* material based on functionalized triazole-ligand (phtptrz) which has been characterized structurally in *LS* and *HS* states.

In line with the results compiled in the previous *Chapters II and III*, the comparative study of **5** and **6** in *Chapter IV* further evidences that the characteristics of the functionalization of the triazole at the 4th position - i.e. nature/bulkiness of the functional group, length of the alkyl spacer, and overall flexibility in the coordination modes of the 4-R-trz ligand - combined with the nature of the anion (geometry, size/volume, charge, and coordination flexibility) drastically impact the inter-metallic interactions/connectivity *via* covalent bonding, and so the genesis of a *SCO* behavior close to room temperature. In summary, the substitution of the organic polynitrile ligands by inorganic $[\text{Pt}(\text{CN})_4]^{2-}$ analogues in the “ $\text{Fe}^{\text{II}}/\text{bntrz}/\text{Anion}$ ” systems enabled the access to extended 1D networks instead of trinuclear complexes, while the replacement of the bntrz ligand by the bulkier (and more flexible) phtptrz ligand in the “ $\text{Fe}^{\text{II}}/\text{R-trz}/[\text{Pt}(\text{CN})_4]^{2-}$ ” systems led us to 3D architectures with a lower degree of cooperativity. In this respect, the compound **5** can be labelled as the first triazole-bridged Fe^{II} 3D complex which displays a *SCO* behaviour.

However, as already pinpointed in the previous chapters and univocally demonstrated with the syntheses of **5** and **6**, any approach - based exclusively on the nature of the precursors to tailor the design of materials with *SCO* behaviors of relevance - would be ultimately inappropriate, or at least incomplete. Indeed, the two compounds **5** and **6** display very different 3D arrangements and magnetic behaviors, even so they have been synthesized from the exact same starting precursors, i.e. $\text{Fe}(\text{ClO}_4)_2 \cdot x\text{H}_2\text{O}$ and $\text{K}_2[\text{Pt}(\text{CN})_4] \cdot 3\text{H}_2\text{O}$ salts, and phtptrz ligands. The latter observation stresses out the decisive and remarkably underestimated role of the crystal engineering conditions (stoichiometry, concentration, nature/mixture of the solvents, and crystallization technique), not only in obtaining single crystals suitable for X-ray diffraction, but also for the decisive input they can have in the structural arrangements and ensuing *SCO* behaviors of the resulting materials. These results once again highlight the highly sensitive complexity to anticipate and predict the design of *SCO* materials with tuned properties, but also the even more pressing need for systematic and refined magneto-structural correlations, notably with access to single-crystal X-ray diffraction studies at both *HS* and *LS* states, to better understand the driving forces of the spin crossover phenomenon in the so called “triazole family”. In that regard, the convenient and flexible route developed in this work has already been defined as a synthetic platform to access a wide range of 4-R-trz ligands, with functional R groups of various natures; these new ligands, in combination with selected anionic candidates with covalent ability, are already under

investigations, with the aim to refine the roles of the functional group of the 4-R-trz ligands and the anion in the *SCO* behavior.

In fine, the aim is to establish thorough and systematic magneto-structural correlations which are essential to understand the physicochemical origin of the strong cooperativity in such striking materials, but also to rationalize the tuning of the *SCO* properties. It is noteworthy to specify the ‘breakthrough’ of the present work from a structural aspect, as all the *SCO* materials presented in this manuscript have been obtained as single crystals and fully characterized by X-ray diffraction. Thus, with very limited structural data currently available about the triazole based materials, the systematic access to extensive structure/properties studies could expand the knowledge about *SCO* behaviours, and allow some rationalization in a consistent way.

Annex I:
Accepted and Submitted Publications

Cooperative 1D Triazole-Based Spin Crossover Fe^{II} Material With Exceptional Mechanical Resilience

Narsimhulu Pittala,[†] Franck Th  tiot,[†] Smail Triki,^{*,†,  } Kamel Boukheddaden,^{  } Guillaume Chastanet,^{  } and Mathieu Marchiv  ^{  }

[†]UMR-CNRS 6521, University de Brest (UBO), 6 Avenue V. Le Gorgeu, C.S. 93837-29238 Brest Cedex 3, France

^{  }GEMaC, UMR-CNRS 8635, University de Paris-Saclay, 45 Avenue des Etats-Unis, 78035 Versailles, France

^{  }CNRS, University de Bordeaux, ICMCB, UPR 9048, 87 Avenue du Dr. A. Schweitzer, 33608 Pessac, France

Supporting Information

The magnetic spin change associated with the spin crossover (SCO) phenomenon represents a paradigm of bistability at the molecular level that is of current interest because of potential applications in the development of new generations of electronic devices such as nonvolatile memories, molecular sensors and displays.^{1–5} The SCO phenomenon is especially observed in Fe^{II} complexes in which the paramagnetic high spin state (HS, *S* = 2) can be switched reversibly to the low spin state (LS, *S* = 0) by several external stimuli such as temperature, pressure or light irradiation.⁶ A huge effort has been devoted to the understanding of the transition mechanisms using inter alia crystallographic tools.^{7,8} The minimal requirements for the latter involve the determination of the crystal structures in both LS and HS states to comprehend the structural parameters at the molecular and intermolecular scales. Although some systems were deeply investigated due to their remarkable switching properties, the absence of any detailed and punctilious structural informations has precluded the definite understanding of these exciting properties. This is particularly the case of the so-called “triazole family”, more specifically the coordination polymer chains of general formula [Fe(Rtrz)₂(trz)](X), where Rtrz is a functionalized 1,2,4-triazole ligand and X a counteranion, which typically display bistability with wide hysteresis loops around or above room temperature.^{9–11} Although known for a few decades, the major lack of high quality single crystals with complete structural data for those materials prevent any deep magneto-structural correlations that are of paramount importance for (i) the understanding of the origin of the thermal hysteresis loop, and (ii) the control of the transition temperature. Indeed, a deep knowledge of the structural data is required to evaluate notably the effects of the rigid triple $\mu_{1,2}$ -trz bridges and/or the characteristics of the intermolecular contacts on the propagation of the elastic interactions. Owing to the great and intensifying attention given to these materials, scarce crystallographic investigations have been recently attempted. Among them, the structural characterizations of the HS and LS states of the [Fe(Htrz)₂(trz)](BF₄) derivative, using distinctively high-resolution synchrotron X-ray powder diffraction combined with Raman spectroscopy¹² or X-ray diffraction data from high-quality crystalline powder,¹³ have been reported. Although the 1D chain structure was proven for both HS and LS states, the rather limited quality of the diffraction patterns could not provide highly precise structural data suitable for

deep magneto-structural correlations. At the same time, a single crystal of the parent Cu^{II} compound [Cu(NH₂trz)₃](NO₃)₂·3H₂O has been finely investigated by Garcia et al. in parallel with the crystal structure of the [Fe(NH₂trz)₃](NO₃)₂ for which only nanosized thin crystallite needles (120–330 nm) could be prepared. However, the powder diffraction pattern of the latter did not fully fit to the diffraction pattern observed for the single crystals of the Cu^{II} compound.¹⁰ Besides, the lone single crystal structural study proving the presumably 1D character of [Fe(NH₂trz)₃](NO₃)₂·2H₂O was only reported in 2011 by Guionneau et al.¹⁴ However, as clearly claimed by the authors, the very low diffraction pattern induced essentially by the sub-micrometric size (>20 × 1 × 1 μ m) of the crystals and the damages due to the X-ray beam during the data collection led to a rather low quality of the structural data that did not allow an accurate detailed discussion of the polymeric chain structure. In addition, the study, performed at 120 K, concerned only the LS state of the sample because the damages caused on the crystals when warming over room temperature have hindered data collection for the HS state. Ultimately, those recent examples clearly expose the challenge to access refined structural data in both spin states in order to apprehend and rationalize fully the conspicuous SCO properties in the Fe^{II}/trz systems.

In the past few years, some Fe^{II} systems based on functionalized triazole ligands (Rtrz) and different counteranions have been reported.¹¹ However, the majority of the involved counterions are rather standard monoanions, whereas the functional groups (R) of the triazole molecules are essentially narrowed to linear or branched alkyl or alkoxyated chains.¹¹ Recently, we have extended this synthetic approach to combinations of triazole ligands and anions that were not used so far within the “triazole family”; among those combinations, triazole ligands involving rigid aryl groups with an alkyl spacer assuring the electronic integrity of the triazole motif, coupled with more sophisticated anions such as polycyanometallates or organic cyanocarbanions which display very diverse sizes, geometries and charges, have been initially considered.^{15,16} In this ongoing work, we have realized at an early stage that this chemical approach involving these unusual building blocks

Received: September 27, 2016

Revised: December 11, 2016

Published: December 22, 2016

tends to improve unprecedentedly the size, the quality and the robustness of the single crystals of the resulting original $\text{Fe}^{\text{II}}/\text{R-trz}$ systems. Ultimately, this synthetic strategy should allow the access to single crystals of novel SCO cooperative materials, which is essential to understand the origin of the unparalleled cooperativity observed in those 1D coordination polymers. Thus, the present work reports the synthesis, the structural and magnetic characterizations, as well as the first accurate single crystal investigations of both HS and LS states of a new triazole-based SCO Fe^{II} 1-D polymer $[\text{Fe}(\text{bntrz})_3][\text{Pt}(\text{CN})_4] \cdot x\text{H}_2\text{O}$ (**1**).

The bntrz ligand was prepared in two steps by reaction of triethyl orthoformate with formylhydrazine and benzylamine under nitrogen atmosphere (S1). Single crystals of $[\text{Fe}(\text{bntrz})_3][\text{Pt}(\text{CN})_4] \cdot x\text{H}_2\text{O}$ (**1**) have been synthesized via diffusion technique in a fine glass tube (3.0 mm diameter) by layering an ethanolic solution of the bntrz ligand onto an aqueous solution containing both $\text{K}_2[\text{Pt}(\text{CN})_4] \cdot x\text{H}_2\text{O}$ and $\text{Fe}(\text{BF}_4)_2 \cdot 6\text{H}_2\text{O}$ salts (S1). The magnetic susceptibility (χ_m) of **1** was measured over the 2–300 K temperature (T) range on a set of single crystals. The $\chi_m T$ versus T plot is displayed in Figure 1. In the high-temperature region, the $\chi_m T$ value (3.45

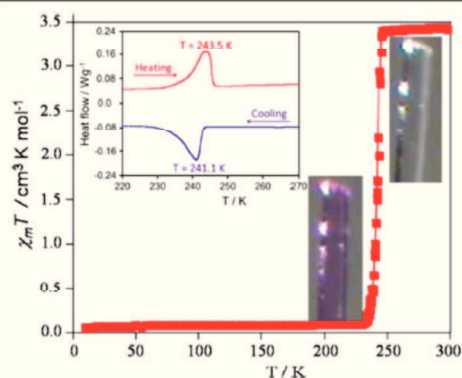


Figure 1. Thermal dependence of the $\chi_m T$ product recorded at 0.4 $\text{K} \cdot \text{mn}^{-1}$ in a settle mode, DSC study recorded at 2 $\text{K} \cdot \text{mn}^{-1}$ (inset), and crystal images in the LS and HS states showing the clear thermochromism from purple to colorless, respectively.

$\text{cm}^3 \cdot \text{K} \cdot \text{mol}^{-1}$) is consistent with a HS ($S = 2$) configuration of the hexacoordinated Fe^{II} ions. Upon cooling, the $\chi_m T$ remains constant down to 240 K, then sharply decreases to ca. 0.0 $\text{cm}^3 \cdot \text{K} \cdot \text{mol}^{-1}$, indicating the presence of a complete sharp HS to LS first-order spin transition ($T_{1/2} = 242$ K). However, no significant thermal hysteresis effects were detected after the warming mode, at the value of the temperature scan rate of 0.4 $\text{K} \cdot \text{mn}^{-1}$. The DSC measurements for **1**, performed in the temperature range 200–260 K with a temperature scan rate of 2 $\text{K} \cdot \text{mn}^{-1}$, reveal exo- and endothermic transitions with maxima at 241.1 and 243.5 K, respectively (inset in Figure 1). Furthermore, the phase transition has been found to occur with an enthalpy and entropy changes of $\Delta H = 16.67 \text{ kJ} \cdot \text{mol}^{-1}$ and $\Delta S = 69.61 \text{ J} \cdot \text{K}^{-1} \cdot \text{mol}^{-1}$, respectively. These values are in the range of those reported in the literature for similar SCO compounds.¹⁷ The presence of a weak hysteresis in the calorimetry data while it was absent in magnetic measurements can be reasonably attributed to the difference of temperature scan rates.

Based on the magnetic and calorimetric measurements, the crystal structure of **1**, defined in the triclinic space group, has been determined at 296 K (HS state, colorless crystal), and at 120 K (LS state, purple crystal) (Table S1). An in-depth examination of the unit cell parameters, at these two temperatures, indicates the absence of any symmetry breaking structural transition within the studied temperature range. The structure of **1** is built from two crystallographically independent Fe^{II} sites, Fe1 and Fe2, and two $[\text{Pt}(\text{CN})_4]^{2-}$ anions located on inversion centers, and three bntrz ligands and one solvent water molecule located on general positions.

The three bntrz ligands act as μ_2 -bridging mode ($\mu_{1,2}$ -bntrz bridges) leading to a regular chain structure running along the [100] direction (Figure 2). The average Fe–N distances and

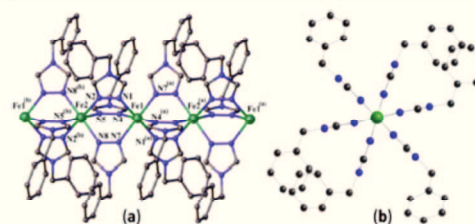


Figure 2. Views of the cationic chain in **1**: (a) linear chain running along the a axis; (b) projection of the chain along the [100] direction. (a) $1-x, -y, 1-z$; (b) $-x, -y, 1-z$.

Table 1. Average Fe–N Distances and Distortion Parameters in **1**

T (K)	296		120	
Fe^{II}	Fe1	Fe2	Fe1	Fe2
$\langle d_{\text{Fe-N}} \rangle$ (Å)	2.190(3)	2.189(3)	1.991(4)	1.998(4)
Σ/Θ (deg)	10/23	10/26	16/40	13/33
spin state	HS	HS	LS	LS

distortion parameters for both spin states are listed in Table 1. The selected Fe–N bond lengths and N–Fe–N bond angles, at 296 and 120 K, are gathered in Table S2. The two crystallographically distinct Fe^{II} ions (Fe1 and Fe2) adopt similar and very regular FeN_6 octahedral geometries, as demonstrated by the unusually low values of Σ and Θ parameters (Table 1).¹⁸ Thus, it is worth noting that the distortion of the octahedrons is higher in the LS state than in the HS state, conversely to what is generally observed. Although more pronounced for Fe1 compared to Fe2, this unusual effect confirms that 1D triazole systems tend to adopt rigid and regular coordination spheres,¹³ but also indicates that the Fe^{II} environment is more constrained in the LS state. The average values of the Fe–N distances, at 296 K (2.190(3), 2.189(3) Å) and 120 K (1.991(4), 1.998(4) Å), are in agreement with the presence of HS and LS states, respectively. The latter observation is consistent with the presence of a complete HS/LS SCO transition, as revealed by the magnetic data.

To understand how the crystal structure is affected by the SCO transition, the temperature dependence of the lattice parameters of a single crystal of **1** was measured in the range 200–280 K. As clearly depicted in Figure 3, the evolution of the

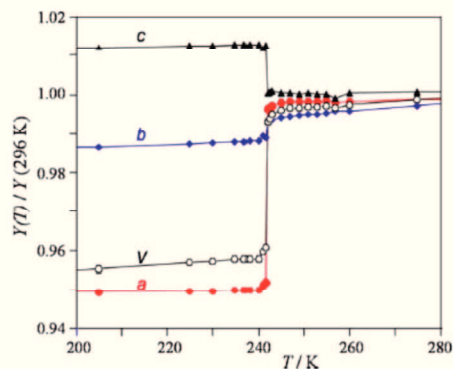


Figure 3. Thermal evolution of the lattice parameters for **1** showing the anisotropic changes upon SCO transition.

unit cell parameters (*a*, *b*, *c*) reveals significant anisotropic changes at the transition temperature (*ca.* 242 K), more precisely a contraction upon heating for the *c* parameter paralleled with positive expansions occurring simultaneously in the *ab* plane. The amplitude of the anisotropic expansion is much more pronounced along the *a* axis, proving that the major structural change accompanying the SCO transition in the overall structure arises along the 1D chain. In comparison with the parent 1D compound $[\text{Fe}(\text{Htrz})_2(\text{trz})](\text{BF}_4)$,¹³ the careful examination of the shortest interchain contacts in **1** reveals the absence of direct H-bonding interchain interactions whereas strong direct H-bonding interchain interactions through the N–H group of the triazole have been identified in $[\text{Fe}(\text{Htrz})_2(\text{trz})](\text{BF}_4)$ (Figures S1 and S2). However, the presence of significant indirect H-bonding, occurring via the $[\text{Pt}(\text{CN})_4]^{2-}$ anions, links the chains in the *b* and *c* directions, leading to an overall 3D packing (Figures 4 and S3). These

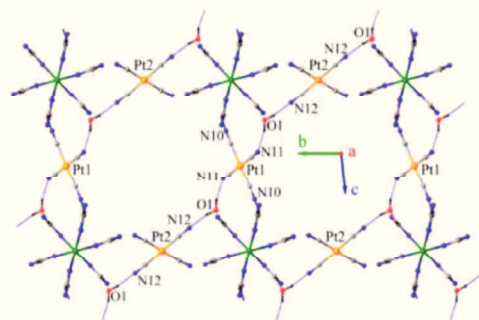


Figure 4. Intermolecular hydrogen bonding contacts in **1** along the *a* direction. Shortest contacts (Å): N11...O1 = 2.944, O1...N12 = 2.995 at 296 K; N11...O1 = 2.888, O1...N12 = 2.883 at 120 K.

interactions in **1** are more pronounced in the *LS* state than in the *HS* state; this observation may explain the more constrained iron geometry along the chain in the *LS* state. The intrachain Fe...Fe distances in **1** are almost similar to those found in $[\text{Fe}(\text{Htrz})_2(\text{trz})](\text{BF}_4)$, in both spin states, whereas the interchain Fe...Fe ones are significantly longer than those

observed in other parent 1D triazole-based derivatives that have been structurally characterized (see Table S3). Moreover, the Fe...Fe intrachain distances in **1** appear also longer in both *HS* and *LS* states than the corresponding distances observed in discrete trinuclear complexes based on triazole ligands,^{19–22} although this latter observation refers only to the few compounds that display “full” *HS* or *LS* states, i.e., involving all the iron centers. Because of the triclinic symmetry of the crystal lattice, the interchain distances do not exactly match the Fe...Fe intermolecular distances, but are shorter because the chains are slightly shifted from each other in the *a* direction (Figure S4). It follows that the interchain distances are different along the *b* and *c* directions. Thus, in the *LS* state, they are shorter in the *b* direction (14.2708(4) Å) compared to the *c* direction (14.5072(4) Å), whereas in the *HS* state, we observe the opposite tendency because the interchain distances along the *b* direction (14.4975(4) Å) are longer than those along the *c* axis (14.2832(4) Å), leading finally to very similar distances in the *LS* and *HS* states, but inverted with respect to *b* and *c* parameters (Figures S5 and S6). These observations indicate a significant motion of the chains with respect to each other in the *bc* plane that co-occurs with a slight gliding along the *a* direction as the chains shift increase during the *LS* to *HS* transition (*ca.* 0.35 Å). Additionally, the *LS* to *HS* transition is accompanied by a rearrangement of the side chain of the triazole ligand, leading to a much better accommodation of the modification of the iron coordination sphere volume in **1** than in the parent compound $[\text{Fe}(\text{Htrz})_2(\text{trz})](\text{BF}_4)$.¹³ Indeed, while the octahedron volume (*V*_p) increases in similar proportions for both compounds (*V*_p increase of 32% for **1** and 36% for $[\text{Fe}(\text{Htrz})_2(\text{trz})](\text{BF}_4)$), the molecular volume remains almost the same for **1** (+0.8%) but increases appreciably for $[\text{Fe}(\text{Htrz})_2(\text{trz})](\text{BF}_4)$ (+4.7%, Table S3). This structural rearrangement of the chains and the related accommodation of the molecular volume to the transition might be responsible for the smaller unit cell volume change at the transition when compared to the parent compound $[\text{Fe}(\text{Htrz})_2(\text{trz})](\text{BF}_4)$ (4.5% vs 11.5%).¹³ Such capability of structural breathing was not observed in $[\text{Fe}(\text{Htrz})_2(\text{trz})](\text{BF}_4)$ and may explain the (i) unusual crystal quality of compound **1** and (ii) its exceptional reliability and mechanical resilience to repeated *LS* to *HS* transition. The latter has been clearly evidenced by crystal mosaicity studies and optical microscopy investigations performed over 20 SCO cycles. Thus, (i) the crystal mosaicity was found to be nearly constant around 0.49(2) between the *LS* and *HS* states (Figure S7), and (ii) no damage or alteration at the resolution of the optical microscopy ($\sim 0.3 \mu\text{m}$) was detected within the single crystal (Figure S8). In addition, an elongation of 5.3% of the crystal upon *LS* to *HS* transition was observed in optical microscopy studies. This value is in excellent agreement with X-ray data that indicates an elongation of 5.32% of the *a* parameter during the *LS*/*HS* thermal transition.

In conclusion, we have prepared and characterized a new triazole-based $[\text{Fe}(\text{bntrz})_3][\text{Pt}(\text{CN})_4] \cdot \text{H}_2\text{O}$ (**1**) salt exhibiting an abrupt spin transition with a transition temperature of *ca.* 242 K. The cationic $[\text{Fe}(\text{bntrz})_3]^{2+}$ complex displays a polymeric chain, similar to that reported for the Fe^{II} triazole-based systems exhibiting magnetic bistability around or above room temperature.^{11–14} The present study clearly evidences the starring roles of the ligand substitution and counterion changes to prevail over the implicit crystallogeneis issue in the Fe^{II} /trz systems, with the association of bntrz ligand and $[\text{Pt}(\text{CN})_4]^{2-}$

C

DOI: 10.1021/acs.chemmater.6b04118
Chem. Mater. XXXX, XXX, XXX–XXX

anion leading for the first time to robust single crystals of high quality and relatively considerable size (up to $0.45 \times 0.04 \times 0.04$ mm) that withstand the *LS/HS* first-order spin transition upon repeated *SCO* cycles. Distinctively from other 1D $\text{Fe}^{\text{II}}/\text{trz}$ systems for which the origin of the strong cooperativity remains strictly indefinite because of the lack of structural information, the characteristics of complex 1 led us to single crystal X-ray data collections of high-quality, allowing highly refined structural characterizations of both high and low spin states, and the thermal evolution of the lattice parameters. The polymeric chain structure of 1, crystallographically determined at 296 and 120 K, is built from two different Fe^{II} centers for which the average values of the Fe–N distances are in agreement with the complete *HS/LS* spin transition revealed by the magnetic data. The crystal structures of the *LS* and *HS* states definitely confirm the perfect linearity of the chains of such polymeric triazole-based *SCO* compounds, even in the *HS* state conversely to what was suggested from the first investigations based on EXAFS and WAXS studies.^{23,24} The thermal variation of the lattice parameters shows anisotropic changes at the transition temperature, and proves that the most pronounced structural changes occur along the 1D covalent chain. The intermolecular interchain contacts occur through hydrogen bonding via the $[\text{Pt}(\text{CN})_4]^{2-}$ anions leading to an overall 3D arrangement. Although displaying cooperativity, the absence of a wide hysteresis loop in the *SCO* of 1 reveals that the strong short-range “ $\text{Fe}^{\text{II}}\text{-(Rtrz)}_5\text{-Fe}^{\text{II}}$ ” interactions along the chain are not sufficient to drive the existence of long lifetime metastable states at the origin of thermal hysteresis; it also confirms that the overall long-range interactions, with an emphasis on the direct contacts between the chains, should play a crucial role to promote significant elastic strains that stabilizes the spin state changes. The exceptional resilience of the present crystals upon repeated switching cycles is most likely due to the accommodation of the molecular volume and the anisotropic expansion/contraction of the unit cell upon *SCO* transition, which allows the existence of a mismatch free *HS/LS* interface resulting from the capability of the “ $\text{Fe}^{\text{II}}\text{-(Rtrz)}$ ” chains to glide from each other and accommodate the structural modifications despite the sharp transition. This observation is similar to that of the spin-crossover single crystals $[\{\text{Fe}(\text{NCSe})(\text{py})_2\}_2(\text{m-bppz})]$ (with *py* = pyridine and *bppz* = 3,5-bis(2-pyridyl)pyrazolate) recently reported by K. Boukheddaden et al.²⁵ In this context, we are currently investigating by optical microscopy the response of a single crystal of 1 upon thermal *SCO* transition in order to visualize the nucleation, the growth, and the propagation of *HS* and *LS* domains accompanying the first-order transition.²⁶ The observation of the orientation and the dynamics of the *HS/LS* interface should allow for a better understanding of the role of the anisotropic changes of the lattice parameters on the exceptional resilience of this material. On the other hand, we are also currently exploring other systems exhibiting similar chain, but with different crystal packing to enhance/control the interchain interactions and produce hysteretic features. *In fine*, the aim is to establish thorough and systematic magneto-structural correlations that are essential to understand the physicochemical origin of the strong cooperativity in such striking materials, and also to rationalize the tuning of the *SCO* properties.

■ ASSOCIATED CONTENT

Supporting Information

The Supporting Information is available free of charge on the ACS Publications website at DOI: 10.1021/acs.chemmater.6b04118.

Experimental details, syntheses of the ligands, the complex 1 and characterizations (PDF)

X-ray crystallographic data for CCDC 1492971 (CIF)

X-ray crystallographic data CCDC 1492972 (CIF)

■ AUTHOR INFORMATION

Corresponding Author

*S. Triki. E-mail: Smail.Triki@univ-brest.fr.

ORCID

Smail Triki: 0000-0003-0130-7461

Author Contributions

All authors contributed equally to this work.

Notes

The authors declare no competing financial interest.

■ ACKNOWLEDGMENTS

This work was supported by the CNRS, the Universities of Brest, Paris-Saday and Bordeaux, the “Agence Nationale de la Recherche” (ANR project BISTA-MAT: ANR-12-BS07-0030-01), the European community (FP7Marie-Curie project: PCIG-GA-2011-304193 NANOCOORD), and the “Région Bretagne” for the funding of this work. We thank M. Sy and G. Bouchez for the optical microscopy measurements.

■ REFERENCES

- (1) Phan, H.; Benjamin, S. M.; Steven, E.; Brooks, J. S.; Shatruk, M. Photomagnetic response in highly conductive $\text{Fe}(\text{II})$ spin-crossover complexes with TCNQ radicals. *Angew. Chem., Int. Ed.* 2015, 54, 823–827.
- (2) Ohkoshi, S.-I.; Tokoro, H. Photomagnetism in cyano-bridged bimetal assemblies. *Acc. Chem. Res.* 2012, 45, 1749–1758.
- (3) Coronado, E.; Galán-Mascarós, J. R.; Monrabal-Capilla, M.; García-Martínez, J.; Pardo-Ibáñez, P. Bistable spin-crossover nanoparticles showing magnetic thermal hysteresis near room temperature. *Adv. Mater.* 2007, 19, 1359–1361.
- (4) Kahn, O.; Jay-Marine, C. Spin transition polymers: from molecular materials toward memory devices. *Science* 1998, 279, 44–48.
- (5) Gülich, P.; Hauser, A.; Spiering, H. Thermal and optical switching of iron(II) complexes. *Angew. Chem., Int. Ed. Engl.* 1994, 33, 2024–2054.
- (6) Halcrow, M. A. *Spin-Crossover Materials: Properties and Applications*, John Wiley & Sons, 2013.
- (7) Halcrow, M. A. Structure: function relationships in molecular spin-crossover complexes. *Chem. Soc. Rev.* 2011, 40, 4119–4142.
- (8) Guionneau, P. Crystallography and spin-crossover. A view of breathing materials. *Dalton Trans.* 2014, 43, 382–393.
- (9) Lavrenova, L. G.; Ikorskii, V. N.; Varnek, V. A.; Oglezneva, I. M.; Larionov, S. V. High-temperature spin transition in coordination compounds of iron(II) with triazoles. *Koord. Khim.* 1986, 12, 207–215.
- (10) Dirtu, M. M.; Neuhausen, C.; Naik, A. D.; Rotaru, A.; Spinu, L.; Garcia, Y. Insights into the origin of cooperative effects in the spin transition of $[\text{Fe}(\text{NH}_2\text{trz})_3](\text{NO}_3)_2$ the role of supramolecular interactions evidenced in the crystal structure of $[\text{Cu}(\text{NH}_2\text{trz})_3](\text{NO}_3)_2 \cdot \text{H}_2\text{O}$. *Inorg. Chem.* 2010, 49, S723–S736.
- (11) Roubeau, O. Triazole-Based One-Dimensional Spin-Crossover Coordination Polymers. *Chem. - Eur. J.* 2012, 18, 15230–15244.
- (12) Urakawa, A.; Van Beek, W.; Monrabal-Capilla, M.; Galán-Mascarós, J.-R.; Palín, L.; Milanesio, M. Combined, modulation

enhanced X-ray powder diffraction and raman spectroscopic study of structural transitions in the spin crossover material $[\text{Fe}(\text{Htrz})_2(\text{trz})](\text{BF}_4)$. *J. Phys. Chem. C* **2011**, *115*, 1323–1329.

(13) Grosjean, A.; Négrier, P.; Bordet, P.; Etrillard, C.; Mondieig, D.; Pechev, S.; Lebraud, E.; Létard, J.-F.; Guionneau, P. Crystal Structures and Spin Crossover in the Polymeric Material $[\text{Fe}(\text{Htrz})_2(\text{trz})](\text{BF}_4)$ Including Coherent-Domain Size Reduction Effects. *Eur. J. Inorg. Chem.* **2013**, *2013*, 796–802.

(14) Grosjean, A.; Daro, N.; Kauffmann, B.; Kaiba, A.; Létard, J.-F.; Guionneau, P. The 1-D polymeric structure of the $[\text{Fe}(\text{NH}_2\text{trz})_n](\text{NO}_3)_2 \cdot n\text{H}_2\text{O}$ (with $n = 2$) spin crossover compound proven by single crystal investigations. *Chem. Commun.* **2011**, *47*, 12382–12384.

(15) Atmani, C.; El Hajj, F.; Benmansour, S.; Marchivie, M.; Triki, S.; Conan, F.; Patinec, V.; Handel, H.; Dupouy, G.; Gómez-García, C. J. Guidelines to design new spin crossover materials. *Coord. Chem. Rev.* **2010**, *254*, 1559–1569.

(16) Milin, E.; Patinec, V.; Triki, S.; Bendeif, E.-E.; Pillet, S.; Marchivie, M.; Chastanet, G.; Boukheddaden, K. Elastic Frustration Triggering Photoinduced Hidden Hysteresis and Multistability in a Two-dimensional photoswitchable Hofmann-like spin-crossover metal-organic framework. *Inorg. Chem.* **2016**, *55*, 11652–11661.

(17) Roubeau, O.; Castro, M.; Burriel, R.; Haasnoot, J. G.; Reedijk, J. Calorimetric Investigation of Triazole-Bridged Fe(II) Spin-Crossover One-Dimensional Materials: Measuring the Cooperativity. *J. Phys. Chem. B* **2011**, *115*, 3003–3012.

(18) Marchivie, M.; Guionneau, P.; Létard, J.-F.; Chasseau, D. Photo-induced spin-transition: the role of the iron(II) environment distortion. *Acta Crystallogr., Sect. B: Struct. Sci.* **2005**, *61*, 25–28.

(19) Gómez, V.; Benet-Buchholz, J.; Martín, E.; Galán-Mascarós, J.-R. Hysteretic Spin Crossover above Room Temperature and Magnetic Coupling in Trinuclear Transition-Metal Complexes with Anionic 1,2,4-Triazole Ligands. *Chem. - Eur. J.* **2014**, *20*, 5369–5379 and refs therein.

(20) Gómez, V.; Sáenz de Pipaón, C.; Maldonado-Illescas, P.; Waerenborgh, J. C.; Martín, E.; Benet-Buchholz, J.; Galán-Mascarós, J.-R. Easy Excited-State Trapping and Record High T_{HIST} in a Spin-Crossover Polyanionic Fe(II) Trimer. *J. Am. Chem. Soc.* **2015**, *137*, 11924–11927.

(21) Sáenz de Pipaón, C.; Maldonado-Illescas, P.; Gómez, V.; Galán-Mascarós, J.-R. Spin Transition Kinetics in the Salt $[\text{H}_2\text{N}(\text{CH}_2)_2]_6[\text{Fe}_3(\text{L})_6(\text{H}_2\text{O})_6]$ ($\text{L} = 4 \cdot (1,2,4\text{-Triazol-4-Yl})\text{-ethanesulfonate}$). *Magnetochemistry* **2016**, *2* (2), 20.

(22) Klein, Y.; Sciortino, N.; Housecroft, C.; Kepert, C.; Neville, S. Structure and Magnetic Properties of the Spin Crossover Linear Trinuclear Complex $[\text{Fe}_3(\text{furtrz})_6(\text{ptol})_2(\text{MeOH})_4] \cdot 4(\text{ptol}) \cdot 4(\text{MeOH})$ (Furtrz: Furanylidene-4H-1,2,4-Triazol-4-Amine Ptol: P-Tolylsulfonate). *Magnetochemistry* **2016**, *2* (1), 7.

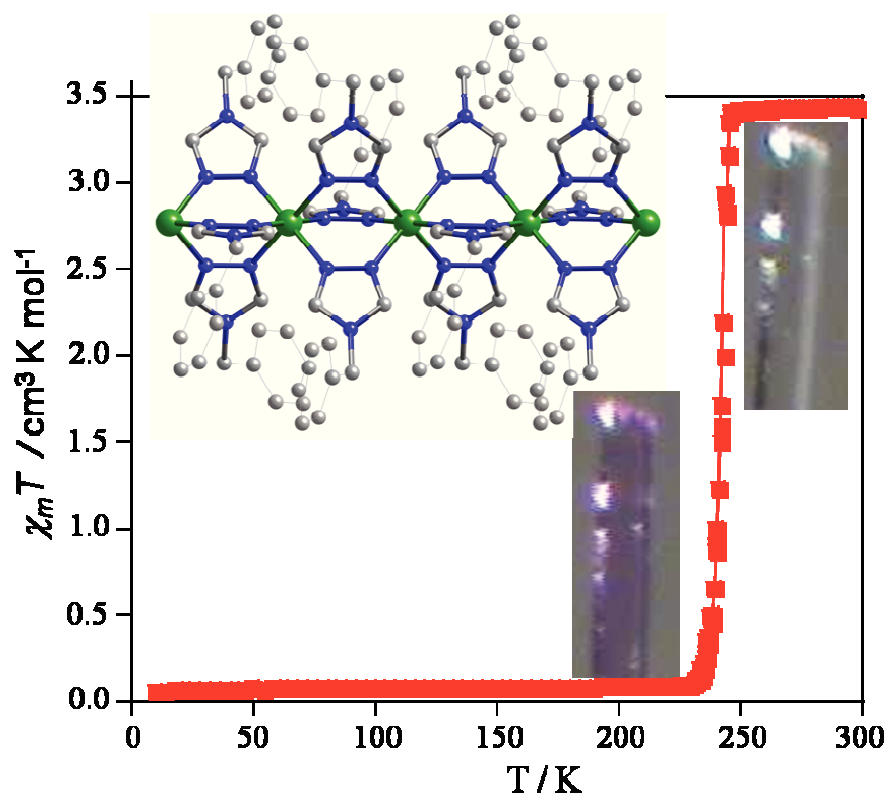
(23) Michalowicz, A.; Moscovici, J.; Ducourant, B.; Cracco, D.; Kahn, O. EXAFS and X-ray powder diffraction studies of the spin transition molecular materials $[\text{Fe}(\text{Htrz})_2(\text{trz})](\text{BF}_4)$ and $[\text{Fe}(\text{Htrz})_3](\text{BF}_4)_2 \cdot \text{H}_2\text{O}$ (Htrz = 1,2,4-4H-triazole; trz = 1,2,4-triazolato). *Chem. Mater.* **1995**, *7*, 1833–1842.

(24) Verelst, M.; Sommier, L.; Lecante, P.; Mosset, A.; Kahn, O. Structural Study by Wide-Angle X-ray Scattering of the Spin Transition Molecular Materials $[\text{Fe}(\text{Htrz})_2(\text{trz})](\text{BF}_4)$ and $[\text{Fe}(\text{NH}_2\text{trz})_3](\text{NO}_3)_2$ (Htrz = 1,2,4-4H-Triazole, trz = 1,2,4-Triazolato). *Chem. Mater.* **1998**, *10*, 980–985.

(25) Sy, M.; Varret, F.; Boukheddaden, K.; Bouchez, G.; Marrot, J.; Kawata, S.; Kaizaki, S. Structure-driven orientation of the high-spin-low-spin interface in a spin-crossover single Crystal. *Angew. Chem., Int. Ed.* **2014**, *53*, 7539–7542.

(26) Sy, M.; Garrot, D.; Slimani, A.; Paez-Espejo, M.; Varret, F.; Boukheddaden, K. Reversible control by light of the high-spin low-spin elastic interface inside the bistable region of a robust spin-transition single crystal. *Angew. Chem., Int. Ed.* **2016**, *55*, 1755–1759.

Table of Contents artwork



Supplementary information

Cooperative 1D Triazole-Based Spin Crossover Fe^{II} Material With Exceptional Mechanical Resilience

Narsimhulu Pittala,[†] Franck Th  tiot,[†] Smail Triki,^{*,†} Kamel Boukheddaden,[‡] Guillaume Chastanet,[§] and Mathieu Marchivie[§]

[†]UMR-CNRS 6521, University de Brest (UBO), 6 Av. V. Le Gorgeu, C.S. 93837 - 29238 Brest Cedex 3 -France

[‡]GEMaC, UMR-CNRS 8635, University de Paris-Saclay, 45 Avenue des Etats-Unis 78035 Versailles, France

[§]CNRS, University de Bordeaux, ICMCB, UPR 9048, 87 avenue du Dr A. Schweitzer, F-33608 Pessac, France

1 - Syntheses

a - General considerations

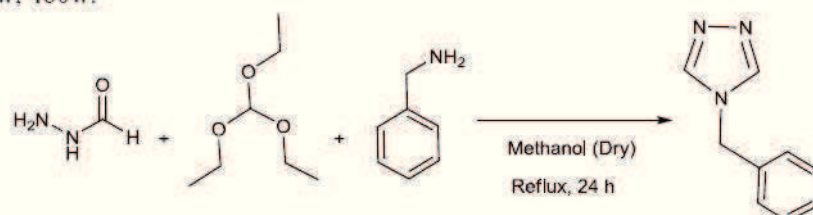
All the starting reagents were purchased from commercial sources (Sigma-Aldrich, Across, Fisher Scientific, Alfa Aesar and Merck) and used without further purification unless otherwise stated. Deuterated solvents were purchased from Sigma-Aldrich and Cambridge Isotope Laboratories. Dried solvents were prepared by refluxing for one day under dinitrogen over the appropriate drying agents (magnesium and iodine for methanol; sodium for ethanol), and then degassed before use. Solvents were stored in glass ampoules under argon. Alternatively, they could be obtained from a solvent purification device (MBRAUN). All glassware and cannula were stored in an oven (>373 K). When appropriate, the reactions were carried out under argon or nitrogen by using a dual manifold vacuum/argon line and standard Schlenk techniques.

b - Synthesis of the functionalized triazole ligand: 4-(benzyl)-1,2,4-triazol (bntrz)

The 4-(benzyl)-1,2,4-triazol (bntrz) ligand was synthesized by modifying a previously reported method (see scheme 1).^{1,2} A solution of triethyl orthoformate (12.0 mL, 72 mmol) and formylhydrazine (3.6 g; 60 mmol) in 50 mL of freshly distilled anhydrous methanol was refluxed for 4 hours. Then, the benzylamine (6.6 mL, 60 mmol) was added to the solution under nitrogen atmosphere, and the mixture was further refluxed for 24 hours. After removal of the solvent

under reduced pressure, the resulting pale pink solid was dissolved in 100 mL of methanol and ether in 8:2 ratio. The resulting solution was kept in a freezer for 2 days. Finally, the product was filtered and washed with ether to obtain a white crystalline powder. Yield: 5.7 g, 60 %.

^1H NMR (300 MHz, CDCl_3) : δ , 5.1 (s, 2H, CH_2), 7.06-7.09(m, 2H, CH), 7.25-7.28 (m, 3H, CH), 8.06 (s, 2H, $\text{CH}=\text{N}$). ^{13}C NMR (300 MHz, CDCl_3) : δ , 48.8 (Ar-C-N), 127.4 (Ar-C), 128.7 (Ar-C), 129.1(Ar-C), 134.1 (Ar-C), 142.7(N-C=N). IR data (ν , cm^{-1}): 3129w, 3084w, 3029w, 2972w, 1679w, 1534w, 1519w, 1496w, 1454w, 1379w, 1365w, 1338w, 1207w, 1181m, 1074w, 1031w, 1001w, 975w, 957w, 891w, 841w, 816w, 768w, 711s, 690m, 638m, 615w, 578w, 460w.



Scheme 1. Synthesis of the triazole derivative 4-(Benzyl)-1,2,4-triazol (bntrz).

c - Single-crystals preparation of complex $[\text{Fe}(\text{bntrz})_3][\text{Pt}(\text{CN})_4]\cdot\text{H}_2\text{O}$ (**1**)

Single-crystals of **1** were prepared by slow diffusion in a fine glass tube (3.0 mm diameter). An aqueous solution (5 mL) of $\text{K}_2[\text{Pt}(\text{CN})_4]\cdot x\text{H}_2\text{O}$ (0.1 mmol, 37.7 mg) and an aqueous solution (5 mL) of $\text{Fe}(\text{BF}_4)_2\cdot 6\text{H}_2\text{O}$ (0.1 mmol, 33.7mg) were mixed with stirring; a white turbid solution was obtained after 1 hour. Then, an ethanol solution (3 mL) of triazole ligand (0.3 mmol, 47.7 mg) was carefully layered onto the above solution with addition of a small amount of pure solvent as buffer between the two solutions to slowdown the diffusion. White needle colorless crystals of **1**, suitable for X-ray analysis, were formed over a period of *ca.* three weeks (Yield 53 %, 45.1 mg). Anal. Calcd for $\text{C}_{31}\text{H}_{20}\text{FeN}_{13}\text{OPt}$: C, 43.7; H, 3.4; N, 21.4 %. Found: C, 44.1; H, 3.4; N, 21.7 %. IR data (ν , cm^{-1}): 3418br, 3054w, 3013w, 2119m, 1608w, 1551m, 1496w, 1496w, 1444w, 1394w, 1221w, 1192w, 1090m, 1026m, 716s, 688w, 644s, 617w, 494w, 469w, 405w, 393w, 359w, 277m, 250m, 229w, 207w, 159s, 128s, 117s, 95m, 78w, 46s, 35m.

It is worth mentioning that the synthetic procedure specifically targeting the formation of 1D derivatives / chains would have been the reaction between the iron(II) salt and the R-trz molecule (1:3 ratio) and addition the $[\text{Pt}(\text{CN})_4]^{2-}$ anion as counter-ion. However, this reaction leads, as expected, to an insoluble amorphous powder of $[\text{Fe}(\text{bntrz})_3](\text{BF}_4)_2$, since the direct reaction of $\text{Fe}(\text{BF}_4)_2\cdot 6\text{H}_2\text{O}$ and bntrz - with the bntrz moiety specifically involving a rigid aryl group with an alkyl spacer assuring the electronic integrity of the triazole motif - favors the formation of the bridging coordination mode of the trz ligand, as observed for the Htrz and NH_2trz ligands.

2 - Physical measurements and characterizations

Single crystal X-ray studies were performed at 296 K and 120 K on Xcalibur 2 κ -CCD diffractometer using Mo K α radiation ($\lambda = 0.71073$ Å). The corresponding structures were solved by direct methods with the SHELXS program and refined on F^2 by weighted full matrix least-squares methods using the SHELXL program.³ All non-hydrogen atoms were refined

anisotropically, hydrogen atoms were located in difference Fourier maps and treated using a riding model. Crystallographic data and refinement details are provided in Table S1. ^1H and ^{13}C NMR spectra were recorded on Bruker AMX-300 spectrometer, and the spectra were referenced internally using residual proton solvent resonances relative to tetramethylsilane ($\delta = 0$ ppm). DSC measurements were performed on a DSC-1/LN2 Mettler Toledo calorimeter setting the heat flow scan rate at $s = 2 \text{ K}\cdot\text{min}^{-1}$. Magnetic measurements were performed with a Quantum Design MPMS-XL-5 SQUID magnetometer in the 2-300 K temperature range with an applied magnetic field of 2 Tesla and scan rate of $0.4 \text{ K}\cdot\text{min}^{-1}$ on single crystals of compound **1** ($m = 6.67 \text{ mg}$) prepared in a sealed polypropylene bag whose diamagnetic contribution was removed. Infrared (IR) spectra were collected in the range $4000\text{--}35 \text{ cm}^{-1}$ on a FT-IR BRUKER ATR VERTEX70 Spectrometer. Elemental analyses were performed at the “Service de microanalyse”, CNRS, 91198 Gif-sur-Yvette, France.

3 - X-ray crystallography

Table S1. Crystal data and structural refinement parameters for compounds **1**.

Compound	1	
Temperature / K	296(2)	120(2)
Empirical formula	C ₃₁ H ₂₉ FeN ₁₃ OPt	C ₃₁ H ₂₉ FeN ₁₃ OPt
Formula weight /g.mol ⁻¹	850.61	850.61
Wavelength / Å	0.71073 Å	0.71073 Å
Space group	<i>P</i> -1	<i>P</i> -1
a / Å	7.8931(2)	7.4945(2)
b / Å	14.5363(4)	14.2896(4)
c / Å	14.6867(4)	14.8234(4)
α / °	94.860(2)	95.640(2)
β / °	103.461(2)	101.855(2)
γ / °	94.187(2)	92.943(2)
Volume / Å ³	1625.41(8)	1541.93(8)
Z	2	2
D _{calc} / g.cm ⁻³	1.738	1.832
Abs. Coef. / mm ⁻¹	4.793	5.052
F(000)	836	836
Crystal size / mm ³	0.27 × 0.03 × 0.03	0.27 × 0.03 × 0.03
2 θ range / °	6.83 - 52.74	6.62 - 52.74
Refl. collected	19574	18768
Unique refl. / R _{int}	6620 / 0.0576	6308 / 0.0608
Data / restr. / N _v	6620 / 2 / 436	6308 / 2 / 436
^a R1/ ^b wR2	0.0350 / 0.0807	0.0342 / 0.1010
^c Goof	1.031	1.089
$\Delta\rho_{\text{max/min}}$ / eÅ ⁻³	1.19/-0.85	1.41 / -1.44
CCDC No.	1492971	1492972

$$^a\text{R1} = \sum |F_o - F_c| / F_o, ^b\text{wR2} = \{\sum [w(F_o^2 - F_c^2)^2] / \sum [w(F_o^2)^2]\}^{1/2}, ^c\text{Goof} = \{\sum [w(F_o^2 - F_c^2)^2] / (N_{\text{obs}} - N_{\text{var}})\}^{1/2}$$

Table S2. Selected Fe-N bond lengths and N-Fe-N bond angles for **1** at 296 K and 120 K

Compound	1	
<i>T</i> / K	296	120
Fe1-N1	2.179(3)	1.988(3)
Fe1-N4	2.210(3)	2.000(4)
Fe1-N7	2.182(3)	1.985(3)
<Fe1-N>	2.190(3)	1.991(4)
Fe2-N2	2.176(3)	1.998(3)
Fe2-N5	2.195(3)	2.001(4)
Fe2-N8 ^(a)	2.195(3)	1.994 (4)
<Fe2-N>	2.189(3)	1.998(4)
N1-Fe1-N7	91.08(12)	91.30(14)
N1-Fe1-N7 ^(a)	88.92(12)	88.70(14)
N1-Fe1-N4	89.28(12)	88.32(14)
N1-Fe1-N4 ^(a)	90.72(12)	91.68(14)
N7-Fe1-N4	90.57(12)	91.09(14)
N7 ^(a) -Fe1-N4	89.43(12)	88.91(14)
^a Σ	10(2)	16(2)
^b Θ	23(3)	40(3)
N2-Fe2-N8	89.50 (12)	89.47(15)
N2-Fe2-N8 ^(b)	90.50(12)	90.53(15)
N2-Fe2-N5 ^(b)	91.04(12)	91.58(15)
N2-Fe2-N5	88.96(12)	88.42(15)
N8-Fe2-N5	90.99(12)	89.01(16)
N8 ^(b) -Fe2-N5	89.01(12)	90.99(16)
^a Σ	10(2)	13(2)
^b Θ	26(3)	33(3)

^aΣ⁴ is the sum of the deviation from 90° of the 12 cis-angles of the FeN₆ octahedron; ^bΘ⁴ is the sum of the deviation from 60° of the 24 trigonal angles of the projection of the FeN₆ octahedron onto its trigonal faces. Symmetry transformations used to generate equivalent atoms: (a) 1-x, -y, 1-z; (b) = -x, -y, 1-z.

Table S3. Comparison of some structural parameters between **1** and parent 1D triazoles bridged compounds $[\text{Fe}(\text{Htrz})_2(\text{trz})](\text{BF}_4)^5$ and $[\text{Fe}(\text{NH}_2\text{trz})_3](\text{NO}_3)_2 \cdot n\text{H}_2\text{O}^6$.

	Compound 1		$[\text{Fe}(\text{Htrz})_2(\text{trz})](\text{BF}_4)$		$[\text{Fe}(\text{NH}_2\text{trz})_3](\text{NO}_3)_2 \cdot n\text{H}_2\text{O}$
Spin State	<i>HS</i>	<i>LS</i>	<i>HS</i>	<i>LS</i>	<i>LS</i>
Fe ^{III} -Fe intra-chain distances (Å)	3.9466(2)	3.7473(2)	3.894(1)	3.6624(6)	3.656(2)
Fe ^{III} -Fe inter-chain distances (Å) (crystallographic direction between chains)	14.5264(4) (010)	14.2896(4) (010)	9.970(1) (101)	9.816(1) (101)	10.562(3) (010)
	14.6867(4) (001)	14.8234(4) (001)	9.564(1) (001)	9.191(1) (001)	11.339(3) (001)
Inter-chain distances (Å) (crystallographic direction between chains)	14.4975(4) (010)	14.2708(4) (010)	9.970(1) (101)	9.816(1) (101)	10.513(3) (010)
	14.2832(4) (001)	14.5072(4) (001)	9.564(1) (001)	9.191(1) (001)	11.226(3) (001)
Shift along the chain direction (Å) (crystallographic direction between chains)	1.0614(4) (010)	0.7328(4) (010)	0 (101)	0 (101)	1.016(1) (010)
	3.4180(4) (001)	3.0454(4) (001)	0 (001)	0 (001)	1.597(1) (001)
V_p^1 (Å ³)	14.0	10.6	14.0	10.3	10.5
Molecular volume ² (Å ³)	1686	1673	737	704	820

¹Volume of the octahedron around the Fe atom calculated using the OLEX2 subroutine *calcvol*⁷.

²Molecular volume calculated from 5 adjacent $\text{Fe}(\text{trz})_3$ units plus one Fe atom using the OLEX2 subroutine *vvol*⁷.

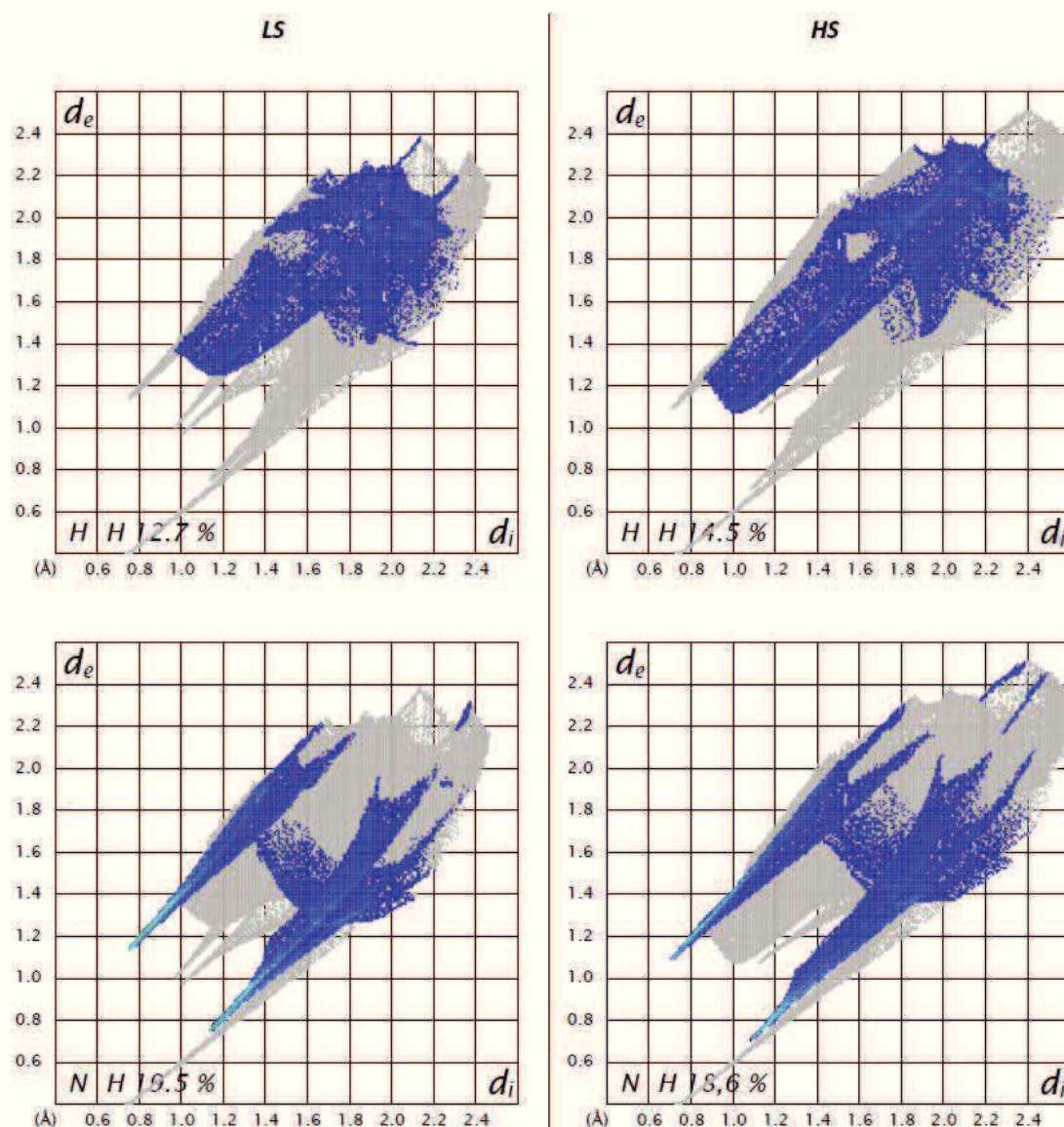


Figure S1. Fingerprints⁸ showing the intermolecular interactions in $[\text{Fe}(\text{Htrz})_2(\text{trz})](\text{BF}_4)_5$ in the *LS* and *HS* states. Top: H-H intermolecular contacts and bottom: N-H intermolecular contacts. Strong direct chain-chain hydrogen bonding interactions are clearly evidenced by sharp spikes on N-H fingerprints with low d_e/d_i couple. These interactions are also present in the *HS* state with slightly lower d_e/d_i . The H-H interactions are strongly affected by the *SCO* as d_i/d_e couples are much lower in the *HS* state than in the *LS* state. This feature that goes against the thermal expansion is likely a consequence of the strong direct inter-chain contacts.

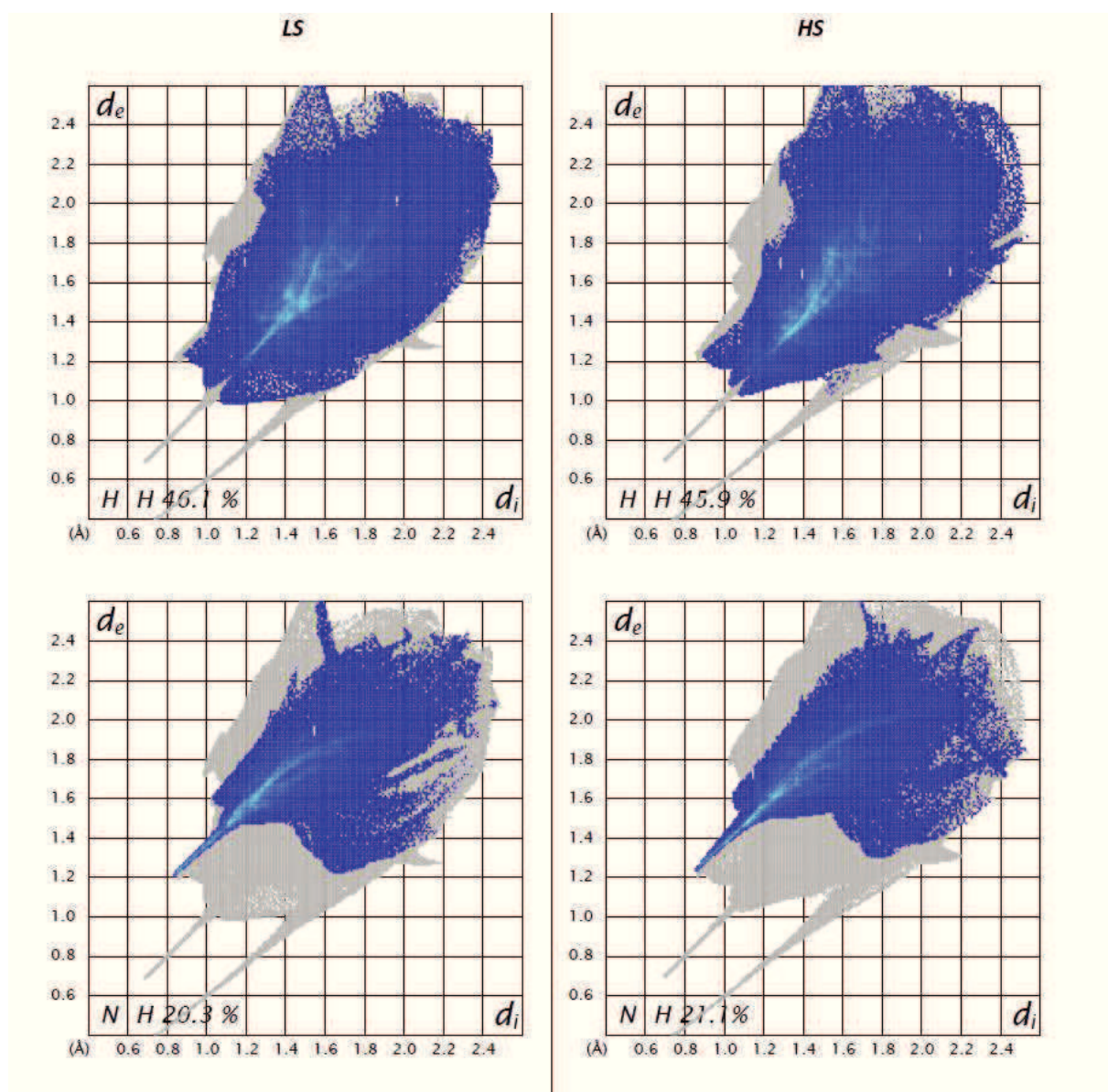


Figure S2. Fingerprints⁸ showing the intermolecular interactions in **1** in the *LS* and *HS* states. Top: H-H intermolecular contacts and bottom: N-H intermolecular contacts. Hydrogen bonding interactions are evidenced by the sharp spike on N-H fingerprints with relatively low d_e/d_i couple. These interactions are also present in the *HS* state with slightly higher d_e/d_i distances and constitute the principal intermolecular contacts. They do not involve directly two different chains but link the chains via the $[\text{Pt}(\text{CN})_4]^{2-}$ anion. The H-H interactions are not affected by the *SCO* as the d_i/d_e couples are slightly higher in the *HS* state than in the *LS* state, in agreement with the thermal expansion.

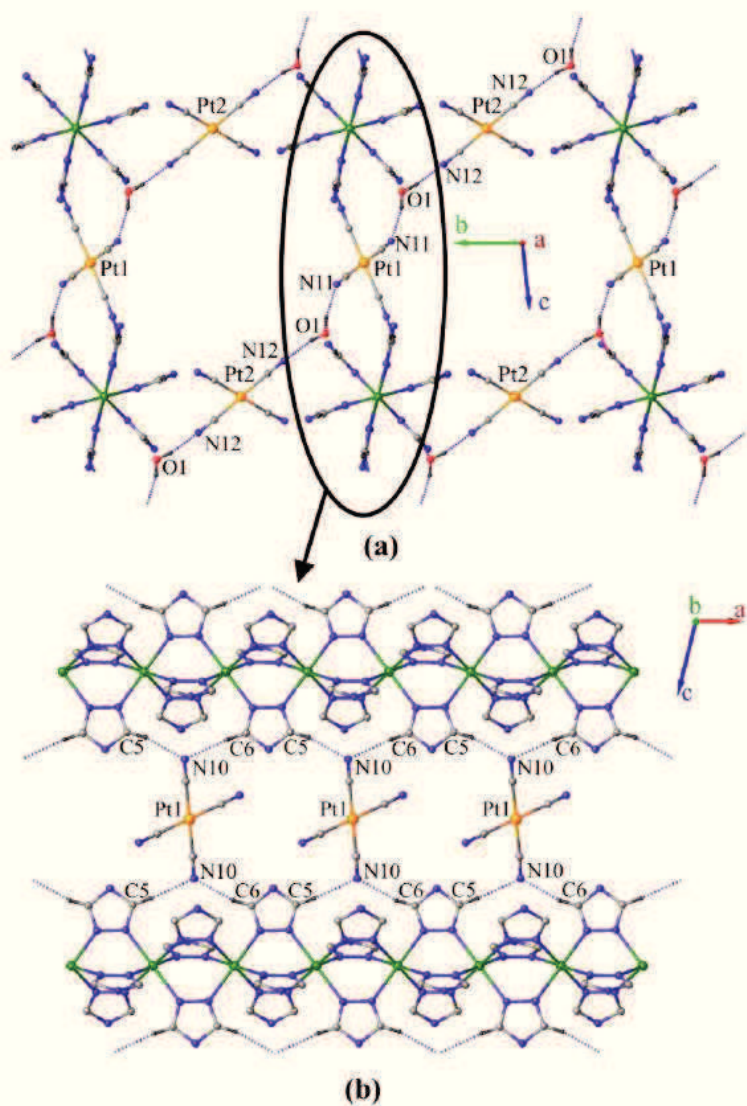


Figure S3 Intermolecular hydrogen bonding contacts in **1** (a) along the *a* direction and (b) along the *b* direction. Shortest contacts (Å): N11 \cdots O1 = 2.944, O1 \cdots N12 = 2.995; C5 \cdots N10 = 3.119; C6 \cdots N10 = 3.219 at 296 K; N11 \cdots O1 = 2.888, O1 \cdots N12 = 2.883; C5 \cdots N10 = 3.054; C6 \cdots N10 = 3.111 at 120 K. (H atoms and benzyl group of the triazole ligand have been omitted for clarity).

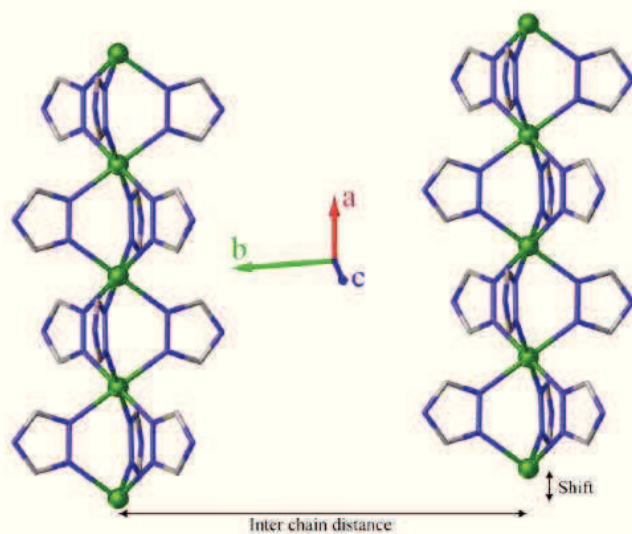


Figure S4. View of **1** showing the inter-chains distance in the *b* direction and the shift of the chain in the *a* direction (H atoms and benzyl group of the triazole ligand, and anions have been omitted for clarity).

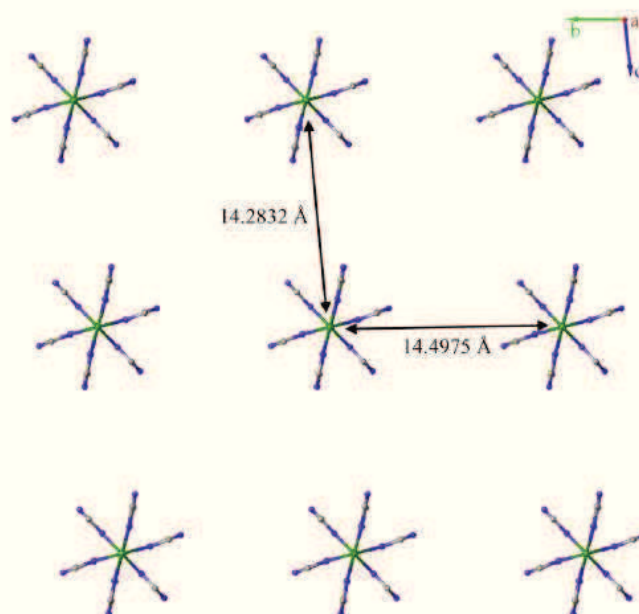


Figure S5. View of **1** along the (100) direction showing the inter-chains distances in the *b* and *c* direction at 296 K in the *HS* state (H atoms and benzyl group of the triazole ligand, and anions have been omitted for clarity).

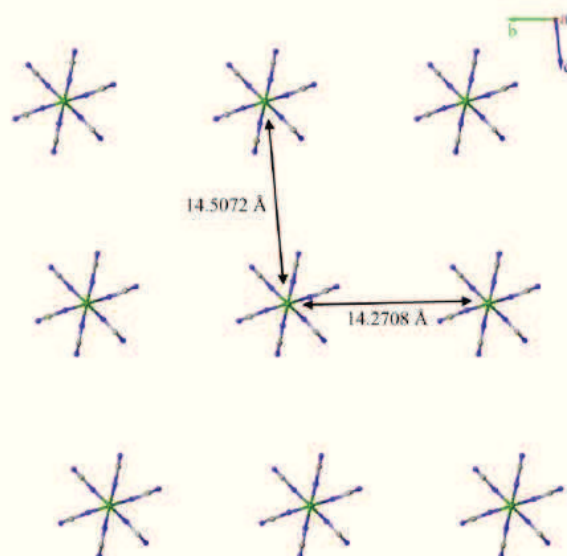


Figure S6. View of **1** along the (100) direction showing the inter-chains distances in the b and c direction at 120 K in the *LS* state (H atoms and benzyl group of the triazole ligand, and anions have been omitted for clarity).

4 - Mechanical resilience study.

a - Crystal mosaïcity studies

The mechanical resilience study has been performed by following the evolution of the crystal mosaïcity upon several thermal cycles, including around the *SCO*. As it was underlined in a earlier study, the mosaïcity given by diffractometers strongly depends on the instrumental setup and the choice of the crystal (i.e. size and shape).⁹ The given value is only relative to the crystal and the chosen experimental setup. Thus, it must be done on the same single crystal and measured in exactly the same conditions.

A colourless single crystal of $0.3 \times 0.05 \times 0.05 \text{ mm}^3$ were mounted on a goniometer head using a Mytigen Kapton® micromount with a little drop of paraffin oil and cooled to 260 K. The whole experiment was performed with the same crystal mounted exactly in the same position on the goniometer. The data collection consisted in a 183 ϕ -scan completed by a 56 ω -scan to get a reasonable completeness of the data to a resolution of 0.76 \AA^{-1} . The value of mosaïcity were obtained by integration using the DENZO program.¹⁰ The *HS-LS-HS* cycles were performed between 260 K in the *HS* state and 200 K in the *LS* state with a cooling or warming rate of 6 K.min^{-1} . The crystal has been firstly cooled down to 200 K, and then warmed up again to 260 K. Data collection has been recorded before the first cycle at 260 K, and then after each cycle between the 1st and the 8th cycle, and finally each two cycles between the 10th and 20th cycle at 260 K. Additionally, data were collected in the same condition at 200 K in the *LS* state during the first cycle to compare the *LS* and *HS* mosaïcity that was found identical (0.48(2) and 0.47(2) respectively). The results are depicted in Figure S7.

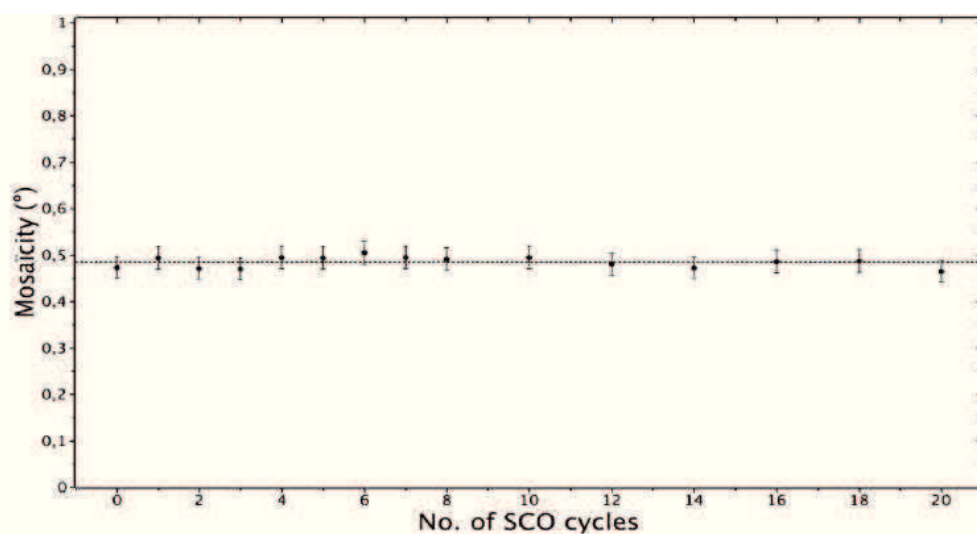


Figure S7. Evolution of the crystal mosaicity of **1** in the *HS* state at 260 K as a function of *SCO* cycles. The dashed line corresponds to the mean observed mosaicity of $0.49(2)^\circ$.

b - Optical microscopy studies

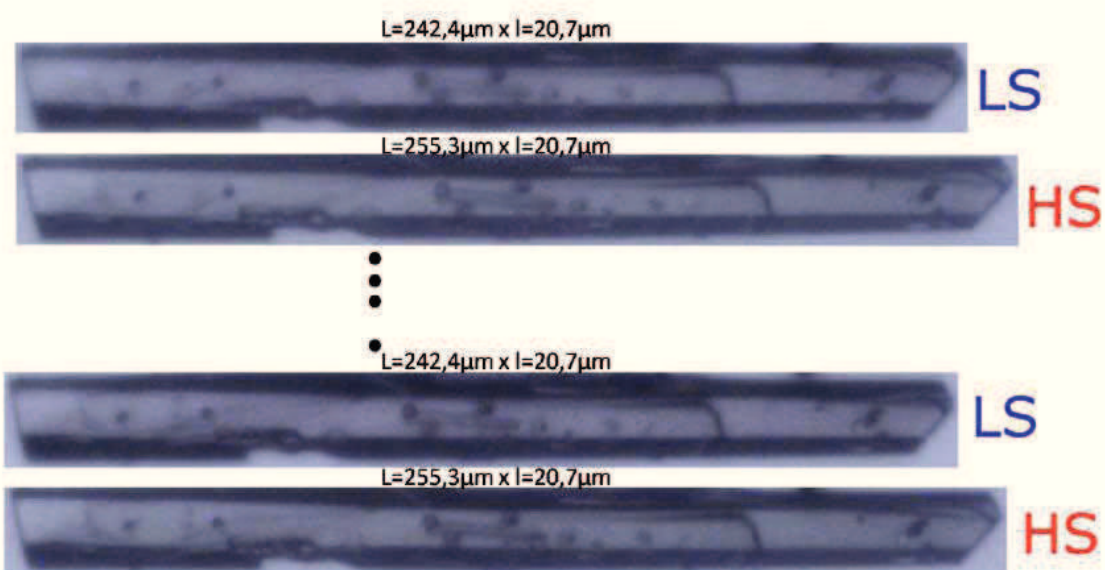


Figure S8. Transmission images of the crystal **1** under study, with a 20x magnification objective (N.A.= 0.4). The crystal size is $\sim 686 \text{ pixel} \times 55 \text{ pixel} \sim 247 \text{ } \mu\text{m} \times 29 \text{ } \mu\text{m}$. The crystal thickness was estimated $\sim 10 \text{ } \mu\text{m}$.

Figure S8 displays the evolution of the crystal quality of **1** by optical microscopy¹¹ during the *HS/LS* cycles after twenty heating and cooling cycles within the same single crystal. The crystal was found to be very robust since no damage or alteration, at the resolution of the optical microscopy (~0.3 micron), was detected. Notice that an elongation of 5.3 % of the crystal upon *LS* to *HS* transition is observed. This value is in excellent agreement with X-rays data which indicates an elongation of 5.32 % of the *a*, parameter during the *LS* to *HS* conversion. On the other hand, the change of the crystal's width at the transition is almost negligible, and in agreement with the relatively weak thermal evolution observed by X-ray diffraction for both *b* and *c* parameters during the *HS/LS* transition.

References

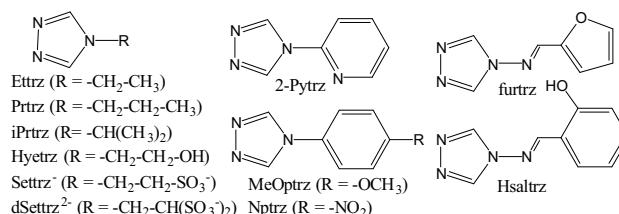
- (1) Bayer, H. O.; Cook, R. S.; von Mayer, W.C.; *US Patent 3821376*, **1974**.
- (2) Bayer, H. O.; Cook, R. S.; von Mayer, W.C.; *US Patent 3647810*, **1972**.
- (3) Sheldrick, G. M., *Acta Cryst.* **2008**, *A64*, 112.
- (4) a) Guionneau, P.; Marchivie, M.; Bravic, G.; Létard, J.-F.; Chasseau, D., *Top. Curr. Chem.* **2004**, *234*, 97-128; b) Marchivie, M.; Guionneau, P.; Létard, J.-F.; Chasseau, D., *Acta Cryst. B*, **2005**, *B61*, 25-28.
- (5) Grosjean, A.; Négrier, P.; Bordet, P.; Etrillard, C.; Mondieig, D.; Pechev, S.; Lebraud, E.; Létard, J. F.; Guionneau, P., *Eur. J. Inorg. Chem.*, **2013**, *2*, 796–802.
- (6) Grosjean, A.; Daro, N.; Kauffmann, B.; Kaiba, A.; Létard, J.-F.; Guionneau, P., *Chem. Commun.*, **2011**, *47*, 12382–12384.
- (7) Dolomanov, O. V.; Bourhis, L. J.; Gildea, R. J.; Howard, J. A. K.; Puschmann, H., *J. Appl. Crystallogr.*, **2009**, *42*, 339–341.
- (8) Spackman, M. A.; McKinnon, J. J., *CrystEngComm*, **2002**, *4*, 378-392; McKinnon, J. J.; Spackman, M. A.; Mitchell, A. S., *Acta Crystallogr. Sect. B Struct. Sci.*, **2004**, *60*, 627–668; S. K. Wolff, D. J. Grimwood, J. J. McKinnon, M. J. Turner, D. Jayatilaka, M. A. Spackman, *CrystalExplorer (Version 3.1)*, University of Western Australia, **2012**.
- (9) Guionneau, P.; Lakhloufi, S.; Lemee-Cailleau, M. H.; Chastanet, G.; Rosa, P.; Mauriac, C.; Létard, J. F., *Chem. Phys. Lett.* **2012**, *542*, 52–55.
- (10) Otwinowski, Z.; Minor, W., *Methods Enzymol.* **1997**, *276*, 307–326.
- (11) Slimani A.; Varret F.; Boukheddaden K.; Garrot D.; Oubouchou H.; Kaizaki S.; *Phys. Rev. Lett.* **2013**, *110*, 087208

Unprecedented complete one-step spin transition above room temperature in a trinuclear Fe(II) triazole-based complex†

Narsimhulu Pittala,^a Franck Th  tiot,^a Smail Triki,^{*a} Kamel Boukheddaden,^b Guillaume Chastanet^c and Mathieu Marchivie.^c

We report an original triazole-based trinuclear Fe^{II} complex [Fe₃(bntrz)₆(tcnset)₆] (1) (bntrz = 4-(benzyl)-1,2,4-triazole, tcnset[−] = 1,1,3,3-tetracyano-2-thioethylpropenide anion) as the first related example to date that displays a complete spin transition. Magnetic and heat capacity measurements, and variable temperature X-ray diffraction revealed a one-step first-order [HS-HS-HS]↔[LS-LS-LS] transition above room temperature ($T_{1/2}$ = 318 K).

Among the molecular switchable materials, the spin crossover (SCO) complexes are particularly of interest, notably because of their potential applications in the development of new generations of electronic devices such as memory, molecular sensing and displays.¹ When the spin pairing energy is close to the splitting energy,^{1,2} a SCO transition between the high-spin state (HS, $S = 2$, $^5T_{2g}$) and low-spin state (LS, $S = 0$, $^1A_{1g}$) can be induced by different external solicitations such as temperature, pressure, magnetic field and light irradiation.^{2,3} To date, Iron (II) metal complexes involving [FeN₆] octahedron coordination spheres have been the most studied SCO compounds. Among the few systems exhibiting remarkable SCO behavior, the binary systems based on the 1,2,4-triazole ligands still remain among the most promising materials for future electronic devices since some of them, such as the coordination polymer chains of general formula [Fe((NH₂-trz)₃](X)₂ and [Fe(Htrz)₂(trz)](X) (NH₂-trz = 4-amino-1,2,4-triazole, Htrz = 4-H-1,2,4-triazole, trz[−] = 1,2,4-triazolato, X[−] = standard monoanions), display wide hysteresis loops around room temperature.⁴ However, the current and longstanding challenge to obtain single crystals of such coordination polymers make difficult to access structural data at the molecular and inter-molecular scales which are essential to understand and fine tune their SCO characteristics such as the origin of their strong cooperativity. Alternatively, new polynuclear triazole-based SCO complexes, involving similar structural features i.e. triple bridges based on functionalized 1,2,4-triazole, similar Fe(II) environments, and/or chain sections, are currently extensively studied.⁵⁻⁹ Such polynuclear systems could assist the modeling of the SCO characteristics of the 1D chain polymers. In this context, several trinuclear triazole-based SCO complexes have been reported, with an archetypal linear molecular structure in which the Fe(II) centers are bridged by substituted 1,2,4-triazole ligands (see Scheme 1).⁵⁻⁸



Scheme 1. Examples of functionalized 1,2,4-triazole ligands in trinuclear Fe(II) SCO complexes.⁵⁻⁸

The polynuclear triazole-based systems can be categorized in two different families: (i) the complexes involving neutral functionalized 1,2,4-triazole ligands, which typically display gradual SCO behavior with a transition temperature in the range 150-330 K;⁵⁻⁷ and (ii) the second family composed of few recent examples based on anionic triazole ligands such as the 4-(1,2,4-triazol-4-yl)ethanesulfonate (Settrtz[−]), and the 4-(1,2,4-triazol-4-yl)ethanedisulfonate substituted triazole molecules (dSettrtz^{2−}).⁸ Referring to the latter, two series have been reported; the first one concerns complexes of formula [Fe₃(Settrtz)₆(H₂O)₆] \cdot nH₂O ($n = 8$) based on the monoanionic ligand Settrtz[−]. the derivative displays a gradual SCO behavior at 150 K and hysteretic transition above room temperature ($T_{1/2}(\uparrow) = 357$ K, $T_{1/2}(\downarrow) = 343$ K when partially dehydrated ($n = 5$).^{8a} The second series is composed from the unique SCO trinuclear anionic complex (Me₂NH₂)₆[Fe₃(dSettrtz)₆(H₂O)₆] that exhibits a large hysteretic cycle above room temperature ($T_{1/2}(\uparrow) = 400$ K, $T_{1/2}(\downarrow) = 310$ K) and a temperature of relaxation, T_{TIESST} , of 240 K which is the highest temperature observed in a switchable molecular material.^{8b}

^a UMR CNRS 6521, Univ. de Brest (UBO), C.S. 93837 - 29238 Brest Cedex 3 – France

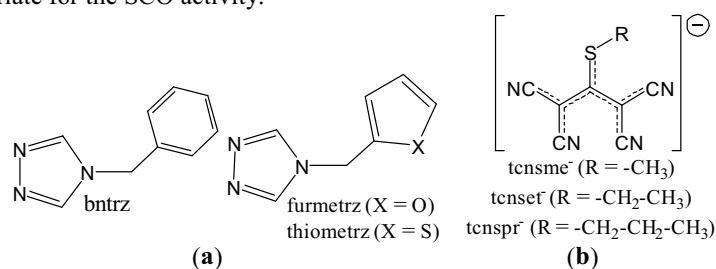
^b UMR-CNRS 8635, Univ. Paris-Saclay, 45 Avenue des Etats-Unis 78035 Versailles, France.

^c CNRS, Univ. Bordeaux, ICMCB, UPR 9048, 87 avenue du Dr A. Schweitzer, F-33608 Pessac, France

*Contact author: smail.triki@univ-brest.fr

† Electronic Supplementary Information (ESI) available: Full experimental details. X-ray crystallographic files (CIF) are available from Cambridge Crystallographic Data Centre (CCDC 1500724, 1500725 and 1500728-1500740). See <http://www.ccdc.cam.ac.uk/contents/retrieving.html>

However, in all these complexes, only the central Fe(II) ion shows a SCO behavior, while the two terminal ones coordinated to two or three water molecules (or other oxygenated solvent molecules and/or anions) remain in the HS state.⁵⁻⁸ Thus, those trinuclear complexes can be viewed as mononuclear SCO complexes in which the single active center displays similar environment than that described for the 1D chain polymers. In addition to deepen the knowledge of the local environment of the Fe(II) active center, the investigations of larger SCO molecular discrete complexes, such as “true” trinuclear systems with three SCO Fe(II) centers, could be critical to better understand the origin of the cooperativity in such striking 1D systems. In this context, we have extended this polynuclear synthetic approach to combinations of new functionalized triazole ligands such as those depicted in scheme 2a, and cyanocarbanions (Scheme 2b) which can act as co-ligands through their N-donor nitrile groups. The strategic use of the latter N-donating based-ligands resides in preventing or limiting the formation of “Fe(II)/1,2,4-triazole” polymeric chains while favoring the coordination of the terminal sites of the polynuclear species by nitrogen groups which are more appropriate for the SCO activity.



Scheme 2. New 1,2,4-triazole ligands (a) and cyanocarbanions (b).

The present work reports the synthesis and full structural and magnetic characterizations of the first example of triazole-based SCO Fe^{II} trinuclear neutral complex [Fe₃(*bntrz*)₆(*tcnset*)₆] (**1**) exhibiting a complete one-step spin transition above room temperature. The 4-(benzyl)-1,2,4-triazole (*bntrz*) molecule was prepared by reaction of triethylorthoformate with formylhydrazine and benzylamine under nitrogen atmosphere (see detailed synthesis, ESI†).¹⁰ The 1,1,3,3-tetracyano-2-thioethylpropenide anion was prepared as potassium salt (K(*tcnset*)) according to a modified procedure (see detailed synthesis, ESI†).¹¹ Single crystals of **1** have been synthesized using diffusion technique in fine glass tube (3.0 mm diameter) by layering methanolic solution of the *bntrz* ligand onto aqueous solution containing K(*tcnset*) and Fe(BF₄)₂·6H₂O (detailed synthesis, ESI†). Compound **1** has been structurally characterized at 360 K (HS state, colorless crystal), 170 K (*LS* state, pink crystal), and around the critical region (280-345 K) (see Tables S1-S2, ESI†). The magnetic susceptibility (χ_m) for **1** was measured over the 2-300 K temperature (*T*) range on a single crystal sample. The thermal variation of the $\chi_m T$ product is displayed in Fig. 1.

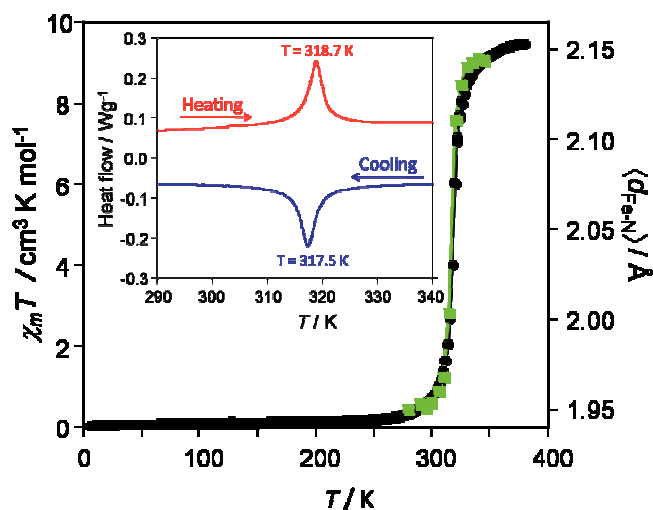


Fig. 1 Thermal evolutions of the $\chi_m T$ product in the 2-380 K range (●), and of the average Fe-N distances (■) around the critical region (280-345 K, $T_{1/2} = 318$ K) for **1**, Inset: DSC study for **1** showing the exo- and endo-thermic transitions.

At 380 K, the $\chi_m T$ value ($9.48 \text{ cm}^3 \cdot \text{K} \cdot \text{mol}^{-1}$) is consistent with three isolated HS ($S = 2$) hexacoordinated Fe(II) ions. Upon cooling, $\chi_m T$ decreases gradually down to a temperature value of *ca.* 320 K. Below this temperature, it sharply decreases to *ca.* $0.0 \text{ cm}^3 \cdot \text{K} \cdot \text{mol}^{-1}$ around *ca.* 250 K, indicating the presence of a sharp and complete *HS* to *LS* SCO first-order phase transition at 318 K. Upon warming and cooling at a scan rate of 1 K/mn in settle mode, no thermal hysteresis effects were detected. The DSC study for **1**, performed in the temperature range 290–340 K with a temperature scan rate of 2 K/mn, shows exo- and endo-thermic transitions with maxima at 317.5 and 318.7 K, respectively (Inset Fig. 1), in agreement with the magnetic data. This phase transition occurs with an enthalpy and entropy changes of $\Delta H = 54.08 \text{ kJ} \cdot \text{mol}^{-1}$ and $\Delta S = 170.00 \text{ J} \cdot \text{K}^{-1} \cdot \text{mol}^{-1}$, respectively. These values are in the same range with those reported in the literature for similar *SCO* compounds.¹² Based on the magnetic observations, the crystal structure of **1** has been determined at 360 K and 170 K. At both temperatures, compound **1** crystallizes in the trigonal *R*-3 space group. Selected Fe–N bond lengths and N–Fe–N bond angles at 360 K and 170 K are gathered in Table S2 (ESI†). Average Fe–N distances and distortion parameters for both metal centers (Fe1 and Fe2) are listed in Table 1 for the two spin states. The unit cell parameters, which are similar at both temperatures, indicate the absence of any structural transition within the studied temperature range (170–360 K). The structure of **1** is built from two crystallographically independent Fe(II) ions (Fe1 and Fe2), located on $(2/3 \ 1/3 \ 5/6)$ and $(2/3 \ 1/3 \ z)$ special positions, respectively, and one *bntrz* molecule and one *tcnset*[−] anion both located on general positions.

The molecular structure of **1** consists of a neutral trinuclear complex of the formula $[\text{Fe}_3(\text{bntrz})_6(\text{tcnset})_6]$ which can be viewed as $[\text{Fe}_2(\text{bntrz})_3\text{Fe}_1(\text{bntrz})_3\text{Fe}_2]$ linear and centrosymmetric fragment in which the central metal ion (Fe1) is bound on both sides to two other Fe(II) centers (Fe2) through three μ_2 -bridging *bntrz* ligands (Fig. 2). The central metal ion (Fe1) is surrounded by six nitrogen atoms from six equivalent μ_2 -*bntrz* ligands, while each external Fe2 ion adopts FeN_3N_3 octahedral environments arising from three equivalent bridging *bntrz* ligands and three unidentate *tcnset*[−] anions (Fig. 2).

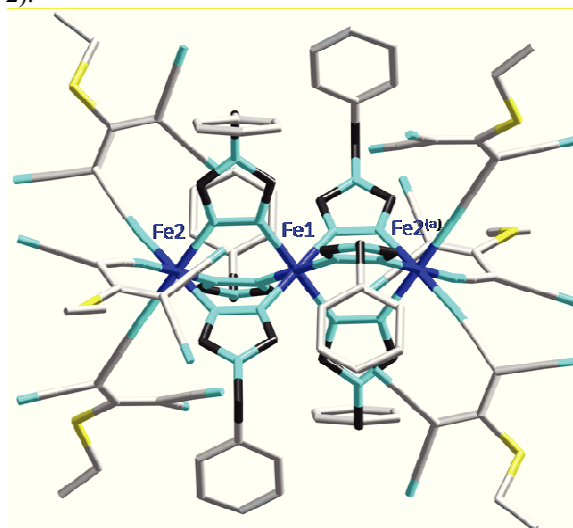


Fig. 2 View of the centrosymmetric trinuclear complex in **1**. (a) $2/3$ -x, $4/3$ -y, $1/3$ -z.

Table 1 Average Fe–N distances ($\langle d_{\text{Fe-N}} \rangle$) and distortion parameters[§] for **1**.

T (K)	170		360	
*Fe ^{II} center	Fe1	Fe2	Fe1	Fe2
Fe1–N1	1.970(3)		2.175(2)	
Fe2–N2		1.962(2)		2.170(2)
Fe2–N4		1.943(3)		2.146(3)
$\langle d_{\text{Fe-N}} \rangle$ (Å)	1.970(3)	1.953(3)	2.175(2)	2.158(3)
$\Sigma \theta$ (°)	4(1) / 5(2)	8(1) / 14(2)	8(1) / 9(2)	24(1) / 39(2)
Spin state	<i>LS</i>	<i>LS</i>	<i>HS</i>	<i>HS</i>

*The two Fe(II) environments are defined by N1 ($[\text{Fe}_1(\text{N1})_6]$) and by N2 and N4 ($[\text{Fe}_2(\text{N2})_3(\text{N4})_3]$) nitrogen atoms.

Examination of the Fe-N bonds and the N-Fe-N bond angles, for both Fe^{II} environments (Fe1 and Fe2), reveals that the central Fe1 ion adopts a regular FeN₆ octahedral geometry which is defined by six equivalent nitrogen atoms ([Fe1(N1)₆]); while the two equivalent external Fe2 centers, surrounded by two different nitrogen atoms ([Fe2(N2)₃(N4)₃]), display a more distorted octahedron geometry, as demonstrated by the values of Σ and Θ parameters[§] (Table 1)¹³ which are relatively low, but significantly higher than those observed for the Fe1 environment. The average values of the Fe-N distances at 360 K ($d_{\text{Fe1-N}} = 2.175(2)$ Å and $\langle d_{\text{Fe2-N}} \rangle = 2.158(3)$ Å) and 170 K ($d_{\text{Fe1-N}} = 1.975(3)$ and $\langle d_{\text{Fe2-N}} \rangle = 1.953(3)$ Å) are in agreement with the presence of HS and LS states, respectively. This observation is consistent with the presence of a complete [HS-HS-HS] \leftrightarrow [LS-LS-LS] SCO transition as initially revealed by the magnetic data. The most intriguing and atypical characteristic in the SCO behavior of compound **1** concerns the presence of a one-step transition despite the presence of two chemically different metal centers (Fe2-Fe1-Fe2) as revealed by the crystal data for the two spin states. Thus, in order to undoubtedly confirm the absence of a two-step transition, and to further understand the evolution of each Fe(II) environment (Fe1 and Fe2) during the transition, the crystal structure of **1** has been solved every 5 K between 280 K and 345 K (see CCDC numbers 1500728-1500740). These additional structural investigations have not revealed any change of symmetry on the whole temperature range, but have shown similar thermal evolution of the average Fe-N distances ($\langle d_{\text{Fe-N}} \rangle$) for the two Fe(II) centers, fitting utterly the thermal magnetic behavior (see Fig. 3). This latter observation clearly suggests that both iron centers of the trinuclear complex, although in different crystallographic environments, are similarly affected by the spin transition, which is consistent with the observed one-step transition from [LS-LS-LS] to [HS-HS-HS] states.

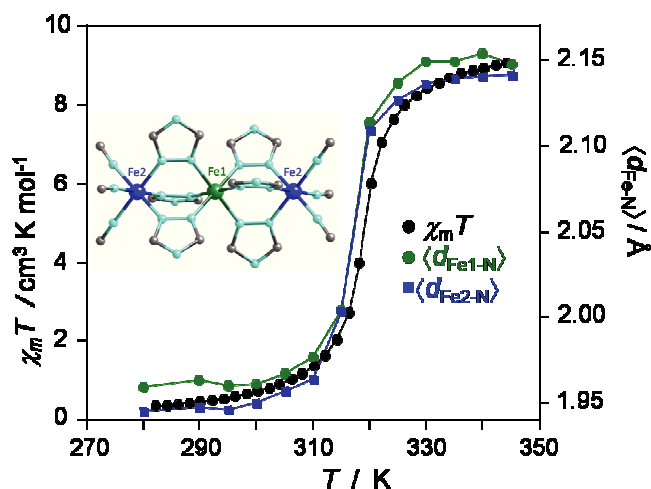


Fig. 3 Thermal evolutions of the average Fe-N distances of each Fe(II) center (Fe1 and Fe2) in the trinuclear units of **1** ([Fe2-Fe1-Fe2]), and of the $\chi_m T$ product in the 280-340 K range.

The careful examination of the shortest inter-molecular contacts (π -stacking, hydrogen bonding and Van der Waals contacts) in **1** reveals that the trinuclear moieties are linked together by six hydrogen bonds involving the triazole ring and the CN branches from the cyanocarbanions of adjacent trinuclear complexes. Such inter-trinuclear contacts lead to a supramolecular chain oriented along the *c* parameter (Fig. 4). The corresponding chains are connected to each other through Van der Waals contacts involving the S-Et groups of the cyanocarbanions. During the HS to LS transition, the inter-trinuclear separations show a decrease of 0.124(3) Å along the *c* axis. This contraction induces a structural rearrangement of the cyanocarbanions and the side chains of the triazoles, leading to an unexpected increase of the inter-chain distances from 15.043 Å to 15.106 Å when cooling from 360 K down to 170K.

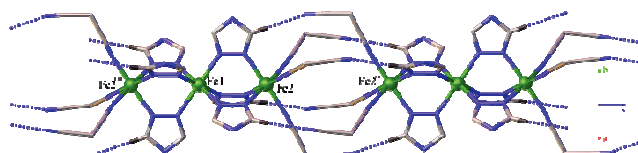


Fig. 4 View of **1** along the direction axis showing the hydrogen bond contacts between trinuclear units: C2...N5 = 3.329 (4) Å at 360 K; C2...N5 = 3.151(4) Å at 170 K. (a) = 2/3-x, 4/3-y, 1/3-z.

In summary, we have prepared and fully characterized a new trinuclear $[\text{Fe}_3(\text{bntrz})_6(\text{tenset})_6]$ (**1**) neutral complex that exhibits a one-step spin transition above room temperature ($T_{1/2} = 318$ K), and defined to our knowledge as the first SCO trinuclear complex exhibiting a complete spin transition. The one-step nature of the magnetic transition has been notably confirmed by detailed structural studies around the critical region that clearly showed that the thermal evolutions for the three Fe(II) environments are similar and fit adequately the one-step transition from [LS-LS] to [HS-HS-HS] states.

We thank the CNRS, the Universities of Brest, Paris-Saclay and Bordeaux, the "Agence Nationale de la Recherche" (ANR project BISTA-MAT: ANR-12-BS07-0030-01), the European community (FP7 Marie-Curie project: PCIG-GA-2011-304193 NANOCOORD), and the "Région Bretagne" for the funding of this work.

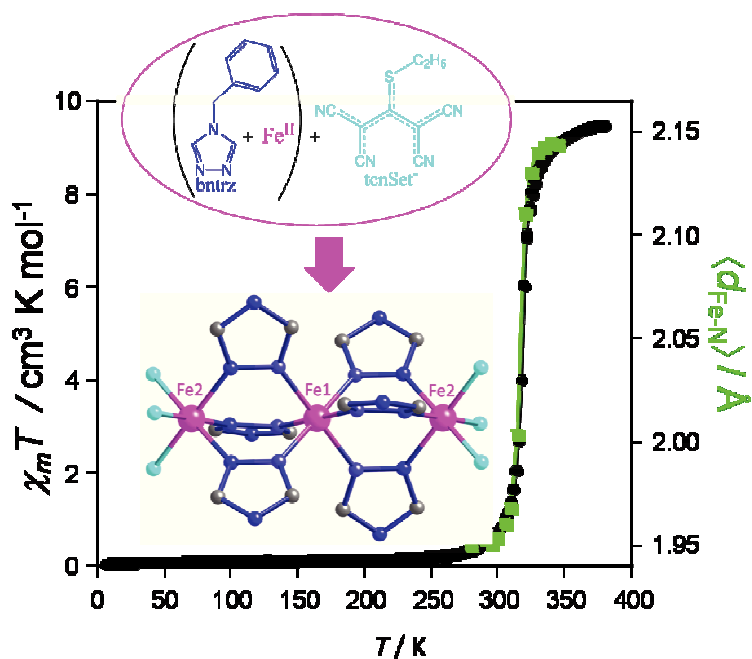
Notes and references

- § *Crystal data* for $\text{C}_{108}\text{H}_{84}\text{N}_{42}\text{S}_6\text{Fe}_3$ (**1**). $T = 170$ K: trigonal $R\bar{3}$ space group, $Z = 3$, $a = 26.164(11)$ Å, $c = 14.267(6)$ Å, $V = 8458(8)$ Å³, 21573 collected reflections, 3393 unique ($R_{\text{int}} = 0.0951$) and 2251 observed, 241 parameters, $R1/wR2 = 0.0506 / 0.0917$, $S = 1.016$. $T = 360$ K: trigonal $R\bar{3}$ space group, $Z = 3$, $a = 26.055(3)$ Å, $c = 14.8240(13)$ Å, $V = 8715(2)$ Å³, 24948 collected reflections, 3544 unique ($R_{\text{int}} = 0.0922$) and 2092 observed, 241 parameters, $R1/wR2 = 0.0554 / 0.0958$, $S = 1.006$.
- (a) E. Coronado, J. R. Galán-Mascarós, M. Monrabal-Capilla, J. García-Martínez and P. Pardo-Ibáñez, *Adv. Mater.* 2007, **19**, 1359; (b) A. Bousseksou, G. Molnar, L. Salmon and W. Nicolazzi, *Chem. Soc. Rev.*, 2011, **40**, 3313; (c) G. Félix, K. Abdul-Kader, T. Mahfoud, I. A. Gural'skiy, W. Nicolazzi, L. Salmon, G. Molnar and A. Bousseksou, *J. Am. Chem. Soc.*, 2011, **133**, 15342.
 - (a) P. Gütllich, A-B. Gaspar and Y. Garcia, *Beilstein J. Org. Chem.*, 2015, **9**, 342; (b) M. Shatruk, H. Phan, B. A. Chrisostomo and A. Suleimenova, *Coord. Chem. Rev.*, 2015, **289-290**, 62; (c) C. Atmani, F. El Hajj, S. Benmansour, M. Marchivie, S. Triki, F. Conan, V. Patinec, H. Handel, G. Dupouy and C. J. Gómez-García, *Coord. Chem. Rev.*, 2010, **254**, 1559.
 - (a) Y. Garcia, V. Niel, M. C. Muñoz and J.-A. Real, *Top. Curr. Chem.*, 2004, **233**, 229-257; (b) S. Hayami, R. Moriyama, Y. Shigeyoshi, R. Kawajiri, T. Mitani, M. Akita, K. Inoue and Y. Maeda, *Inorg. Chem.*, 2005, **44**, 7295; (c) R. Ishikawa, K. Matsumoto, K. Onishi, T. Kubo, A. Fuyuhiko, S. Hayami, K. Inoue, S. Kaizaki and S. Kawata, *Chem. Lett.*, 2009, **38**, 620; (d) G. Morgan, K. D. Murnaghan, H. Muller-Bunz, V. McKee and C. J. Harding, *Angew. Chem. Int. Ed.*, 2006, **45**, 7192; (e) M. A. Halcrow, *Chem. Soc. Rev.*, 2011, **40**, 4119; (f) P. Guionneau, *Dalton Trans.*, 2014, **43**, 382.
 - (a) M. M. Dîrtu, C. Neuhausen, A. D. Naik, A. Rotaru, L. Spinu and Y. Garcia, *Inorg. Chem.*, 2010, **49**, 5723; (b) O. Roubeau, *Chem. Eur. J.*, 2012, **18**, 15230.
 - (a) L. Antolini, A. C. Fabretti, D. Gatteschi and R. Sessoli, *Inorg. Chem.*, 1990, **29**, 143; (b) Y. M. Klein, N. F. Sciortino, C. E. Housecroft, C. J. Kepert and S. M. Neville, *Magnetochemistry*, 2016, 2.
 - (a) O. G. Shakirova, L. G. Lavrenova, Y. G. Shvedenkov, G. A. Berezovskii, D. Y. Naumanov, L. A. Sheludyakova, G. V. Dolgushin and S. V. Larionov, *Russ. J. Coord. Chem.*, 2004, **30**, 473; (b) M. Thomann, O. Kahn, J. Guilhem and F. Varret, *Inorg. Chem.*, 1994, **33**, 6029.
 - (a) H. Z. Scott, T. M. Ross, B. Moubaraki, K. S. Murray and S. M. Neville, *Eur. J. Inorg. Chem.*, 2013, 803; (b) Y. Garcia, P. Guionneau, G. Bravic, D. Chasseau, J. A. K. Howard, O. Kahn, V. Ksenofontov, S. Reiman and P. Gütllich, *Eur. J. Inorg. Chem.*, 2000, 1531; (c) G. Vos, R. A. le Febre, R. A. G. de Graaff, J. G. Haasnoot and J. Reedijk, *J. Am. Chem. Soc.*, 1983, **105**, 1682; (d) J. J. A. Kolnaar, G. van Dijk, H. Kooijman, A. L. Spek, V. Ksenofontov, P. Gütllich, J. G. Haasnoot and J. Reedijk, *Inorg. Chem.*, 1997, **36**, 2433; (e) D. Savard, C. Cook, G. D. Enright, I. Korobkov, T. J. Burchell and M. Murugesu, *CrystEngComm*, 2011, **13**, 5190.
 - (a) V. Gómez, J. Benet-Buchholz, E. Martin and J. R. Galan-Máscaros, *Chem. Eur. J.*, 2014, **20**, 5369; (b) V. Gómez, C. S. de Pipaón, P. Maldonado-Illescas, J. C. Waerenborgh, E. Martin, J. Benet-Buchholz and J. R. Galan-Máscaros, *J. Am. Chem. Soc.*, 2015, **137**, 11924.
 - (a) X. Cheng, Q. Yang, C. Gao, B.-W. Wang, T. shiga, H. Oshio, Z.-M. Wang, S. Gao, *Dalton Trans.*, 2015, **44**, 11282; (b) Y. Garcia, F. Robert, A. D. Naik, G. Zhou, B. Tinant, K. Robeyns, S. Michotte and L. Piroux, *J. Am. Chem. Soc.*, 2011, **133**, 15850; (c) X. X. Wu, Y. Y. Wang, P. Yang, Y. Y. Xu, J. Z. Huo, B. Ding, Y. Wang and X.-G. Wang, *Cryst. Growth. Des.*, 2014, **14**, 477; (d) J. J. A. Kolnaar, M. I. de Heer, H. Kooijman, A. L. Spek, G. Schmitt, V. Ksenofontov, P. Gütllich, J. G. Haasnoot and J. Reedijk, *Eur. J. Inorg. Chem.*, 1999, 881.
 - N. Pittala, F. Thétiot, S. Triki, K. Boukheddaden, G. Chastanet, and M. Marchivie, *Chem. Mater.*, 2016; DOI: 10.1021/acs.chemmater.6b04118.
 - (a) S. Lethu and J. Dubois, *Eur. J. Org. Chem.*, 2011, 3920; (b) P. G. Baraldi, F. Fruttarolo, M. A. Tabrizi, D. Preti, R. Romagnoli, H. El-Kashef, A. Moorman, K. Varani, S. Stefania Gessi, S. Merighi and P. A. Borea, *J. Med. Chem.*, 2003, **46**, 1229; (c) G. Dupouy, M. Marchivie, S. Triki, J. Sala-Pala, J.-Y. Salaün, C. J. Gómez-García and P. Guionneau, *Inorg. Chem.*, 2008, **47**, 8921.
 - P. Gütllich and H. A. Goodwin, *Top. Curr. Chem.*, **2004**, 233, 1-47.
 - M. Marchivie, P. Guionneau, J.-F. Létard and D. Chasseau, *Acta Cryst. B*, 2005, **B61**, 25.

Unprecedented complete one-step spin transition above room temperature in a trinuclear Fe(II) triazole-based complex

Narsimhulu Pittala, Franck Th  tiot, Smail Triki, Kamel Boukheddaden, Guillaume Chastanet and Mathieu Marchivie.

We report an original triazole-based trinuclear Fe^{II} complex [Fe₃(bntz)₆(tcnset)₆] (**1**) (bntz = 4-(benzyl)-1,2,4-triazole, tcnset[−] = 1,1,3,3-tetracyano-2-thioethylpropenide anion) as the first related example to date that displays a complete spin transition. Magnetic and heat capacity measurements, and variable temperature X-ray diffraction revealed a one-step first-order [HS-HS-HS]↔[LS-LS-LS] transition above room temperature (*T*_{1/2} = 318 K).



Supplementary information

One-step complete spin transition above room temperature in a trinuclear Fe^{II} neutral complex

Narsimhulu Pittala,^a Franck Thétiot,^a Smail Triki,^{*a} Kamel Boukheddaden,^b Guillaume Chastanet^c and Mathieu Marchivie.^c

^a*UMR CNRS 6521, Chimie, Electrochimie Moléculaires, Chimie Analytique, Université de Bretagne Occidentale, C.S. 93837 - 29238 Brest Cedex 3 – France*

^{*}E-mail: smail.triki@univ-brest.fr

^bGroupe d'Etudes de la Matière Condensée, UMR-CNRS 8635, Université Paris-Saclay, 45 Avenue des Etats-Unis 78035 Versailles, France.

^cCNRS, Université Bordeaux, ICMCB, 87 Av. Doc. A. Schweitzer, F-33608 Pessac, France.

1 - Syntheses

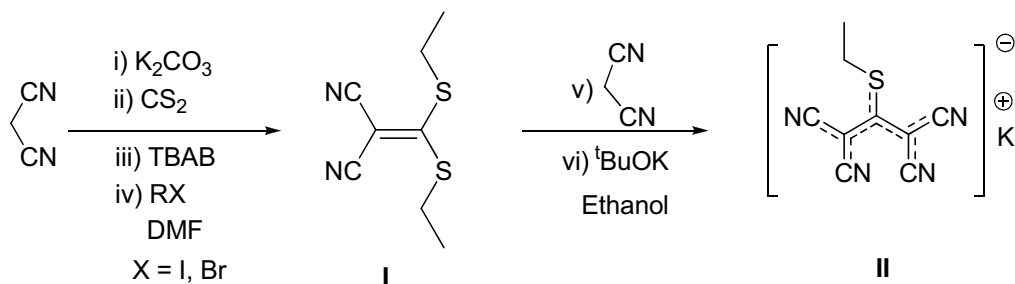
a - General Considerations

All the starting reagents were purchased from commercial sources (Sigma-Aldrich, Across, Fisher Scientific, Alfa Aesar and Merck) and used without further purification unless otherwise stated. Deuterated solvents were purchased from Sigma-Aldrich and Cambridge Isotope Laboratories. Dried solvents were prepared by refluxing for one day under nitrogen over the appropriate drying agents (calcium hydride for acetonitrile, dichloromethane, and hexane; magnesium and iodine for methanol; sodium for ethanol, and molecular sieves for DMF), and then degassed before use. Solvents were stored in glass ampoules under argon. All the glassware and cannula were stored in an oven (>373 K). When appropriate, the reactions were carried out under argon or nitrogen by using a dual manifold vacuum/argon line and standard Schlenk techniques.

b - Syntheses of the ligands

Triazole-based Ligand. The 4-(Benzyl)-1,2,4-triazole (bntrz) ligand was synthesized using the previously reported method.^{1,2}

Cyanocarbanion salt.³ The potassium 1,1,3,3-tetracyano-2-thioethylpropenide (K(tcnset)) was prepared in two steps (Scheme 2) according to modified literature methods.³ In the first step, 2-[(bis-ethylthio)methylene]malononitrile was synthesized from malononitrile and alkyl halide following the reported methods.^{3a-b} Then, potassium [1,1,3,3-tetracyano-2-thioethylpropenide] salt [K(tcnset)] was obtained from the corresponding ketene thioacetal after reaction with malononitrile in the presence of potassium tert-butoxide.^{3c}



Scheme 2: Synthesis of K(tcnset).

2-[(bis-ethylthio)methylene]malononitrile (I). To a solution of malononitrile (4.0 g, 60.55 mmol) in DMF (25 mL) was added K_2CO_3 (8 g, 57.88 mmol). After stirring for 30 min at room temperature, CS_2 (3.6 mL, 66.6 mmol) was added dropwise, and the reaction mixture was stirred at room temperature for an additional 10 min before ethylhalide (121.1 mmol) and tetrabutylammonium bromide (4 g, 10 mmol) were successively added. After further stirring for 30 minutes at room temperature, the reaction mixture was then refluxed for 2 h at 50 °C. Subsequently, after stirring for 24-48 h at room temperature while monitoring the reaction status with TLC (2:98 Ethylacetate: Hexane), the reaction mixture was diluted with water (200 mL) and extracted with Et_2O (4×200 mL). The combined organic layers were washed with Brine solution (100 mL) and dried over $MgSO_4$, then filtered and concentrated under reduced pressure. The crude product was purified by chromatography on silica gel [hexane/ $EtOAc$, 10:0 to 9.5:0.5 (v/v)] to provide ketene dithioacetal as pale green solid (yield: 60 %, 7.170 g).

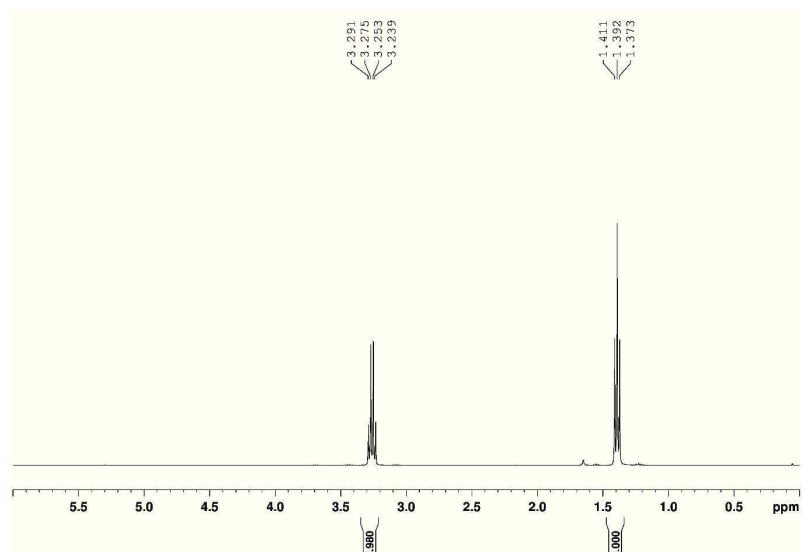


Figure S1. ^1H NMR (400 MHz, CDCl_3 , 298 K) of 2-[bis(ethylthio)methylene]malononitrile (**I**).
 ^1H NMR : δ , 3.27 (q, 4H, -SCH₂-), 1.39 (t, 6H, -CH₃).

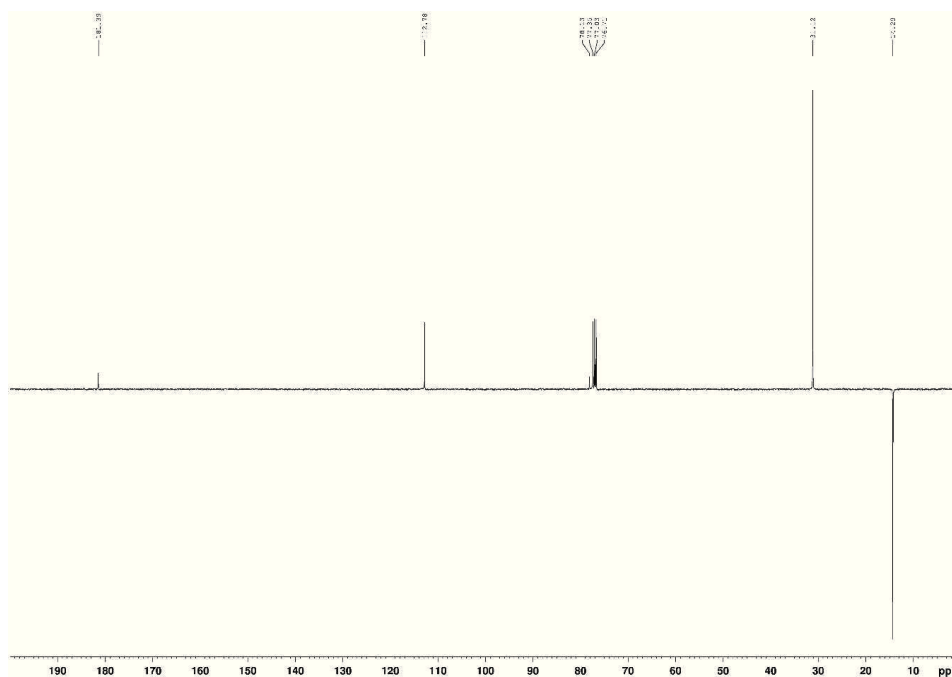


Figure S2. ^{13}C NMR (400 MHz, CDCl_3 , 298 K) of 2-[bis(ethylthio)methylene]malononitrile (**I**).
 ^{13}C NMR : δ , 181.4 (-C(S-Et)₂), 112.8 (-CN), 78.1 (-C(CN)₂), 31.1 (-SCH₂-), 14.3 (-CH₃).

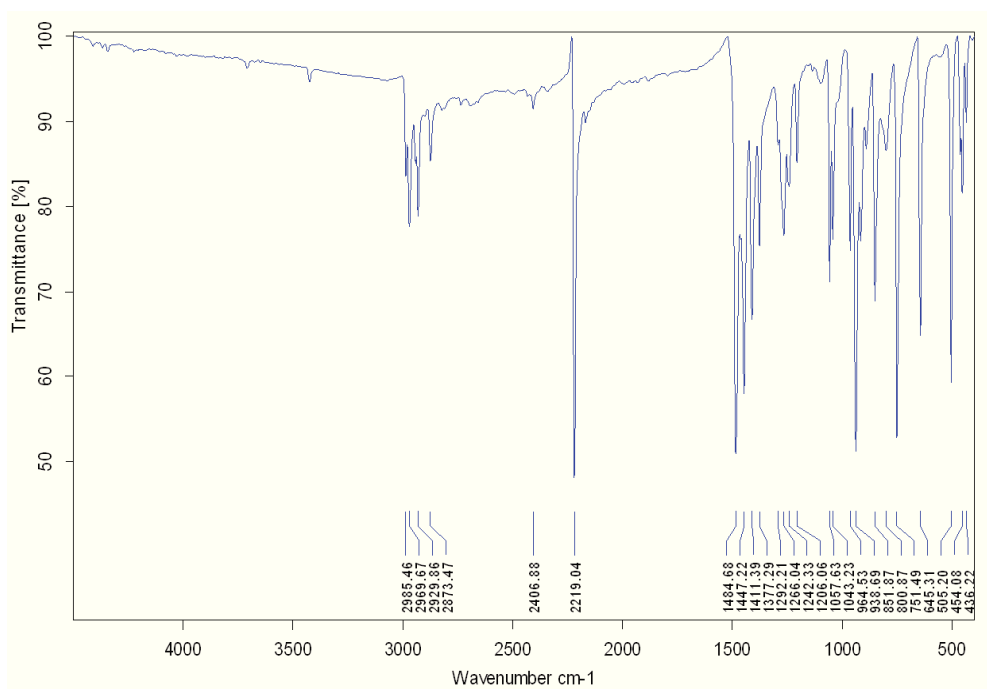


Figure S3. Infrared Spectrum of 2-[bis(ethylthio)methylene]malononitrile (**I**). IR data (ν , cm^{-1}) : 2970w, 2930w, 2874w, 2407w, 2349w, 2322w, 2219s, 1486s, 1463m, 1411w, 1377w, 1265w, 1240w, 1206w, 1057m, 1043m, 964s, 939w, 852w, 801w, 751w, 646m, 505m, 454m, 436w.

K(tenaset) (II). In this second step, a warm ethanolic solution (30 mL) of the previously synthesized 2-[(bis-ethylthio)methylene]malononitrile (**I**) (1.983 g, 10 mmol) was added dropwise to an ethanolic solution (10 mL) of malononitrile (0.66 g, 10 mmol) and t-BuOK (1.12 g, 10 mmol). The resulting mixture was refluxed for 1h, and then cooled to room temperature and kept at 4 °C for two days. The compound was filtered on a sintered-glass funnel, washed with distilled diethyl ether, and finally dried under vacuum to obtain the potassium salt of [1,1,3,3-tetracyano-2-thioalkylpropenide] (K(tenaset), **II**) as a white crystalline powder (yield: 86%, 2.076 g).

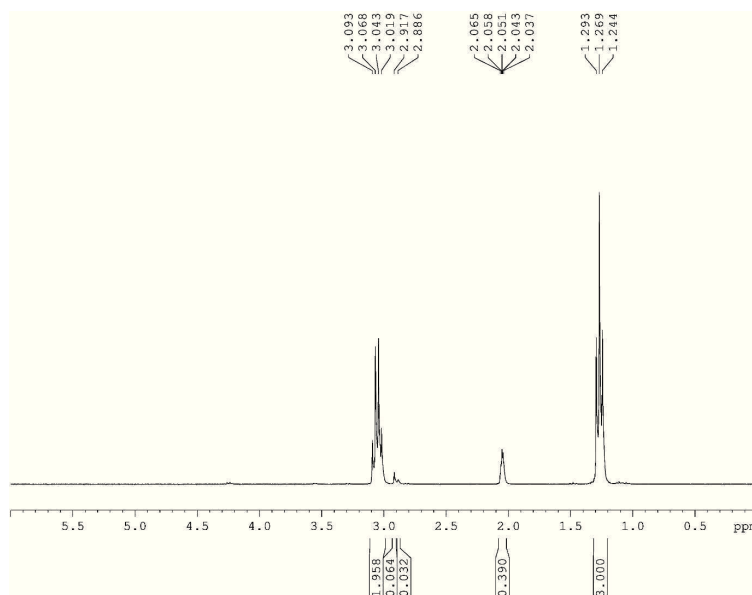


Figure S4. ^1H NMR (300 MHz, Acetone- D_6 , 298 K) of K(tcnsset) (**II**). ^1H NMR : δ , 3.06 (q, 2H, -SCH₂-), 1.27 (t, 3H -CH₃).

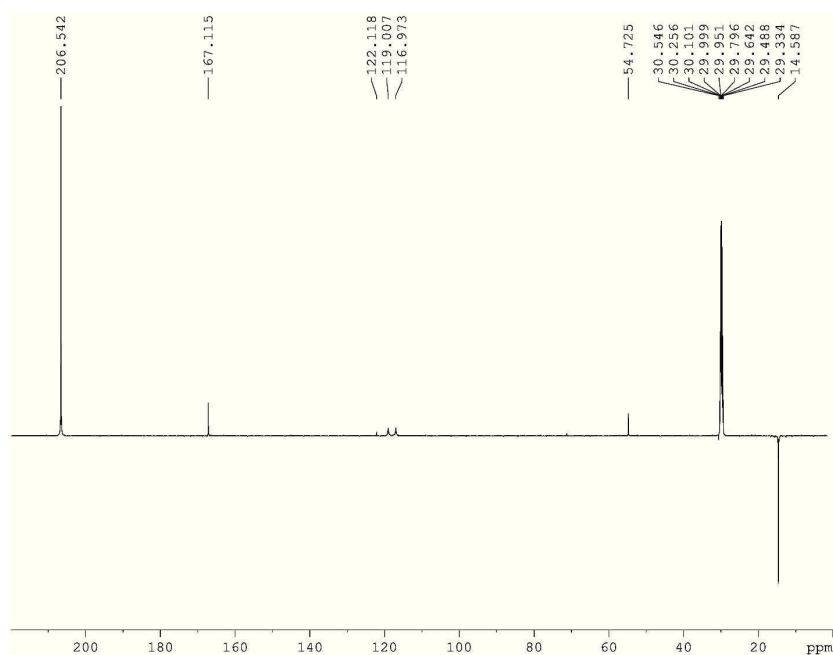


Figure S5. ^{13}C NMR (500 MHz, Acetone- D_6 , 298 K) of K(tcnsset) (**II**). ^{13}C NMR : δ , 167.1 (-C(S-Pr)₂), 119.1 (-CN), 116.9 (-CN), 54.7 (-C(CN)₂), 29.8 (-SCH₂-), 14.6 (-CH₃).

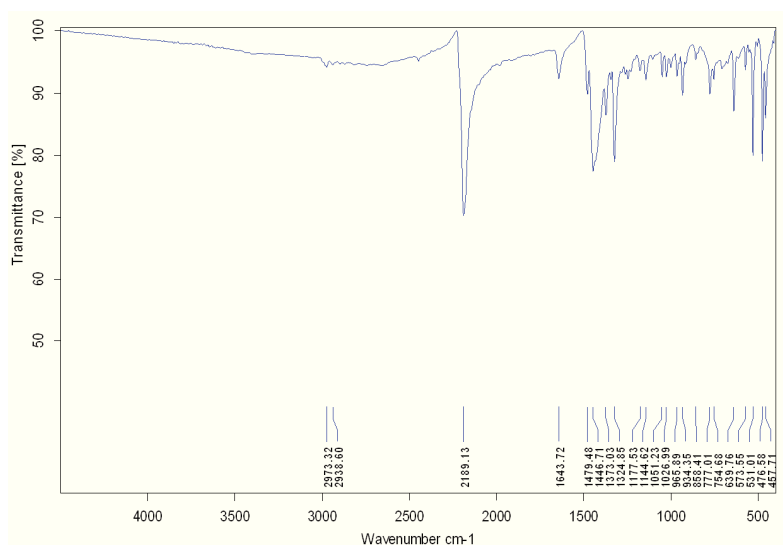


Figure S6. Infrared Spectrum of K(tcnsset). IR (ν , cm^{-1}) : 2189s, 1644w, 1445s, 1373w, 1325w, 934w, 777w, 640w, 531w, 477w, 458w.

c - Single-crystals preparation of $[\text{Fe}_3(\text{bntrz})_6(\text{tcnsset})_6]$ (**1**)

Single-crystals of linear trinuclear Fe(II) SCO complex $[\text{Fe}_3(\text{bntrz})_6(\text{tcnsset})_6]$ were prepared by slow diffusion, in a fine glass tube (3.0 mm diameter). An aqueous solution of $\text{Fe}(\text{BF}_4)_2 \cdot 6\text{H}_2\text{O}$ (33.755 mg, 0.1 mmol) and K(tcnsset) (48 mg, 0.2 mmol) in 10 mL of distilled water with a small amount of ascorbic acid and a solution of bntrz (47.7 mg, 0.3 mmol) in 2.5 mL of methanol were initially prepared. The aqueous solution of Fe^{II} was placed in the bottom of a fine tube of 3.0 mm, upon which a solvent mixture of water and methanol - with a ratio of 2:1 - was carefully added. Then, a methanolic solution of bntrz of methanol was carefully layered on top of the buffer layer. In fine, pink single crystals of **1** suitable for X-ray diffraction were grown at the interface over a period of three weeks. Alternatively, an aqueous solution of $\text{Fe}(\text{BF}_4)_2 \cdot 6\text{H}_2\text{O}$ placed at the bottom of a glass tube was covered with water mixture, over which an aqueous solution of the bntrz ligand and K(tcnsset salt) was layered. The same pink single crystals of **1** were obtained in smaller size compared to the above-mentioned experimental conditions. Anal. Calcd for $\text{C}_{108}\text{H}_{84}\text{Fe}_3\text{N}_{42}\text{S}_6$: C, 55.6; H, 3.6; N, 25.2 %. Found: C, 56.1; H, 3.5; N, 24.8 %.

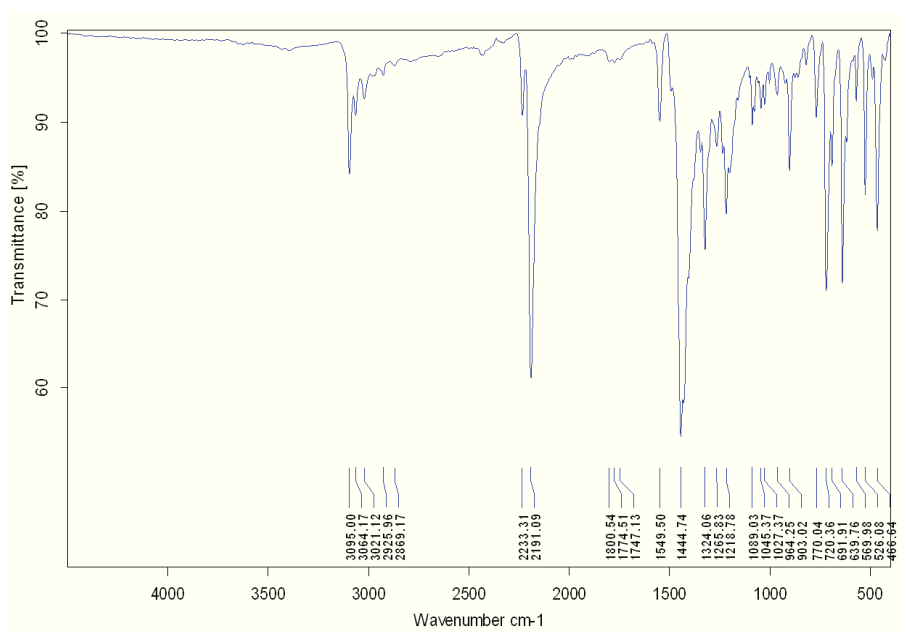


Figure 16. IR Spectrum of the Single-Crystals of $[\text{Fe}_3(\text{bntrz})_6(\text{tcnsct})_6]$ (**2**) ($4000\text{--}450\text{ cm}^{-1}$). IR (ν, cm^{-1}) : 3095w, 3064w, 3021w, 2233w, 2191s, 1549w, 1445s, 1324s, 1219m, 1089w, 1045w, 1027w, 903w, 721m, 641m, 527w, 467w.

2 - Physical Measurements and characterizations

Single crystal X-ray studies were performed at 296 K and 120 K on Xcalibur 2 κ -CCD diffractometer using Mo $K\alpha$ radiation ($\lambda = 0.71073\text{ \AA}$). The corresponding structures were solved by direct methods with the SHELXS program and refined on F^2 by weighted full matrix least-squares methods using the SHELXL program.⁴ All non-hydrogen atoms were refined anisotropically, hydrogen atoms were located in difference Fourier maps, and treated using a riding model. Crystallographic data and refinement details are provided in Table S1. $^1\text{H}/^{13}\text{C}$ -NMR spectra were recorded on Bruker AMX-300, AMX-400 and AMX-500 spectrometers, and the spectra were referenced internally using residual proton solvent resonances relative to tetramethylsilane ($\delta = 0\text{ ppm}$). Magnetic measurements were performed with a Quantum Design MPMS-XL-5 SQUID magnetometer in the 2-300 K temperature range with an applied magnetic field of 2 Tesla and scan rate of $0.4\text{ K}\cdot\text{min}^{-1}$ on single crystals of compound 1 (mass of 4.25 mg). DSC measurements were performed on a DSC-1/LN2 Mettler Toledo calorimeter setting the heat flow scan rate at $s = 2\text{ K}\cdot\text{min}^{-1}$ on single crystals of 1 (mass of 4.40 mg). Infrared (IR) spectra were collected in the range $4000\text{--}200\text{ cm}^{-1}$ on a FT-IR BRUKER ATR VERTEX70

Spectrometer. Elemental analyses were performed at the “Service de microanalyse”, CNRS, 91198 Gif-sur-Yvette, France.

3 - X-ray crystallography

Table S1. Crystal data and structural refinement parameters for compound **1**.

Compound	1	
Temperature / K	360(2)	170(2)
Color	Yellow	Pink
Empirical formula	C ₁₀₈ H ₈₄ Fe ₃ N ₄₂ S ₆	C ₁₀₈ H ₈₄ Fe ₃ N ₄₂ S ₆
Formula weight / g.mol ⁻¹	2330.08	2330.08
Wavelength / Å	0.71073 Å	0.71073 Å
Crystal system	Trigonal	Trigonal
Space group	<i>R</i> -3	<i>R</i> -3
a / Å	26.055(3)	26.164(11)
c / Å	14.8240(13)	14.267(6)
Volume / Å ³	8715(2)	8458(8)
Z	3	3
D _{calc} / g.cm ⁻³	1.332	1.372
Abs. coef. / cm ⁻¹	5.43	5.60
F(000)	3600.0	3600.0
Crystal size / mm ³	0.25 × 0.02 × 0.02	0.25 × 0.02 × 0.02
2θ range / °	5.51 to 50.738	5.988 to 50.482
Refl. collected	24948	21573
Unique refl. / R _{int}	3544 / 0.0922	3393 / 0.0951
Data / restr. / N _v	2092 / 0 / 241	2251 / 0 / 241
Final R indexes [<i>I</i> ≥ 2σ (<i>I</i>)]	R ₁ = 0.0554, wR ₂ = 0.0958	R ₁ = 0.0506, wR ₂ = 0.0917
Final R indexes [all data]	R ₁ = 0.1214, wR ₂ = 0.1129	R ₁ = 0.1002, wR ₂ = 0.1048
°GooF	1.006	1.016
Δρ _{max/min} / eÅ ⁻³	+0.342 / -0.381	0.527 / -0.471
CCDC No.	1500725	1500724
	280 K-345 K, every 5K (CCDC numbers 1500728-1500740).	

$$^a R_1 = \sum |F_o - F_c| / F_o. \quad ^b wR_2 = \{ \sum [w(F_o^2 - F_c^2)^2] / \sum [w(F_o^2)^2] \}^{1/2}. \quad ^c \text{GooF} = \{ \sum [w(F_o^2 - F_c^2)^2] / (N_{\text{obs}} - N_{\text{var}}) \}^{1/2}$$

Table S2. Fe-N bond lengths and N-Fe-N bond angles at 360 and 170 K for **1**.

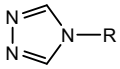
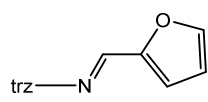
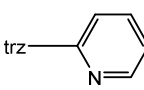
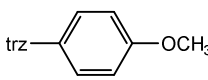
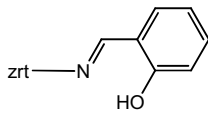
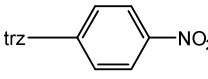
T / K	360 (<i>HS</i> State)	170 (<i>LS</i> State)
Fe1-N1 ^(b)	2.175(2)	1.970(2)
Fe1-N1 ^(a)	2.175(2)	1.970(2)
Fe1-N1 ^(d)	2.175(2)	1.970(3)
Fe1-N1 ^(e)	2.175(2)	1.970(2)
Fe1-N1	2.175(2)	1.970(2)
Fe1-N1 ^(c)	2.175(2)	1.970(3)
Fe2-N2	2.170(2)	1.962(2)
Fe2-N2 ^(b)	2.170(2)	1.962(2)
Fe2-N2 ^(c)	2.170(2)	1.962(2)
Fe2-N4 ^(c)	2.146(3)	1.943(3)
Fe2-N4	2.146(3)	1.943(3)
Fe2-N4 ^(b)	2.146(3)	1.943(3)
N1 ^(b) -Fe1-N1 ^(d)	89.34(8)	89.63(10)
N1 ^(b) -Fe1-N1 ^(d)	89.34(8)	89.63(10)
N1-Fe1-N1 ^(e)	89.34(8)	89.64(10)
N1 ^(b) -Fe1-N1 ^(e)	180.0	180.00(10)
N1 ^(a) -Fe1-N1 ^(e)	90.67(8)	90.37(9)
N1 ^(d) -Fe1-N1 ^(c)	180.0	180.0
N1-Fe1-N1 ^(c)	90.66(8)	90.37(9)
N1 ^(b) -Fe1-N1	90.66(8)	90.37(10)
N1 ^(b) -Fe1-N1 ^(a)	89.33(8)	89.63(10)
N1 ^(d) -Fe1-N1	89.34(8)	89.63(10)
N1 ^(b) -Fe1-N1 ^(c)	90.66(8)	90.37(10)
N1 ^(a) -Fe1-N1	180.0	180.0
N1 ^(d) -Fe1-N1 ^(a)	90.66(8)	90.37(9)
N1 ^(a) -Fe1-N1 ^(c)	89.34(8)	89.63(10)
N1 ^(d) -Fe1-N1 ^(e)	90.66(8)	90.37(9)
N1 ^(e) -Fe1-N1 ^(c)	89.33(8)	89.63(9)
N2-Fe2-N2 ^(c)	90.27(9)	90.07(10)
N2 ^(b) -Fe2-N2 ^(c)	90.27(9)	90.06(10)
N2 ^(b) -Fe2-N2	90.27(9)	90.07(10)
N4 ^(c) -Fe2-N2	177.19(9)	178.95(11)
N4-Fe2-N2	87.01(9)	88.89(10)
N4-Fe2-N2 ^(b)	177.19(9)	178.94(11)
N4-Fe2-N2 ^(c)	89.03(9)	89.78(10)
N4 ^(b) -Fe2-N2	89.03(9)	89.78(10)
N4 ^(b) -Fe2-N2 ^(c)	177.19(9)	178.95(11)
N4 ^(c) -Fe2-N2 ^(c)	87.01(9)	88.89(10)
N4 ^(c) -Fe2-N2 ^(b)	89.03(9)	89.78(10)
N4 ^(b) -Fe2-N2 ^(b)	87.01(9)	88.89(10)
N4 ^(c) -Fe2-N4	93.65(9)	91.26(10)
N4 ^(b) -Fe2-N4	93.65(9)	91.26(10)
N4 ^(b) -Fe2-N4 ^(c)	93.65(9)	91.26(10)

*The two Fe(II) environments are defined by N1 ([Fe1(N1)₆]) and by N2 and N4 ([Fe2(N2)₃(N4)₃]) nitrogen atoms.

^a Σ^5 is the sum of the deviation from 90° of the 12 cis-angles of the FeN₆ octahedron; ^b Θ^5 is the sum of the deviation from 60° of the 24 trigonal angles of the projection of the FeN₆ octahedron onto its trigonal faces. Symmetry transformations used to generate equivalent atoms: (a) = 2/3-x, 4/3-y, 1/3-z; (b) = 1-y, 1+x-y, +z; (c) = +y-x, 1-x, +z; (d) = 2/3-y+x, 1/3+x, 1/3-z; (e) = -1/3+y, 1/3-x+y, 1/3-z.

4 - Trinuclear Fe(II) complexes based on functionalized triazole ligands

Table S3. Trinuclear Fe₃ complexes with triple triazole bridges

	Trinuclear complex	SCO behavior / T _{1/2}	Ref.
trz—CH ₂ —CH ₂ —CH ₃	[Fe ₃ (Prtrz) ₆ (ReO ₄) ₄ (H ₂ O) ₂](ReO ₄) ₂ ·H ₂ O	gradual / T _{1/2} =185 K	6a
	[Fe ₃ (furtrz) ₆ (ptol) ₂ (MeOH) ₄](ptol) ₄ ·4(MeOH)	gradual / T _{1/2} ~170 K	6b
	[Fe ₃ (Pytrz) ₈ (H ₂ O) ₄](NO ₃) ₆	Gradual / T _{1/2} =208 K	7a
	[Fe ₃ (Pytrz) ₈ (H ₂ O) ₄](ClO ₄) ₆	HS	7a
	[Fe ₃ (Pytrz) ₈ (H ₂ O) ₄](Br) ₆	HS	7a
	[Fe ₃ (MeOptrz) ₈ (H ₂ O) ₄](BF ₄) ₆ ·2H ₂ O	HS	7b
	[Fe ₃ (MeOptrz) ₆ (H ₂ O) ₆](Tos) ₆ ·4H ₂ O	gradual / T _{1/2} =245 K	7b
	[Fe ₃ (MeOptrz) ₆ (H ₂ O) ₆](Tos) ₆	gradual / T _{1/2} =330 K	7b
	[Fe ₃ (Hsaltrz) ₆ (H ₂ O) ₂ (EtOH) ₄](ClO ₄) ₆ ·2EtOH	HS	8a
trz—CH ₂ —CH ₂ —OH	[Fe ₃ (Hyetrz) ₆ (H ₂ O) ₆](CF ₃ SO ₃) ₆	gradual / T _{1/2} =290 K	8b
trz—CH ₂ —CH ₃	[Fe ₃ (Ettrz) ₆ (H ₂ O) ₆](CF ₃ SO ₃) ₆	abrupt / T _{1/2} =205 K	8c
trz—CH(CH ₃) ₂	[Fe ₃ (iPrtrz) ₆ (H ₂ O) ₆](Tos) ₆ ·2H ₂ O	gradual / T _{1/2} =242 K	8d
	[Fe ₃ (iPrtrz) ₆ (H ₂ O) ₆](CF ₃ SO ₃) ₆	gradual / T _{1/2} =185 K	8d
	[Fe ₃ (Nptrz) ₆ (H ₂ O) ₂ (EtOH) ₄](ptol) ₆ ·4EtOH	gradual / T _{1/2} =148 K	8e
trz—CH ₂ —CH ₂ —SO ₃ [−]	[Fe ₃ (Settrz) ₆ (H ₂ O) ₆].5H ₂ O	spin transition with T _{1/2} (↑)=357 K, T _{1/2} (↓)=343K	9a
trz—CH ₂ —CH(SO ₃) ₂	(Me ₂ NH ₂) ₆ [Fe ₃ (dSettrz) ₆ (H ₂ O) ₆]	spin transition with T _{1/2} (↑)=400 K, T _{1/2} (↓)=310K	9b

MeOptrz = 4-(p-methoxyphenyl)-1,2,4-triazole; Tos = p-toluenesulfonate; Hsaltrz = N-salicylidene 4-amino-1,2,4-triazole; Prtrz = 4-propyl-1,2,4-triazole; Hyetrz = 4-(2'-hydroxyethyl)-1,2,4-triazole; Ettrz = 4-ethyl-1,2,4-triazole; iPrtrz = 4-isopropyl-1,2,4-triazole; Nptrz = 4-(4'-nitrophenyl)-1,2,4-triazole; ptol = p-tolylsulfonate; Pytrz = 4-(2-pyridyl)-1,2,4-triazole; bpy = 2,2'-bipyridyl; tpen = tetrakis(2-pyridylmethyl)ethylenediamine; HC(3,5-Mepz)₃ = tris(3,5-dimethylpyrazol-1-yl)methane; ddb = N₂,N₂,N₄,N₄-tetrabutyl-N₆,N₆-di(pyridin-2-yl)-1,3,5-triazine-2,4,6-triamine; pytepy = 2-(1H-pyrazol-1-yl)-6-(1H-tetrazol-5-yl)pyridine; Settrz = 4-(1,2,4-triazol-4-yl)ethanesulfonate; dSettrz = 4-(1,2,4-triazol-4-yl)ethanedisulfonate; furtrz = 1,2,4-triazole ligand furanylidene-4H-1,2,4-triazol-4-amine.

References

- (1) N. Pittala, F. Thétiot, S. Triki, K. Boukheddaden, G. Chastanet, and M. Marchivie, *Chem. Mater.*, **2016**; DOI: 10.1021/acs.chemmater.6b04118.
- (2) H. O. Bayer, R. S. Cook and W. C. Von Mayer, *US Patent*, **1974**, 3821376.
- (3) a) S. Lethu, J. Dubois, *Eur. J. Org. Chem.*, **2011**, 3920-3931; b) P. G. Baraldi, F. Fruttarolo, M. A. Tabrizi, D. Preti, R. Romagnoli, H. El-Kashef, A. Moorman, K. Varani, S. Stefania Gessi, S. Merighi, P.A. Borea, *J. Med. Chem.*, **2003**, *46*, 1229-1241. c) G. Dupouy, M. Marchivie, S. Triki, J. Sala-Pala, J.-Y. Salaün, C. J. Gómez-García, P. Guionneau, *Inorg. Chem.*, **2008**, *47*, 8921-8931.
- (4) Sheldrick, G. M., *Acta Cryst.*, **2008**, *A64*, 112.
- (5) a) P. Guionneau, M. Marchivie, G. Bravic, J.-F. Létard and D. Chasseau, *Top. Curr. Chem.* **2004**, **234**, 97-128; b) M. Marchivie, P. Guionneau, J.-F. Létard and D. Chasseau, *Acta Cryst. B*, **2005**, **B61**, 25-28.
- (6) M. B. Bushuev, L. G. Lavrenova, Yu. G. Shvedenkov, A. V. Virovets, L. A. Sheludyakova, and S. V. Larionov, *Russ. J. Inorg. Chem.*, **2007**, *52*, 46-51; b) Y. M. Klein, N. F. Sciortino, C. E. Housecroft, C. J. Kepert, and S. M. Neville, *Magnetochemistry*. **2016**, 2-8.
- (7) a) O. G. Shakirova, L. G. Lavrenova, Y. G. Shvedenkov, G. A. Berezovskii, D. Y. Naumanov, L. A. Sheludyakova, G. V. Dolgushin, S. V. Larionov, *Russ. J. Coord. Chem.*, **2004**, *30*, 473-479; b) M. Thomann, O. Kahn, J. Guilhem, F. Varret, *Inorg. Chem.*, **1994**, *33*, 6029-6037.
- (8) a) H. Z. Scott, T. M. Ross, B. Moubaraki, K. S. Murray, S. M. Neville, *Eur. J. Inorg. Chem.*, **2013**, 803-812; b) Y. Garcia, P. Guionneau, G. Bravic, D. Chasseau, J. A. K. Howard, O. Kahn, V. Ksenofontov, S. Reiman, P. Gülich, *Eur. J. Inorg. Chem.*, **2000**, 1531-1538; c) G. Vos, R. A. le Febvre, R. A. G. de Graaff, J. G. Haasnoot, J. Reedijk, *J. Am. Chem. Soc.*, **1983**, *105*, 1682-1683; d) J. J. A. Kolnaar, G. van Dijk, H. Koojiman, A. L. Spek, V. Ksenofontov, P. Gülich, J. G. Haasnoot, J. Reedijk, *Inorg. Chem.*, **1997**, *36*, 2433-2440; e) D. Savard, C. Cook, G. D. Enright, I. Korobkov, T. J. Burchell, M. Murugesu, *CrystEngComm.*, **2011**, *13*, 5190-5197.
- (9) a) V. Gómez, J. Benet-Buchholz, E. Martin and J. R. Galan-Mascarós, *Chem. Eur. J.* **2014**, *20*, 5369-5379; b) V. Gómez, C. S. de Pipaón, P. Maldonado-Illescas, J. C. Waerenborgh, E. Martin, J. Benet-Buchholz and J. R. Galan-Mascarós, *J. Am. Chem. Soc.*, **2015**, *137*, 11924-11927.

Titre: « Contribution à l'étude de matériaux à transition de spin à base de Fe^{II} et de triazole : Avancées et nouvelles questions. »

Ces dernières années, les matériaux à transition de spin (*TS*) ont suscité un intérêt marqué en raison de leurs applications potentielles, notamment en tant que capteurs ou dispositifs électroniques; typiquement, ces complexes présentent - *via* un stimulus externe (ex.: température, rayonnement) - une transition de spin réversible "Haut Spin (HS) \leftrightarrow Bas Spin (BS)". Dans ce contexte, le travail présenté a porté sur la conception et les études magnéto-structurales de monocristaux de nouveaux systèmes Fe^{II} à *TS* à base de ligands 4-R-1,2,4-triazole comprenant un espaceur alkyl, en combinaison avec soit (i) des entités tétracyanométallates inorganiques ($[\text{M}(\text{CN})_4]^{2-}$, $\text{M} = \text{Ni}^{\text{II}}$, Pt^{II} , Pd^{II}) ou (ii) des cyanocarbanions organiques spécifiques ($(\text{tcnsR}')^-$: anions 1,1,3,3-tétracyano-2-thioalkylpropénide) - et ce afin de comprendre *in fine* l'origine physico-chimique de la forte coopérativité dans ces matériaux remarquables, mais aussi de rationaliser le contrôle et l'optimisation des propriétés de *TS*. Dans un premier temps, un nouveau sel de polymère 1D $[\text{Fe}(\text{bntrz})_3][\text{Pt}(\text{CN})_4]\cdot\text{H}_2\text{O}$ (**1**) - présentant une *TS* abrupte et une résilience exceptionnelle lors de cycles répétés de commutation - a été synthétisé; les études structurales fines - réalisées sur monocristaux - des états HS et BS ont clairement révélé l'impact des interactions à longue distance sur les propriétés de la *TS* dans ce système. Ensuite, la substitution de l'anion « rigide » tétracyanométallate ($[\text{Pt}(\text{CN})_4]^{2-}$) par l'entité plus « flexible » $(\text{tcnset})^-$ nous a conduit au premier exemple de complexe neutre trinuéculaire à base de triazole $[\text{Fe}_3(\text{bntrz})_6(\text{tcnset})_6]$ (**2**) présentant une *TS* complète en une seule étape au-dessus de la température ambiante. La variation systématique du substituant R' de l'anion fonctionnalisé $(\text{tcnsR}')^-$ a permis l'obtention de deux nouveaux systèmes à *TS*, à savoir le complexe trinuéculaire neutre $[\text{Fe}_3(\text{bntrz})_6(\text{tcnspr})_6]$ (**3**) et le dérivé 1D $[\text{Fe}_3(\text{bntrz})_8(\text{tcnsme})_4](\text{tcnsme})_2\cdot 4\text{H}_2\text{O}$ (**4**), avec des caractéristiques structurales et des comportements de *TS* distincts. Enfin, dans le but d'évaluer précisément l'impact de différents substituants en 4ème position sur le ligand 1,2,4-triazole, deux nouveaux matériaux 3D basés sur le triazole 2-(3-(4H-1,2,4-triazol-4-yl)propyl)isoindoline-1,3-dione (phtptrz) - *i.e.* $\{\text{Fe}_3(\mu_2\text{-phtptrz})_6[\mu_2\text{-Pt}(\text{CN})_4]_3\}\cdot\text{C}_2\text{H}_5\text{OH}\cdot 5.5\text{H}_2\text{O}$ (**5**) et $\{\text{Fe}(\text{phtptrz})[\text{Pt}(\text{CN})_4]\cdot\text{H}_2\text{O}\}$ (**6**) - ont été synthétisés et caractérisés; une *TS* en deux étapes est observée pour le composé **5**, tandis que le dérivé **6** exprime un comportement paramagnétique caractéristique de l'état de spin $S = 2$.

Mots clés: Ligands, 1,2,4-Triazole, Complexes, Matériaux, Réseau moléculaire, Transition de spin, Coopérativité, Haut spin, Bas spin, Interactions intermoléculaires, Monocristaux.

Title: « Contribution to the Triazole-Based Fe(II) Spin-Crossover (SCO) Materials: Some Achievements and New Questions. »

In recent years, the spin-crossover (*SCO*) materials have attracted much interest because of their potential applications such as sensors or electronic displays; these complexes typically exhibit - *via* an external disturbance (e.g. temperature, radiation) - a reversible “High Spin (*HS*) \leftrightarrow Low Spin (*LS*)” spin transition. In this context, the present work has focused on the design and the magneto-structural investigations of single crystals of novel Fe^{II} *SCO* systems based on 4-R-1,2,4-triazole ligands including an alkyl spacer - with either (i) inorganic tetracyanometallates ($[M(CN)_4]^{2-}$, $M = Ni^{II}, Pt^{II}, Pd^{II}$) or (ii) specific organic cyanocarbanions ($(tcnsR')^-$: 1,1,3,3-tetracyano-2-thioalkylpropenide anions) - in order to ultimately understand the physicochemical origin of the strong cooperativity in such striking materials, but also to rationalize the tuning of the *SCO* properties. At first, a new 1D polymer $[Fe(bntrz)_3][Pt(CN)_4].H_2O$ (**1**) salt - exhibiting an abrupt spin transition and an exceptional resilience upon repeated switching - has been synthesized; the accurate single crystal investigations of both *HS* and *LS* states of the latter clearly revealed the impact of the long-range interactions on *SCO* properties in this system. Then, the substitution of the ‘rigid’ $[Pt(CN)_4]^{2-}$ tetracyanometallate anion by the more ‘flexible’ $(tcnset)^-$ entity lead us to the first example of triazole-based *SCO* Fe^{II} trinuclear neutral complex $[Fe_3(bntrz)_6(tcnset)_6]$ (**2**) exhibiting a complete one-step spin transition above room temperature. The systematic variation of the R' substituent from the functionalized $(tcnsR')^-$ anion resulted in two new Fe^{II} *SCO* systems, *i.e.* the neutral trinuclear complex $[Fe_3(bntrz)_6(tcnspr)_6]$ (**3**) and the 1D $[Fe_3(bntrz)_8(tcnsme)_4](tcnsme)_2.4H_2O$ (**4**) derivative, with distinct structural characteristics and *SCO* behaviours. Finally, with the purpose to further evaluate the impact of different substituents at the 4th position onto 1,2,4-triazole ligand, two new 3D materials based on the functionalised triazole 2-(3-(4H-1,2,4-triazol-4-yl)propyl)isoindoline-1,3-dione (phtptrz) - $\{Fe_3(\mu_2-phtptrz)_6[\mu_2-Pt(CN)_4]_3\}.C_2H_5OH, 5.5H_2O$ (**5**) and $\{Fe(phtptrz)[Pt(CN)_4].H_2O\}$ (**6**) - have been synthesized and characterized; a two-step *SCO* behaviour is observed only in **5**, while **6** shows a characteristic paramagnetic behavior.

Keywords: Ligands, 1,2,4-Triazole, Complexes, Materials, Molecular network, Spin transition, Cooperativity, High spin, Low spin, Intermolecular interactions, Single crystals.